

Correlated TEM-NanoSIMS investigation of foraminiferal metabolism

THÈSE N° 8054 (2017)

PRÉSENTÉE LE 27 OCTOBRE 2017
À LA FACULTÉ DE L'ENVIRONNEMENT NATUREL, ARCHITECTURAL ET CONSTRUIT
LABORATOIRE DE GÉOCHIMIE BIOLOGIQUE
PROGRAMME DOCTORAL EN GÉNIE CIVIL ET ENVIRONNEMENT

ÉCOLE POLYTECHNIQUE FÉDÉRALE DE LAUSANNE

POUR L'OBTENTION DU GRADE DE DOCTEUR ÈS SCIENCES

PAR

Charlotte Madeleine Nicole LEKIEFFRE

acceptée sur proposition du jury:

Prof. A. Buttler, président du jury
Prof. A. Meibom, Prof. E. Geslin, directeurs de thèse
Prof. N. Risgaard-Petersen, rapporteur
Prof. K. Sabbe, rapporteur
Prof. R. Bernier-Latmani, rapporteuse



ÉCOLE POLYTECHNIQUE
FÉDÉRALE DE LAUSANNE

Suisse
2017

Acknowledgements

Ma thèse a représenté une merveilleuse expérience tant au niveau scientifique qu'humain, et de nombreuses personnes que je souhaite remercier ici ont contribué à rendre ces quatre années aussi enrichissantes.

La première personne que je souhaiterais remercier ici est ma co-encadrante de thèse Emmanuelle Geslin sans qui rien de tout ceci n'aurait été possible. Merci de m'avoir fait découvrir dès la première année de master avec Christine Barras le monde merveilleux des foraminifères ! Et merci de m'avoir fait confiance et supporter tout au long de mon stage de master 2 et de ma thèse. Je remercie également Anders Meibom de m'avoir offert l'opportunité de réaliser cette thèse au sein de son laboratoire, merci pour son soutien et son enthousiasme (très communicatif) !

Je remercie également les membres du jury de thèse, Alexandre Buttler, président du jury, Rizlan Bernier-Latmani, examinateur interne, Nils Risgard-Petersen et Koen Sabbe, examinateurs externes, d'avoir accepté d'examiner ce manuscrit.

J'ai eu la chance pendant ces quatre années à l'EPFL de côtoyer de formidables collègues que je suis heureuse de pouvoir compter à présent parmi mes amis. Merci à Stephanie, Louise, Melany, Mustafa, Thomas, Béatrice, Stéphane, Florent, Julia, Tian et Bohumil et les deux Caroles. Mention spéciale à Emma, qui aura partagé mon bureau pendant presque deux ans :-) Je tiens tout particulièrement à remercier Yuhei pour tout son soutien durant les deux premières années de ma thèse, merci pour tous tes conseils !

Mais pour les conversations sur les foraminifères, ce sont mes collègues du LPG-BIAF d'Angers que je dois remercier ! J'ai eu la chance de collaborer étroitement avec ce laboratoire tout au long de ma thèse. Je remercie toutes les personnes du BIAF et en particulier Sophie pour son aide sur le terrain et au labo, ainsi que pour sa gentillesse, Magali pour nos discussions franco-suisse et génétiques, Edouard pour la location de bureau (et l'aide en géochimie), Sandrine pour m'avoir fait une place quand Edouard n'a plus voulu de moi dans son bureau, ainsi que Frans et Hélène pour leurs conseils avisés. Et enfin je remercie Thierry pour son enthousiasme et son aide pour une grosse partie de ma thèse ! Ça a été un réel plaisir que de collaborer avec lui, tant sur le terrain qu'au bureau, et d'enlever toutes les virgules de mes manuscrits qu'il m'avait faites ajouter.

Ce travail de thèse a aussi été enrichi de nombreuses collaborations, ce qui a été l'occasion de faire de très belles et enrichissantes rencontres tant sur le plan scientifique qu'humain. Je tiens donc à remercier Joan Bernhard pour toute son aide et pour avoir partagé son expérience avec moi. Pour

Acknowledgements

leur aide et leur gentillesse je remercie également Helena Filipsson, Bruno Jesus et Olivier Maire (aussi pour avoir fait de moi une (quasi)-experte de la pêche sous-marine). Parmi les voyages que j'ai faits au cours de cette thèse, j'ai eu la chance d'aller par deux fois au Wrigley Marine Institute of Santa Catalina en Californie. Pour ça je remercie Howie Spero qui m'en a donné l'opportunité, grâce à lui j'ai pu rencontrer d'autres fantastiques personnes dont Oscar, Ann, Jen, Kate et Edward.

Parmi la communauté « foram » il y a plusieurs personnes que je tiens tout particulièrement à remercier pour leur amitié, leur support et de longues conversations foram, mais pas que ;-) Merci d'abord à Clare, je suis extrêmement heureuse d'avoir pu te rencontrer et de pouvoir te compter maintenant parmi mes amies. Merci aussi à Briz (dont je tairais le surnom) et à Laurie (ma biche).

Ma recherche n'aurait pas été possible sans l'aide de beaucoup de personnes que je remercie ici. Tout particulièrement je remercie Jorge Spangenberg pour l'immense travail qu'il a fourni tout au long de ma thèse et pour m'avoir aidée à promouvoir mon travail. Vraiment, merci pour son aide, sa patience et sa gentillesse. Ensuite je voudrais remercier Céline pour toute son aide, de toujours avoir répondu à mes questions et pour son amitié. Je remercie aussi Jean, Antonio, Caroline et Damien pour toute leur aide et leur patience à la plateforme de microscopie électronique de Lausanne et d'avoir toujours accepté de reprogrammer en dernière minute mes séances de TEM :-). Merci aussi à Florence, Guillaume et Romain de la plateforme de microscopie d'Angers pour toute l'aide qu'ils m'ont apportée. Enfin merci à Stan Fakan pour tous ses conseils.

Finalement je tiens à remercier tous mes amis d'avoir grandement enrichi ses quatre dernières années. Merci à mon petit lapin Lorenzo, Didrik, Catherine, Arun (le meilleur des colocataires, sauf quand il y a une araignée dans la poubelle, et le meilleur chasseur de mites que j'ai jamais vu), Emma, Louise et Tor, Stéphanie et Thomas. Merci aussi à Tsing-Lee et Alexis pour tous ces moments passés ensemble, merci à eux d'avoir choisi de se marier à trois semaines de la date du rendu de mon manuscrit de thèse, je leur souhaite tout le bonheur possible dans leur nouvelle vie à deux (et un nouveau canapé qui ne penche pas sur le côté pour mes prochaines visites). Merci à Jean-Marc et Michel et tous « mes gosses » de l'équipe M13 de handball des clubs de Lausanne et Renens. J'ai passé trois inoubliables années à vous coatcher ! Evidemment je remercie ma famille (en particulier Irma) pour tous ces formidables moments passés ensemble (puisse les bulles toujours couler à flots !) et Lapin pour les prêts à répétition (presque de bonne grâce) de sa voiture. Et merci à David <3

Abstract

Foraminifera are ubiquitous eukaryotic protists inhabiting all types of marine environments. The chemical and isotopic compositions of their carbonate tests are commonly used as proxies for paleo-environmental conditions. However, while foraminifera represent a large fraction of the meiofauna and could therefore play a significant role in biogeochemical cycles, little is known about their biology. For the last 30 years, studies have revealed a wide range of physiological functions and metabolic pathways, in both planktic and benthic foraminifera: symbiosis, denitrification, kleptoplasty, dormancy, etc. However, the detailed metabolic processes involved in this large variety of physiological functions remain poorly understood.

NanoSIMS, the main analytical technique used in this work, is a powerful analytical technique to simultaneously visualize, with a high spatial resolution (~ 100 nm), and quantify the incorporation of isotopically labeled compounds in organisms. In this study, NanoSIMS analysis was combined with TEM to investigate the spatio-temporal dynamics of isotopically labeled compound assimilation at a sub-cellular scale.

The first chapter presents an inventory of TEM pictures of the main organelles found in benthic foraminifera based on the literature, complemented by new TEM observations of nine benthic species. This work is essential to interpret the data of the chapters that follow. Using NanoSIMS combined with TEM, the second chapter investigates the heterotrophic metabolism, under oxic and anoxic conditions, of the intertidal benthic foraminifera, *Ammonia* cf. *tepida*. A sharp decrease of the metabolic activity observed in anoxia strongly suggests dormancy in response to the lack of oxygen. The third chapter is dedicated to kleptoplasty in benthic species. Incubation with labeled ^{13}C -bicarbonate, ^{15}N -ammonium, and ^{34}S -sulfate were made, and the assimilation and fate of these molecules and their metabolites within the foraminiferal cell were traced with correlated TEM-NanoSIMS. A number of key observations were made: (1) assimilation of inorganic C was shown in the kleptoplastic *Haynesina germanica* under light conditions, but was not observed under dark conditions, indicating a photosynthetic uptake via the kleptoplasts. (2) In a different species, *Elphidium williamsoni*, photosynthetic assimilation of inorganic C was also observed, but the observed ^{13}C -enrichments were much lower and not found in the same organelles as in *H. germanica*, indicating differences in the metabolic pathways among kleptoplastic species. (3) Assimilation of NH_4^+ and SO_4^{2-} was documented in both kleptoplastic and akleptoplastic species, strongly suggesting the existence of a cytoplasmic pathway for NH_4^+ and SO_4^{2-} assimilation. Thus, the role of kleptoplasts in N and S foraminiferal metabolism remains unclear and need further investigations. Finally the last chapter applied a similar

Abstract

protocol to study the C assimilation dynamics in symbiotic dinoflagellates and subsequent transfer the planktonic foraminiferal host cell. Dinoflagellates are transferring large amounts of photosynthates to the foraminifera, mainly in the form of lipid droplets.

In conclusion, correlated TEM and NanoSIMS imaging is an efficient tool to study foraminiferal metabolism. Through this study it has led to progress in the knowledge of their ultrastructure and metabolic pathways, and ultimately shed light on their potential role in the biogeochemical cycles of marine ecosystems.

Key words: foraminiferal ultrastructure, dormancy, kleptoplasts, symbiosis, photosynthesis, metabolite exchange, NanoSIMS

Résumé

Les foraminifères sont des organismes eucaryotes, protistes, peuplant tous types de milieux marins. La composition chimique et isotopique de leur test carbonaté est couramment utilisé comme proxy des conditions paléo-environnementales. Cependant, bien que les foraminifères représentent une fraction importante de la méiofaune et peuvent donc potentiellement jouer un rôle important dans les cycles biogéochimiques, on sait peu de choses sur leur biologie. Durant les trente dernières années, des études ont montré un large panel de fonctions physiologiques et de voies métaboliques, é la fois chez les foraminifères benthiques et planctoniques : symbiose, dénitrification, kleptoplasty, dormance, etc. Or les processus métaboliques impliqués dans ces fonctions physiologiques restent méconnus.

Le NanoSIMS; le principal outil analytique utilisé dans ce travail, est une technique permettant de simultanément visualiser (avec une résolution spatiale de l'ordre de 100 nm) et quantifier l'incorporation de composés marqués isotopiquement dans un organisme. Dans cette thèse, le NanoSIMS sera utilisé en combinaison avec le TEM pour étudier la dynamique spatio-temporelle de l'assimilation de composés isotopiquement marqués, et ce à une échelle subcellulaire.

Le premier chapitre présente un inventaire d'images TEM des principaux organites observés chez les cellules de foraminifères benthiques, complété par de nouvelles observations faites sur neuf autres espèces benthiques. Ce travail a été essentiel pour l'interprétation des données des chapitres suivants. Via l'utilisation du NanoSIMS combiné au TEM, le chapitre 2 étudie le métabolisme hétérotrophique, en conditions oxiqne et anoxiqne, de l'espèce benthique *Ammonia cf. tepida*. L'observation d'une nette diminution de l'activité métabolique en anoxie suggère fortement la dormance comme réponse au manque d'oxygène. Le troisième chapitre est dédié à l'étude des foraminifères benthiques kleptoplastes. Les foraminifères ont été incubés en présence de ^{13}C -bicarbonate, ^{15}N -ammonium, and ^{34}S -sulfate ; et l'assimilation et le devenir de ces composés et de leur métabolites dans la cellule du foraminifère a été suivie grâce au NanoSIMS combiné au TEM. Plusieurs observations clés ont été faites : (1) l'assimilation de C inorganique a été montré chez l'espèce kleptoplastique *Haynesina germanica* seulement en présence de lumière (pas d'assimilation à l'obscurité) ; ce qui indique une assimilation photosynthétique via les kleptoplastes. (2) Chez une espèce différente, *Elphidium williamsoni*, l'assimilation photosynthétique de C inorganique a aussi été démontré, mais le ^{13}C assimilé n'a pas été retrouvé dans les mêmes structures que chez *H. germanica* ; ce qui montre des processus métaboliques différents selon les espèces kleptoplastiques. (3) L'assimilation de NH_4^+ et SO_4^{2-} a été noté chez à la fois chez des espèces kleptoplastiques et non

kleptoplastiques, ce qui suggère fortement une voie cytoplasmique pour leur assimilation. De ce fait, le rôle des kleptoplastes dans les métabolismes azoté et soufré des foraminifères reste incertain et requiert d'autres investigations. Finalement, le quatrième chapitre présente l'application d'un protocole similaire pour l'étude des dynamiques de l'assimilation du C par des dinoflagellés symbiotiques, et son transfert à la cellule hôte d'un foraminifère planctonique. Les dinoflagellés transfèrent une quantité importante de photosynthétas vers le foraminifère, principalement pour y être accumulé sous forme de lipides.

Pour conclure, la corrélation entre l'imagerie TEM et NanoSIMS est un outil approprié pour l'étude du métabolisme des foraminifères. Cette étude a mené à de large progrès sur la connaissance de leur l'ultrastructure et de leur processus métaboliques, et a finalement mis en lumière leurs rôles potentiels dans les cycles biogéochimiques des écosystèmes marins.

Mots-clés : ultrastructure, dormance, kleptoplastes, symbiose, photosynthèse, échange de métabolites, NanoSIMS

Contents

Acknowledgements.....	i
Abstract	iii
Résumé.....	v
Contents	vii
List of Figures.....	xiii
List of Tables.....	xvii
List of Abbreviations.....	xix
Introduction.....	1
Literature review on foraminiferal physiology and metabolism	3
1 Trophic mechanisms.....	3
1.1 Heterotrophy.....	3
1.1.1 Grazing and deposit feeding.....	3
1.1.2 Carnivory	4
1.1.3 Suspension feeding, parasitism and direct uptake of DOC	5
1.2 Mixotrophy.....	6
1.2.1 Symbiosis between photosynthetic microalgae and planktonic foraminifera.....	6
1.2.2 Kleptoplasty: sequestration of chloroplasts within the foraminiferal cytoplasm.....	9
1.2.3 Symbiosis with prokaryotes.....	13
2 Aerobic and anaerobic metabolisms.....	14
2.1 Aerobic metabolism: low respiration rate	15
2.2 Anaerobic metabolism	15
2.2.1 Known alternative anaerobic metabolism: Denitrification	16
2.2.2 Hypothetic alternative anaerobic metabolisms	17
3 Concluding remarks about foraminiferal physiological and metabolic mechanisms	20
4 TEM studies on foraminiferal cell.....	21
5 NanoSIMS: a tool to study foraminiferal metabolism.....	23
5.1 Fundamentals of NanoSIMS	23
5.2 Metabolic dynamics within biological material and symbiotic system explored with NanoSIMS	24
5.3 TEM-NanoSIMS correlation: an adapted tool to visualize the fate of labeled compounds within the foraminiferal cell	25
Thesis objectives and content	27
Note about the nomenclature of the species <i>Ammonia cf. tepida</i>	29

Chapter 1: An overview of cellular ultrastructure in benthic foraminifera: New observations in the context of existing literature	31
Abstract	33
1. Introduction.....	35
2. Material and methods.....	36
2.1. Collection sites	36
2.2. Chemical fixation and TEM observations	37
3. TEM observations of benthic foraminiferal cells.....	38
3.1. Cell body and “empty” vacuoles	38
3.2. Organelles with known function	40
3.2.1. Nucleus	40
3.2.2. Mitochondria	44
3.2.3. Endoplasmic reticulum	46
3.2.4. Peroxisomes	48
3.2.5. Golgi apparatus	50
3.2.6. Organelles involved in feeding metabolism	53
3.2.6.1. Degradation vacuoles	53
3.2.6.2. Residual bodies.....	55
3.2.6.3. Lipid droplets.....	56
3.2.7. Paracrystals of tubulin.....	58
3.3. Organelles with unknown function	59
3.3.1. Prokaryotes and sequestered chloroplast.....	59
3.3.2. Fibrillar vesicles.....	59
3.3.3. Electron-opaque bodies	61
3.3.4. Multivesicular bodies	63
4. Conclusion	64
Chapter 2: Surviving anoxia in marine sediments: The metabolic response of ubiquitous benthic foraminifera (<i>Ammonia tepida</i>)	677
Abstract	699
1 Introduction.....	71
2 Results	733
2.1 Experiment I: Survival and growth rate of <i>A. tepida</i> under oxic and anoxic conditions	733
2.2 Experiment II: Feeding behavior of <i>A. tepida</i> under oxic and anoxic conditions.....	733
3 Discussion	833

Contents

3.1	Survival and growth.....	833
3.2	Feeding and metabolism: bulk data	833
3.3	Feeding and metabolism: subcellular observations.....	844
3.4	Fatty acid composition and synthesis	855
4	Conclusion	877
5	Material and methods.....	888
5.1	Experiment I: Survival and growth rate of <i>A. tepida</i>	888
5.2	Experiment II: Feeding behavior of <i>A. tepida</i> under oxic and anoxic conditions.....	899
5.2.1	TEM and NanoSIMS analysis	90
5.2.2	Fatty acids.....	90
5.2.3	Stable isotope analyses by isotope ratio mass spectrometry (IRMS)	91
5.2.4	Statistical analysis.....	91
	Supporting information.....	922
Chapter 3: Kleptoplasty in benthic foraminifera from photic environments		101
Chapter 3.1: Ultrastructure and distribution of sequestered chloroplasts in benthic foraminifera from shallow-water (photic) habitats.....		103
	Abstract	1055
1	Introduction.....	1077
2	Material and methods.....	1088
2.1	Specimen collection and field sample fixations	1088
2.2	Species identifications	10909
2.3	Ultrastructural observations by TEM	110
3	Results and discussion.....	11111
3.1	<i>Haynesina germanica</i>	11111
3.2	<i>Elphidium williamsoni</i>	1144
3.3	<i>Elphidium "excavatum"</i> species complex.....	1166
3.3.1	<i>Elphidium oceanense</i>	1166
3.3.2	<i>Elphidium selseyense</i>	1188
3.4	<i>Elphidium</i> aff. <i>E. crispum</i>	12020
3.5	<i>Planoglabratella opercularis</i>	122
3.6	<i>Ammonia aomoriensis</i>	1255
3.7	General discussion.....	1288
Chapter 3.2: Inorganic carbon and nitrogen assimilation by a benthic kleptoplastic foraminifera.....		133

Contents

Abstract	1355
1 Introduction.....	1366
2 Material and methods.....	1388
2.1 Experiment 1: light/dark cycle incubation with $\text{H}^{13}\text{CO}_3^-$ and $^{15}\text{NH}_4^+$	1388
2.2 Experiment 2: Incubation in continuous darkness with $\text{H}^{13}\text{CO}_3^-$ and $^{15}\text{NH}_4^+$	1399
2.3 Preparation for TEM-NanoSIMS studies.....	1399
2.4 Stable isotope mapping with NanoSIMS	1399
2.5 Statistical analysis.....	140
3 Results	141
3.1 TEM observations of the foraminiferal cytoplasm.....	141
3.2 Uptake of $\text{H}^{13}\text{CO}_3^-$ within the foraminiferal cell.	14343
3.3 Uptake of $^{15}\text{NH}_4^+$ in the foraminiferal cell.	1455
4 Discussion	1488
4.1 Ultrastructural observations	1488
4.2 Assimilation of C.....	1488
4.3 Assimilation of N.....	150
4.4 Advantages of a mixotrophic strategy	151
5 Conclusion	151
Supporting information.....	153
Chapter 3.3: Carbon, ammonium and sulfate uptake by benthic foraminifera: A comparison between kleptoplastic and non-kleptoplastic species from a photic environment	1577
1 Introduction.....	1588
2 Material and methods.....	16161
2.1 Sampling and incubation in light condition with $\text{H}^{13}\text{CO}_3^-$, $^{15}\text{NH}_4^+$ and $^{34}\text{SO}_4^{2-}$	161
2.2 Preparation for TEM-NanoSIMS studies.....	161
2.3 Stable isotope mapping with NanoSIMS	162
2.4 Respiration rates	162
3 Results	1644
3.1 Ultrastructural observations	1644
3.2 Inorganic carbon, ammonium and sulfate uptake and fate within the foraminiferal cell	1677
3.3 Respiration rates	170
4 Discussion.....	171
4.1 Ammonium and sulfate assimilation.....	171
4.2 Photosynthesis and inorganic carbon uptake	172

Contents

4.3	Kleptoplast ultrastructure and cellular distribution.....	173
4.4	Specific organelles isotopically enriched.....	1744
4.5	Trophic mechanism impacts on cellular ultrastructure	1755
5	Conclusion	1755
Chapter 4: Assimilation and translocation of carbon between photosynthetic symbiotic dinoflagellates and their planktonic foraminifera host		1799
	Abstract	181
1	Introduction.....	18282
2	Material and Methods.....	183
2.1	Collection of the foraminifera	183
2.2	Experiment: incubation with $\text{NaH}^{13}\text{CO}_3$ during a light-dark cycle	183
2.3	TEM – NanoSIMS sample preparation	184
2.4	Statistical analysis.....	185
3	Results	1866
3.1	Dinoflagellate migration in and out of the foraminiferal endoplasm	1866
3.2	Carbon uptake and storage by the symbiotic dinoflagellates.....	1888
3.3	Transfer of carbon to the foraminiferal host cell	191
3.4	Dinoflagellate cell division within the foraminiferal host cell	193
4	Discussion	195
4.1	Diurnal patterns of symbiont distribution.....	195
4.2	Dinoflagellate mitosis and photosynthesis: role of the foraminifera?.....	195
4.3	Photosynthate assimilation and turnover in the symbiotic dinoflagellates	1977
4.4	Photosynthate translocation and fate inside the host cell	1988
5	Conclusion	201
General discussion and perspectives		203
1	NanoSIMS advantages and limitations.....	203
2	Ultrastructure of benthic foraminiferal cells.....	204
3	Dormancy in response to anoxia.....	205
4	Kleptoplasty in coastal benthic foraminifera	2066
5	Carbon metabolism in symbiotic planktonic foraminifera	2099
6	Conclusion	210
	References.....	213
	Curriculum vitae	243

List of Figures

- Figure 0.1:** Heterotrophic mechanisms in benthic and planktonic foraminifera.
- Figure 0.2:** Symbiosis between photosynthetic microalgae and planktonic foraminifera.
- Figure 0.3:** Concentrations of O₂ and CO₂ at the shell surface of the planktonic symbiotic species *Orbulina universa*.
- Figure 0.4:** TEM micrographs of kleptoplasts in two benthic species.
- Figure 0.5:** Schematic representation of the roles (potentially) played by kleptoplasts in the foraminiferal cell.
- Figure 0.6:** TEM micrographs of the cytoplasm of two species inhabiting low O₂ environments.
- Figure 0.7:** Number of publications dealing with benthic foraminiferal ultrastructure from the 1950s to present, sorted by topics
- Figure 0.8:** Schematic representation of the NanoSIMS
- Figure 0.9:** TEM-NanoSIMS imaging technique example with the foraminiferal species *Ammonia* sp.
- Figure 1.0:** Foraminiferal life cycle (modified from Goldstein, 1998).
- Figure 1.1:** Light micrographs of the foraminifera from the Atlantic French coast intertidal mudflat and the Gullmar fjord.
- Figure 1.2:** Light micrographs of semi-thin sections of the foraminifera from the Atlantic French coast intertidal mudflat and the Gullmar fjord.
- Figure 1.3:** Transmission electron micrographs of benthic foraminiferal nuclei.
- Figure 1.4:** Schematic ultrastructure of a foraminiferal nucleus.
- Figure 1.5:** Transmission electron micrographs of benthic foraminiferal mitochondria.
- Figure 1.6:** Transmission electron micrographs of benthic foraminiferal endoplasmic reticulum.
- Figure 1.7:** Transmission electron micrographs of benthic foraminiferal peroxisomes.
- Figure 1.8:** Schematic ultrastructure and relations between the reticulum endoplasmic, Golgi apparatus and fibrillar vesicles in the foraminiferal cell.
- Figure 1.9:** Transmission electron micrographs of benthic foraminiferal Golgi apparatus.
- Figure 1.10:** Transmission electron micrographs of different types of degradation vacuoles.
- Figure 1.11:** Transmission electron micrographs of benthic foraminiferal residual bodies.
- Figure 1.12:** Transmission electron micrographs of benthic foraminiferal lipid droplets.
- Figure 1.13:** Transmission electron micrographs of paracrystals of tubulin.
- Figure 1.14:** Transmission electron micrographs of benthic foraminiferal fibrillar vesicles.
- Figure 1.15:** Transmission electron micrographs of benthic foraminiferal electron-opaque bodies.
- Figure 1.16:** Transmission electron micrographs of benthic foraminiferal multivesicular bodies.
- Figure 2.1:** TOC concentration and ¹³C atomic fraction of *A. tepida* under oxic and anoxic conditions.
- Figure 2.2:** Time-evolution of ¹³C uptake and transfer within the cytoplasm of *A. tepida* under oxic conditions.
- Figure 2.3:** Time-evolution of ¹³C uptake and transfer within the cytoplasm of *A. tepida* under anoxic conditions.
- Figure 2.4:** Percentages of cytoplasmic occupation and ¹³C atomic fraction of key cell ultrastructures.

Figure 2.5: Relative abundances (%) of the dominant fatty acids extracted from the biofilm of diatoms and in *A. tepida* endoplasm.

Figure 2.S1: Survival rate Experiment I.

Figure 2.S2: Growth rate Experiment I.

Figure 2.S3: Typical cellular structures of *Ammonia tepida* cytoplasm.

Figure 3.1.1: *Haynesina germanica* (elphidiid phylotype S16) isolated from Bourgneuf Bay (France).

Figure 3.1.2: *Haynesina germanica* (elphidiid phylotype S16) isolated from Wadden Sea (Texel, Netherlands).

Figure 3.1.3: *Elphidium williamsoni* (elphidiid phylotype S1) isolated from Gullmar fjord (Sweden).

Figure 3.1.4: *Elphidium oceanense* (elphidiid phylotype S3) isolated from Bourgneuf Bay (France).

Figure 3.1.5: *Elphidium selseyense* (elphidiid phylotype S5) isolated from Wadden Sea (Texel, Netherlands).

Figure 3.1.6: *Elphidium* aff. *E. crispum* isolated from Yugawara (Kanagawa prefecture, Japan).

Figure 3.1.7: *Planoglabratella opercularis* isolated from Yugawara (Kanagawa prefecture, Japan).

Figure 3.1.8: Transmission electron micrographs of *P. opercularis*.

Figure 3.1.9: *Ammonia aomoriensis* (*Ammonia* phylotype T6) from Bourgneuf Bay (France).

Figure 3.1.10: Transmission electron micrographs of *A. aomoriensis*.

Figure 3.2.1: Schematic of Experiments 1 and 2, exposing *H. germanica* to different light conditions.

Figure 3.2.2: TEM micrographs of the cytoplasm and organelles of *Haynesina germanica*.

Figure 3.2.3: TEM micrographs of one chloroplast in *Haynesina germanica* cytoplasm.

Figure 3.2.4: Time-evolution of ^{13}C and ^{15}N uptake and fate within the cytoplasm of *H. germanica* during Experiment 1.

Figure 3.2.5: Foraminiferal organelles enriched in ^{13}C - and/or ^{15}N -enriched in Experiment 1 at different time points.

Figure 3.2.6: Average ^{13}C and ^{15}N enrichment of the cytoplasm of *H. germanica* (n=3) as a function of time.

Figure 3.2.7: ^{13}C and ^{15}N uptake and fate within the cytoplasm of *H. germanica* during Experiment 2.

Figure 3.2.S1: Time-evolution of ^{13}C uptake and fate within the cytoplasm of *H. germanica* during Experiment 1.

Figure 3.2.S2: Time-evolution of ^{15}N uptake and fate within the cytoplasm of *H. germanica* during Experiment 1.

Figure 3.3.1: TEM micrographs of the cytoplasm of *Elphidium williamsoni*.

Figure 3.3.2: TEM micrographs of the cytoplasm of *Ammonia cf. tepida*.

Figure 3.3.3: ^{13}C , ^{15}N and ^{34}S cellular localization in the cytoplasm of *Elphidium williamsoni*.

Figure 3.3.4: ^{13}C , ^{15}N and ^{34}S cellular localization in the cytoplasm of *Ammonia cf. tepida*.

Figure 3.3.5: Oxygen production/consumption profiles for *E. williamsoni* over time, under dark and light conditions.

Figure 4.1: The *O. universa* incubation experiment time line.

Figure 4.2: *Orbulina universa* during day (left column) and night (right column).

Figure 4.3: Time-evolution of starch production and ^{13}C incorporation by the symbiotic dinoflagellates in *Orbulina universa* endoplasm.

Figure 4.4: Dinoflagellate starch grain abundance and their ^{13}C -enrichments.

Figure 4.5: Average ^{13}C -enrichment in *O. universa* lipid droplets in the endoplasm as a function of time.

List of Figures

Figure 4.6: Translocation of ^{13}C -enriched lipids from the symbiotic dinoflagellates to *Orbulina universa* endoplasm.

Figure 4.7: ^{13}C -enriched small electron-opaque and fibrillar bodies.

Figure 4.8: Dinoflagellate mitosis.

Figure 5.1: Schematic representation of the C, N and S assimilation pathways in kleptoplastic foraminiferal cell.

List of Tables

Table 1.1: Species, sampling location, and number of specimens observed or reported in this study.

Table 2.1: Percentage of intact diatoms (frustule containing cytoplasm) in the foraminiferal cytoplasm.

Table 2.2: Concentrations of fatty acids in *A. tepida*.

Table 2.3: ^{13}C atomic fraction of dominant fatty acids in the cytoplasm of *A. tepida*.

Table 2.S1: Carbonate uptake and shell ^{13}C -enrichment

Table 2.S2: Sensors used in Experiment I and II

Table 3.1.1: Available DNA sequences for specimens from the same population or the same location as TEM studied specimens.

Table 3.1.2. Synopsis of the ecology, sequestered plastid abundance, plastid distribution and other specifics for seven species of benthic foraminifera from shallow-water photic habitats.

List of Abbreviations

ANOVA	analysis of variance	LSU	large subunit
APS	adenosine 5-phosphosulphate	Mg	magnesium
ASW	artificial sea water	N	nitrogen
ATP	adenosine 5'-triphosphate	N₂	gaseous nitrogen
C	carbon	N₂O	nitrous oxide
Ca	calcium	NaCaco	Sodium cacodylate
CO₂	carbon dioxide	NaCl	sodium chloride
Cs⁺	cesium ion	NaOCl	sodium hypochlorite
Cu	copper	NO	nitric oxide
DIC	dissolved inorganic carbon	NO₂⁻	nitrite ion
DNA	deoxyribonucleic acid	NO₃⁻	nitrate ion
DOC	dissolved organic carbon	NH₄⁺	ammonium ion
EA/IRMS	elemental analysis / isotope ratio mass spectrometry	NMR	nuclear magnetic resonance
EDTA	ethylenediaminetetraacetic acid	O⁻	oxygen ion
EDS	energy- dispersive X-rays	O₂	dioxygen
ER	endoplasmic reticulum	OMZ	oxygen minimum zone
FA	fatty acid	OsO₄⁻	osmium tetroxide
FAMES	fatty acid methyl esters	P-ER	peroxisome-endoplasmic reticulum complex
FDA	fluorescein diacetate	PCR	polymerase chain reaction
FISH	fluorescence in situ hybridization	PUFA	polyunsaturated fatty acid
FLEC	fluorescently labeled embedded core	rDNA	ribosomal deoxyribonucleic acid
FSW	filtrated sea water	RER	rough endoplasmic reticulum
GAGs	glycosaminoglycans	ROIs	Regions of interest
GC/C/IRMS	gas chromatography/combustion/isotope ratio mass spectrometry	S	sulfur
GS/FID	gas chromatography / flame ionization detection ToF-SIMS	SD	standard deviation
GC/MS	gas chromatography / mass spectrometry	SEM	scanning electron microscopy
GDH	glutamate dehydrogenase	SER	smooth endoplasmic reticulum
GOGAT	glutamine oxoglutarate aminotransferase	SSU	small subunit
GS	glutamate synthase	SO₃²⁻	sulfite ion
H₂O₂	hydrogen peroxide	SO₄²⁻	sulfate ion
HCO₃⁻	bicarbonate ion	TEM	transmission electron microscopy
IRMS	isotope ratio mass spectrometry	TGA	triacylglycerol
ITS	internal transcribed space	TOC	total organic carbon
LBF	large benthic foraminifera	ToF-SIMS	time-of-flight secondary ion mass spectrometry
LC-MS	liquid chromatography-mass spectrometry		

List of Abbreviations

Introduction

Foraminifera are unicellular eukaryote protists that can be differentiated into three groups according to their habitats and life strategies: (i) planktonic foraminifera living in the water column in the open sea, (ii) large benthic foraminifera thriving in warm shallow water and bearing photosynthetic symbionts, (iii) « small » benthic foraminifera inhabiting the sediment. In this thesis, we will mainly focus on « small » benthic foraminifera (lately referred as “benthic foraminifera”). But as the last chapter will consider the planktonic foraminifera, they will also be briefly discussed in this literature review.

Foraminifera are ubiquitous in all marine environments, from tropical to polar latitudes and from estuaries to the deep-sea (Arnold and Parker, 1999; Murray, 2006). They possess two specific features: their granuloreticulopodia, which are anastomosed pseudopods with a granular texture when observed at the microscope; and their envelop (called “test”), protecting their cell (Goldstein, 1999). Foraminifera are usually divided into three major groups according to their test composition: (i) organic, (ii) agglutinated, i.e. composed of mineral grains taken from the surrounding environment, and (iii) calcareous, i.e. a shell made of calcite secreted by the foraminifera. The latter group is the most intensively studied because they are widely used in paleoenvironmental reconstructions (Lea, 1999; Rohling and Cooke, 1999). The calcite shells produced by foraminifera are found in marine sedimentary records since the Ordovician (~ 290 million years ago). Thanks to their abundance, variability and rapid evolution, they are powerful tools for biostatigraphic studies. The study of their assemblage composition, their relative taxonomic abundances (different species adapted to specific environmental conditions), as well as the elemental (e.g. Mg/Ca) and isotopic (e.g. $\delta^{18}\text{O}$) composition of their shells are frequently used to reconstruct global climate changes (Lea, 1999; Rohling and Cooke, 1999).

Despite the large number of publications about foraminifera as paleoceanographic and paleoclimate proxies, little is known about their biology. Only a few biological aspects were studied whereas recent discoveries show a huge diversity of life strategies and metabolisms (heterotrophy, bacterial and algal symbiosis, kleptoplasty, denitrification, dormancy, etc.). Benthic foraminifera may represent up to 50 % of sediment biomass and they constitute an important part of benthic meiofauna (Gooday et al., 1992; Moodley et al., 1997, 2000; Snider et al., 1984). They may play a significant role in the biogeochemical cycles, especially carbon and nitrogen cycles (Cesbron et al., 2016; Gooday et al., 1990, 2008; Høglund et al., 2008; Moodley et al., 2002, 2008; Piña-Ochoa et al., 2010a; Woulds et al., 2007). The broad conditions under which marine foraminifera live includes zones of O_2 -depletion

(Bernhard and Sen Gupta, 1999; Cesbron et al., 2016; Koho and Piña-Ochoa, 2012), deep-sea sulfidic habitats (Bernhard, 2003), hydrocarbon seeps (Sen Gupta et al., 1997; Sen Gupta and Aharon, 1994), or transitional environments (Debenay et al., 2000). Over their evolution foraminifera have developed many different metabolisms in order to adapt to all the various ecosystems in which they live, and to survive the stressful conditions they encounter.

Literature review on foraminiferal physiology and metabolism

1 Trophic mechanisms

Trophic mechanisms are diverse among foraminifera and have been shown to include heterotrophy and mixotrophy. The heterotrophy mechanisms discussed below comprise of grazing on algal and/or bacterial biofilm, deposit feeding, suspension feeding, carnivory, parasitism, and direct uptake of the DOC (dissolved organic carbon). Some foraminifera can possess different trophic mechanisms, and even present a complementary autotrophy metabolism if acquired through symbiosis: a strategy called mixotrophy. It is also noteworthy that although foraminifera are commonly thought to be unable to uptake inorganic nutrients directly; it seems that there is no evidence in the literature to support this notion.

1.1 Heterotrophy

1.1.1 Grazing and deposit feeding

Grazing, described in shallow-water foraminifera, involves the individual moving across a surface and collecting food particles, mainly algal cells, with their pseudopods (Goldstein, 1999). Deposit feeders are defined as omnivorous foraminifera that use their pseudopods to gather the sediment around them, collecting the food particles (bacteria, algal cells, organic detritus, etc.) in their environments (Pascal et al., 2008b). It is observed both in shallow water and deep sea species: the shallow water species feeding on fresh microalgae while the deep water species rely on phytodetritus sinking to depths they inhabit (Goldstein and Corliss, 1994; Nomaki et al., 2006). These two processes are similar and will be discussed in the same section. They both result in a cyst (mound) being formed by the foraminifera (Fig. 1.1): in the case of grazing this cyst is made of discarded algal envelopes (Goldstein, 1999), so it is made after the feeding process. In the deposit feeders the cyst is gathered by the pseudopods to construct a feeding cyst made of sediment, then portions of this cyst are then ingested by phagotrophy in the terminal chamber of the foraminifera (Goldstein and Corliss, 1994; Nyholm, 1957). The ingestion of feeding cyst portion seems to be, at least in some species, a selective process where the foraminifera can discriminate food and non-food particles (Langezaal et al., 2005). Foraminifera can use both bacteria and algal cells as food sources (Goldstein and Corliss, 1994; Heinz et al., 2002; Mojtahid et al., 2011; Nomaki et al., 2005b, 2005a, 2006, 2008). Some species are omnivorous and ingest both, this is for example the case of *Ammonia* sp. (Pascal et al., 2008a, 2009) or deep-sea species (Heinz et al., 2002) while other species are selective for specific bacterial strains

or microalgal types (Lee et al., 1966; Lee and Muller, 1973; Muller, 1975; Nomaki et al., 2005a; Suhr et al., 2003a). It is interesting to note that in the deposit feeding strategy, some organic detritus are made available for foraminifera thanks to bacterial recycling (Levinton, 1979), so bacteria are not only a common prey in foraminifera but they are also an important trophic link. Based on an experiment showing different ingestion patterns of ^{13}C -labeled bacteria and algae by eight different deep-sea species, (Nomaki et al., 2006) defined three main feeding strategies: (i) the phytophagy, i.e. selective ingestion of phytodetritus (or fresh algae) by grazing, (ii) the seasonal phytophagy, i.e. ingestion of organic matter when no phytodetritus are available (in deep-environments the flux of phytodetritus sinking to the bottom is not regular), and (iii) deposit feeding, this category feeds at random on sedimentary organic matter.

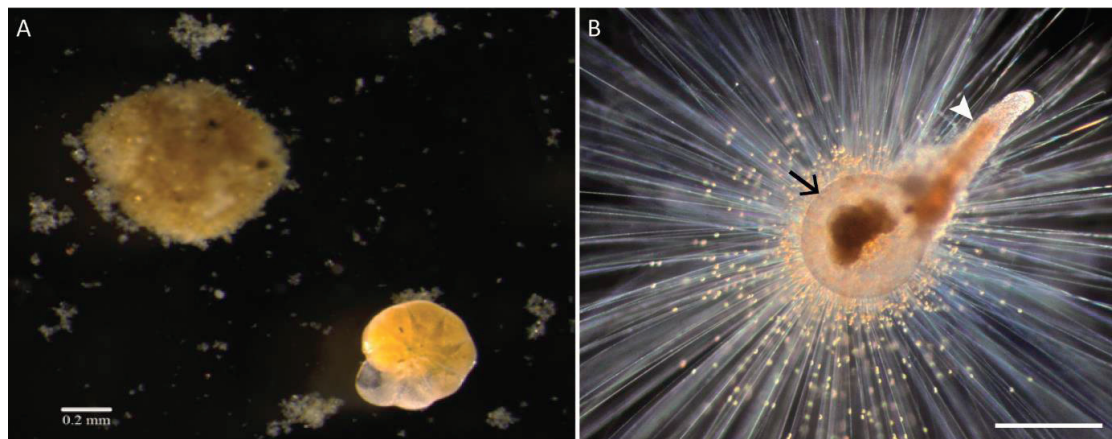


Figure 0.1: Heterotrophic mechanisms in benthic and planktonic foraminifera. A: Grazing by the benthic *Ammonia cf. tepida* (courtesy of E. Geslin). Bottom right: a specimen without surrounding particles, cleaned with a fine brush. Top left: a specimen within a cyst made of discarded products. B: Carnivory in the planktonic *Orbulina universa* (courtesy of H. Spero). The foraminifer (black arrow) caught an *Artemia salina* (brine shrimp, white arrowhead) in its pseudopods on the spines, and is digesting it extracellularly. The bright yellow dots on the spines are symbiotic dinoflagellates (see section 1.2.1). Scale bar: 500 nm.

1.1.2 Carnivory

Carnivory has already been documented in a few benthic species (Boltovskoy and Wright, 1976; Buchanan and Hedley, 1960; Dupuy et al., 2010; Hallock and Talge, 1994), and is more widely encountered in planktonic species (Anderson et al., 1979; Anderson and Bé, 1976a; Bé et al., 1977; Bé and Hutson, 1977). The range of prey include copepods and shrimp nauplii, small crustaceans

(cumaceans, caprellids), echinoid larvae and even large foraminifera (Fig. 1.1). Carnivorous foraminifera seem to have developed specific pseudopodia to capture prey that are stronger than non-carnivorous and have a special extracellular matrix (Bowser et al., 1992). Carnivory might be an alternative strategy to grazing in some species; for example, the benthic *Ammonia* sp. is known to actively graze on algal and bacterial biofilm (Pascal et al., 2008a, 2008b, 2009), but was also seen in laboratory to feed on nematodes, copepods larval gastropods (Dupuy et al., 2010).

1.1.3 Suspension feeding, parasitism and direct uptake of DOC

Other trophic mechanisms, which won't be discussed in this thesis work, include suspension feeding, parasitism and direct uptake of DOC. Briefly, suspension feeding occurs in epiphytic foraminifera and benthic foraminifera that inhabit the upper layer of soft sediments (by the extension of their pseudopods in the water column) (Goldstein, 1999; Lipps, 1983). Lipps (1983) suggested a passive mechanism of uptake as foraminifera lack structures to create water currents. Parasitism has only been recorded in a few species. The parasitic species were reported infesting various organisms, and usually one species can only infect only one type of organism: other foraminifera, scallops, bivalves or macrophytic algae (Alexander and Delaca, 1987; Collen, 1998; Le Calvez, 1947; Pawlowski, 1989; Pawlowski and Lee, 1992; Todd, 1965); except one species, *Hyrrokin sacrophaga*, which is able to infest multiple host (bivalves, sponges and corals) by penetrating their wall to feed on soft tissues (Cedhagen, 1994; Freiwald and Schönfeld, 1996). To date only one foraminifera, the agglutinated species *Notodendrodes antarctikos*, has been reported to uptake dissolved organic matter (DOC) directly as a carbon source from its environment (DeLaca et al., 1981; DeLaca, 1982). In these studies, labeled glucose and amino acids were rapidly taken up and metabolized by the foraminifera. As (Goldstein, 1999) specified in her review on trophic mechanisms in foraminifera, the direct uptake of DOC might be more widespread, and is thought to be scarce only because of the little attention it received. Indeed, among meiofauna the direct uptake of dissolved organic matter is not rare (Montagna, 1995).

1.2 Mixotrophy

1.2.1 Symbiosis between photosynthetic microalgae and planktonic foraminifera

Symbiosis with algae is encountered in many planktonic (Fig. 1.2) and large benthic foraminifera, but was never described to our knowledge in “small” benthic foraminifera. Only the planktonic foraminifera will be discussed here. Symbionts associated with planktonic foraminifera are mainly dominated by dinoflagellates, but chrysophytes have been found in symbiosis with a few species (Anderson and Lee, 1991; Faber et al., 1988; Gastrich, 1987; Hemleben et al., 1989) (Fig. 1.2). The density of the algal symbionts in foraminiferal cells is high: it may reach 2×10^4 dinoflagellate cells per individual in *Orbulina universa* (Spero and Parker, 1985), and symbionts occupy 75 – 85 % of the host cytoplasmic volume in *Globigerinoides ruber* (Lee et al., 1965).

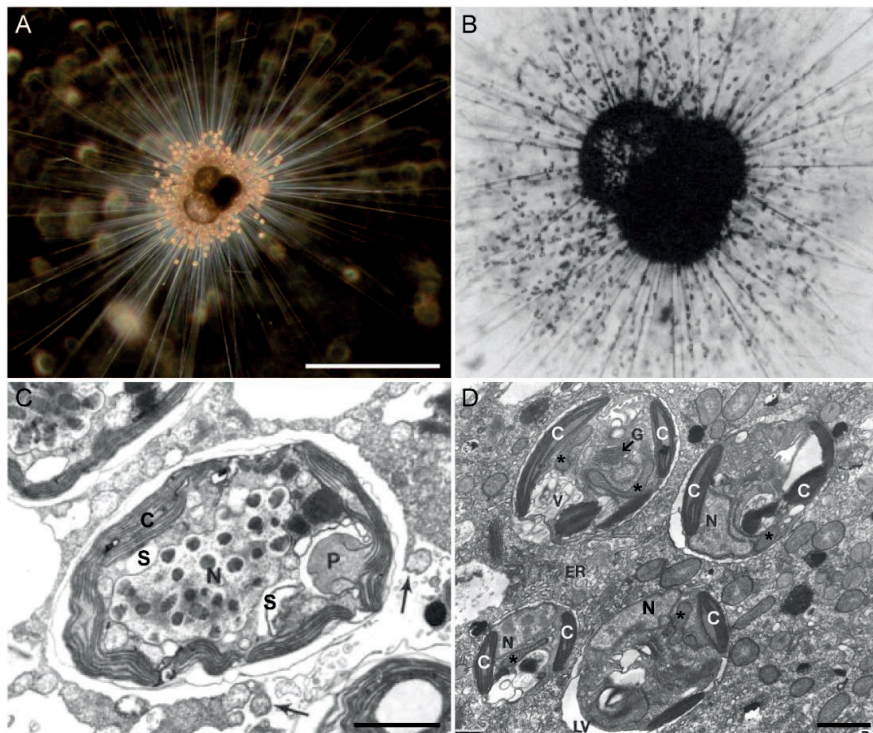


Figure 0.2: Symbiosis between photosynthetic microalgae and planktonic foraminifera. A, B: Light microscopy images. A: *Orbulina universa* (courtesy of H. Spero); scale bar: 500 μm ; and B: *Globigerinoides ruber* (from Bé et al., 1977); magnification $\times 90$. Symbiotic dinoflagellates are dispersed along the spines of both specimens. Scale bar: 500 μm . C: TEM micrograph of the fine structure of a dinoflagellate in the cytoplasm of *O. universa* (modified from Spero, 1987). Arrows: ends of host cytoplasm, C: chloroplast, N: nucleus, P: pyrenoid, S: starch grain. Scale bar: 1 μm . D: TEM micrograph of chrysophyte symbionts (type I) in the cytoplasm of *Globigerinoides siphonofera* (*aequilateralis*) (modified from Faber et al., 1988). Asterisks: chrysophyte mitochondria, C: chloroplast, ER: endoplasmic reticulum, G: Golgi apparatus, LV: lucent vacuole (potential artefact fixation), N: nucleus, P: pyrenoid, V: vacuole. Scale bar: 2 μm .

1.2.1.1 Symbiotic microalgae impact on planktonic foraminiferal physiology

The symbiosis between microalgae and planktonic foraminifera was first formally described at the beginning of the last century (Rhumbler, 1911), but the experimental evidence of the microalgae symbiotic function date from the 1980s (Bé et al., 1982; Caron et al., 1981). The elimination of the symbionts in *Globigerinoides sacculifer* resulted in shorter foraminiferal life time and showed that symbionts are essential for the growth of the foraminifera (Bé et al., 1982). The light intensity, by regulating the symbionts photosynthesis, was shown to impact the growth rate and life time of *G. sacculifer* (Caron et al., 1981) and *Heterostegina depressa* (Röttger and Berger, 1972). Moreover, the symbionts have an effect on the host cytoplasmic organization: depending on its symbiotic chrysophyte type (I or II), the foraminifera *Globigerinoides siphonofera (aequilateralis)* exhibited different pseudopodial network arrangement and distribution of the symbionts within this network, besides effects on its growth rate and life time (Faber et al., 1988, 1989).

1.2.1.2 Photosynthesis, oxygen and carbon production

While only a few papers examine the primary production of symbiotic planktonic foraminifera, it was shown that together with Acantharia (protists inhabiting sea surface) they may contribute to a significant part (~ 5%) of the total annual production in surface waters (Caron et al., 1995). For example, the symbiotic planktonic species *Orbulina universa* alone would contribute to 1% of the total inorganic carbon fixation by all primary producers for a density of only 5 individuals per m³ (Spero and Parker, 1985).

Many studies have confirmed the essential role of symbionts in planktonic foraminiferal physiology, especially during vegetative growth (Bé et al., 1983; Hemleben and Spindler, 1983; Jørgensen et al., 1985; Spero and Parker, 1985). The efficiency of the dinoflagellate photosynthesis was assessed by microsensors measurements in two species: *G. sacculifer* and *O. universa* (Fig. 1.3) (Jørgensen et al., 1985; Köhler-Rink and Kühl, 2005; Rink et al., 1998). Gross photosynthesis was calculated as being 18.1 and 5.3 ± 2.7 nmol O₂ h⁻¹ individual⁻¹ in *G. sacculifer* (Jørgensen et al., 1985) and *O. universa* (Rink et al., 1998), respectively. (Jørgensen et al., 1985) estimated that photosynthetic symbionts could provide enough organic carbon to *G. sacculifer* to sustain its metabolism (energy requirements) and growth. Furthermore, by comparing the symbiotic dinoflagellate photosynthesis rate with *Orbulina universa* respiration rate, it was shown that carbon is assimilated in excess of what this species needs for its growth; suggesting that some carbon might be exported to the environment, potentially to attract prey (Lombard et al., 2009). However other studies showed that to maintain

growth; feeding the foraminifera with prey was necessary (Bé et al., 1982; Caron et al., 1981). Photosynthate translocation from the symbionts would be enough to provide the foraminiferal host cell with carbon, and feeding would rather be a way to obtain major nutrients as nitrogen and phosphorus (see below). Finally, although carbon translocation from the symbiotic dinoflagellates to planktonic foraminiferal cell was shown, there is no detailed understanding of the metabolic processes. The molecules involved, the translocation pathways and the time scale that these changes are happening over are still unknown.

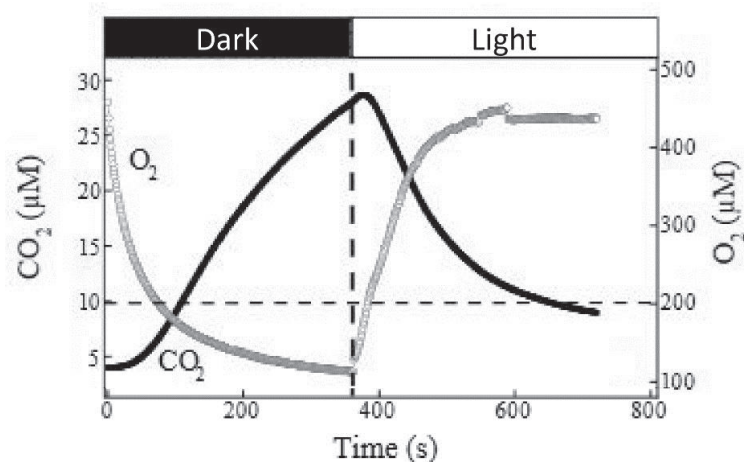


Figure 0.3: Concentrations of O₂ and CO₂ at the shell surface of the planktonic symbiotic species *Orbulina universa*. Variations of the O₂ and CO₂ concentrations measured with microsensors during an experimental light – dark cycle. The horizontal dotted line represents ambient seawater conditions during the experiment (modified from (Köhler-Rink and Kühl, 2005)).

1.2.1.3 Symbiosis benefits for the dinoflagellates

In the symbiotic planktonic foraminifera inhabiting oligotrophic environments (Bé and Hutson, 1977; Giraudeau, 1993; Tolderlund and others, 1971), carnivory can be a great advantage for the symbiont-host system. Indeed, in low nutrient environments, capturing prey might provide the host with nitrogen and phosphorus compounds, that it could transfer to its symbionts in exchange of photosynthates (Jørgensen et al., 1985; Uhle et al., 1999). In addition, the foraminiferal cell could also provide the host with CO₂ through its respiration. In the case of *O. universa*, foraminiferal respiration (production of CO₂) corresponds to ~ 50 % of the gross photosynthesis (uptake of CO₂ by the dinoflagellates), which makes it a valuable source of inorganic carbon for dinoflagellate photosynthesis (Rink et al., 1998). A time lag in the CO₂ concentration exists after switching from light to dark

conditions and *vice-versa*, which was interpreted as the consequence of an internal CO₂ supply mechanism (i.e. the foraminifera provides CO₂ to the symbionts by releasing CO₂ in the microenvironment; (Köhler-Rink and Kühl, 2005).

1.2.2 Kleptoplasty: sequestration of chloroplasts within the foraminiferal cytoplasm

Kleptoplasty, i.e. the ability of an organism to sequester algal chloroplasts inside its “host” cell while the other algal components are either discarded or digested, is encountered in a few organisms: sea slugs (sacoglossans, e.g., (Pelletreau et al., 2011; Rumpho et al., 2001; Serôdio et al., 2014), dinoflagellates (Kim et al., 2012; Nagai et al., 2008; Nishitani et al., 2012), ciliates (Dolan, 1992), and « small » benthic foraminifera (Bernhard and Bowser, 1999). In benthic foraminifera kleptoplastic species are encountered in coastal environments, both in photic and aphotic zones (Bernhard and Bowser, 1999). Until now, most of the studies concerning kleptoplasty in benthic foraminifera have focused on TEM observations (Fig 1.4) and the genetic analysis of sequestered chloroplasts (also called kleptoplasts), which revealed that most are of diatom origin (Cevasco et al., 2015; Correia and Lee, 2000, 2002a; Lechlitter, 2014; Pillet et al., 2011; Pillet and Pawlowski, 2013; Tsuchiya et al., 2015), although a dinoflagellate origin of chloroplasts has also been proposed (Cedhagen, 1991).

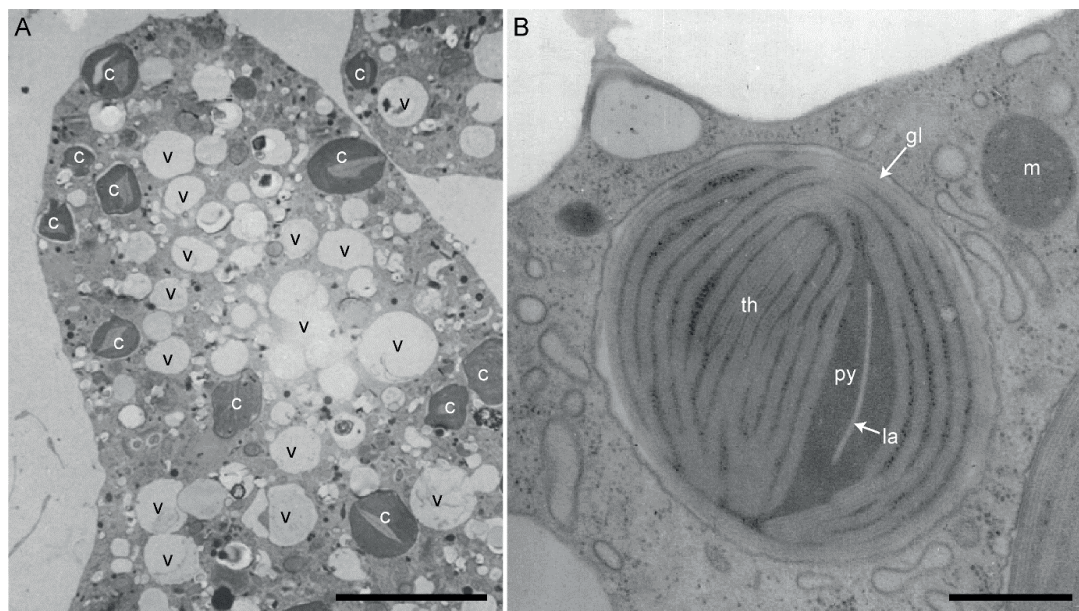


Figure 0.4: TEM micrographs of kleptoplasts in two benthic species. A: Kleptoplast distribution in *Elphidium williamsoni* (modified from Lopez, 1979); c: chloroplast, v: vacuole. Scale bar: μm . B: Fine structure of a kleptoplast in *Elphidium* sp. (modified from Bernhard and Bowser, 1999); gl: girdle lamella, la: lamella, m: mitochondria, py: pyrenoid, th: thylakoids. Scale bar: 500 nm.

1.2.2.1 Life-time of the kleptoplasts within the foraminifera cell

The life time of kleptoplasts within foraminiferal cells varies depending on the species: ranging from days in *H. germanica* (Jauffrais et al., 2016) to weeks in *E. excavatum* (Correia and Lee, 2002b). The kleptoplast retention time is longer under dark conditions (Correia and Lee, 2002a, 2002b; Jauffrais et al., 2016), for example in *H. germanica* kleptoplasts were maintained for a maximum of 12 days under light but were kept for 21 days in the dark (Jauffrais et al., 2016). The longer preservation of the kleptoplasts in the dark can be explained by the fact that a large part of the genes coding for chloroplast protein renewal are present in the algal nucleus which is not kept by the foraminiferal cell; besides there is no horizontal gene transfer from the algae to the foraminiferal cell (Pillet and Pawlowski, 2013). Under light, the chloroplast proteins are used and then degraded, especially the light harvesting and photosynthetic apparatus proteins, and cannot be replaced; while in the dark the enzymatic machinery is preserved longer (Jauffrais et al., 2016). For example the protein D1, a major component in the chloroplast photosystem II, is encoded in the chloroplast (Tyystjärvi and Aro, 1996). But its synthesis requires other proteins encoded in the algae nucleus (Yamaguchi et al., 2005), which is not preserved within the foraminiferal cell but digested or discarded. Thus to perform photosynthesis the foraminifera can only use the pre-existing pool of proteins contained in the kleptoplasts at the time of their incorporation in the cell.

1.2.2.2 Benefit for the foraminiferal “host” cell

Inorganic carbon assimilation

One of the main advantages of sequestering chloroplasts is the photosynthesis, both for the mixotrophy strategy it provides to the host, i.e. the production of photoassimilates from inorganic carbon (via the Calvin-Benson cycle) that are transferred to the host (Fig. 1.5); and for oxygen production by the kleptoplast within the host cell. The latter will be discussed in the section 2.2.2.1. The assimilation of inorganic carbon via sequestered chloroplasts was already demonstrated in the kleptoplastic sea slugs (reviewed in Rumpho et al., 2001). Based on natural isotopic values of the sea slugs and the algae they feed on, it was estimated that up to 60 % of the host carbon input come from the kleptoplast photosynthesis (Raven et al., 2001). In addition, in the sea slug cells, the lipid droplets accumulating around the kleptoplasts have an high abundance of the fatty acid 20:5, which is known to be algal-derived (Pelletreau et al., 2014). The incubation of sea slugs in seawater spiked with $\text{H}^{14}\text{CO}_3^-$ clearly indicated assimilation of carbon within the sea slug cells, at a rate that was higher even, than in the algal cells (Rumpho et al., 2001). To our knowledge, there is only one study that has examined

carbon assimilation via kleptoplast photosynthesis in benthic foraminifera (Lopez, 1979): by following the incorporation of $\text{H}^{14}\text{CO}_3^-$ in the foraminiferal cell, a maximum assimilation rate of $2.3 \mu\text{g C mg}^{-1} \text{h}^{-1}$ was recorded for the coastal species *E. williamsoni* (Lopez, 1979). This study also showed that substantial variability exists between kleptoplastic species as *H. germanica* was shown to have a much lower rate of carbon assimilation (five times lower); and a third species, *E. excavatum*, did not incorporate any carbon despite harboring sequestered chloroplasts in its cytoplasm. However, the time and cellular dynamics of the process are still unknown and many questions (such as which is the form of carbon during the transfer) are not answered for this inorganic carbon assimilation and subsequent transfer to the host cell.

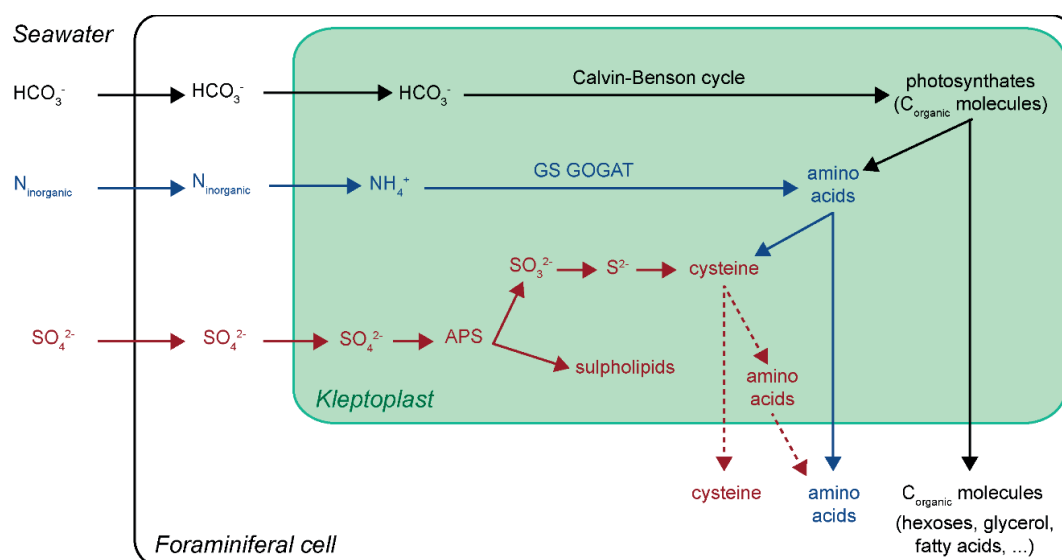


Figure 0.5: Schematic representation of the roles (potentially) played by kleptoplasts in the foraminiferal cell. In black the incorporation of inorganic carbon in the foraminiferal cell, its transfer to the kleptoplast, its assimilation via the Calvin-Benson cycle (driven by energy acquired through the photosynthesis light reactions) into carbonated organic molecules (sugars) and finally its transfer to the foraminiferal cell. In blue the potential role of kleptoplast in the foraminiferal nitrogen metabolism through inorganic nitrogen incorporation and assimilation thanks to the GS/GOGAT enzymatic machinery in the kleptoplast. The amino acids formed would then be transferred to the foraminiferal cell to be further transformed and/or used. In red the potential role of kleptoplast in the foraminiferal sulfate assimilation. Sulfate (SO_4^{2-}) is first incorporated within the kleptoplast, and converted into adenosine 5-phosphosulphate (APS) via the ATP sulfurylase enzyme. Then the APS can either be used to form sulpholipids or further processes to be assimilated on amino-acids to form cysteine. Cysteine is the primer amino acids to form others sulfated amino-acids such as methionine; however according to literature it remains unclear whether these processes (represented with dotted arrows) happen in the chloroplasts or in the cytoplasm in algal cells. Modified from (Giordano and Raven, 2014; Pyke, 2009; Takahashi et al., 2011).

Other functions: putative role in the nitrogen and sulfur metabolism?

Interestingly, sequestered chloroplasts are also observed in deep species inhabiting aphotic environments (Bernhard and Bowser, 1999). One of this species, *Nonionella stella* collected in the Santa Barbara basin (USA) was shown to harbor structurally intact chloroplasts within its cytoplasm and up to one year after sample collection, still contained functional proteins encoded both in the chloroplast and in the algal nucleus (Grzymski et al., 2002). As these species are unlikely to perform photosynthesis, there might be another explanation for their sequestration than the advantage provided by photosynthate or O₂ production. Note that most of the deep kleptoplastic species are encountered in hypoxic to anoxic regions (Bernhard and Bowser, 1999). In plant cells, the chloroplasts have many other roles than photosynthesis, which provide many paths to be explored in the case of kleptoplasty. In diatoms, the microalgae from which foraminifera are stealing their kleptoplasts, the chloroplasts also play a role in the nitrogen metabolism of the cell. They are able to incorporate ammonium to form amino acids through the GS/GOGAT (glutamate synthase and glutamine oxoglutarate aminotransferase) enzymatic machinery (Syrett, 1981; Zehr et al., 1988; Zehr and Falkowski, 1988). It is therefore possible that the kleptoplasts in foraminifera play a similar role, they could be able to assimilate inorganic nitrogen through the GS/GOGAT machinery to produce amino acids subsequently transferred to the foraminifera cell (Fig. 1.5) (Grzymski et al., 2002). This alternative pathway of nitrogen assimilation would provide a net advantage to kleptoplastic foraminifera over other meiofaunal species relying solely on food to meet their nitrogen requirements. In the study by Grzymski et al. (2002), the deep species *N. stella*, was sampled in the Santa Barbara basin, an environment often subjected to periods dominated by low O₂ concentrations and which are associated with high sulfide concentration. Sulfide is extremely toxic for the cell as it poisons the cytochrome c complex and thus disrupts mitochondrial respiration (Beauchamp et al., 1984; Reiffenstein et al., 1992). Thus a role of the kleptoplast in the tolerance to high sulfide concentration was proposed. The authors suggested a substitution of the mitochondrial respiration by chlororespiration, before concluding this would be unlikely as in the environment a high concentration of sulfide is spatially and temporarily separated from the presence of oxygen required for chlororespiration (as for mitochondrial respiration). However, the kleptoplasts could play another role in the sulfur metabolism in the foraminiferal cell, like they do in plant and algal cells for the production of sulfated amino acids (cysteine, methionine) and sulfolipids (Fig. 1.5) (Giordano and Raven, 2014; Takahashi et al., 2011). This would provide the foraminifera with a great advantage in their environment if they could rely on another source than feeding to obtain these cell functioning essential molecules. The sulfolipids formation is an interesting pathway to study in foraminifera because it is known that diatoms exhibit higher sulfolipids concentrations than other algae or plants (Goss and Wilhelm, 2009; Vieler et al.,

2007). These particular lipids are essential components of the thylakoids and chloroplast membranes in nearly all photosynthetic organisms (Benning and Garavito, 2008).

These putative roles in nitrogen and sulfur cell metabolisms are only hypothetical in benthic foraminifera at the current time and require investigation. Can foraminifera take up inorganic nitrogen in their cell and transfer it to the kleptoplasts where it could be assimilate into amino acids? If so, we can suggest that kleptoplasts might in return transfer these amino acids in the foraminiferal cell to be used in the metabolism. And, is there a kleptoplastic pathway for sulfate assimilation which could lead to the production of sulfated molecules, such as sulfated amino acids or sulfolipids, by kleptoplasts?

1.2.3 Symbiosis with prokaryotes

To our knowledge, most of the studies revealing the presence of bacterial symbionts associated to foraminiferal cell were carried out on foraminifera inhabiting extreme environments (see section 2.2.2.1); where the authors looked specifically for an explanation of the survival to these conditions, and thus looked for potential symbiotic prokaryotes. It is possible that symbiosis with prokaryotes may be more widespread than the scarcity of the observations suggests and this field would be worth further investigation.

It is noteworthy that in addition to the putative denitrifying, sulfate reducers, sulfide oxidizers or sulfur oxidizers prokaryotic symbionts that have been described in some foraminifera (see section 2.2.2.1); a benthic species, *Furkensonia rotundata*, and a planktonic species *Globigerina bulloides* were shown to harbor the photosynthetic cyanobacteria *Synechococcus* (Bird et al., 2017; Buck and Bernhard, 2004). In *G. bulloides*, inhabiting the photic zone, these cyanobacteria might bring a valuable advantage for the planktonic species through their phototrophic metabolism and capacity to store polyphosphate and proteins (Bird et al., 2017). The benthic *F. rotundata* inhabits the Santa Barbara basin (USA) and is unlikely to receive any light; so the cyanobacterial role remains unknown (Buck and Bernhard, 2004).

2 Aerobic and anaerobic metabolisms

One of the most studied topic in benthic foraminiferal physiology is their ability to tolerate periods of hypoxia or anoxia. Benthic ecosystems, especially coastal environments, are increasingly affected by hypoxic/anoxic events (Diaz and Rosenberg, 2008; Helly and Levin, 2004; Rabalais et al., 2010). During these events, while large fractions of the benthic meio- and macrofauna (size range >1 mm) die off (Bianchi et al., 2000; Josefson and Widbom, 1988; Stachowitsch, 1991; Wetzel et al., 2001); foraminifera are consistently among the most resistant species (Gooday et al., 2000; Levin et al., 2009; Moodley et al., 1997).

Various terms are used to qualify the oxygenation state of an environment, they are all reviewed in (Bernhard and Sen Gupta, 1999). In this thesis only the term “anoxic” and “hypoxic” will be used. Hypoxic conditions are reached for dissolved oxygen concentrations of less than $62.5 \mu\text{M}$ / (or $1.42 \text{ mL O}_2 \text{ L}^{-1}$ and anoxia refers to the total absence of detectable oxygen, with or without hydrogen sulfides (Koho and Piña-Ochoa, 2012). It has to be noted that for *in situ* observations the precise O_2 concentrations are not always precisely known and can vary over time. For example (Tsuchiya et al., 2015) found the species *Virgulina fragilis* in environment with dissolved oxygen concentrations ranging from “dysoxic” (i.e. $5 - 45 \mu\text{mol O}_2 \text{ L}^{-1}$) to “microxic” (i.e. $0 - 5 \mu\text{mol O}_2 \text{ L}^{-1}$) conditions. Thus for the *in situ* observations, the depleted oxygen conditions will be referred as “low O_2 environments” (or with “low O_2 conditions”); except when the precise O_2 concentrations are specified and did not vary.

Laboratory experiments showed that under anoxic conditions some benthic foraminiferal species migrate towards the oxygenated surface of the sediment column to find suitable redox conditions while other species do not (Geslin et al., 2004; Pucci et al., 2009). This suggests that at least some species possess an alternative metabolism that allows them to survive in environments with low O_2 concentrations. Tolerance to low- O_2 conditions is not rare among foraminifera and was encountered in many different species, both in laboratory experiment (Heinz and Geslin, 2012) and in *in situ* experiments and observations (Bernhard and Reimers, 1991; Bernhard and Sen Gupta, 1999; Glud et al., 2009; Kitazato and Ohga, 1995; Langlet et al., 2013). Besides, benthic foraminifera can be moved deep into the sediment by bioturbation, which can expose them to low O_2 levels (Bouchet et al., 2009; Maire et al., 2016; Thibault de Chanvalon et al., 2015). Several metabolisms were suggested until now to explain the survival of some benthic foraminiferal species to extended periods of hypoxia or anoxia.

2.1 Aerobic metabolism: low respiration rate

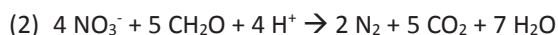
Benthic foraminifera were shown to have a relatively low rate of aerobic respiration (from 0.09 to 5.27 nl O₂ cell⁻¹ h⁻¹) compared to other meiofaunal species such as nematodes, copepods, ostracods, ciliates and flagellates (Geslin et al., 2011). Thus in the case of hypoxia, even low O₂ concentrations could be enough to maintain an aerobic respiration and normal activity level in foraminiferal cells.

2.2 Anaerobic metabolism

Both laboratory and *in situ* observations have showed that foraminifera are capable of surviving anoxia (Bernhard and Alve, 1996; Bernhard and Reimers, 1991; Heinz and Geslin, 2012; Langlet et al., 2013; Moodley et al., 1997), but foraminifera appear to exhibit different responses to anoxia. A laboratory experiment showed three different responses: (1) species that are tolerant of the lack of oxygen i.e. there was no impact on their survival or their intracellular ATP content (a proxy for metabolic activity), (2) species capable of surviving extended anoxic incubations but that experience a decrease in intracellular ATP concentrations and (3) species impacted by anoxia that exhibit changes in both survival rate and ATP concentrations (Bernhard and Alve, 1996). Different responses were also observed in an *in situ* experiment under anoxic conditions. Over a ten month incubation some foraminiferal species saw their abundances decreasing while other species exhibited stable abundances (Langlet et al., 2014). One species exhibited a particularly unique response to long-term exposure to anoxia: its abundance first increased until 30 days and decreased until the end of the experiment (i.e. 10 months). This was interpreted as an opportunistic strategy: where the increased organic matter availability in the first two weeks of the incubation led to either increased juvenile growth or to a reproduction event. The first hypothesis seems more likely. Indeed one intertidal and two fjord species were shown to calcify in anoxia, adding chambers during laboratory incubations (Nardelli et al., 2014). This latter finding is important as it suggests efficient alternative anaerobic metabolisms exist which provide enough energy not only to keep the foraminifera alive, but also to sustain its growth. However, *in situ* observations revealed that the benthic species *N. stella* is unable to survive extended anoxia (Bernhard and Reimers, 1991). And during a long-term *in situ* experiment under anoxic conditions, the standing stocks of foraminifera globally decreased throughout the experiment, which lasted ten months (Langlet et al., 2013). Together, these observations may indicate that foraminifera cannot complete their life cycle, i.e. some species may survive, even calcify, but not perform reproduction; thereby suggesting that the alternative anaerobic metabolisms implemented during anoxia events are not as efficient in terms of energy yield compared to normal aerobic respiration.

2.2.1 Known alternative anaerobic metabolism: Denitrification

In 2006, it was demonstrated for the first time that one species, *Globobulimina pseudospinescens*, is able to carry out complete denitrification under anoxic conditions, i.e. full reduction of nitrates (NO_3^-) to gaseous nitrogen (N_2) in the absence of oxygen as shown in the following equation (Risgaard-Petersen et al., 2006).



(1) Equation of denitrification, i.e. full reduction of nitrate into gaseous nitrogen (from (Kamp et al., 2015). Foraminifera have been shown to be able to carry a complete denitrification (from NO_3^- to N_2), however some species seem to lack the nitrous oxide reductase and reduce NO_3^- only to N_2O (Piña-Ochoa et al., 2010a; Risgaard-Petersen et al., 2006). NO_3^- : nitrate, NO_2^- : nitrite, NO : nitric oxide, N_2O : nitrous oxide, N_2 : gaseous nitrogen.

(2) Stoichiometric equation of denitrification from nitrate to N_2

This capacity was shown to be widespread among foraminiferal species (Piña-Ochoa et al., 2010a). Many of which can store nitrates in their cell and then use them after the establishment of anoxic conditions (Bernhard et al., 2012a; Glud et al., 2009; Koho et al., 2011; Piña-Ochoa et al., 2010b, 2010a; Risgaard-Petersen et al., 2006). Before the study by Risgaard-Petersen et al. (2006), only bacteria and fungi were thought to denitrify. These findings therefore have great importance in understanding the ecosystems that these foraminiferal species live in. Indeed, foraminifera are now known to be major contributors of nitrate removal from the sediment (Høglund et al., 2008), and can contribute, depending on the environment, up to 80 % of the total denitrification occurring in the sediment (Piña-Ochoa et al., 2010a). In foraminifera the denitrification can be performed either by the foraminifera itself, or by bacterial endobionts (Fig. 1.6A). Indeed denitrification was demonstrated in foraminifera lacking any type of prokaryotic symbiont, meaning the foraminifera is able to perform denitrification by itself (Bernhard et al., 2012a; Risgaard-Petersen et al., 2006). And in allogromiid species, genetic analysis of the foraminifera and their endobionts revealed that the denitrification potential comes from the endobionts, which are likely denitrifying *Pseudomonas* (Bernhard et al., 2012b, 2012a).

2.2.2 Hypothetic alternative anaerobic metabolisms

2.2.2.1 Symbiosis to obtain an alternate anaerobic metabolism

Symbiosis with bacteria possessing an alternative anaerobic metabolism, either ectobionts (Bernhard et al., 2010a) or endobionts (Bernhard et al., 2000; Bernhard, 2003; Nomaki et al., 2014; Tsuchiya et al., 2015), or chloroplast sequestration (Bernhard and Bowser, 1999; Grzymiski et al., 2002) were also suggested to explain foraminifera tolerance to low O₂ conditions.

Symbiosis with prokaryotes

To our knowledge prokaryotic symbiosis (Fig 1.6) were described mainly in the cytoplasm of foraminifera inhabiting extreme environments such as basins with low O₂ environments or hydrocarbon seeps (Bernhard et al., 2000, 2001; Bernhard, 2003; Bernhard et al., 2006, 2010a, 2010b, 2012b, 2012a; Buck and Bernhard, 2004; Nomaki et al., 2014; Tsuchiya et al., 2015). In all these studies, the symbiosis with prokaryotes was explained as a way for foraminifera to survive extreme conditions (hypoxia, anoxia, presence of sulfides, etc.) thanks to an alternative metabolism (like denitrification or sulfate reduction) performed by the prokaryotes; although most of the time the identity of these prokaryotes is unknown. Their ultrastructure observations with TEM are not enough to determine their nature, the use of genetic analysis is needed to clarify the origin of the symbionts in a benthic species (but is rare due to expensive and time consuming methods). For example, the DNA sequencing of *Virgulinema fragilis* endosymbionts revealed their δ -proteobacteria origin (Tsuchiya et al., 2015). These symbionts are thought to be sulfate-reducing bacteria (Bernhard et al., 2010a; Tsuchiya et al., 2015), with the ability to produce energy by reducing sulfate to sulfide in anoxic conditions. Moreover in this species, the bacteria were observed to be contained in vacuoles, surrounded by mitochondria (Bernhard et al., 2010a; Tsuchiya et al., 2015). The close association observed between these endosymbionts and mitochondria was ascribed either to mitochondria detoxifying sulfide ability (Bernhard et al., 2010a) or mitochondrial oxygen consumption to maintain the anaerobic bacteria within the cell (Tsuchiya et al., 2015). Specimens of another species, *Bolivina pacifica*, collected in an O₂ depleted basin, were shown to harbor ectobionts on the calcite shell pores (Bernhard et al., 2010a). Bernhard et al. (2010a) hypothesized that these putative symbiotic bacteria were sulfide oxidizers or sulfur oxidizers, thus playing a role in the foraminiferal resistance to sulfidic conditions, which are linked to anoxia. In this species specific ultrastructural adaptations were observed and also described as features that enable *B. pacifica* to thrive in strongly hypoxic environments. These ultrastructural adaptations, already observed by Leutenegger and Hansen (1979), are the occurrence of numerous

mitochondria and the presence of plasma membrane invaginations under the pores (Fig. 1.6B). The pores are thought to be gas exchange pathways that exist between the foraminiferal cytoplasm and the surrounding environment (Berthold, 1976) and the plasma membrane invaginations extend the surface area with the surrounding environment. Thus the presence of mitochondria under the pores associated with the plasma membrane invaginations was interpreted as a way to facilitate oxygen diffusion from the surrounding environment, and to bring oxygen directly to the mitochondria to maintain aerobic respiration under hypoxic conditions.

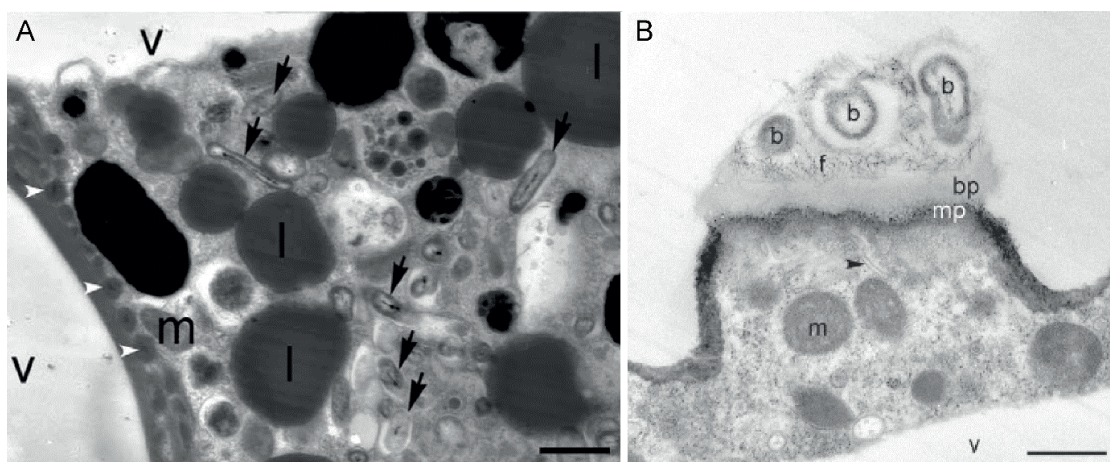


Figure 0.6: TEM micrographs of the cytoplasm of two species inhabiting low O₂ environments. A: Presence of endobionts in the cytoplasm in *Buliminella tenuata*, a denitrifying species (from Bernhard et al. 2012a). Arrows: bacteria (endobionts), arrowheads: peroxisomes, m: mitochondria, v: vacuoles. Scale bar: 1 μ m. B: Pore structure in *Bolivina pacifica* (from Bernhard et al. 2010). Arrowhead: plasma membrane invagination b: bacteria (ectobionts), bp: basal plate, f: fibrils, m: mitochondria, mp: microporous plate. Scale bar: 500 nm.

Chloroplast sequestration

The sequestration of chloroplasts (see section 1.3.2), was also described as a potential alternative metabolism to survive anoxia. Several foraminiferal species that frequently encounter low-O₂ environments actively sequester chloroplasts (Bernhard and Bowser, 1999). In such environments, provided they are photic, the kleptoplasts could provide the foraminiferal cell with oxygen from photosynthesis (Bernhard, 2003; Cesbron et al., 2017; Tsuchiya et al., 2015) as has been observed in ciliate species (Esteban et al., 2009). This advantage would be especially valuable for coastal species as their environments are the most likely affected by periods of low O₂ concentration (Diaz and Rosenberg, 2008; Middelburg and Levin, 2009; Zhang et al., 2010).

While the production of oxygen by the sea slug kleptoplast is well known for many different species (Gibson et al., 1986; Green et al., 2000; Rumpho et al., 2000; Taylor, 1971), only two studies have examined the oxygen production of the kleptoplasts in benthic foraminifera (Cesbron et al., 2017; Jauffrais et al., 2016). Using microsensors, the O_2 production in the intertidal species *Haynesina germanica* was estimated to range from 200 to 1000 $\mu\text{mol } O_2 \text{ cell}^{-1} \text{ d}^{-1}$ (Cesbron et al., 2017; Jauffrais et al., 2016). Besides the functionality of the photosystems in the photosynthetic reactions, the xanthophyll pigment cycle was also shown to be effective, meaning the kleptoplasts must possess a photoprotection mechanism (Jauffrais et al., 2017). The kleptoplast oxygen production might bring a valuable advantage to their host by providing them with a source of oxygen for species inhabiting photic zones; especially in coastal areas submitted to hypoxic/anoxic events, or for species inhabiting areas subjected to high bioturbation.

2.2.2.2 Dormancy

Finally, an alternative metabolism that has also been proposed to explain the tolerance to anoxia is dormancy. Dormancy is defined as “suspension of active life, arrested development, and reduced or suspended metabolic activity, mediated either by internal physiological factors (known as diapause) or exogenous factors (known as quiescence)” (Ross and Hallock, 2016). (Bernhard and Alve, 1996) observed a decrease of the molecule adenosine 5'-triphosphate (ATP, energy of the cell) pool in different foraminiferal species (*Bulimina marginata*, *Stainforthia fusiformis* and *Adercotryma glomeratum*) exposed to anoxia. This, as they suggested, might indicate a state of dormancy: because when cell metabolism is shut down, less ATP is required to maintain cellular functions. Based on the existing literature it was suggested that the dormancy might be a basic and widespread adaptation in foraminifera that would allow them (i) to survive environmental stressors and (ii) rapidly recover after the return of favorable conditions (Ross and Hallock, 2016). However this hypothesis was never proven and several questions remain: to which point do foraminifera lower their metabolic activity under anoxic conditions? And what are the implications of dormancy for physiological functions such as feeding, growth or reproduction?

3 Concluding remarks about foraminiferal physiological and metabolic mechanisms

This literature review about foraminiferal metabolism highlights the important variability of the metabolic pathways among the foraminiferal species. Many species possess different trophic metabolisms, allowing them to pass from heterotrophic to mixotrophic strategies. They can therefore use different nutrient sources and switch from one source to another one when the main food source is no longer available. For example, most of the carnivorous species possess another trophic mechanism: *Astrorhiza limicola* described earlier is also a suspension feeder (Buchanan and Hedley, 1960); the omnivorous *Ammonia* sp. feeds on bacteria and microalgae biofilm as well as copepods, nematodes or gastropod larvae (Dupuy et al., 2010; Pascal et al., 2008b); and many carnivorous planktonic species also perform symbiosis with microalgae (Anderson and Bé, 1976a; Bé et al., 1977; Hemleben et al., 1989). Possessing different trophic energetic mechanisms provides foraminifera with a great advantage in an environment with high competition for resources with other foraminifera or other meiofaunal species. This variability certainly explains their ubiquitous distribution in all the marine environments. However for most of the trophic mechanisms as well as their tolerance to low O₂ conditions, little is known about the intracellular metabolic pathways. Chapters 2, 3 and 4 of this thesis will investigate the intracellular processes of different foraminiferal species inhabiting different environments and/or exhibiting different metabolisms. To do so, the main technique chosen is Transmission Electron Microscopy (TEM) - NanoSIMS correlation which allows to describe the cellular organization, and subsequently link it to exchange of isotopically labeled metabolites.

4 TEM studies on foraminiferal cell

The cellular ultrastructure of foraminifera is one of the most documented topics in foraminiferal biology. However compared to other organisms, (in particular the protists), little is known about the identity and function of many of the observed organelles; especially in benthic foraminifera. The first studies that used Transmission Electron Microscopy (TEM) to study the foraminiferal cell and observe their ultrastructure date from the 1950 to the 1970's. However, during this period and until the end of the 80s, almost all focused on planktonic foraminifera (e.g., (Anderson and Bé, 1976a; Bé and Anderson, 1976; Bé et al., 1977, 1980, 1983; Dahlgren, 1967; Faber et al., 1988, 1989; Febvre-Chevalier, 1971; Hemleben et al., 1985; Lee et al., 1965; Spero, 1987, 1988; Spindler et al., 1978; Spindler and Hemleben, 1982), larger foraminifera, especially because of their relationship with symbiotic microalgae, (Hottinger, 1982; Hottinger and Dreher, 1974; Lee et al., 1979, 1983, 1988, Leutenegger, 1977a, 1977b, 1977c, 1977d, 1983; McEnery and Lee, 1981; Müller-Merz and Lee, 1976) and monothalamous foraminifera (Arnold, 1982, 1984, Dahlgren, 1964, 1967; Nyholm and Nyholm, 1975; Schwab, 1976, 1977; Schwab and Schwab-Stey, 1979); while only a few TEM images were published for "small" benthic foraminifera (Alexander and Banner, 1984; Angell, 1967; Heeger, 1988; Leutenegger and Hansen, 1979; Lopez, 1979).

The ultrastructure of benthic foraminifera had been studied, but ultrastructural observations were performed to look at specific organelles, in order to understand a specific physiological function (Fig. 1.7, data from Bernhard and Geslin (in press)). The physiological functions that have been studied include reproduction (Goldstein, 1997; Goldstein and Moodley, 1993; Pawlowski et al., 1995), nutrition (Goldstein and Corliss, 1994), symbiosis with endobionts or kleptoplasts (Bernhard, 2003; Bernhard and Bowser, 1999; Cesbron et al., 2017; Tsuchiya et al., 2015) and motility (Bowser and Travis, 2000). Since the 1990s, TEM studies have tended to examine the ultrastructural modifications observed in foraminifera that inhabit or were incubated under particular environmental conditions; mainly to understand how foraminifera are able to survive low-oxygen conditions (Bernhard, 2003; Bernhard et al., 2010a, 2012a; Bernhard and Alve, 1996; Bernhard and Reimers, 1991; Nomaki et al., 2014; Sen Gupta et al., 1997), but also more recently to look at the impacts of pollutants (Frontalini et al., 2015, 2016; Le Cadre and Debenay, 2006). Since 2004, a few publications have described methodologic developments (Fig 1.7) such as the cryo-fixation procedure (Goldstein et al., 2004), the fluorescently labeled embedded core (FLEC) combined with TEM to correlate the ultrastructure with the foraminiferal microenvironment (Bernhard and Richardson, 2014), or TEM combined with complementary approaches such as carbonate carbon isotopic analysis (Bernhard et al., 2010b; Martin et al., 2010) or NanoSIMS (Nomaki et al., submitted).

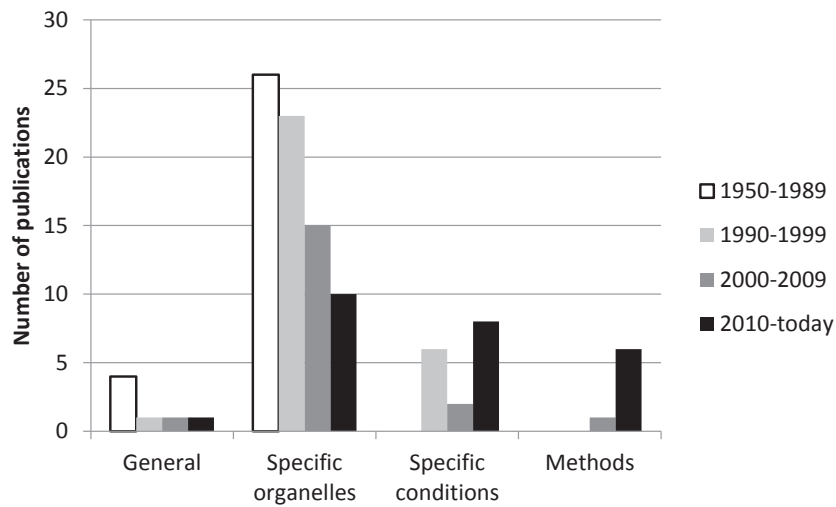


Figure 0.7: Number of publications dealing with benthic foraminiferal ultrastructure from the 1950s to present, sorted by topics. Modified from Bernhard and Geslin (in press).

Despite the high number of publications examining the ultrastructure of foraminifera, including benthic foraminifera, only a little fraction of the organelles observed have been yet identified (Bernhard and Geslin, in press). In their review, Bernhard and Geslin (in press), emphasize the need for further research into cellular structures in order to better understand the foraminiferal cell ultrastructure and learn more about foraminiferal metabolism. To do so, there is a need to gather all information already known about the foraminiferal ultrastructure to better orientate future research. Such reviews already exist for planktonic (Anderson and Bé, 1978; Anderson and Lee, 1991; Hemleben et al., 1989) but not for benthic foraminifera. The chapter 1 of the thesis, which will be the first article of a special issue dedicated to benthic foraminiferal ultrastructure, is intended to fill this gap.

5 NanoSIMS: a tool to study foraminiferal metabolism

Although they allow the discovery of specific cellular features, ultrastructural observations alone are not sufficient to understand foraminiferal metabolism and unravel cellular pathways. There is a need for complementary techniques such as imaging to link cytoplasm organization and structure to specific physiological process. The main analytical tool used in the present work is the NanoSIMS, an ion microprobe for isotopic analysis at high spatial resolution.

5.1 Fundamentals of NanoSIMS

The NanoSIMS (nanoscale Secondary Ion Mass Spectrometry) instrument provides the remarkable capability to quantify isotopic ratios on a length scale of about 100 nm, which is enough to resolve all sub-compartments and structures in normal cells. The basic principles of the NanoSIMS can be found in the literature (Hoppe et al., 2013). Briefly, the NanoSIMS has the ability to perform mass-spectrometry on secondary ions sputtered from a solid sample by the impact of a primary beam of charged particles. Secondary ions are sputtered from the top few atomic monolayers of the sample. Therefore, although NanoSIMS is strictly speaking a destructive analytical technique, the level of damage to the sample is usually considered negligible. The NanoSIMS instrument delivers a primary beam of Cs^+ or O^- to the sample surface, focused to a spot size of $\sim 50\text{-}100$ nanometers. Secondary ions extracted from the sample surface and charged opposite to the primary beam are transferred to the high mass-resolution, multi-collection mass-spectrometer (Fig. 1.8). Ion images of the sample surface are created by rastering the primary beam across the sample surface. This technology enables high-spatial resolution imaging of variations in element distributions, as well as isotopic composition, in biological materials, and on length scales of about 100 nm. The NanoSIMS N50L used in this work is equipped with a multi-collector system that allows simultaneous collection of up to 7 different isotopes, i.e. seven different images can be simultaneously recorded from the same analyzed area. This capability can be used to create images or maps of elemental and isotopic variation within a sample. Such images can be generated from the lightest elements, such as C ($^{13}\text{C}/^{12}\text{C}$ ratios), N ($^{15}\text{N}/^{14}\text{N}$ ratios), and S (e.g. $^{34}\text{S}/^{32}\text{S}$ ratios) to the heaviest elements in the periodic table, including uranium. This instrument is therefore the perfect analytical instrument in combination with biological labelling experiments where high spatial resolution is required.

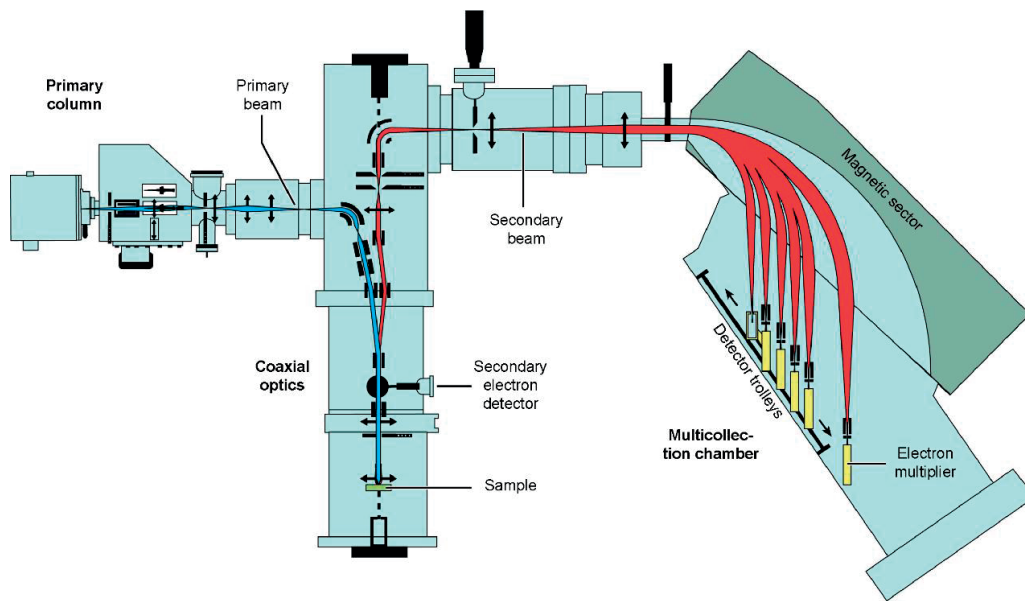


Figure 0.8: Schematic representation of the NanoSIMS (Boxer et al., 2009). The primary ion beam (Cs^+ or O^-) generated in the primary column is directed to the sample surface. The sputtered secondary ions are directed to the magnetic sector to be separated according to their mass over charge (m/z) ratio and are collected by detectors.

5.2 Metabolic dynamics within biological material and symbiotic system explored with NanoSIMS

The use of NanoSIMS combined with stable isotope labelling has started to be successfully applied to biological samples over the last decade (Hoppe et al., 2013). These studies involve various organisms, from prokaryotes and single cells to mammal or plant cells, and use many different stable isotopes (Boxer et al., 2009; Herrmann et al., 2007; Kilburn et al., 2010; Lechene et al., 2006; McMahon et al., 2006; Moore et al., 2012). However, to date, only one study has applied this analytical method to the foraminiferal cell: (Nomaki et al., 2016) used NanoSIMS combined with TEM observations to follow the assimilation and fate of $^{15}\text{NO}_3^-$ and $^{34}\text{SO}_4^{2-}$ within foraminiferal cells incubated in either hypoxic or anoxic conditions.

The NanoSIMS technique has already been used on other organisms to follow stable isotopes assimilation and their subsequent transfer within symbiotic systems. One of the main model organisms that has been studied in this regard is coral, which is associated with symbiotic photosynthetic dinoflagellates. The assimilation of inorganic compounds (nitrogen, ammonium, bicarbonate and sulfate) could be measured, as well as their transfer within the different compartments of the

dinoflagellates and coral host tissues (Kopp et al., 2013, 2015a; Pernice et al., 2012; Raina et al., 2017). In the present work, similar methods will be applied to symbiotic foraminiferal species.

5.3 TEM-NanoSIMS correlation: an adapted tool to visualize the fate of labeled compounds within the foraminiferal cell

One of the most remarkable advantage of NanoSIMS, and that will of great importance in this work, is that the isotopic mapping can be carried out on tissue sections previously imaged with TEM. This allows us to precisely assign quantified isotopic ratios to specific sub-cellular structures. An example is shown in Fig. 1.9, which show data from within a foraminiferal cell. The NanoSIMS technique allowed us to follow the fate of the ^{13}C -enriched diatom material after digestion by the foraminiferal cell (see chapter 2). The ^{13}C -signal could be traced within the different compartments of the foraminiferal cytoplasm. This figure illustrates the capability to obtain high quality isotopic images on thin sections on which high quality TEM imaging has been carried out prior to NanoSIMS analyses. This capability is essential for the project presented here, because TEM imaging will allow us to target precisely the sub-cellular structures that contain either the isotopically enriched compounds given to the foraminifera, or the metabolized compounds produced after their assimilation.

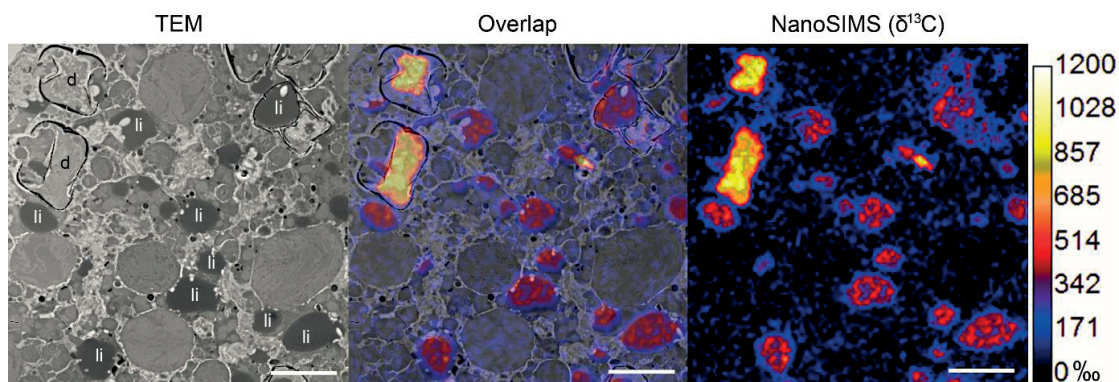


Figure 0.9: TEM-NanoSIMS imaging technique example with the foraminiferal species *Ammonia* sp. The observed specimen was fed with ^{13}C -enriched microalgae (diatoms) and then incubated in anoxic artificial seawater for 28 days. On the TEM micrograph (left) some diatoms (d) can be seen in the foraminiferal cytoplasm, along with lipid droplets (li). On the right the NanoSIMS image represent the $\delta^{13}\text{C}$ (expressed in ‰) repartition in the imaged cytoplasm area. As it can be seen on the central image, the NanoSIMS image can be perfectly overlapped with the TEM image, allowing a direct visualization of the ^{13}C -enriched sub-cellular compartments (here the diatoms and the lipid droplets). Scale bars: 5 μm .

Thesis objectives and content

The main objective of this thesis is to bring new knowledge about the intracellular metabolic pathways involved for different metabolisms encountered in foraminifera. Emphasis will be placed on feeding strategy under anoxia and the role of symbionts (sequestered chloroplasts and dinoflagellates) in different species, inhabiting different environments.

Chapter 1 (LeKieffre et al., submitted) gives an overview of the cellular ultrastructure of benthic foraminifera. This work combines a review of the existing literature with novel TEM observations from nine benthic species sampled from three distinct environments: an intertidal mudflat, a fjord and a basin. A description of commonly encountered organelles is given, followed by a discussion of their role(s) and function(s) within the cell. This chapter will aid subsequent interpretation of the TEM observations made in the following chapters.

Chapter 2 (LeKieffre et al., 2017) presents a study on the feeding behavior and the metabolic response of an intertidal species (*Ammonia* sp.) incubated under anoxic conditions with ^{13}C -labeled diatoms. This species is widely distributed and abundant in coastal areas, and is, as many other benthic foraminiferal species, known to survive weeks to months without oxygen. However, the metabolic adaptations that enable foraminifera to achieve this are still unknown. This experiment has two objectives: (1) to follow food uptake and processing within a foraminiferal cell and (2) to compare this feeding metabolism between foraminifera incubated under oxic vs. anoxic conditions in order to unravel the mechanisms by which *Ammonia* sp. survive extended periods of anoxia.

Chapter 3 is dedicated to the study of the nutrients exchanges in kleptoplastic foraminifera. The objective was to observe the intracellular exchanges of metabolites between the sequestered chloroplasts and the foraminiferal host cell. In the literature the kleptoplasty has been shown to be functional in some species, but many questions remain unanswered. In the foraminifera inhabiting photic areas, what are the intracellular structures involved in the carbon translocation from the kleptoplasts to the foraminiferal cell? Do the kleptoplasts play any role in the nitrogen and sulfur metabolisms of foraminiferal cells? And, are the metabolic pathways involved similar among all the kleptoplastic species, especially in species inhabiting aphotic environments? The first sub-chapter 3.1 (Jauffrais, LeKieffre et al., submitted) presents the fine structure of kleptoplasts sequestered by different species and shows the ultrastructural variability among the species. Then in chapters 3.2, 3.3 and 3.4. foraminiferal labeling experiments with ^{13}C -bicarbonate, ^{15}N -ammonium and ^{34}S -sulfate were performed to better understand the role of sequestered chloroplasts in the foraminiferal cell. Carbon uptake through photosynthesis and putative roles in the nitrogen and sulfur metabolism are

investigated and compared among species as well as with non-kleptoplastic species. The species examined are *Haynesina germanica* and *Elphidium williamsoni*, common kleptoplastic species in intertidal photic ecosystems; and *Nonionellina labradorica*, a species inhabiting aphotic areas in the Gullmar fjord (Sweden).

Chapter 4 (LeKieffre et al., in prep) presents inorganic carbon assimilation in the case of a “full” symbiosis between a photosynthetic dinoflagellate and the planktonic species *Orbulina universa*. This pulse-chase experiment using ^{13}C -bicarbonate allows the visualization of the carbon uptake through dinoflagellate photosynthesis and transfer dynamics to the foraminiferal host cell. It also gives insights of the benefits that dinoflagellates gain from the symbiosis, and their mitosis mechanism.

Finally the last part gives a general discussion on all the results gathered in this thesis in an attempt to place them in a larger perspective.

Note about the nomenclature of the species *Ammonia cf. tepida*

The specimens of *Ammonia* used in this thesis work in chapters 1, 2 and 3 came from two sampling locations: the mudflat of Bourgneuf bay (France) and a small mudflat near the Gullmar fjord (Sweden), both populations were genetically characterized and belong to the same phylotype, T6 (Magali Schweizer, pers. com.) following the classification that Hayward et al. (2004) established for the genus *Ammonia*. This phylogenetic analysis indicated that there are a number of well-defined subclades nested within the genus or clade *Ammonia*, each of which could be given a distinct species name, hence the use of the term “phylotype” (Moreira and López-García (2011)). Since our specimens are morphologically similar to the morphospecies *Ammonia tepida*, we will use the name *Ammonia cf. tepida* (Cushman, 1926) to refer to this phylotype. However, different names have been used for this phylotype through this PhD thesis: chapters 1 and 3.1. have been submitted and the chapter 2 accepted before we could homogenize the nomenclature; in these chapters *Ammonia cf. tepida* is referred to as *Ammonia* sp., *Ammonia aomoriensis* and *Ammonia tepida*, respectively.

Chapter 1: An overview of cellular ultrastructure in benthic foraminifera: New observations in the context of existing literature

Chapter 1 presents a manuscript submitted to the special issue “Foraminiferal ultrastructure” of the Marine Micropaleontology journal. In this chapter the cellular ultrastructure of nine benthic foraminiferal species is investigated and the role of observed organelles is discussed.

PhD student’s contribution: the PhD student designed the experiment with EG and JMB; CL collected the samples with HLF and EG and analyzed the samples (except the samples of the species *Bulimina tenuata* which were analyzed by JMB); interpreted the TEM micrographs with GM and JMB; discussed the results with JMB and EG and wrote the manuscript with comments and edits from all the authors.

Note about the life cycle of foraminifera

Foraminifera have a complex life cycle with an alternation of sexual and asexual generations (see Goldstein, 1999 for a review). The adult gamont has a single nucleus and produces gametes (in foraminifera the gametogenesis only involves mitosis, and not meiosis). The gametes then fuse and form a diploid zygote, which will result in an adult agamont. This adult agamont is multinucleate and produces by multiple fission (meiosis occurs at this stage) haploid young individuals that either mature into uni-nucleate gamonts, or into a second asexual generation, the schizonts (see Figure 1.0 below). This life cycle may vary from one species to another. The discussion about the nucleus ultrastructure in the following chapter is concerned with the “gamont” stage.

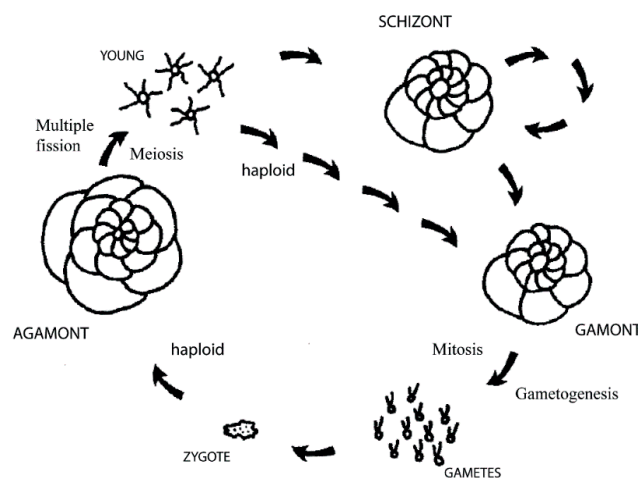


Figure 1.0: Foraminiferal life cycle (modified from Goldstein, 1998).

An overview of cellular ultrastructure in benthic foraminifera: New observations in the context of existing literature

Charlotte LeKieffre^{1*}, Joan M. Bernhard², Guillaume Mabilieu³, Helena L. Filipsson⁴,
Anders Meibom^{1,5}, Emmanuelle Geslin⁶

¹ Laboratory for Biological Geochemistry, School of Architecture, Civil and Environmental Engineering (ENAC), Ecole Polytechnique Fédérale de Lausanne (EPFL), Switzerland

² Department of Geology and Geophysics, Woods Hole Oceanographic Institution, Woods Hole, MA, USA

³ Service commun d'imageries et d'analyses microscopiques (SCIAM), Institut de Biologie en Santé, University of Angers, France

⁴ Department of Geology, Lund University, Sölvegatan 12, 223 62 Lund, Sweden

⁵ Center for Advanced Surface Analysis, Institute of Earth Sciences, University of Lausanne, Switzerland

⁶ UMR CNRS 6112 - LPG-BIAF, University of Angers, France

* Corresponding author: charlotte.lekieffre@epfl.ch

Abstract

We report systematic transmission electron microscope (TEM) observations of the cellular ultrastructure of selected, small rotalid benthic foraminifera. Nine species from different environments (intertidal mudflat, fjord, and basin) were investigated: *Ammonia* sp., *Elphidium oceanense*, *Haynesina germanica*, *Bulimina marginata*, *Globobulimina* sp., *Nonionellina labradorica*, *Nonionella* sp., *Stainforthia fusiformis* and *Buliminella tenuata*. All the observed specimens were fixed just after collection from their natural habitats allowing description of intact and healthy cells. Foraminiferal organelles can be divided into two broad categories: (1) organelles that are present in all eukaryotes, such as the nuclei, mitochondria, endoplasmic reticulum, Golgi apparatus, and peroxisomes; and (2) organelles specific to foraminifera, generally with unknown function, such as fibrillar vesicles or electron-opaque bodies. Although the organelles of the first category were observed in all the observed species, their appearance varied. For example, subcellular compartments linked to feeding and metabolism exhibited different sizes and shapes between species, likely due to differences in their diet and/or trophic mechanisms. The organelles of the second category were common in all foraminiferal species investigated and, according to the literature, are frequently present in the cytoplasm of many different species, both benthic and planktonic. This study, thus, provides a detailed overview of the major ultrastructural components in benthic foraminiferal cells from a variety of marine environments, and also highlights the need for further research to better understand the function and role of the various organelles in these fascinating organisms.

Key-words: Protist, organelles, TEM, cytology, mudflat, Gullmar Fjord.

1. Introduction

Despite a number of studies regarding the ultrastructure of benthic foraminifera revealed by transmission electron microscope (TEM) observations, only a small fraction of the organelles in these single-celled organisms have been identified and their function understood (see compiled review of prior publications in Bernhard and Geslin (submitted). Recent studies have attempted to correlate ultrastructural imaging of the cytoplasmic structures to physiological processes using correlative imaging approaches (Bernhard and Bowser, 2008; LeKieffre et al., 2017; Nomaki et al., 2016). The inability to confidently link form and structure with function warrants an improved understanding of the foraminiferal cell at the ultrastructural level.

Based on the literature, we present here an inventory of the common organelles found in benthic foraminifera, to which we add new TEM observations on the cytoplasm of nine benthic rotalid foraminiferal species. These foraminifera were sampled in three different locations and environments (Fig. 1.1 and Table 1.1): *Ammonia* sp. (phylotype T6, Hayward et al., 2004; Holzmann, 2000), *Elphidium oceanense* (*excavatum* species complex, Darling et al., 2016), and *Haynesina germanica* (Ehrenberg, 1980) from an intertidal mudflat in Bourgneuf Bay on the Atlantic coast of France; *Bulimina marginata* (d'Orbigny, 1826), *Globobulimina* sp., *Nonionellina labradorica* (Dawson, 1860), *Nonionella* sp., and *Stainforthia fusiformis* (Williamson, 1848) from the Gullmar Fjord in Sweden, which is a silled basin with restricted circulation, and *Buliminella tenuata* from the silled, typically stagnant, Santa Barbara Basin (USA, samples from Bernhard and Bowser, 2008). These species are all small (< 500 µm) rotalid benthic foraminifera for which a description of each typical organelle is presented along with discussion of their known or inferred function(s).

Table 1.1: Species, sampling location, and number of specimens observed or reported in this study.

Species	Site	Numbers of specimens analyzed
<i>Ammonia</i> sp. genetic type T6 (<i>tepida</i> morphocomplex)	Bourgneuf Bay, Atlantic coast, intertidal mudflat, France	3
<i>Elphidium oceanense</i> (<i>excavatum</i> species complex)		3
<i>Haynesina germanica</i>		4
<i>Bulimina marginata</i>	Gullmar Fjord, Sweden (70 m / 117 m depth)	1
<i>Globobulimina</i> sp.		3
<i>Nonionellina labradorica</i>		6
<i>Nonionella</i> sp.		4
<i>Stainforthia fusiformis</i>		3
<i>Buliminella tenuata</i>	Santa Barbara Basin, California, USA (~ 580 - 598 m) (Bernhard and Bowser, 2008)	2

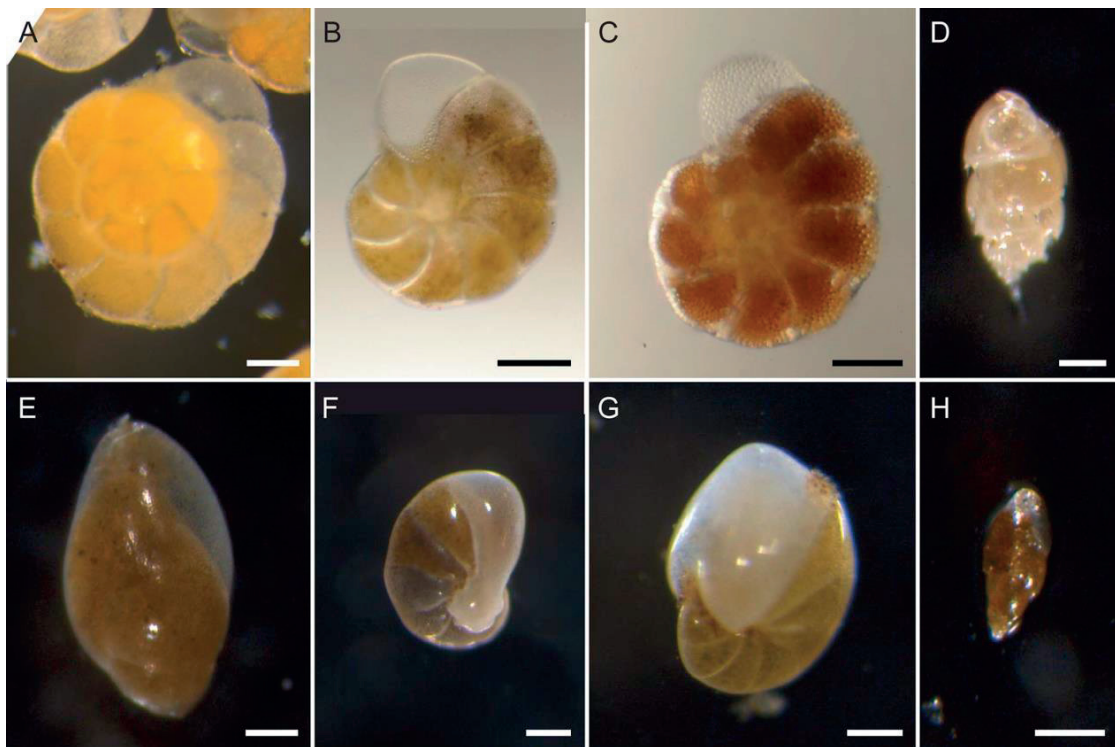


Figure 1.1: Light micrographs of the foraminifera from the Atlantic French coast intertidal mudflat and the Gullmar fjord. A: *Ammonia* sp. (*tepida* morphocomplex); B: *Haynesina germanica*; C: *Elphidium oceanense* (*excavatum* species complex), D: *Bulimina marginata*; E: *Globobulimina* sp.; F: *Nonionella* sp.; G: *Nonionellina labradorica*; H: *Stainforthia fusiformis*. Scales: A-D, F = 100 μ m; E, G, H = 200 μ m.

2. Material and methods

2.1. Collection sites

Foraminifera from intertidal environments (*Ammonia* sp., *E. oceanense* and *H. germanica*) were sampled on March 7, 2016, on the intertidal mudflat in the bay of Bourgneuf at la Couplassse station (Loire-Atlantique, France; 47°0'47"N, 2°1'17"W). The top 2 cm of sediment was collected at low tide, transferred to plastic jars, and immediately chemically fixed (1:1 volume sediment : fixative solution; see below). Living foraminifera from the Gullmar fjord, Sweden (*B. marginata*, *Globobulimina* sp., *N. labradorica*, *Nonionella* sp. and *S. fusiformis*) were collected on October 22, 2014, at two locations using the R/V Skagerak of the Sven Lovén Centre for Marine Science (University of Gothenburg): site DF3 (117-m depth; 58°19.096'N, 11°32.398'E) and site DF70-2 (70-m depth, 58°17.071'N, 11°30.636'E). At the time of collection, both locations were characterized by a temperature of approximately 8 °C and salinity of 34.6. Sediment samples were collected with a box

corer. Immediately after the cores were brought on board, the top 2 cm (approximately) of the sediment was collected in plastic jars and chemically fixed (1:1 volume sediment : fixative solution; see below). *Buliminella tenuata* specimens were collected as described in Bernhard and Bowser (2008) from sediments in the Santa Barbara Basin (centered on 34°16'N, 120°02'W).

2.2. Chemical fixation and TEM observations

The fixative solution contained 4 % glutaraldehyde and 2 % paraformaldehyde diluted in cacodylate buffer solution (NaCaco 0.1 M, Sucrose 0.4M, NaCl 0.1M). Following fixation and rinsing with the cacodylate buffer, cytoplasm-bearing foraminifera were, based on the color of their cytoplasm, picked using a binocular microscope (Leica, M165C) and transferred individually into microtubes for decalcification in 0.1 M Ethylenediaminetetraacetic Acid (EDTA) diluted in 0.1 M cacodylate buffer solution. They were then post-fixed with 2 % osmium tetroxide (OsO₄) for 1 h at room temperature, dehydrated in successive ethanol baths (50, 70, 95 and 100 %) and finally embedded in LR White acrylic resin. Embedded individuals were cut into 70-nm sections with an ultramicrotome (Reichert ultracut S) equipped with a diamond knife (Diatome, Ultra 45°) and placed on formvar-carbon coated copper TEM slot grids. The sections were post-stained for 10 mins with 2 % uranyl acetate and observed with a transmission electron microscope (TEM), either a Philips 301 CM100 at the Electron Microscopy Facility of the University of Lausanne (Switzerland) or a JEOL JEM 1400 at the SCIAM (Service Commun d'Imagerie et d'Analyses Microscopiques) platform at the University of Angers (France). Semi-thin sections (500 nm) for light microscopy observation were also cut and stained with toluidine blue and basic fuchsin. Both thin and semi-thin sections were taken in the middle of the foraminiferal cell in order to obtain sections bisecting the maximum number of chambers. *Buliminella tenuata* specimens were processed, and imaged as described in Bernhard and Bowser (2008).

3. TEM observations of benthic foraminiferal cells

The TEM micrographs presented in this study depict foraminifera that were alive when collected and preserved. The vitality of each specimen was checked by observing the appearance of mitochondria and membranes as described by Nomaki et al. (2016). Only specimens with well-preserved mitochondria and membranes are reported here.

Two regions of cytoplasm in foraminifera are usually distinguished in thin sections: the cell body (located inside the test (shell); also called “endoplasm”) and the reticulopodial net (reticulated pseudopods) typically, but not always, located outside the test (the reticulopodial net can also be gathered within the younger chambers of the foraminifer) (Alexander and Banner, 1984; Anderson and Lee, 1991). The cell body is usually denser (i.e., contains more electron-opaque organelles and thus appears darker in TEM images) than reticulopodial net, which has a granular appearance (Alexander and Banner, 1984). The cell body is the focus of the present study.

3.1. Cell body and “empty” vacuoles

The appearance of the cell body was highly variable among foraminiferal species, both between conspecifics and between chambers within a single individual. A main difference between intertidal and fjord/basin species was the numerous, large (between 10 to 200 μm in diameter) empty vacuoles, which were typical in the cell body of most of the fjord species, except *B. marginata* (Fig. 1.2). These vacuoles certainly had lost their soluble compounds during sample preparation. Similar, albeit smaller (i.e., 5 - 20 μm diameter) vacuoles were sometimes observed in the youngest chambers of species from intertidal mudflats (for instance in *H. germanica* and *E. oceanense*, Figs. 1.2B and C). Portions of the cell body in the two or three youngest chambers of a foraminifera had a particular appearance: they contained very few lipid droplets but more “empty” and degradation vacuoles (and thus appeared less dense) than the cell body portions of older chambers. Besides these cell body portions of the youngest chambers often had a patchy aspect: that is, more electron-opaque organelles were grouped in certain areas within the cell body, thus appearing darker in TEM images than the surrounding cytosol (e.g. Fig. 1.2C).

Because *Globobulimina* sp. from Gullmar Fjord and several other species inhabiting the same type of environment, such as *Stainforthia fusiformis* or *Nonionella* sp., are known to store nitrate in their cell (Piña-Ochoa et al., 2010), it is possible that the large “empty” vacuoles play a role as internal reservoirs of nitrate, as suggested by Bernhard et al. (2012). The intertidal species *Ammonia tepida*

(same type T6 as our specimens) and *Haynesina germanica* are not known to contain any intracellular nitrate (Piña-Ochoa et al., 2010). Thus the vacuoles observed in the cell body of intertidal species may have a different origin and/or function than the common, large “empty” vacuoles observed in fjord specimens. As hypothesized in some studies (e.g. Erez, 2003; Bentov et al., 2009)), the vacuoles in intertidal species could serve as storage for ions intended for test formation inside the foraminiferal cell body (pool of HCO_3^- ions in *Amphistegina lobifera*). The brighter appearance of the cell body portions of the youngest chambers is likely due to its location near the aperture from where the reticulopods extend, as this requires the presence of numerous microtubules which are not electron-dense organelles (Alexander and Banner, 1984). The numerous degradation vacuoles sometimes observed can also be explained by the proximity to the aperture, where food is internalized by phagocytosis.

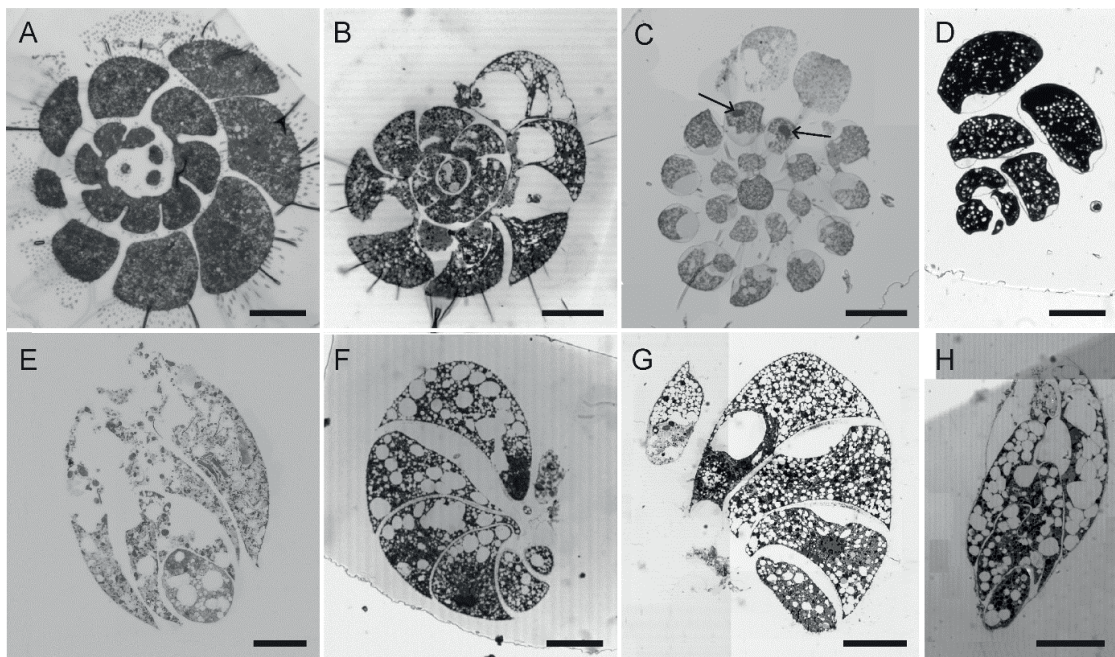


Figure 1.2: Light micrographs of semi-thin sections of the foraminifera from the Atlantic French coast intertidal mudflat and the Gullmar fjord. A: *Ammonia* sp. (*tepida* morphocomplex); B: *Haynesina germanica*; C: *Elphidium oceanense* (*excavatum* species complex); D: *Bulimina marginata*; E: *Globobulimina* sp.; F: *Nonionella* sp.; G: *Nonionellina labradorica*; F: *Stainforthia fusiformis*. Arrows: nuclei. Scales: A, B, C, E, F, H = 100 μm ; D, G = 200 μm .

3.2. Organelles with known function

3.2.1. Nucleus

The nucleus can be located at different locations within the foraminiferal cell, from older to younger chambers in multi-chambered species (reviewed in Anderson and Lee, 1991). In our spiral-shaped foraminifera, the nucleus in one *Ammonia* sp. (phylotype T6) and two *E. oceanense* occurred in chambers of the penultimate whorl. In all specimens where a nucleus was observed, it seemed that these individuals were uninucleate, except for one *E. oceanense* where two nuclei were noted (Fig. 1.2C). The uninucleate feature seemed to be typical for foraminiferal gamonts (e.g. Enery and Lee, 1976; Goldstein, 1997, 1988; Goldstein et al. 2010; Raikov et al., 1998). The observed nuclei exhibited various shapes, from nearly spherical to partially lobate. Published accounts also document nuclei with various shapes, from spherical to multilobate (reviewed in Raikov et al., 1998). The lobate forms may derive from the spherical form in response to an increased need of membrane before gametogenesis (Raikov et al., 1998).

In the rotalid species investigated in this study, the nucleus had a size typically ranging from about 20 to 50 μm in diameter with numerous nucleoli and a lamina (Figs. 1.3 and 4A), which is in the same range than previously observed nuclei in different monothalamous or rotalid species (e.g. Altin et al., 2009; Altin-Ballero et al., 2013; Anderson and Lee, 1991; Dahlgren, 1967a, b; Goldstein and Richardson, 2002; Goldstein et al., 2010; Raikov et al., 1998; Schwab, 1972; Schwab and Schwab-Stey, 1979). The lamina is a layer of nucleoplasm (i.e., matrix of the nucleus) in contact with the inner membrane of the nuclear envelope (Fig. 1.3). Although the lamina appears very similar to the nucleoplasm, the former is easily visualized because of the space it creates between the nuclear envelope and the nucleoli (Fig. 1.4B). The lamina between the nucleoli and the inner membrane has been described in other species (e.g. Dahlgren, 1967a and b). In the allogromiid foraminifer *Myxotheca* sp. a “prominent non-chromatin containing” space was also observed between the nucleoli and the nuclear envelope but was not interpreted as a lamina (Goldstein and Richardson, 2002). However it might not exist in all species because it was not observed in *Heterostegina depressa* and *Globobulimina turgida* (Hottinger and Dreher, 1974). At higher magnification (Fig. 1.4B), the double-membrane nuclear envelope was observable. The distribution of the nucleoli in the nucleus varied among species: all the nucleoli we observed were distributed at the periphery of the nucleus, flattened against the lamina or nuclear envelope as illustrated for *S. fusiformis* (Fig. 1.4C). Sometimes, however, additional small nucleoli were seen in the central part of the nucleus as in *N. labradorica* (Fig. 1.4D). The literature also notes that different distributions of nucleoli occur in different species (see Raikov

et al. 1998). For example, Spindler et al. (1978) described a central dispersion of the nucleoli in the planktonic species *Hastigerina pelagica*, without nucleoli adjacent to the nuclear envelope, while Anderson and Lee (1991) reported nucleoli distribution either centrally or at the periphery of the nucleus. A peripheral repartition of nucleoli was also observed in the monothalamous *Hippocrepinella alba*, the rotalid *Globobulimina turgida* (Dahlgren 1967b) and the allogromiid *Hyperammina* sp. (Goldstein and Richardson, 2002).

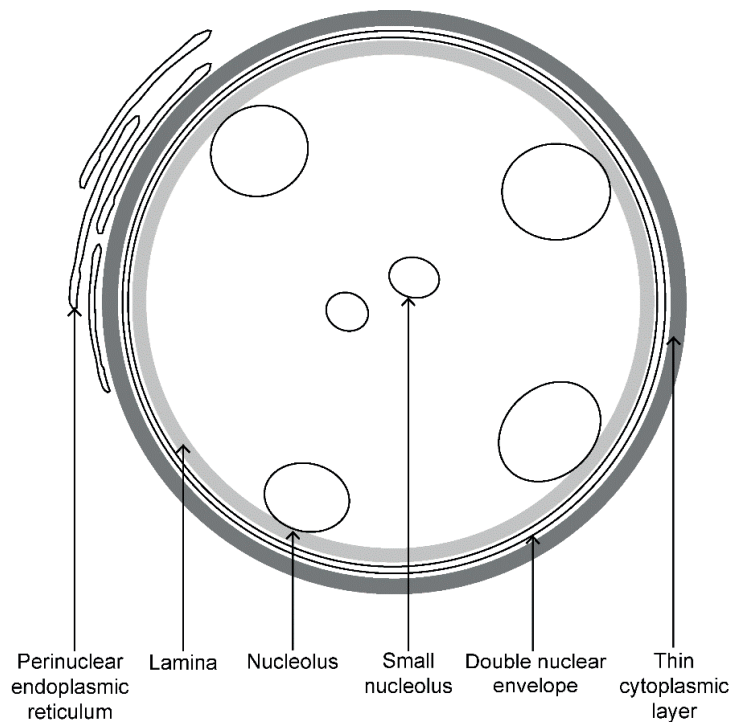


Figure 1.3: Schematic ultrastructure of a foraminiferal nucleus. The double nuclear envelop is surrounded by a thin cytoplasmic layer against which perinuclear endoplasmic reticulum stand in a continuous or intermittent layer. On the inner part of the nuclear envelop a lamina can be seen, separating the peripheral nucleoli from the envelop. Smaller nucleoli can also occupy a central position. The nucleus is represented in a circular shape for convenience as it can also be in a lobate form (see details in the text).

Perinuclear endoplasmic reticulum was often noted on the outside of the nuclear envelope (see section 3.2.3). A thin layer (approximately 200 nm) of cytoplasmic material with a particular fibrous aspect surrounded the nuclei in some species, such as *Nonionella* sp. or *Nonionellina labradorica* (Figs. 1.4A, B and D). This layer was absent from the nucleus of *S. fusiformis* (Fig. 1.4C). The

thin layer of fibrous cytoplasm around the nuclei has been described in larger benthic foraminifera (Soritidae) and planktonic species (Leutenegger, 1977) where it was separated from the cytosol by small vesicles or lacunas (electron-light cytoplasmic layer). Small vesicles surrounding the nucleolar membrane were also observed in different monothalamous species: *Psammophaga sapela*, *Xiphophaga minuta*, *Niveus flexilix*, *Myxotheca* sp., *Cribrorothammmina alba* and *Hyperammmina* sp. (Altin et al., 2009; Altin-Ballero et al., 2013; Goldstein and Richardson, 2002; Goldstein et al., 2010). However in the present study, the thin layer of cytoplasm with a fibrous aspect surrounding the nuclei in some rotalid species was not clearly separated from the rest of the cytosol and no accumulation of small vesicles was detected. This feature could correspond to the “nuclear villi” observed by Dahlgren (1967a) in the monothalamous species *Ovammmina opaca* and described as protrusions projected in the cytoplasm from the nuclear envelope. The double nucleated *E. oceanense* exhibited atypical nuclei with outgrowths (Fig. 1.4E). At higher magnification (Fig. 1.4F), the circular nuclear envelope was distinguished between the nucleus and the “outgrowths”. These “outgrowths” were formed of an electron-dense matrix and included various organelles like lipid droplets or electron-opaque bodies. This matrix was probably linked to the thin layer of cytoplasm, although its role remains unknown. It could also be a fixation artefact.

The TEM micrographs of our study did not allow us to observe the pores of the nuclear envelope, but other studies have noted their presence in both planktonic and benthic species (e.g. Altin et al. 2009; Anderson and Lee, 1991; Dahlgren, 1967b; Goldstein, 1997; Hemleben et al., 1989; Leutenegger, 1977). These pores may allow communication with the cell body, in particular the migration of RNA (Anderson and Lee, 1991).

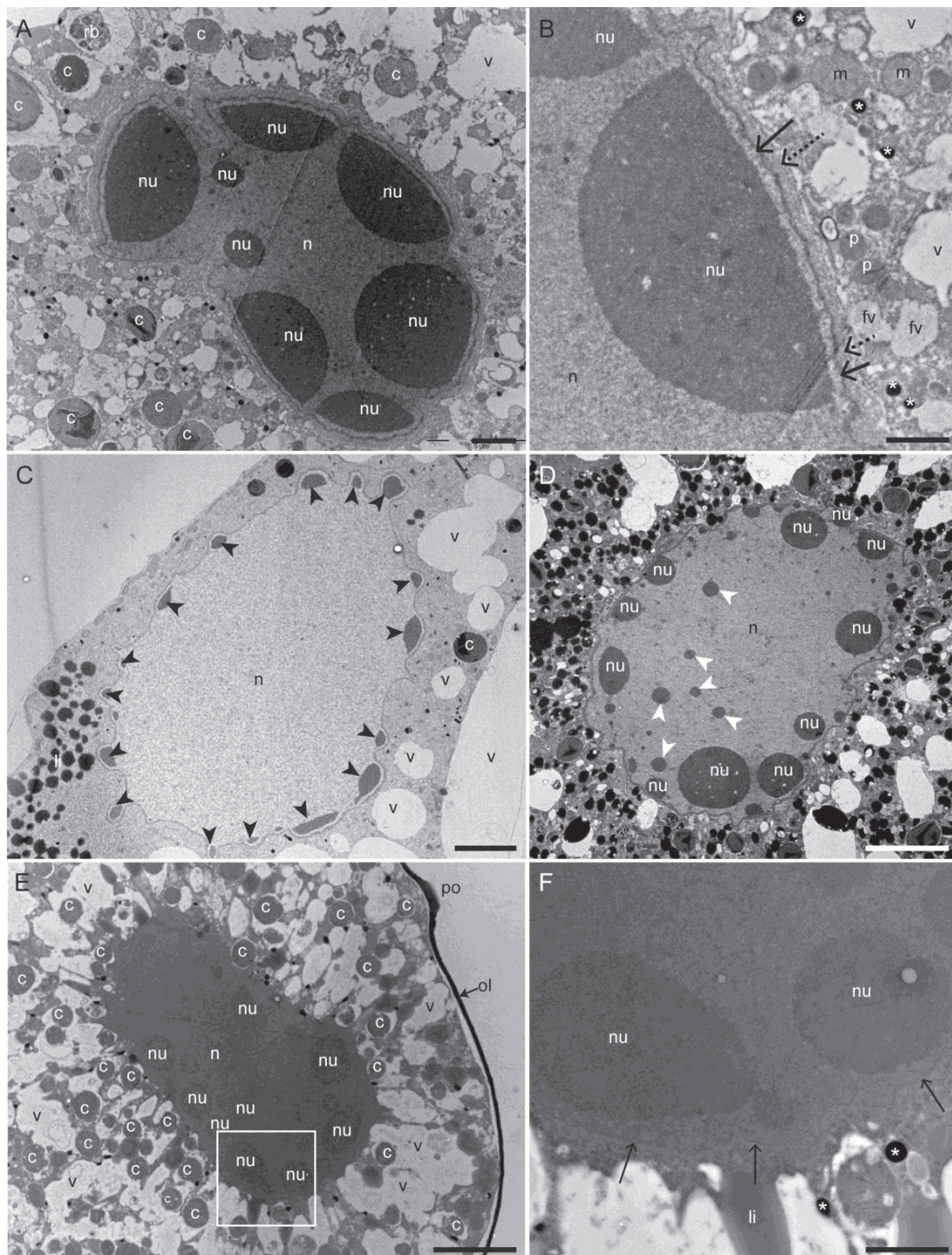


Figure 1.4: Transmission electron micrographs of benthic foraminiferal nuclei. A: *Nonionella* sp. nucleus with numerous nucleoli. B: Higher magnification of *Nonionella* sp. nucleus showing a nucleolus at the nucleus periphery and the nuclear membrane (arrows) with a thin cytoplasmic layer (dotted arrows). C: *S. fusiformis* nucleus with numerous small peripheral nucleoli (black arrowheads). D: *Nonionellina labradorica* nucleus with a few small central nucleoli (white arrowheads). E: *Elphidium oceanense* nucleus with "cytoplasmic outgrowths". F: Higher magnification of the nucleus of *Elphidium oceanense* (arrows: nucleoplasm). Arrows: nuclear membranes, dotted arrows: thin cytoplasmic layer, white asterisks: electron opaque bodies, c: chloroplasts, fv: fibrillar vesicles, li: lipid droplets, m: mitochondria, n: nucleus, nu: nucleolus, ol: organic lining, p: peroxisomes, po: pore, rb: residual bodies, v: vacuoles. Scales: A = 2 μ m; B, F = 1 μ m; C, E = 5 μ m; D = 10 μ m.

3.2.2. Mitochondria

Mitochondria were studied in all the observed specimens. As they are the site of Adenosine TriPhosphate (ATP) production (Sherratt, 1991), their presence and integrity are one of the main tools to attest to the vitality of the specimen at the time of fixation (Nomaki et al., 2016). Main features of mitochondria, which are also observed in our study (Fig. 1.5A), is the double membrane and the presence of cristae in their matrix (Sherratt, 1991). Mitochondria usually appeared oval or kidney shaped in cross section with a length in the range of 0.5 to 1 μm (Figs. 1.5A-C), although they can be bigger and take various shapes (Figs. 1.5B and C). In some foraminiferal species mitochondria with atypical morphologies could be observed. In two of the observed *N. labradorica*, the mitochondria exhibited tubular inclusions (Fig. 1.5D). Also, in other specimens of *N. labradorica*, as well as in *H. germanica* and *Nonionella* sp., a less electron opaque central area was seen in the mitochondria (Fig. 1.5E). At higher magnification, filaments could be identified in this less electron-dense central part (Fig. 1.5E inset).

In all analyzed specimens except those of *Stainforthia fusiformis*, the mitochondria seemed to be homogeneously distributed throughout the cell body. However in the three analyzed individuals of *S. fusiformis*, although a few mitochondria were seen dispersed through the entire cell body, most of them were clearly concentrated close to the plasma membrane of the external parts of the chambers, i.e., parts of the chambers that are in contact with the environment (or were in contact before the addition of a new chamber (Figs. 1.5F and G).

To our knowledge, the tubular inclusions observed in some mitochondria have not been described in any other type of organism. We suggest here that they could be elongated cristae. The less electron-opaque central part of mitochondria observed in some species of this study can also be seen in the mitochondria of the planktonic species *Hastigerina pelagica* and *Globigerinoides ruber* (Hemleben et al., 1989). Seen at higher magnification, the filaments resembled fibrils of mitochondrial DNA (Nass and Nass, 1963). The accumulation of mitochondria under the pores is known in some benthic foraminiferal species such as *Nonionella stella* and *Bolivina pacifica* (Bernhard et al., 2010a; Leutenegger and Hansen, 1979). This specific distribution was interpreted as an adaptation to low-oxygen environments. In the *S. fusiformis* specimens studied here, the mitochondria were not only distributed under the pores but all along the plasma membrane of the external part of the chambers. Thus we cannot conclude that a similar role occurs in this species.

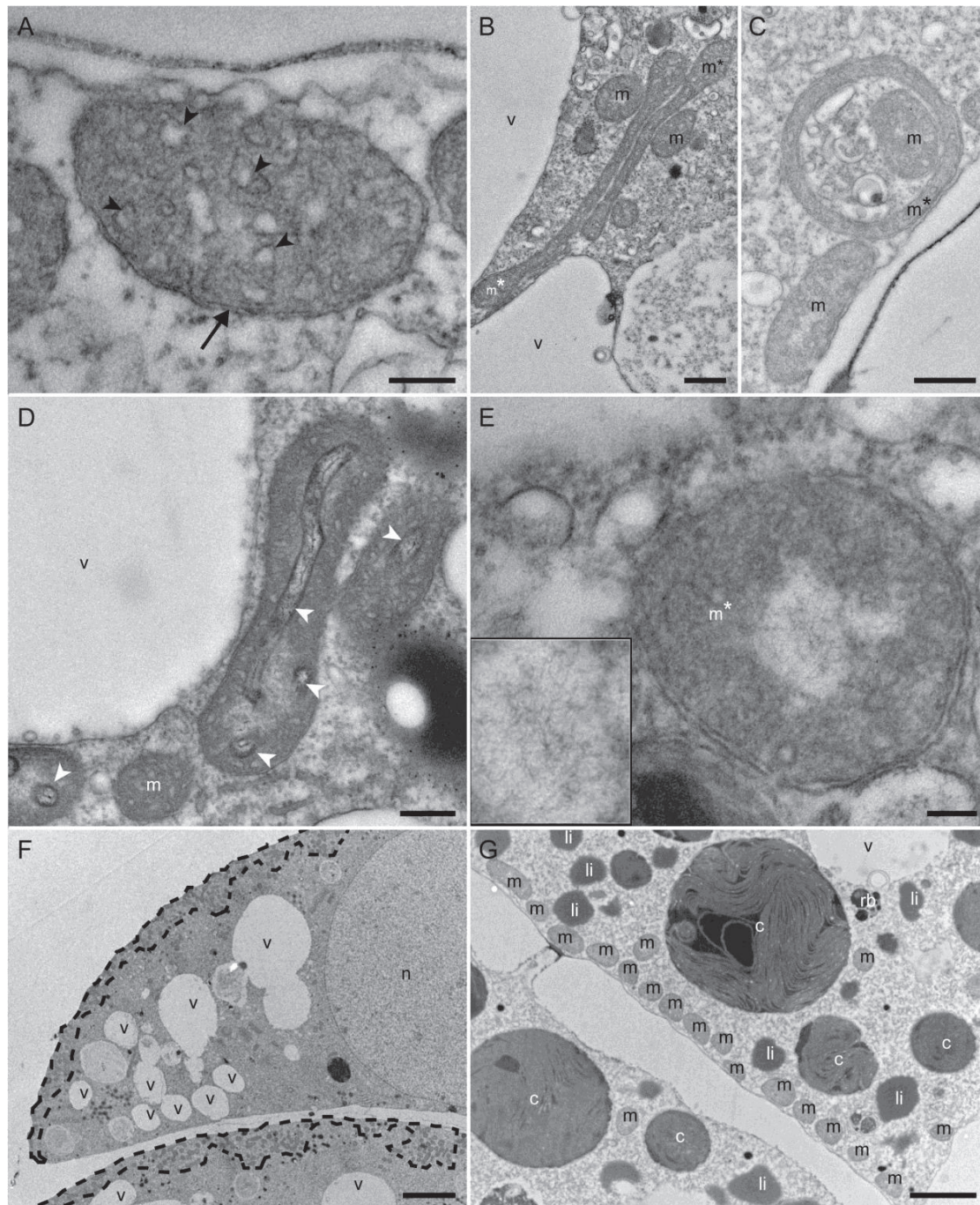


Figure 1.5: Transmission electron micrographs of benthic foraminiferal mitochondria. A: Classic structure of a mitochondrion observed in *Stainforthia fusiformis* (arrowheads: cristae, arrows: double membrane). B: Elongated mitochondria (asterisks) in *Nonionella* sp. C: Circular mitochondrion (asterisk) aside two classic mitochondria in *Nonionella* sp. D: Tubular inclusions (white arrowheads) in two mitochondria of a specimen of *Nonionellina labradorica*. E: Mitochondria with a less electron opaque central part (white asterisks) in *Nonionella* sp. Inset: High-magnification micrograph of the fibrils in this central part. F and G: Numerous mitochondria at the periphery of the chambers (areas surrounded by a dashed black line in F) in *Stainforthia fusiformis*. c: chloroplasts, m: mitochondria, li: lipid droplets, n: nucleus, rb: residual bodies, v: vacuoles. Scales: A, D = 200 nm; B, C = 500 nm; E = 100 nm; F = 5 μ m; G = 2 μ m.

3.2.3. Endoplasmic reticulum

Generally in eukaryotic cells, two types of endoplasmic reticulum occur: rough endoplasmic reticulum (RER) that has ribosomes on its membrane, and smooth endoplasmic reticulum (SER) that lacks ribosomes (Vertel et al., 1992). The former type is a site of protein synthesis, while the latter is involved in lipid synthesis and other synthesis activities (Vertel et al., 1992). Because the visualization of ribosomes at the resolution of the TEM is not assured, in this contribution both types will be grouped under the name of “endoplasmic reticulum”.

Endoplasmic reticulum (ER) was observed in all foraminiferal species studied here (e.g., Fig. 1.6A and B), and has been documented in many other foraminiferal species (reviewed in Anderson and Bé, 1978). The ER is very often observed associated with Golgi apparatus (Figs. 1.6D and E) and peroxisomes (Figs. 1.6E and F - see sections 3.2.4. and 3.2.5.). It was also present around each nucleus observed in this study, as shown in Figs. 1.6C and D. In Figures 1.6E-G, structures apparently made of ER can be observed. These structures, all observed in *S. fusiformis* specimens, were formed of numerous ER cisternae stacked in parallel.

The particular association of ER with the nucleus was established in different foraminiferal species, rotalid or monothalamous (e.g. Altin et al., 2009; Altin-Ballero et al., 2013; Anderson and Bé, 1978; Dahlgren, 1967a, b; Hottinger and Dreher, 1974) and described as “perinuclear reticulum”, however it seems to be absent in some monothalamous species such as *Myxotheca* sp., *Cribrorothalammina alba* and *Hyperammina* sp. (Goldstein and Richardson, 2002). In certain specimens of *S. fusiformis*, this perinuclear ER was intermittent (Fig. 1.6C), while in specimens of *N. labradorica* it formed a continuous layer around the nucleus (Fig. 1.6D). Finally, the ER organized in parallel stacks (Figs. 1.6E-G) were similar to the annulate lamellae of the planktonic foraminifer *Hastigerina pelagica* (d'Orbigny) (Anderson and Lee, 1991; Hemleben et al., 1989; Spindler and Hemleben, 1982). These annulate lamellae made of ER are formed before the gametogenesis of a foraminifera and may provide membranous material for the formation of nuclear envelop of the new nuclei (Anderson and Lee, 1991; Hemleben et al., 1989; Spindler and Hemleben, 1982). Goldstein (1997) also described a pregametic nucleus surrounded by several layers of endoplasmic reticulum in the rotalid *Ammonia* sp. She also hypothesized that those structures are involved in foraminiferal gametogenesis.

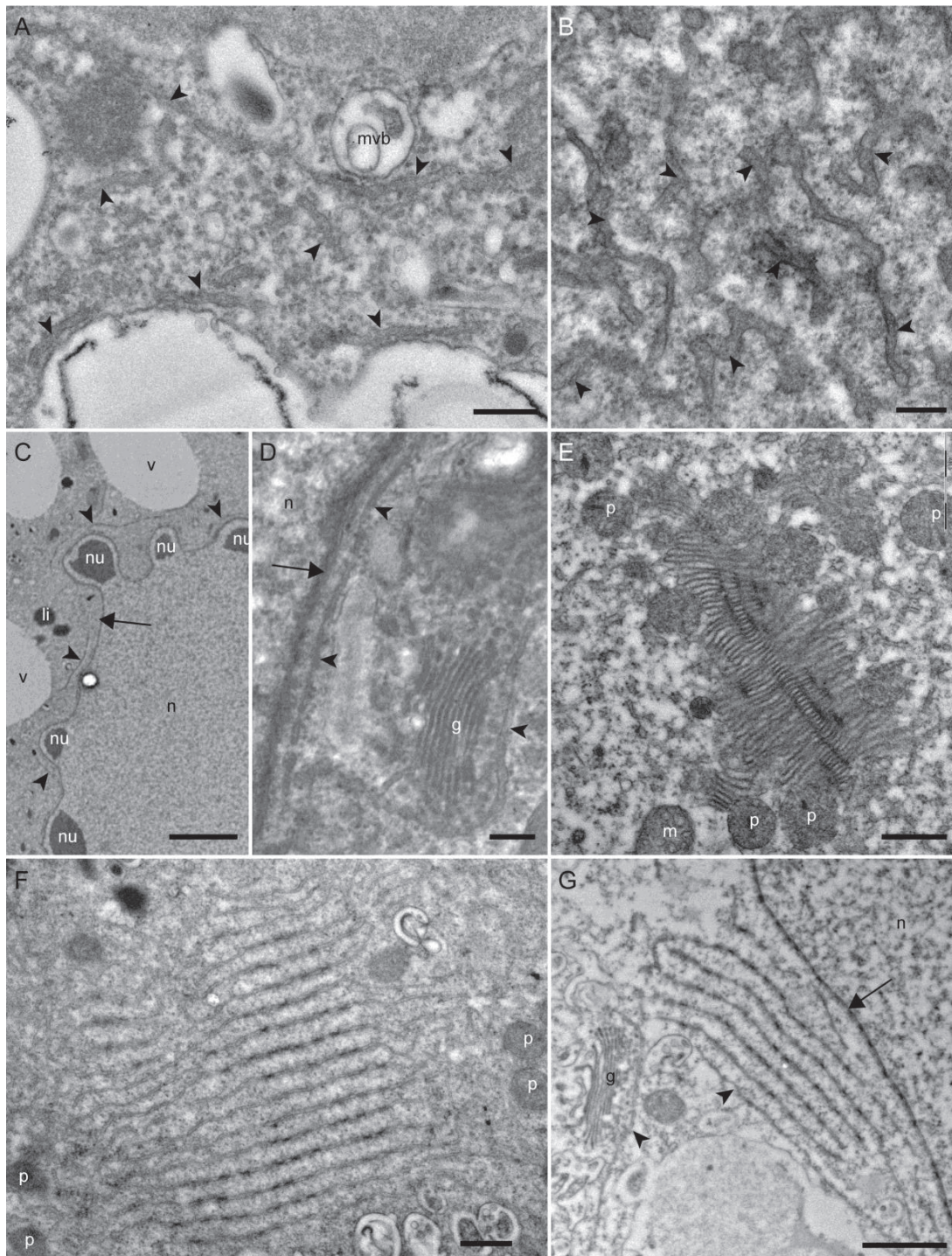


Figure 1.6: Transmission electron micrographs of benthic foraminiferal endoplasmic reticulum. A: Area of the cytoplasm rich in endoplasmic reticulum in *Nonionella* sp. B: Higher magnification of endoplasmic reticulum in *Nonionellina labradorica*. C, D: Endoplasmic reticulum at the periphery of a nucleus in C: *Nonionellina labradorica* and D: *Stainforthia fusiformis*. E: Particular structure made of endoplasmic reticulum in one specimen of *Stainforthia fusiformis*. F, G: Endoplasmic reticulum stacked in a parallel pattern in another specimen of *Stainforthia fusiformis*. Black arrowheads: endoplasmic reticulum, arrows: nucleoplasm, g: Golgi apparatus, m: mitochondria, mvb: multivesicular bodies, n: nucleus, nu: nucleolus, li: lipid droplets, p: peroxisomes. Scales: A, B, D = 200 nm; C = 2 μ m; E, F = 500 nm; G = 1 μ m.

3.2.4. Peroxisomes

Peroxisomes, which were observed in all the specimens from the three sites, are spherical vesicles, approximately 500 nm in diameter and containing a crystalline structure (Fig. 1.7A). At high magnification, the regular organization of the crystalline structure was observed (Fig. 1.7B inset). Peroxisomes were always observed associated with ER (Figs. 1.7A, C and D) and, in the cell body of *S. fusiformis* and *Globobulimina* sp., they were organized in a particular structure: numerous peroxisomes were associated with a high density of ER (Fig. 1.7E).

The existence of peroxisomes in the cytoplasm of foraminifera was first demonstrated in planktonic foraminifera by Anderson and Tuntivate-Choy (1984), who used cytochemical analysis to document the presence of peroxidases, which are enzymes typical of peroxisomes. Peroxidase activity was also demonstrated in benthic foraminiferal peroxisomes (Bernhard and Bowser 2008). Furthermore, Bernhard and Bowser (2008) measured the spacing of the benthic foraminiferal peroxisomal internal crystals, documenting its identity as catalase, which is present in all peroxisomes (De Duve and Beaudhuin, 1966). Catalase is an enzyme that converts hydrogen peroxide (H_2O_2) into water and oxygen, a reaction which produces metabolically useful molecules. Another role that peroxisomes play in eukaryotic cells, including foraminifera, is gluconeogenesis, i.e., the production of carbohydrates (Hemleben et al., 1989).

The association of peroxisomes with ER has been established previously for other benthic foraminiferal species (Bernhard et al., 2001; Bernhard and Alve, 1996; Bernhard and Reimers, 1991; Nyholm and Nyholm, 1975). Also, the specific organization of stacks of peroxisomes associated with copious endoplasmic reticulum (so-called peroxisome-endoplasmic reticulum complexes; P-ER; Fig. 1.7E) has been observed in benthic foraminifera inhabiting chemocline environments, such as low-oxygen areas or seeps (reviewed in Bernhard and Bowser, 2008) (Figs. 1.7F and G). Our observations are consistent with these prior studies because we noted P-ER complexes in both *S. fusiformis* and *N. labradorica* from the Gullmar Fjord, which often exhibits episodes of hypoxia (Filipsson and Nordberg, 2004; Nordberg et al., 2000).

Peroxisomes can also be closely associated with mitochondria (Bernhard and Bowser 2008; Fig. 1.7F) and large vacuoles (Bernhard and Bowser 2008; Fig. 1.7G). Bernhard and Bowser (2008) hypothesized the conversion of peroxide to oxygen and water allowed mitochondrial use of oxygen; the association of peroxisomes with vacuoles suggests a potential source of reactive oxygen species in the vacuoles.

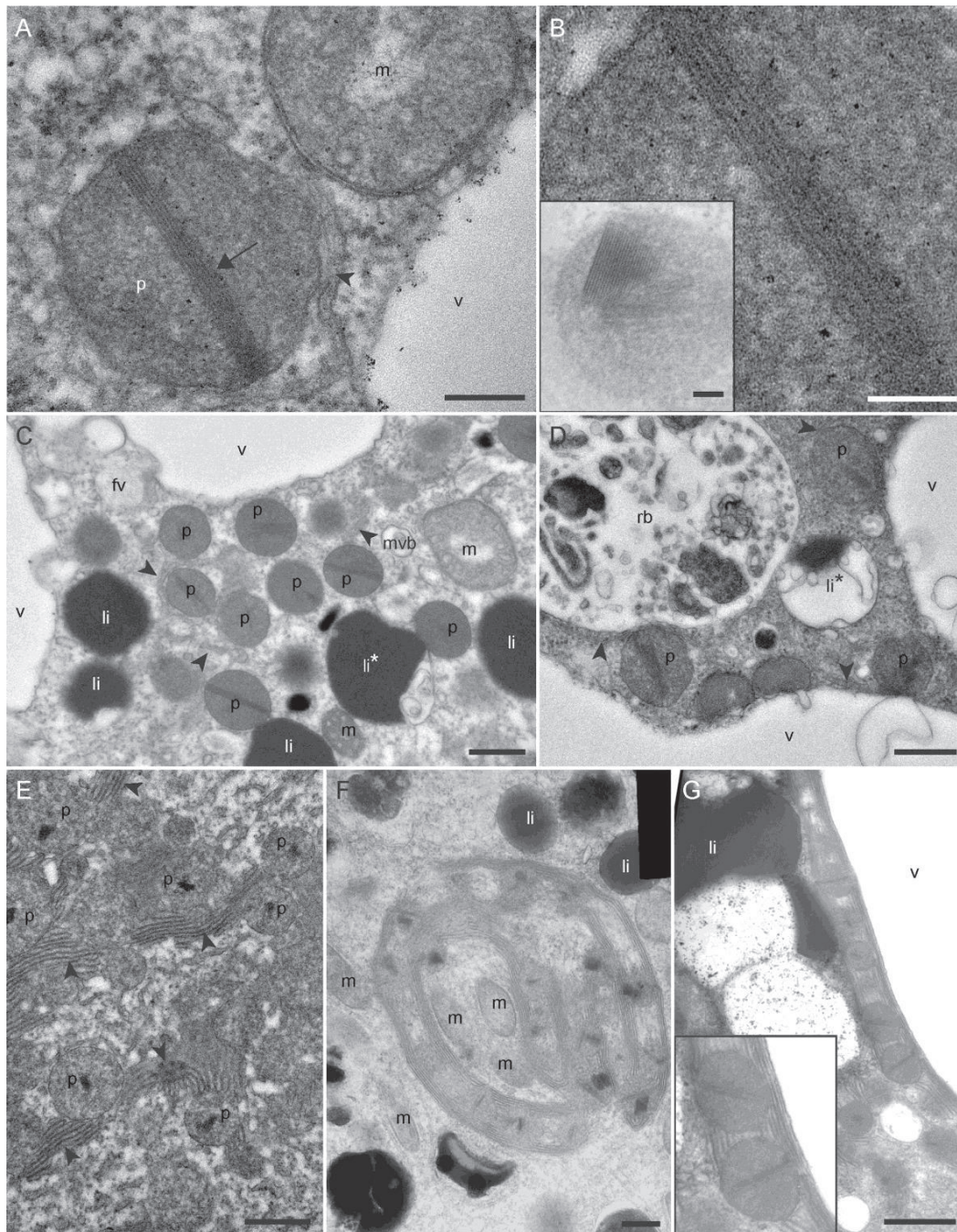


Figure 1.7: Transmission electron micrographs of benthic foraminiferal peroxisomes. A: Classic structure of a peroxisome surrounded by endoplasmic reticulum (ER) in *Nonionellina labradorica*. B: High-magnification image of the crystalline structure of the peroxisome seen in A; inset: triangular core in *Bulimina tenuata* peroxisome (specimen from Bernhard and Bowser, 2008). C and D: Peroxisomes in the cytoplasm of C: *Nonionella* sp. and D: *Nonionellina labradorica*. E: Peroxisome-endoplasmic reticulum (P-ER) complex in *Stainforthia fusiformis*. F: Circular P-ER ring encircling mitochondria in *Bulimina tenuata* (specimen from Bernhard and Bowser, 2008). G: "Railroad track" of P-ER along the edge of a large vacuole in *Bulimina tenuata* (specimen from Bernhard and Bowser, 2008). Inset: higher magnification showing two of the peroxisomes forming the track and the fibrils of ER linking them. Arrowheads: ER, arrow: crystalline inclusion, fv: fibrillar vesicles, li: lipid droplets, li*: lipid droplets in lysis, m: mitochondria, mvb: multivesicular bodies, p: peroxisomes, rb: residual bodies, v: vacuoles. Scales: A = 200 nm; B = 100 nm; C, D = 500 nm; F, G = 1 µm.

3.2.5. Golgi apparatus

Generally, the Golgi apparatus plays a role in the maturation of proteins, as well as in the formation of some lipids (and polysaccharides in plant cells) (Farquhar and Palade, 1998; Staehelin and Moore, 1995). The Golgi processes proteins received from the endoplasmic reticulum through incoming transport vesicles on the *cis* face. These proteins are then sent to their next destination from the *trans* face in secretory vesicles (Farquhar and Palade, 1998; Staehelin and Moore, 1995; Fig. 1.8). The Golgi apparatus is made of membrane stacks surrounded by different types of vesicles, these membranes form tubular vesicles called cisternae; the space within the cisternae is called the lumen (Farquhar and Palade, 1998; Staehelin and Moore, 1995; see Fig. 1.8). In our study, Golgi apparatus observed in the rotalid species' cell bodies also presented this specific organization (Fig. 1.9).

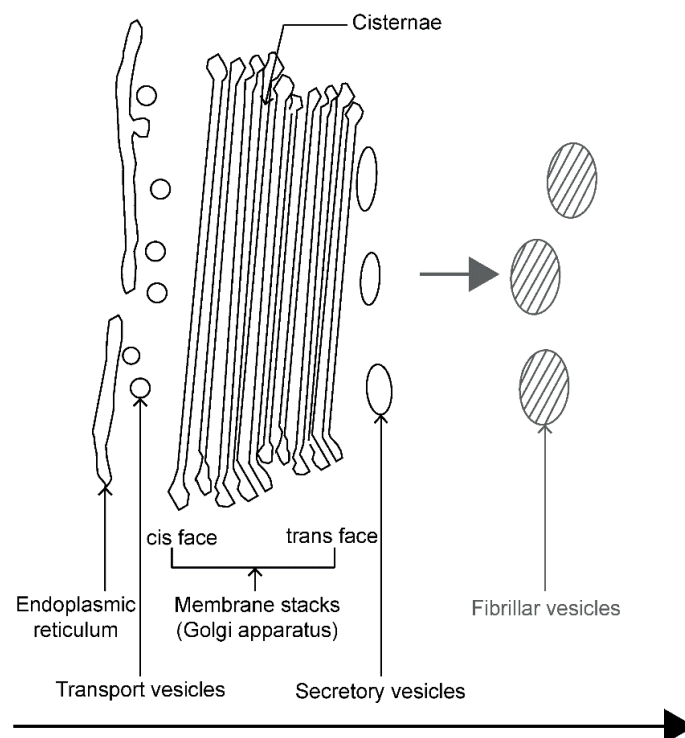


Figure 1.8: Schematic ultrastructure and relations between the reticulum endoplasmic, Golgi apparatus and fibrillar vesicles in the foraminiferal cell. The endoplasmic reticulum (ER) is secreting the transport vesicles containing the ER secretory products (proteins or lipids) which arrive on the *cis* face of the Golgi apparatus. After maturation through the Golgi saccules the proteins (or lipids) are excreted on the *trans* face in secretory vesicles. The grey part is speculative: the secretory vesicles would further be transformed into fibrillar vesicles (see details in the text). The arrow represents the direction of the metabolic process, from the secretion by the endoplasmic reticulum to the excretion in secretory vesicles and putative transformation in fibrillar vesicles. Modified from (Anderson and Lee, 1991).

The Golgi apparatus observed in our foraminiferal cells had a typical structure where the different elements described above can be clearly identified (Fig. 1.9A). The membrane stacks were made of about ten cisternae and were often surrounded by ER on the *cis* face, with spherical transport vesicles about 70 nm in diameter existed between the ER and the cisternae (Figs. 1.9A, B and C). The secretory vesicles on the *trans* face were elongated and slightly longer (150 – 200 nm) (Fig. 1.9A). Frequently, a single stack of membrane was observed (Fig. 1.9B) but groups of two and sometimes more were also noted (Fig. 1.9C).

The Golgi apparatus is a common organelle that has been described in planktonic (e.g., Anderson and Bé, 1976a; Anderson and Lee, 1991), benthic (e.g., Bernhard et al., 2010a, 2010b; Frontalini et al., 2015), and large benthic foraminifera (LBF) (e.g., Hottinger and Dreher, 1974; Leutenegger, 1977). In planktonic foraminiferal cells they may be involved in the formation of fibrillar vesicles (see section 3.3.1.).

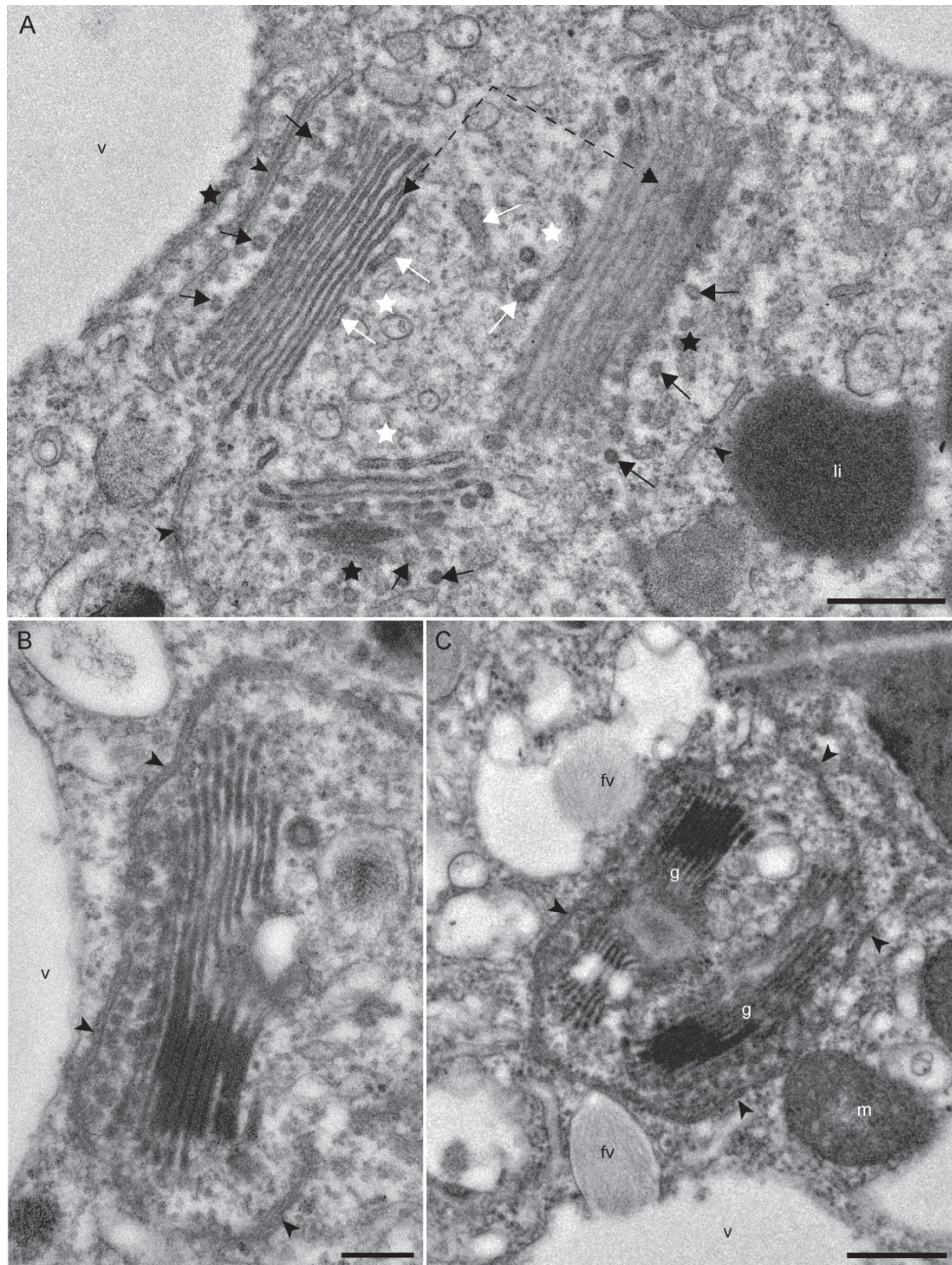


Figure 1.9: Transmission electron micrographs of benthic foraminiferal Golgi apparatus. A: Golgi apparatus made of three membrane stacks in *Stainforthia fusiformis*. B and C: Membrane stacks of Golgi apparatus alone (B) or organized in pair (C) surrounded by endoplasmic reticulum in *Nonionellina labradorica*. Black stars: cis face, white stars: trans face, arrowheads: endoplasmic reticulum, dotted arrows: cisternae, black arrows: incoming transport vesicles, white arrows: secretory vesicles, fv: fibrillar vesicles, m: mitochondria, li: lipid droplets, v: vacuoles. Scales: A, C = 500 nm; B = 200 nm.

3.2.6. Organelles involved in feeding metabolism

3.2.6.1. Degradation vacuoles

Often in the literature the degradation vacuoles containing food are described and referred to as either food vacuoles or digestive vacuoles. Anderson and Bé (1976b) and Hemleben et al. (1989) differentiated between food vacuoles and digestive vacuoles: the former are vacuoles containing food that has recently been ingested, but not yet degraded; and the latter are vacuoles in the next stage, i.e., after a food vacuole has fused with a primary lysosome carrying digestive enzymes that have triggered onset of degradation. In our study no food vacuoles with clearly identifiable food particles were observed. Concerning the digestive vacuoles, it is challenging to determine from TEM images if the source of the degraded material is an external source (food) or autophagocytosis of foraminiferal organelles (i.e., self-digestion of damaged or non-functional organelles). Thus, we do not distinguish between digestive vacuoles, and autophagocytosis and consequently lump them together under the label of “degradation vacuoles”.

Degradation vacuoles had highly variable dimensions (Figs. 1.10A, B, C and D), with diameters ranging between 2-10 μm . They were mainly localized in the younger chambers of the foraminiferal cell, close to the aperture where food is phagocytosed. They were observed in all specimens examined in this study, in varied abundances. In *Ammonia* sp. (phylotype T6), diatoms at different stages of digestion could be seen in the youngest chambers (n to $n - 5$, i.e., the last six chambers from the aperture).

The different sizes and abundances of degradation vacuoles might depend on the foraminiferal metabolism and feeding strategies. Indeed, a starved foraminifer or a foraminifer with an alternative metabolism, such as denitrification, mixotrophy, or symbiosis with algae (or bacteria) might contain fewer endoplasmic degradation vacuoles. Furthermore, the morphological appearance of these vacuoles might depend on the nature of the ingested food and/or feeding strategy (reviewed by Goldstein and Corliss, 1994). In our study, one example is illustrated by the particular appearance of degradation vacuoles in *Ammonia* sp. (phylotype T6). As *Ammonia* sp. feeds on diatoms, including the diatom frustules, the cell body portions of the youngest chambers in this species exhibited diatoms at different stages of digestion: from the nearly intact diatoms with identified organelles to empty frustules (Fig. 1.10E). Engulfed frustules have been observed in other studies of *Ammonia* spp. (Goldstein and Corliss, 1994, LeKieffre et al., 2017, second chapter) as well as in the large benthic foraminifera *Amphisorus hemprichii* and *Amphistegina lessonii* (McEnery and Lee, 1981).

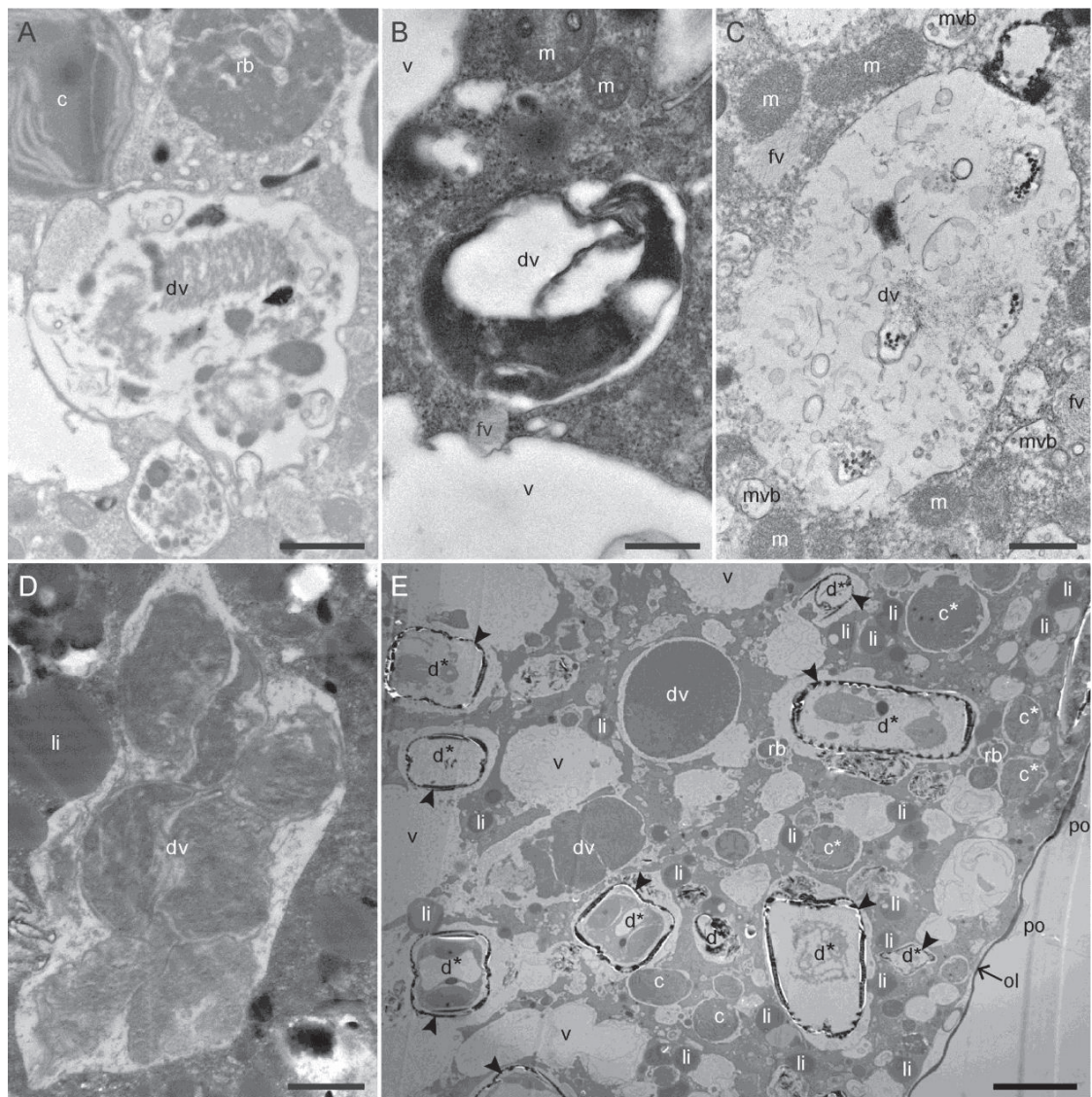


Figure 1.10: Transmission electron micrographs of different types of degradation vacuoles. Degradation vacuoles in the cytoplasm of A: *Nonionella* sp. B: *Nonionellina labradorica*, C and D: *Ammonia* sp. E: Cytoplasm of the antepenultimate chamber in *Ammonia* sp. exhibiting numerous diatom frustules (arrowheads), in which the diatom cytoplasm is being digested (d*) and diatom chloroplasts are in degradation (c*). c: chloroplasts, c*: chloroplasts in degradation, d*: diatom in degradation, dv: degradation vacuoles, fv: fibrillar vesicles, li: lipid droplets, m: mitochondria, ol: organic lining, po: pore, rb: residual bodies, v: vacuoles. Scales: A, C, D = 1 μ m; B = 500 nm; E = 5 μ m.

3.2.6.2. Residual bodies

Residual bodies are vacuoles with heterogeneous content, often with electron-dense circular particles (Hemleben et al., 1989; Leutenegger, 1977). In this study, residual bodies were circular with diameters from 1 to 5 μm (Fig. 1.11A, B), except in the species *B. marginata* where they were slightly bigger (4 to 8 μm) with irregular shapes (Fig. 1.11C). These residual bodies were observed in all species studied here, although in different abundances, and appear equivalent to the residual bodies observed in the cell body of LBF Amphisteginidae and Nummulitidae (Leutenegger 1977), and to inclusions in *Heterostegina depressa* with “strikingly inhomogeneous content” (Hottinger and Dreher (1974). Leutenegger (1977) described the residual bodies as autophagocytosis vacuoles, i.e., autolysis vacuoles containing foraminiferal organelles in degradation. Note that there was no clear evidence for degrading organelles in any of the residual bodies observed in this study. In general, it is difficult to establish if the electron-dense particles inside these residual bodies result from the degradation of external material (food) or from foraminiferal organelle autophagocytosis. Hemleben et al. (1989) described residual bodies as vacuoles containing non-digestible debris, which is consistent with the observed accumulation of isotopic labeled compounds derived from diatoms in residual bodies of *Ammonia* sp. (LeKieffre et al., 2017, second chapter). Le Cadre and Debenay (2006) and Morvan et al. (2004) noted that residual bodies proliferated when *Ammonia tepida* specimens were under stress from different forms of pollution or contamination of their environment.

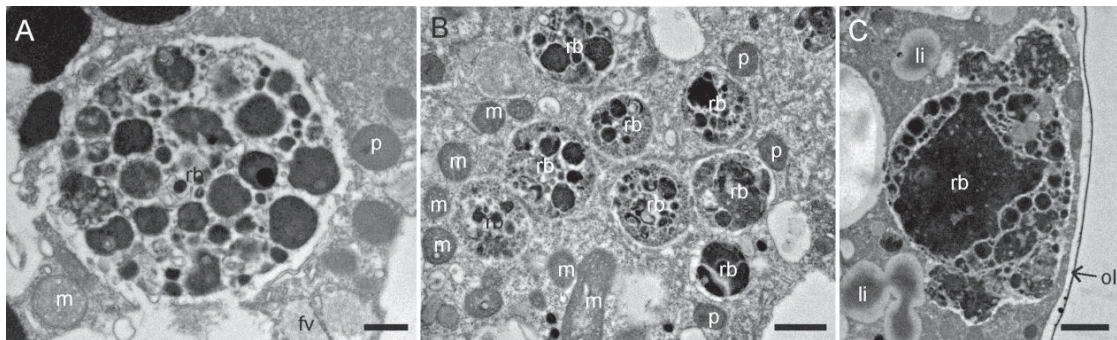


Figure 1.11: Transmission electron micrographs of benthic foraminiferal residual bodies. A: Round shaped residual body in *Nonionella* sp. B: High abundance of residual bodies in the cytoplasm of *Nonionellina labradorica*. C: Irregular shaped residual body in *Bulimina marginata*. fv: fibrillar vesicles, m: mitochondria, ol: organic lining, p: peroxisomes, rb: residual bodies. Scales: A = 500 nm; B, C = 1 μm .

3.2.6.3. Lipid droplets

Lipid droplets were often spheroidal (Fig. 1.12A), but can take a variety of shapes in the cytoplasm (Fig 1.12B, C). A particular feature of lipid droplets was the absence of apparent enclosing membrane(s). Sizes vary from about 500 nm to 10 μm in diameter, with an average diameter approximately 2 μm . In nearly all specimens studied by us, a few lipid droplets were observed in degradation (i.e., part of the lipid droplet was missing, 'replaced' by apparently empty space in the TEM micrographs; Fig. 1.12B). Sometimes the opacity of the lipid droplets was not uniform; it could be brighter on the periphery than in the center, as observed, e.g., in *N. labradorica* and *B. marginata* (Figs. 1.12C and D).

Described as the primary carbon storage in foraminiferal cells (Hottinger, 1982; Hottinger and Dreher, 1974; Leutenegger, 1977; Pawlowski et al., 1995), lipid droplets are osmiophilic vesicles and thus they appear electron dense in TEM micrographs. The level of opacity depends on the osmium tetroxide (OsO_4) concentration of incubation media, as well as on the degree of fatty acid saturation, which might explain observed variations among different species, assuming identical sample preparation procedures, including OsO_4 staining (which is the case in our study). Metabolic state and diet can contribute to this variability. LeKieffre et al. (2017, second chapter) have demonstrated a clear link between lipid droplets and food in digestive vacuoles by tracing ^{13}C -enrichment from ingested food, via degradation vacuoles, to lipid droplets.

Lipid droplet distribution in the cell body in the present study was in agreement with previous studies. Anderson and Lee (1991) also observed such droplets in all chambers, except in the last (youngest) and penultimate chambers, from where benthic foraminifera extend their reticulopods. The proportion of lipid droplets in a state of degradation is highly variable, likely depending on metabolic state of the individual. In a 28-day incubation in which foraminifera were fed only once, at the beginning of the experiment, LeKieffre et al. (2017, second chapter) observed how lipid droplets were initially formed and then were gradually consumed nearly to the point of disappearance.

A relatively high abundance of lipids has been observed under stressful conditions in different experimental studies testing the response of foraminifera to heavy-metal contamination (Frontalini et al., 2015; Le Cadre and Debenay, 2006) and anoxia (Koho et al. this special issue). Finally, lipid droplets with a brighter periphery were also observed in the case of contamination with lead and described as "electron-dense core lipid vacuoles" (Frontalini et al., 2015). In our study we suggest that the lipid brighter at the periphery observed in *N. labradorica* and *B. marginata* could be a fixation artifact, although we are not able to explain it.

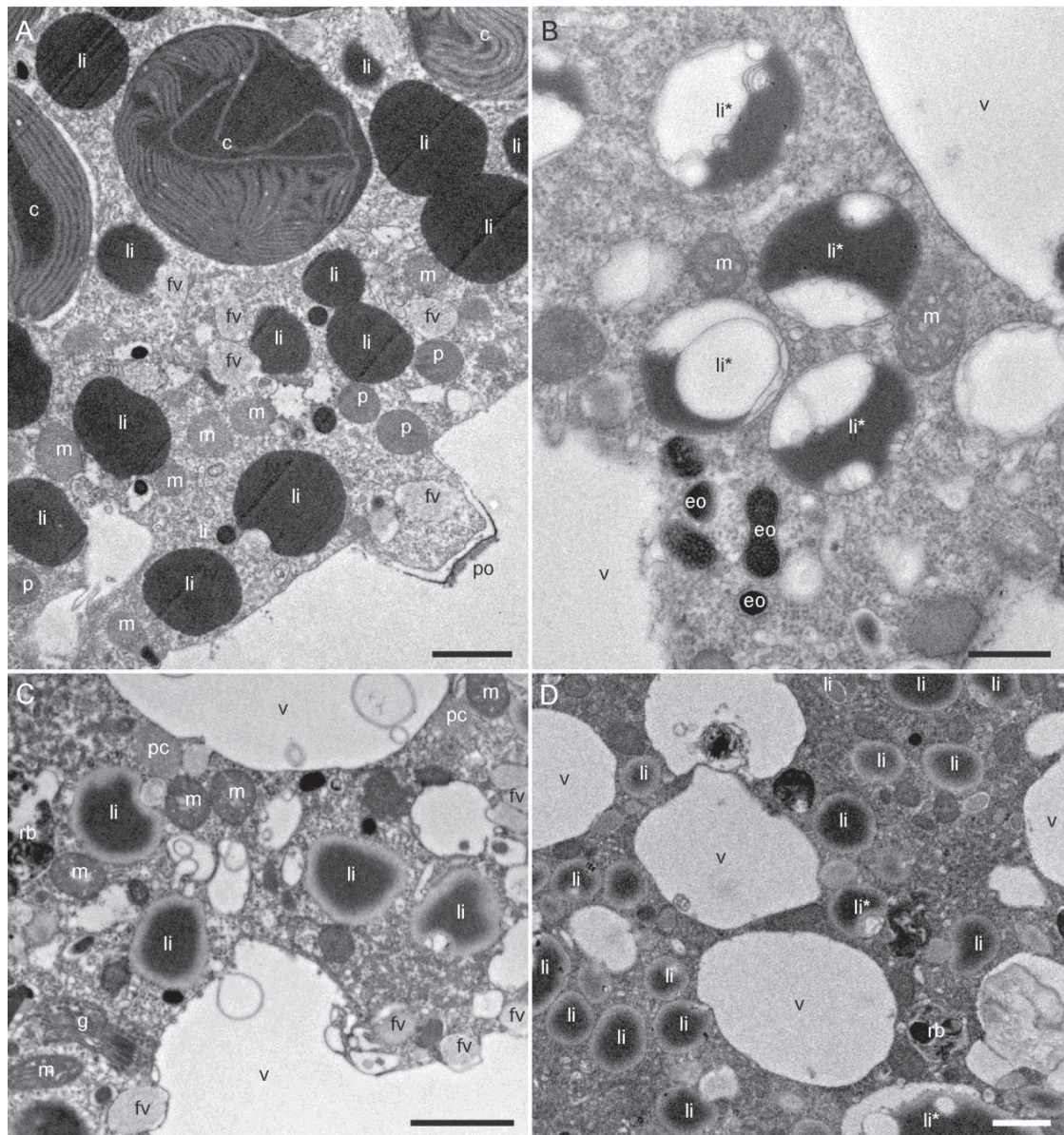


Figure 1.12: Transmission electron micrographs of benthic foraminiferal lipid droplets. A: Lipid droplets in the cytoplasm of *Nonionella* sp. B: Lipid droplets in degradation in *Nonionellina labradorica*. C, D: Less electron-opaque lipid droplets at the periphery of *Nonionellina labradorica* (C) and *Bulimina marginata* (D). c: chloroplasts, eo: electron-opaque bodies, fv: fibrillar vesicles, li: lipid droplets, li*: degraded lipid droplets, m: mitochondria, p: peroxisomes, po: pore, rb: residual bodies, v: vacuoles. Scales: A, C, D = 1 μ m; B = 500 nm.

3.2.7. Paracrystals of tubulin

Paracrystals of tubulin provide the cell with molecular building blocks for their microtubular network supporting, e.g., the foraminiferal reticulopods (reviewed in Travis and Bowser, 1991), which are the primary mean of foraminiferal food acquisition. They are elongated structures from 2 to 50 μm in length (Fig. 1.13A) and recognizable due to their regular organization at high magnification (Fig. 1.13B), sometimes exhibiting regular crystalline pattern akin to a honeycomb structure (Figs. 1.13C and D) depending on the plane of section. We observed these structures in the cell body of Gullmar Fjord species *N. labradorica*, *Nonionella* sp. and *Globobulimina* sp. (Fig. 1.13A), but not in intertidal foraminiferal species. Note that the higher density of the cell body in the latter might have partially obstructed their observation. Our observations are similar to the paracrystals in the cell body and reticulopodial net of other benthic foraminiferal species (reviewed in Travis and Bowser, 1991).

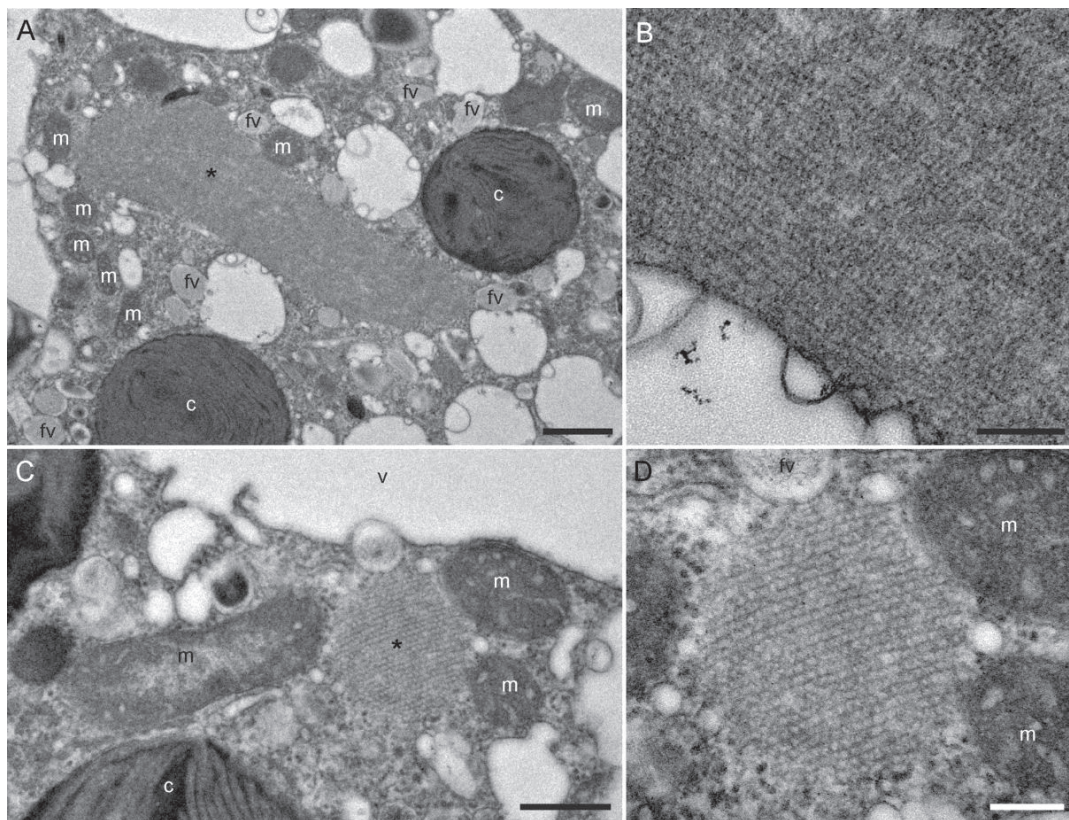


Figure 1.13: Transmission electron micrographs of paracrystals of tubulin in the cytoplasm of *Nonionellina labradorica*. A: Longitudinal section of a tubulin paracrystal. B: High-magnification image revealing the regular pattern of the crystalline structure observed in A. C: Cross section of the crystalline structure. D: High-magnification image revealing the regular pattern of the crystalline structure observed in C. Asterisks: paracrystals of tubulin, c: chloroplasts, fv: fibrillar vesicles, li: lipid droplets, m: mitochondria. Scales: A = 1 μm ; B, D = 200 nm, C = 500 nm.

3.3. Organelles with unknown function

3.3.1. Prokaryotes and sequestered chloroplasts

Many benthic foraminiferal species are known to have prokaryotic associates and/or sequester chloroplasts in their cytoplasm (see Bernhard et al., submitted, Jauffrais et al., (chapter 3.1) for reviews). The prokaryotes seemingly can be symbionts beneficial to the host foraminifer or can be parasites, which are detrimental to the foraminiferal host. Kleptoplasts are believed to confer considerable advantage to the foraminiferal host. While the role of these subcellular entities clearly impacts the foraminifer, details on the functions of these structures are not well understood. We refrain from further discussion of these entities and direct the reader to the noted publications.

3.3.2. Fibrillar vesicles

Fibrillar vesicles were abundant in all foraminiferal species observed in this study (Fig. 1.14A). These structures are small oval vesicles approximately 500 nm in length. They contained fibrils that, depending on the cutting plane, appeared as thin threads or as nanometer-scale spots (Fig. 1.14B). In some TEM micrographs, we observed a space between the fibrils and the membrane enclosing them (Fig. 1.14C), which may be a fixation artifact. Fibrillar vesicles were sometimes observed to exocytose into white “empty” vacuoles or to be fused with residual bodies (Figs. 1.14D, E, F and G).

First described by Angell (1967), small fibrillar vesicles have been observed both in planktonic and benthic foraminifera throughout the cell body as well as in the reticulopods (Anderson and Bé, 1976a; Goldstein and Barker, 1988; Hemleben et al., 1989; Leutenegger, 1977). Different authors have hypothesized that the fibrillar vesicles are formed by the stacks of membranes of the Golgi apparatus (Anderson and Bé, 1976b, 1976a; Anderson and Lee, 1991; Leutenegger, 1977) (Fig. 8). Similar fibrillar vesicles were also observed in dinoflagellate cells (Dodge, 1974; Leadbeater and Dodge, 1966) where they were identified as Golgi vesicles. Langer (1992) hypothesized that the fibrillar vesicles are involved in the transport of glycosaminoglycans (GAGs; sulfated polysaccharides) from their production site in the Golgi apparatus, to the place they would be used. Some studies have argued that the fibrillar vesicles could play a role in the secretion of mucilaginous substances for the reticulopods (Anderson and Bé, 1976b, 1976a). Because of the small size of fibrillar vesicles and their abundance in the peripheral cytoplasm of the species studied, Leutenegger (1977) suggested a role in the formation of organic matrix, such as organic linings, which seems consistent with observations of high densities of fibrillar vesicles in the last chamber of foraminifera, prior the formation of a new chamber in planktonic foraminifera (Angell, 1967; Leutenegger, 1977; Spero, 1988).

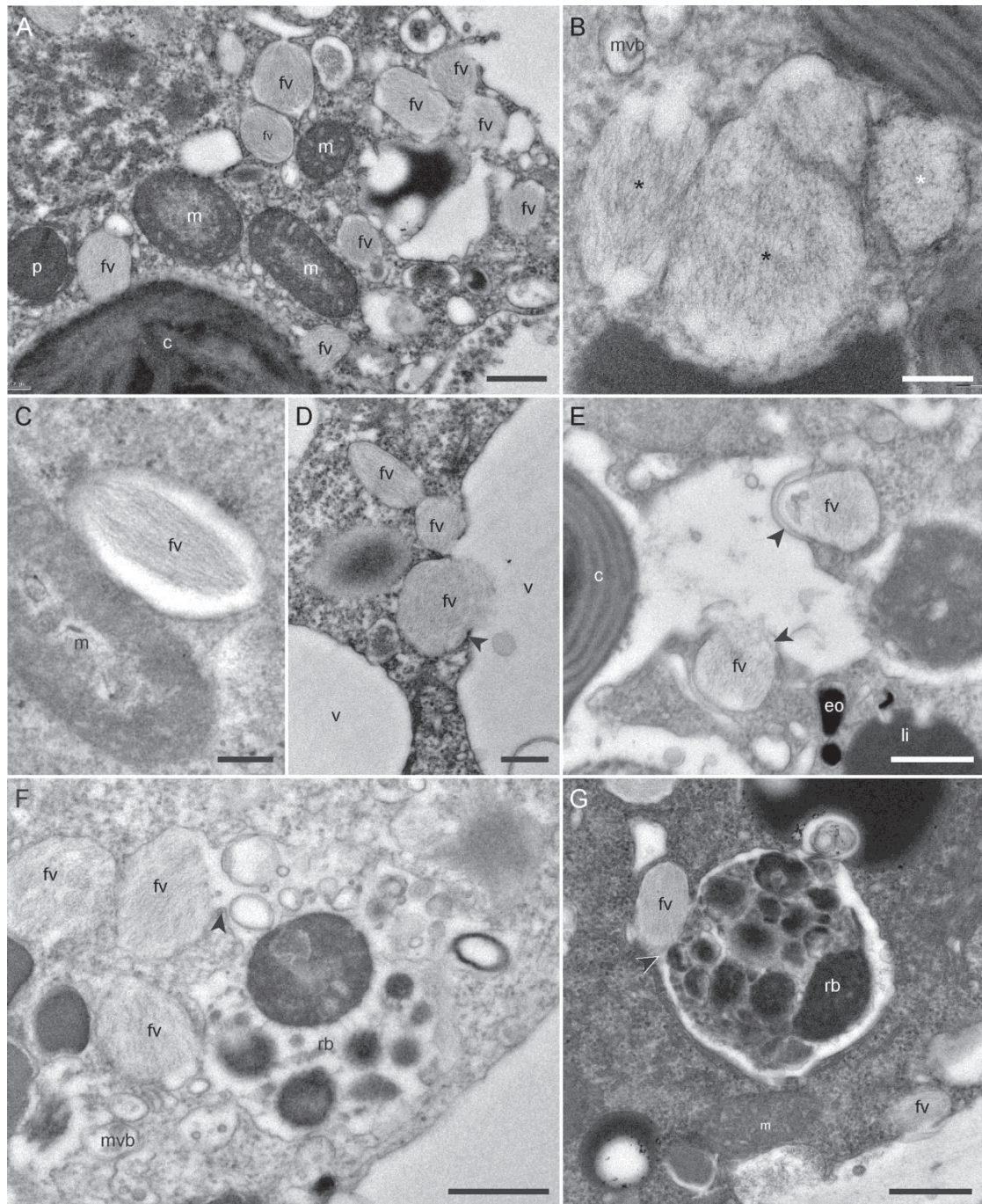


Figure 1.14: Transmission electron micrographs of benthic foraminiferal fibrillar vesicles. A: Fibrillar vesicles in the cytoplasm of *Nonionellina labradorica*. B: High-magnification image of a group of fibrillar vesicles in *Nonionella* sp.; sections parallel (black asterisks) or perpendicular (white asterisk) to the fibrils. C: Fibrillar vesicle surrounded by a space between the fibrils and the vesicle membrane in *Haynesina germanica*. D and E: Fibrillar vesicles merging with vacuoles (arrowheads) in D: *Nonionellina labradorica* and E: *Nonionella* sp. F and G: Fibrillar vesicles merging with residual bodies (arrowheads) in F: *Stainforthia fusiformis* and G: *Nonionellina labradorica*. c: chloroplast, eo: electron-opaque bodies, li: lipid droplet, m: mitochondria, mvb: multivesicular bodies, p: peroxisomes, rb: residual body, fv: fibrillar vesicles. Scales: A, E, F, G = 500 nm; B, C, D = 200 nm.

Note that the fibrillar vesicles observed here differ from the fibrillar system (also called fibrillar bodies or microvillus system) observed in planktonic foraminifera (Anderson and Bé, 1976a; Anderson and Lee, 1991; Hemleben et al., 1989; Leutenegger, 1977; Spero, 1988). The fibrillar system in planktonic foraminifera is made of larger fibrillar bodies, which are vacuoles containing larger fibrils with a tubular aspect; possibly serving as flotation devices (Anderson and Bé, 1976a; Hemleben et al., 1989; Leutenegger, 1977), or playing a role as Ca storage vacuoles (Spero, 1988).

3.3.3. Electron-opaque bodies

Electron-opaque bodies are small (200 to 500-nm in diameter) spherical (Fig. 1.15A) to oval-shaped (Fig. 1.15B) dense bodies. Some of these bodies were surrounded by a seemingly empty space and a membrane (Figs. 1.15A-C, G-H); the space below the membrane could be due to shrinkage during chemical fixation. Others did not seem to possess a space below the membrane (Figs. 1.15C-H), and they are so electron-opaque that the presence of a membrane is difficult to establish. Such electron-opaque bodies, i.e., with or seemingly without membrane, were observed in the cell body of all species studied here, sometimes equally distributed but occasionally clustered at the cell periphery, as in *Ammonia* sp. cell body (Fig. 1.15C). The visualization of the membrane might also depend on the plane section view and could explain that it was clearly visible in some cases, and sometimes not.

We assume that whether or not they possess a seemingly empty space and a membrane, all the electron-opaque bodies are in fact the same structure, but further studies are required. Leutenegger (1977) did not differentiate the osmiophilic granules observed in the cell body of larger foraminifera, whether a membrane could be distinguished or not (e.g., Plate 17, Fig. c; Plate 29, Fig. d and Plate 43, Figs. b and c in Leutenegger 1977). The Leutenegger osmiophilic granules were approximately the same size as the electron-opaque bodies observed in our study. It is noted that these structures occur in the TEM micrographs of several publications, both on planktonic and benthic foraminiferal cells, although they have not always been described (e.g., Anderson and Bé, 1976a; Bernhard et al., 2010; Hemleben et al., 1989; Le Cadre and Debenay, 2006). They may correspond to the “electron-dense bodies” surrounded by membranes observed by Nomaki et al. (2016), who observed these structures clustered close to the cell periphery, but only in specimens incubated in anoxia. Although their role is not understood, it has been shown that these structures had a relatively high sulfur content when compared to other types of organelles (Nomaki et al., 2016).

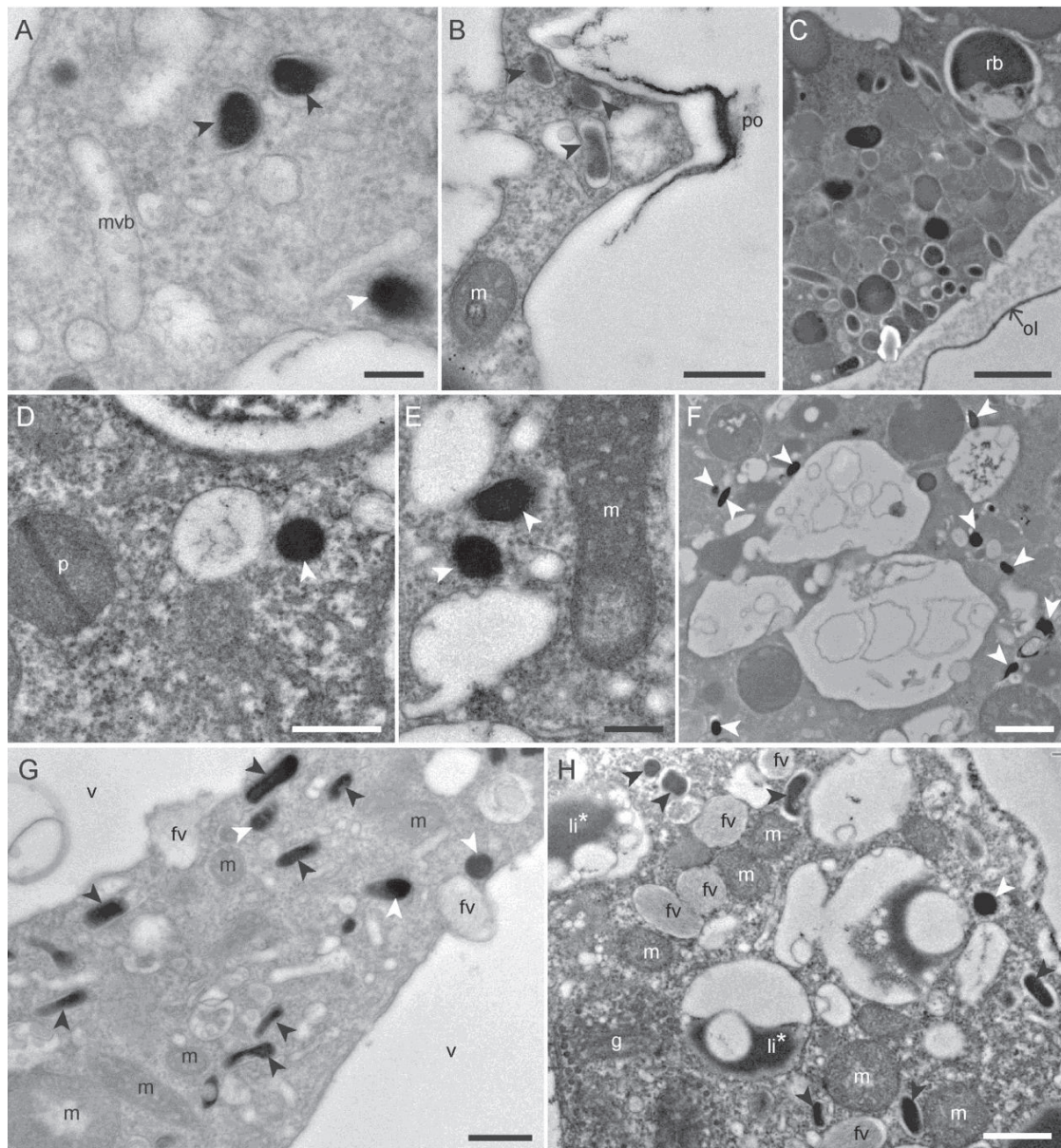


Figure 1.15: Transmission electron micrographs of benthic foraminiferal electron-opaque bodies. A and B: Electron-opaque bodies with membranes (black arrowheads) in the cytoplasm of A: *Nonionella* sp. and B: *Nonionellina labradorica*. C: Clusters of electron-opaque bodies in the cytoplasm of *Ammonia* sp. C, D and E: Electron-opaque bodies without distinguishable membranes (white arrowheads) in the cytoplasm of C, D: *Nonionellina labradorica* and E: *Haynesina germanica*. G, H: Both shapes of electron-opaque bodies in the cytoplasm of G: *Nonionella* sp. and H: *Nonionellina labradorica*. Black arrowheads: electron-opaque bodies with membranes, white arrowheads: indistinguishable membrane electron-opaque bodies, fv: fibrillar vesicles, g: Golgi apparatus, li*: lipid droplets in lysis, m: mitochondria, mvb: multivesicular bodies, p: peroxisomes, rb: residual bodies, v: vacuoles. Scales: B, D-F = 500 nm; A, G = 200 nm; C, H: 1 µm.

3.3.4. Multivesicular bodies

Multivesicular bodies are tiny spheroidal vacuoles with a diameter of 200 – 500 nm (Figs. 1.16A and B). They contain vesicles of 10 to 50 nm; the number of these vesicles can vary from one or two to more than a dozen per multivesicular body. They were observed in the cell body of all the species studied here and were more abundant in the younger chambers (arrowheads in Fig. 1.16B).

The role and function of these multivesicular bodies are unknown. These structures could correspond to the multivesicular bodies in the microtubule-transport model of Langer (1992 [Fig. 3]). Vesicles attached to microtubules were also observed by Anderson and Lee (1991, [Fig 27]), although they were simply referred to as “vesicles”. They could also correspond to the “fuzzy coated vesicles” associated with microtubules in the reticulopods (Bowser and Travis, 2000 [Fig. 2b]; Travis and Allen, 1981 [Fig. 3]; Travis and Bowser, 1991 [Fig. 9]): these fuzzy coated vesicles are more elongated than spheroids but their size is similar to the structures observed here. Similar vesicles were also observed in the canal plasma of *Operculina ammonoides*. However, in that case, the vesicles were associated with microtubules (Hottinger and Dreher, 1974 [Fig. 11]). Finally, the same kind of vesicles was also seen in the reticulopodial net of *Peneroplis planatus* and near a pore in *Amphistegina lobifera* (Leutenegger, 1977 [Plate 45, Fig. a; Plate 52, Fig. a]). All these observations are consistent with the higher abundances of multivesicular bodies in younger chambers. Whatever their function, it seems that multivesicular bodies are ubiquitous among benthic foraminiferal species.

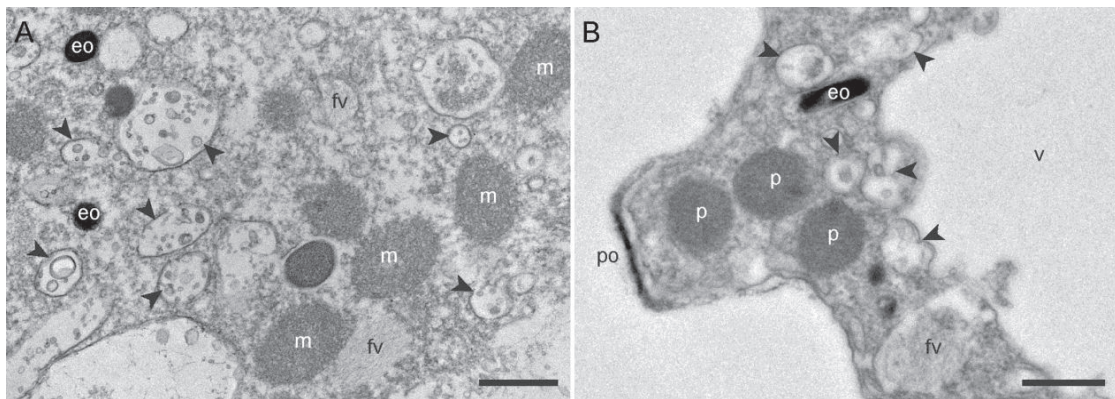


Figure 1.16: Transmission electron micrographs of benthic foraminiferal multivesicular bodies. Multivesicular bodies in the cytoplasm of A: the penultimate chamber of one *Ammonia* sp. specimen and B: *Nonionella* sp. Black arrowheads: multivesicular bodies, eo: electron opaque bodies, fv: fibrillar vesicles, m: mitochondria, p: peroxisomes. Scales: A, B = 500 nm.

4. Conclusion

The ultrastructure of foraminifera is highly variable among species. First, the overall aspect of the cell body is variable, mainly because of the absence/presence and abundance of large vacuoles. Second, although organelles involved in basic functioning of the cell (e.g., nucleus, mitochondria, ER, Golgi apparatus, peroxisomes) are present in all the species, their appearance, size, abundance, or location vary. Third, the degradation vacuoles are found in all the species studied here but because there are many different types of feeding metabolism, there are also many different types of degradation vacuoles. Moreover, the physiological state (environmental stress, starvation state, stage in the reproduction cycle, etc.) of a specimen can have an impact on its cellular ultrastructure, resulting in ultrastructural variations within conspecifics (Koho et al., in press; Frontalini et al., in press).

Finally, this work emphasizes the need for further ultrastructural investigations to determine the role of recurrent but poorly understood organelles, such as fibrillar vesicles, electron-opaque bodies, or multivesicular bodies, as well as the metabolic interactions between all types of organelles.

Acknowledgements:

Florence Manero from the SCIAM platform at the University of Angers (France), the electron microscopy platform at the University of Lausanne (Switzerland), and the crew of the R/V Skagerak are thanked for help and technical assistance. We are also grateful for the help and advice provided by Stan Fakan (Laboratory for Biological Geochemistry at EPFL) and Thierry Jauffrais (LPG-BIAF, Angers University) as well as comments on an earlier manuscript version from two anonymous reviewers. This contribution was edited by Prof. Richard Jordan.

Funding sources:

This work was supported by the Swiss National Science Foundation (grant no. 200021_149333) and The Investment in Science Fund at WHOI.

Chapter 2: Surviving anoxia in marine sediments: The metabolic response of ubiquitous benthic foraminifera (*Ammonia tepida*)

Chapter 2 presents an article published in the journal PLoS ONE (LeKieffre et al., 2017). The feeding metabolism of a benthic foraminiferal species is investigated and compared between oxic and anoxic conditions. This article can be access online: <https://doi.org/10.1371/journal.pone.0177604>

PhD student's contribution: the PhD student collected the samples from the field designed the Experiment I with EG; analyzed and interpreted data of Experiment I with GM and EG; designed the Experiment II with JS, AM and EG; analyzed the TEM-NanoSIMS results, interpreted the NanoSIMS results with SE and AM, performed the statistical analysis; discuss the results with EG, JS and AM and wrote the manuscript with comments and edits from all the authors. JS analyzed and interpreted fatty acids and IRMS results and was a major contributor in writing the manuscript.

Surviving anoxia in marine sediments: The metabolic response of ubiquitous benthic foraminifera (*Ammonia tepida*)

Charlotte LeKieffre^{1,*}, Jorge E. Spangenberg², Guillaume Mabilieu³, Stéphane Escrig¹,
Anders Meibom^{1,4,*}, Emmanuelle Geslin^{5,*}

¹ Laboratory for Biological Geochemistry, School of Architecture, Civil and Environmental Engineering (ENAC), Ecole Polytechnique Fédérale de Lausanne (EPFL), Lausanne, Switzerland

² Stable Isotope and Organic Geochemistry Laboratories, Institute of Earth Surface Dynamics (IDYST), University of Lausanne, Lausanne, Switzerland

³ Service commun d'imageries et d'analyses microscopiques (SCIAM), Institut de Biologie en Santé, University of Angers, Angers, France

⁴ Center for Advanced Surface Analysis, Institute of Earth Sciences, University of Lausanne, Lausanne, Switzerland

⁵ UMR CNRS 6112 - LPG-BIAF, University of Angers, Angers, France

* Corresponding authors

Abstract

High input of organic carbon and/or slowly renewing bottom waters frequently create periods with low dissolved oxygen concentrations on continental shelves and in coastal areas; such events can have strong impacts on benthic ecosystems. Among the meiofauna living in these environments, benthic foraminifera are often the most tolerant to low oxygen levels. Indeed, some species are able to survive complete anoxia for weeks to months. One known mechanism for this, observed in several species, is denitrification. For other species, a state of highly reduced metabolism, essentially a state of dormancy, has been proposed but never demonstrated. Here, we combined a 4 weeks feeding experiment, using ¹³C-enriched diatom biofilm, with correlated TEM and NanoSIMS imaging, plus bulk analysis of concentration and stable carbon isotopic composition of total organic matter and individual fatty acids, to study metabolic differences in the intertidal species *Ammonia tepida* exposed to oxic and anoxic conditions. Strongly contrasting cellular-level dynamics of ingestion and transfer of the ingested biofilm components were observed between the two conditions. Under oxic conditions, within a few days, intact diatoms were ingested, degraded, and their components assimilated, in part for biosynthesis of different cellular components: ¹³C-labeled lipid droplets formed after a few days and were subsequently lost (partially) through respiration. In contrast, in anoxia, fewer diatoms were initially ingested and these were not assimilated or metabolized further, but remained visible within the foraminiferal cytoplasm even after 4 weeks. Under oxic conditions, compound specific ¹³C analyses showed substantial *de novo* synthesis by the foraminifera of specific polyunsaturated fatty acids

(PUFAs), such as 20:4(*n*-6). Very limited PUFA synthesis was observed under anoxia. Together, our results show that anoxia induced a greatly reduced rate of heterotrophic metabolism in *Ammonia tepida* on a time scale of less than 24 hours, these observations are consistent with a state of dormancy.

Keywords: Benthic foraminifera, Anoxia, Dormancy, NanoSIMS, Mass spectrometry, Fatty acids, Cell ultrastructure

1 Introduction

Benthic foraminifera are eukaryote unicellular protists and ubiquitous in marine sediments from shallow water estuaries to the deep ocean (Murray, 2006). Representing up to 50 % of top sediment biomass, they constitute an important part of benthic meiofauna (Gooday et al., 1992; Snider et al., 1984) and may play a significant role in the carbon and nitrogen cycles, depending on the habitat, species assemblage, and feeding patterns (Gooday et al., 1990, 2008; Moodley et al., 2008; Woulds et al., 2007). The broad spectrum of conditions under which marine foraminifera live includes zones of O₂-depletion (Caulle et al., 2014; Gooday et al., 2000; Høglund et al., 2008; Mallon et al., 2012), deep-sea sulphidic habitats (Bernhard, 2003), hydrocarbon seeps (Sen Gupta et al., 1997; Sen Gupta and Aharon, 1994), and intertidal environments (Debenay et al., 2000). Of particular interest here is the striking capability of some benthic foraminifera to adapt to a sudden decrease in the availability of O₂. Hypoxic and anoxic events strongly and more frequently affect benthic ecosystems, in particular on continental shelves and in coastal areas where renewal of bottom water is slow and/or organic input is high (Diaz and Rosenberg, 2008; Helly and Levin, 2004; Rabalais et al., 2010). During such events, large fractions of the benthic meio- and macrofauna (size range >1 mm) can die off (Bianchi et al., 2000; Josefson and Widbom, 1988; Stachowitsch, 1991; Wetzel et al., 2001). However, foraminifera are consistently among the most resistant species (Gooday et al., 2000; Levin et al., 2009; Moodley et al., 1997). High survival rates of foraminifera under low O₂ conditions have been documented both *in-situ* (Bernhard and Gupta, 2003; Bernhard and Reimers, 1991; Glud et al., 2009; Kitazato and Ohga, 1995; Langlet et al., 2013) and in laboratory experiments (Heinz and Geslin, 2012; Nardelli et al., 2014) and ascribed, in part, to relatively low rates of O₂-respiration compared to other meiofauna species (Geslin et al., 2011). Experimental studies of *Ammonia* sp. combining TEM and NanoSIMS observations suggest higher global metabolic activity in hypoxia than in anoxia (Nomaki et al., 2016). Various anaerobic pathways have been suggested as alternative metabolic strategies to achieve resistance to low-O₂ conditions, including symbiosis with ectobionts (Bernhard, 2003; Bernhard et al., 2010a) or endobionts (Nomaki et al., 2014), and sequestered chloroplasts (Bernhard and Bowser, 1999; Grzymski et al., 2002). It has been demonstrated that some species are capable of nitrate respiration (denitrification) under anoxia (Kamp et al., 2015; Piña-Ochoa et al., 2010a; Risgaard-Petersen et al., 2006). Bernard et al. (Bernhard and Alve, 1996) observed a decrease of the adenosine 5'-triphosphate (ATP) pool in foraminifera *Bulimina marginata*, *Stainforthia fusiformis* and *Adercotryma glomeratum* from Drammensfjord (Norway) exposed to anoxia, and suggested that this might indicate a state of dormancy. Indeed, dormancy or quiescence, defined as reduced or suspended metabolic activity in response to exogenous factors, might be a more widespread adaptation strategy of benthic foraminifera to environmental stress than previously acknowledged (Ross and Hallock, 2016). Even

during periods with normal oxic conditions in bottom waters, foraminifera and other benthic meiofauna species can be (and frequently are) exposed to low O₂ levels simply because bioturbation mechanically moves them deeper into the sediments (Bouchet et al., 2009; Jorissen, 1999). *Ammonia tepida*, for example, which is among the most abundant species in intertidal sediments (Debenay et al., 2000) is normally residing in the top few centimeters of the sediments, where O₂ concentration is high. Here, it grazes on algal biofilm (Pascal et al., 2008a). However, *A. tepida* is also regularly found alive at depths of 4 to 26 cm, *i.e.* below the O₂ penetration depth, as a result of bioturbation (Alve and Murray, 2001; Thibault de Chanvalon et al., 2015). These observations raise questions about the mechanism(s) that enable foraminifera to survive sudden changes to anoxia, often for extended periods of time.

In this study, we present results of two experiments: Experiment I aimed to determine the survival and growth rates of algae-fed *A. tepida* under anoxia, compared with oxic conditions. Experiment II aimed to investigate the metabolism of *A. tepida* following a sudden shift to anoxic conditions. In the latter experiment, using ¹³C-enriched diatom-containing biofilm and a combination of transmission electron microscopy (TEM) and NanoSIMS isotopic imaging, we have visualized and quantified with subcellular resolution (*in situ, ex vivo*) the incorporation and transfer of isotopically labeled heterotrophic compounds, under both oxic and anoxic conditions. These subcellular-level observations were combined with concentrations and stable carbon isotopic analysis by isotope ratio mass spectrometry of total organic carbon (TOC) and individual fatty acids. Our results are discussed in context of previous experiments using ¹³C-labeled food, which have already yielded important insights into the metabolism of foraminifera under a variety of environmental conditions (Enge et al., 2014; Larkin et al., 2014; Linshy et al., 2014; Moodley et al., 2000; Nomaki et al., 2005b, 2006, 2009; Pascal et al., 2008b).

2 Results

2.1 Experiment I: Survival and growth rate of *A. tepida* under oxic and anoxic conditions

After 13 days of incubation, the survival rates of fed adult or juvenile specimens of *A. tepida* were indistinguishable ($p > 0.05$) between oxic and anoxic conditions (2.S1 Fig): 95 ± 11 % and 87 ± 12 % for adults and 84 ± 2 % and 83 ± 8 % for juveniles, respectively. The average growth rate of juvenile specimens was significantly ($p < 0.05$) higher under oxic (1.3 ± 0.7 % per day) compared with anoxic (0.2 ± 0.1 % per day) conditions (2.S2 Fig). The growth rate under anoxic conditions was not significantly different from zero (t -test, $p > 0.05$).

2.2 Experiment II: Feeding behavior of *A. tepida* under oxic and anoxic conditions

Under anoxic conditions the foraminifera rapidly (within around 24 hours) ceased to move. At the end of the incubation there was still diatom biofilm left in the vials in the anoxic aquarium, while the biofilm had been completely consumed by the foraminifera in the oxic aquarium.

Under oxic conditions, the average total organic carbon (TOC) content per cell of the *A. tepida* specimens increased during the first 7 days from 0.65 ± 0.06 to 1.29 ± 0.14 $\mu\text{g C} \times \text{ind}^{-1}$ (Fig 2.1A). At this point it was observed that all the biofilm had been ingested. After 14 days, the TOC content had decreased to 1.10 ± 0.18 $\mu\text{g C} \times \text{ind}^{-1}$ and continued to decrease to reach a value of 0.94 ± 0.05 $\mu\text{g C} \times \text{ind}^{-1}$ at the end of the experiment (*i.e.* Day 28). Under anoxia the TOC content showed a modest increase during the first 3 days of the incubation, reaching maxima of 1.0 ± 0.1 $\mu\text{g C} \times \text{ind}^{-1}$. At Day 7, the TOC had dropped to 0.8 ± 0.1 $\mu\text{g C} \times \text{ind}^{-1}$ and this level was maintained for the rest of the experiment ($p > 0.05$) (Fig 2.1A).

Average ^{13}C atomic fractions in TOC ($x(^{13}\text{C})_{\text{TOC}}$ in %) as a function of time are shown in Fig 2.1. Under both oxic and anoxic conditions, a sharp ^{13}C -enrichment indicating an uptake of ^{13}C -enriched diatoms occurred at the beginning of the experiment, reaching plateaus on different time scales. Under oxic conditions, a sharp increase in $x(^{13}\text{C})_{\text{TOC}}$ up to 1.86 ± 1.16 % occurred during the Day 1, followed by a slower increase to 2.24 ± 1.22 % on Day 7, after which $x(^{13}\text{C})_{\text{TOC}}$ stabilized ($p > 0.05$). Under anoxia, $x(^{13}\text{C})_{\text{TOC}}$ increased to 1.41 ± 1.18 % during the Day 1, after which no statistically significant changes were observed ($p > 0.05$). The final $^{13}\text{C}_{\text{TOC}}$ -enrichment was about 4 times higher under oxic than anoxic conditions.

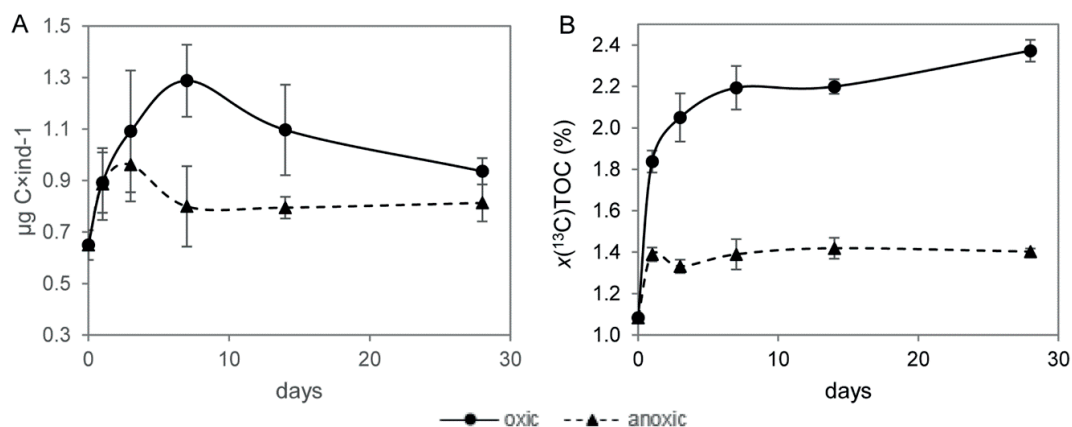


Figure 2.1: TOC concentration and ^{13}C atomic fraction of *A. tepida* under oxic and anoxic conditions. (A) Average total organic carbon (TOC in $\mu\text{g C} \times \text{ind}^{-1}$) concentration and (B) ^{13}C atomic fraction of the TOC ($\chi(^{13}\text{C})_{\text{TOC}}$ in %), both as a function of time. Continuous lines: oxic conditions, dotted lines: anoxic conditions. Error bars are ± 1 SD ($n=3$).

Average carbonate uptake (calculated as the difference in C content of the shells in individuals from Day 28 and control specimens) and the enrichment in ^{13}C of the shells from Day 28 over that of control samples are given in 2.S1 Table. Under oxic conditions, an average of $4.9 \pm 1.8 \mu\text{g C} \times \text{ind}^{-1}$ was added to the shells over 28 days and their average $\chi(^{13}\text{C})_{\text{car}}$ was 0.05 % higher than the unlabeled control samples. Under anoxia, the specimens did not add new carbonate to their shells and therefore no significant $^{13}\text{C}_{\text{car}}$ -enrichment was observed ($p > 0.05$), consistent with a growth rate statistically indistinguishable from zero (Fig 2.1B).

Results of TEM and NanoSIMS analyses are presented in Figs 2.2 and 2.3. The figure 2.S3 exhibits typical cellular structures in the antepenultimate chamber of an *A. tepida* specimen collected directly from the mudflat that provided samples for Experiment II. Recognizable structures include lipid droplets, residual bodies, and diatomic frustules. The presence of mitochondria and the integrity of intact double membranes and crests indicated vitality at the time of the chemical fixation; all observed specimens exhibited these ultrastructures. Time sequences of TEM and NanoSIMS isotopic images permit to follow the ingestion and metabolism of isotopically enriched diatom biofilm components under oxic and anoxic conditions (Figs 2.2 and 2.3). Fig 2.4 shows the relative surface areas occupied by diatoms, lipid droplets, and residual bodies in a representative cytoplasm area, with the corresponding average ^{13}C atomic fractions for each structural component.

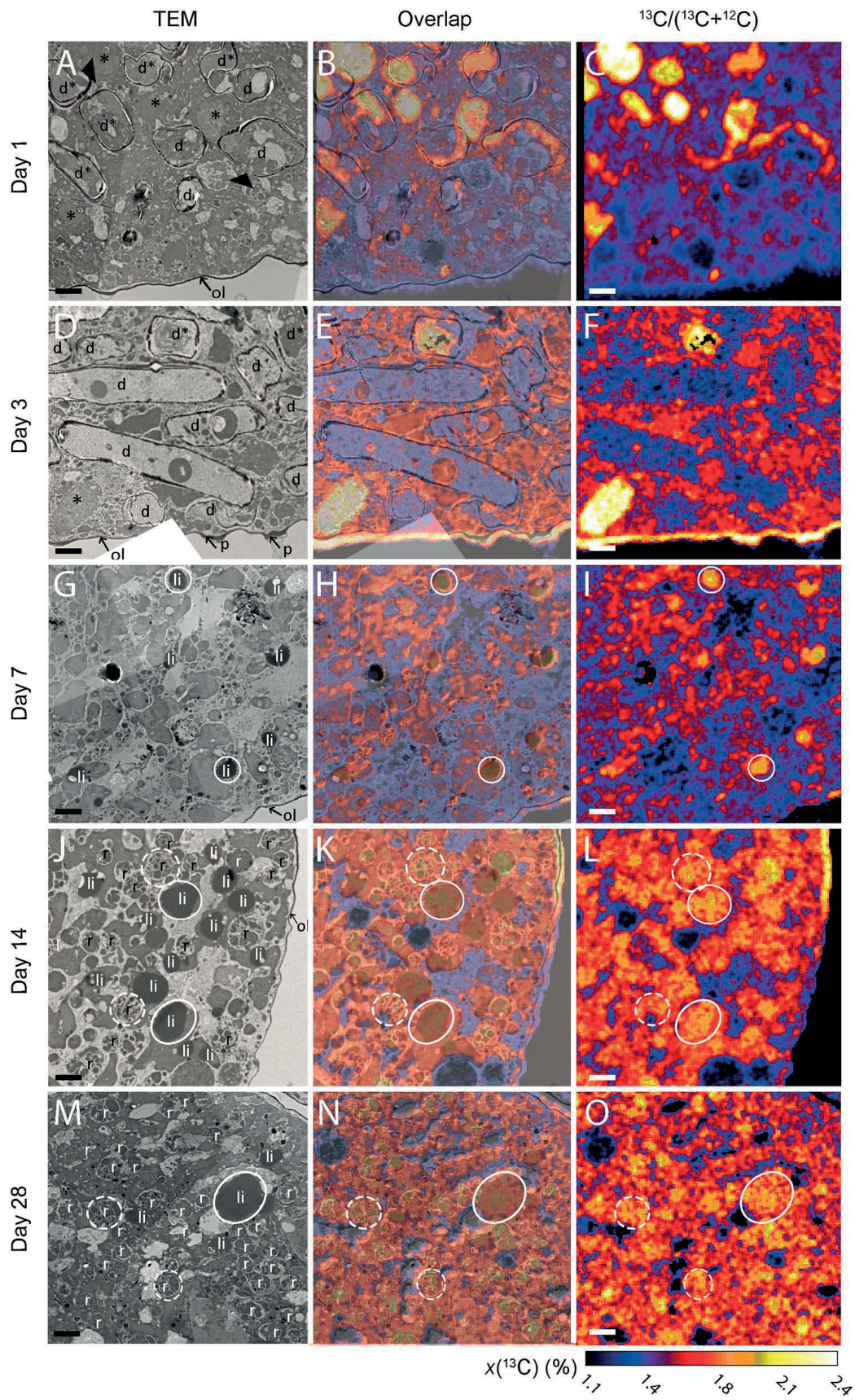
Under oxic conditions, abundant diatoms with frustules were visible after Day 1 as free-floating objects (i.e. not surrounded by vesicles/vacuoles) that occupied about 30 % of the cytoplasm area (Figs 2.2A and 2.4A). About 75 % of these ingested diatoms still held their original cellular matrix, which was clearly distinguishable by strong ^{13}C enrichment; the remaining 25 % had lost their content to the foraminiferal cytoplasm (Figs 2.2A-C, Table 2.1). After Day 3, diatom frustules were still clearly observable (Fig 2.2D), but ca. 83 % of them had lost their original content of cellular matrix (Figs 2.2D-F, Table 2.1). After Day 7, frustules were no longer observed (Figs 2.2G, J, and M). However ^{13}C -enriched lipid droplets (not observed before Day 7) were numerous (Fig 2.4C). Between Day 7 and 14, lipid droplets were present in roughly constant abundance (ca. 10 %; Fig 2.4C) with $\delta^{13}\text{C}$ of approximately 1.65 ‰ (Fig 2.4D). After Day 28 only a few lipid droplets were observed in the cytoplasm of the foraminifera (Figs 2.2M and 2.4C). In contrast, ^{13}C -enriched residual bodies appeared after Day 14 (Figs 2.2J and 2.4F) occupying about 5 % of the cytoplasm area with an average ^{13}C atomic fraction around 1.70 ‰ (Figs 2.4E-F); this did not significantly change before the end of the experiment ($p>0.05$). In 5 out of 15 observed foraminifera cells, the organic lining (i.e. the thick membrane between the plasma membrane and the calcite shell) was enriched in ^{13}C (Figs 2.2E, F, K and L); two of these had the ^{13}C -enrichment of their organic lining concentrated in the vicinity of pores in the shell.

Table 2.1: Percentage of intact diatoms (frustule containing cytoplasm) in the foraminiferal cytoplasm. Percentage of the diatoms present in the cytoplasm of *A. tepida* still holding their original cellular contents, as a function of time for both experimental conditions ($n=3$).

Days	Diatoms filled with diatomic material (%)	
	Oxic	Anoxic
1	75 \pm 11	91 \pm 8
3	17 \pm 10	73 \pm 22
7	0	28 \pm 22
14	0	17 ^a
28	0	47 \pm 46

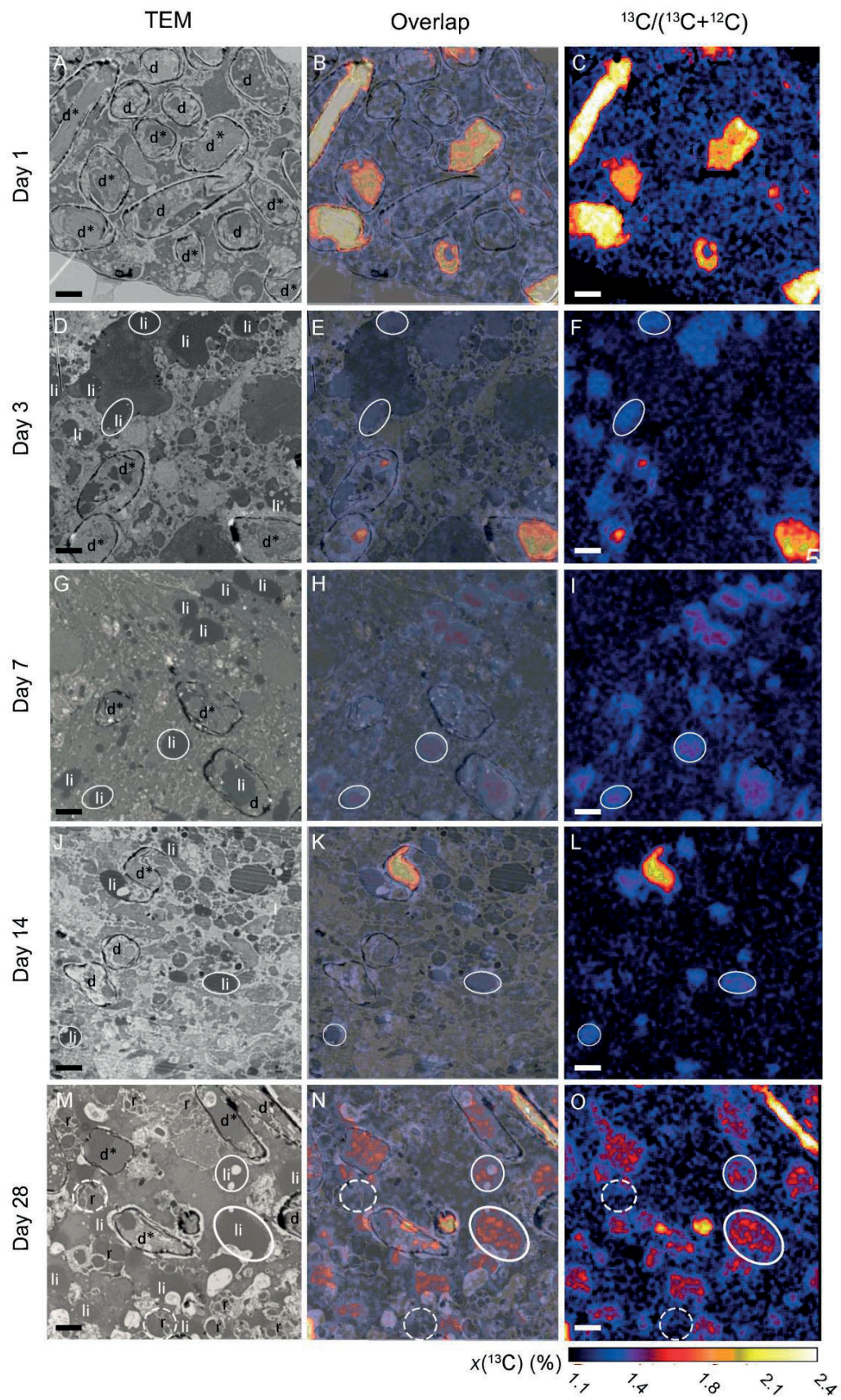
^a : diatoms were present only in 1 of the 3 specimens analyzed, SD could not be calculated.

Figure 2.2 (p. 74): Time-evolution of ^{13}C uptake and transfer within the cytoplasm of *A. tepida* under oxic conditions. A, D, G, J and M: TEM images; C, F, I, L and O: NanoSIMS images of corresponding $^{13}\text{C}/^{12}\text{C}$ distributions. B, E, H, K, and N: Direct correlation of TEM and NanoSIMS images. d*: Intact diatoms; d: frustules without their original contents; *: diatomic material free in the foraminiferal cytoplasm; li: lipid droplets; ol: organic lining; p: pores; r: residual bodies. Arrowheads show aperture of opened diatom frustules. Circles are drawn around a few organelles to facilitate their visualization on the different images: white circles: lipid droplets, dotted circles: residual bodies. Scale bars: 2 μm .



Under anoxic conditions, the content of the foraminiferal cytoplasm after Day 1 was essentially identical to that observed at the same time under oxic conditions (Fig 2.3A). No lipid droplets or residual bodies were visible, and the cytoplasm was occupied by ^{13}C -labeled intact diatoms (*i.e.* diatomic material surrounded by the silica frustule; roughly 30 % of the imaged area) (Figs 2.3A-C and 2.4A-B). However, the fraction of ingested diatoms still containing their original ^{13}C -labeled material was higher under anoxic conditions (roughly 91 % vs. 75 %; Table 2.1). After Day 3 diatoms were still observed in the cytoplasm (Fig 2.3D) with about 75 % of them containing original cellular materials; *i.e.*, 4 times more than under oxic conditions at the same time point (Table 2.1). The proportion of diatoms in the foraminifera cytoplasm remained roughly constant between Days 3 and 28, in the range from 3 to 12 % (Fig 2.4A). Among these, the proportion containing original ^{13}C -labeled material decreased to ca. 30 % between Days 3 and 7, and then did not significantly change until the end of the experiment ($p>0.05$; Table 2.1). Lipid droplets appeared after Day 3 under anoxic conditions, in contrast to Day 7 under oxic conditions (Figs 2.3D and 2.4C). Their proportion in the cytoplasm varied between 4 % and 19 % with corresponding average ^{13}C atomic fractions between 1.27 % and 1.38 %; *i.e.* 2 to 3 times less ^{13}C -enrichment than under oxic conditions (Figs 2.4C D). Residual bodies, which were observed only in specimens sampled on Day 28, and only in 2 out of 3 imaged foraminifera, were much less abundant (4 ± 4 %) than under oxic conditions (Figs 2.3M and 2.4E). Most of these residual bodies were only slightly enriched, with an average $\delta(^{13}\text{C})$ of 1.20 ± 0.03 ‰ compared to 1.69 ± 0.14 ‰ under oxic conditions (Fig 2.4F).

Figure 2.3 (p. 76): Time-evolution of ^{13}C uptake and transfer within the cytoplasm of *A. tepida* under anoxic conditions. A, D, G, J and M: TEM images; C, F, I, L and O: NanoSIMS images of corresponding $^{13}\text{C}/^{12}\text{C}$ distributions. B, E, H, K, and N: Direct correlation of TEM and NanoSIMS images d*: Intact diatoms; d: frustules without their original contents; *: diatomic material free in the foraminiferal cytoplasm; li: lipid droplets; ol: organic lining; p: pores; r: residual bodies. Arrowheads show aperture of opened diatom frustules. Circles are drawn around a few organelles to facilitate their visualization on the different images: white circles: lipid droplets, dotted circles: residual bodies. Scale bars: 2 μm .



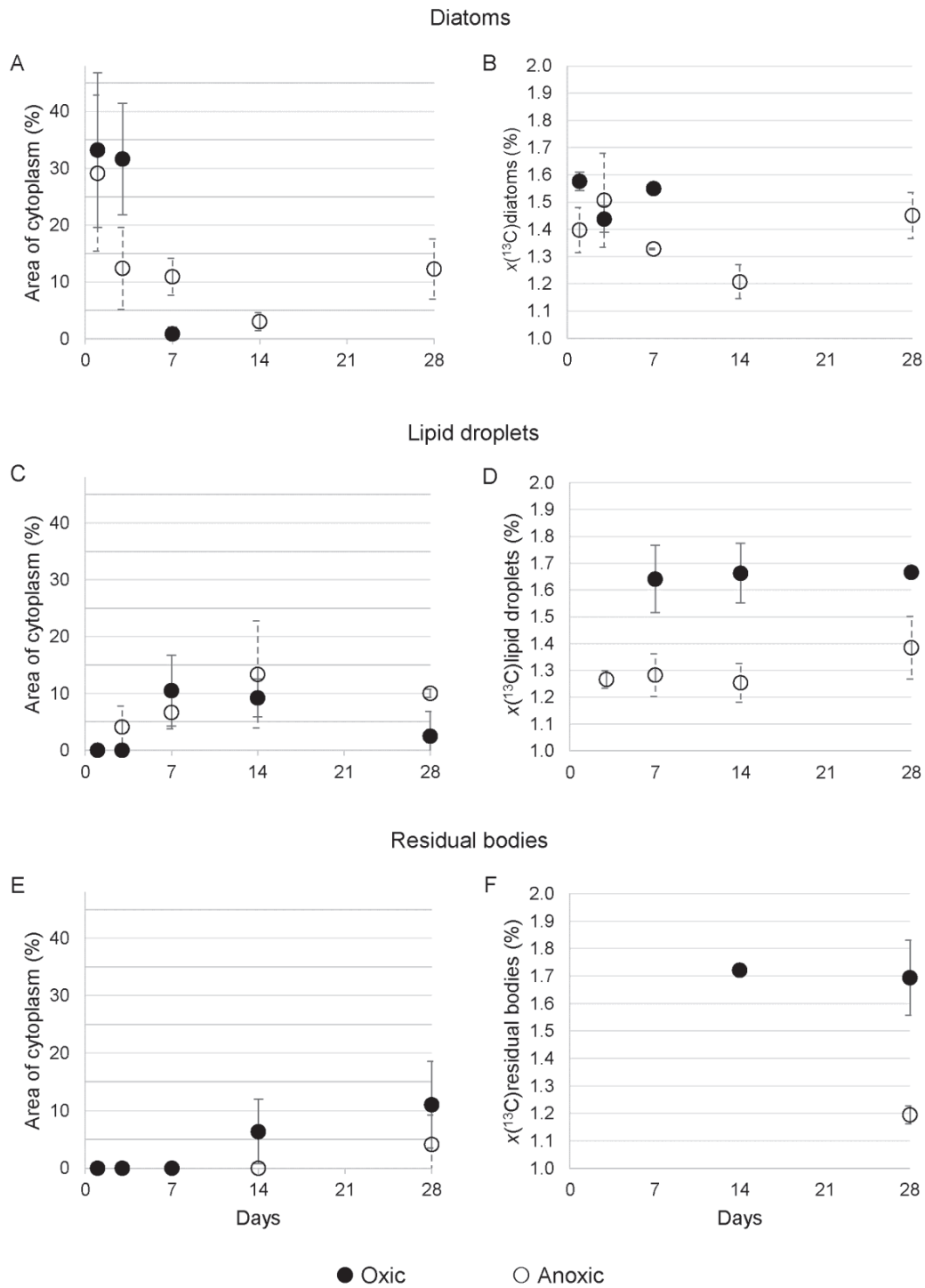


Figure 2.4: Percentages of cytoplasmic occupation and ^{13}C atomic fraction of key cell ultrastructures. Percentage of occupation of cytoplasm area (A, C and E) and ^{13}C atomic fraction ($x(^{13}\text{C})$ in %; B, D and F) over time for key components in *A. tepida*: A, B: diatoms; C, D: lipid droplets; E, F: residual bodies. Errors bars are ± 1 SD ($n=3$).

Fatty acids (FAs) studied here included triglycerides, phospholipid and free acids, as well as other acid lipids extracted from diatom and foraminifera samples. In the following, FAs are abbreviated as x:y(z) where 'x' is the number of carbon atoms, 'y' the number of double bonds and 'z' the position of the double bond relative to the terminal methyl group. The main saturated FAs in the labeled diatom biofilm were 14:0 and 16:0, with relative abundances of 7.4 % and 28.2 %, respectively (Fig 2.5A). The mono-unsaturated FAs 16:1 and 18:1 (isomers) were observed in relative abundances of 42.0 and 3.8 %, respectively (Fig 2.5A). The sums of all the positional (mainly *n*-9, *n*-7 and *n*-5) and geometric (*cis* and *trans*) isomers of hexadecenoic and octadecenoic acid were included in the designations 16:1 and 18:1. The main polyunsaturated FAs (PUFA) were 20:5(*n*-3) (9.6 %) with trace amount of 20:4(*n*-6) and 22:5(*n*-3) and 22:6(*n*-3), which accounted for less than 0.2 % of the total FAs.

Table 2.2: Concentrations of fatty acids in *A. tepida*. Concentrations in ng×ind⁻¹ of the fatty acids found in *A. tepida* cell before the experiment (control), after Day 7 and Day 28; under oxic and anoxic conditions.

Fatty acid	Control	Oxic		Anoxic	
		7 days	28 days	7 days	28 days
Total	322.6±22.4	408.3±33.5	344.24±31.8	360.1±22.1	380.8±13.1
14:0	27.0±1.8	25.7±1.5	22.3±2.4	27.2±0.9	28.4±0.8
15:0	4.8±0.2	4.1±0.3	3.4±0.2	4.9±0.2	5.2±0.4
15:1		1.5±0.2	2.2±0.4		
16:0	66.7±4.3	97.3±7.4	81.1±8.2	74.1±5.7	77.0±3.4
16:1	49.1±3.8	51.1±6.4	21.2±3.5	64.0±5.1	64.9±2.7
16:2	11.4±0.8	9.3±3.3	3.2±2.7	14.0±0.4	14.7±0.4
16:3	3.1±0.2	2.9±0.5		2.9±0.3	3.3±0.5
17:0	3.3±0.4	1.1±0.3		3.4±0.2	3.6±0.1
17:1	3.2±0.4	3.7±0.3	2.8±0.2	2.1±1.3	2.3±1.5
18:0	8.6±0.4	14.6±1.5	11.3±0.5	8.3±1.5	8.7±0.4
18:1	27.9±2.2	48.1±4.95	37.6±5.5	28.7±2.5	22.9±1.3
18:2(<i>n</i> -6)	5.2±0.6	6.4±0.6	3.4±0.4	5.3±0.4	5.6±0.4
18:4(<i>n</i> -3)	3.4±0.3	3.1±0.2	2.2	4.3±0.3	4.7±0.1
20:1(<i>n</i> -9)	4.1±0.2	6.2±0.6	4.6±0.2	3.9±0.7	4.3±0.1
20:4(<i>n</i> -3)	2.6±0.2	2.6±0.2	3.0±0.1	2.9±0.2	2.9±0.2
20:4(<i>n</i> -6)	26.2±1.8	40.4±2.5	58.7±5.0	33.2±2.5	39.0±2.0
20:5(<i>n</i> -3)	62.3±4.3	75.6±6.3	72.5±7.5	66.6±4.3	71.7±3.1
22:6(<i>n</i> -3)	8.7±0.7	9.6±0.7	8.7±0.7	9.7±0.4	10.8±0.2
22:5(<i>n</i> -3)	4.8±0.4	6.9±0.3	9.3±0.6	5.3±0.3	5.9±0.3

All analyzed foraminifera samples showed roughly similar FAs distributions in the C₁₄ to C₂₂ range. The observed small quantities of odd-chain and traces or complete absence of branched-chain FAs indicate minimal bacterial contamination. In the control foraminifera, the most abundant saturated FAs were 14:0, 16:0 and 18:0, with a preference for 16:0 (Table 2.2 and Figs 2.5B and C). The most abundant monounsaturated FA was 16:1 and the most abundant PUFAs were 20:4(*n*-6) and 20:5(*n*-3) (Table 2.2 and Fig 2.5).

Under oxic conditions, the FA content in foraminifera increased during the first 7 days from 322±22 to 408±33 ng×ind⁻¹ ($p<0.05$), and then decreased to 344±32 ng×ind⁻¹ after Day 28 ($p<0.1$ between 7 and 28 days) (Table 2.2). Under anoxia, the total foraminifera FA content continuously increased during the experiment from 322±22 up to 380±13 ng×ind⁻¹ ($p<0.05$) (Table 2.2). Under oxic conditions, the relative abundances of 16:0 and 18:1 isomers increased between 0 and 7 days ($p<0.05$), and remained stable between Day 7 and 28 (Fig 2.5B). The relative abundances of 14:0 and 16:1(*n*-7) decreased between Days 0 (control) and 7 ($p<0.05$). Between Days 7 and 28, the relative abundance of 14:0 remained constant, while that of 16:1(*n*-7) continued to decrease. The abundance of 20:5(*n*-3) first decreased between Days 0 (control) and 7, and then increased to its highest level at Day 28 ($p<0.05$) (Fig 2.5B). Despite being present in small amounts in the diatom biofilm, the PUFAs 20:4(*n*-6) and 22:5(*n*-3) significantly increased in relative abundance along the experiment ($p<0.05$); most pronounced for 20:4(*n*-6) from 8.1 % in the control to 17.1 % (Fig 2.5A-B). Significant variation in the abundance of 22:6(*n*-3) was not observed during the experiment ($p>0.05$).

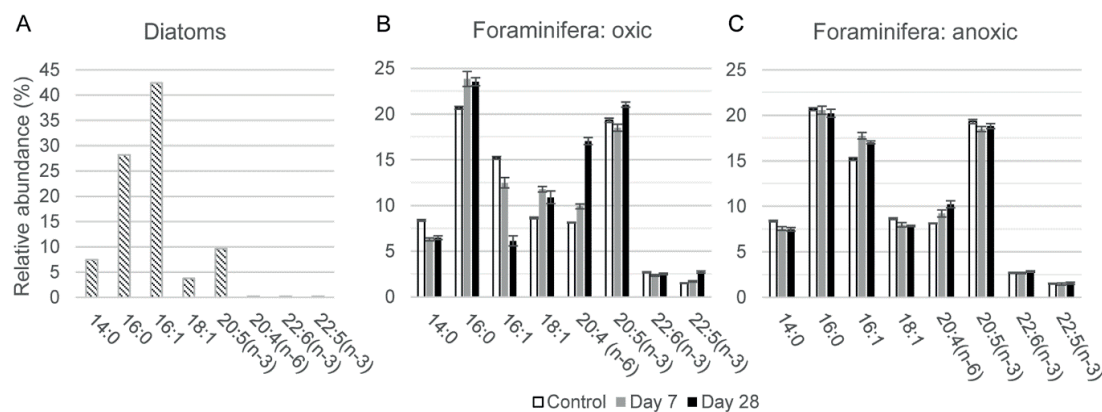


Figure 2.5: Relative abundances (%) of the dominant fatty acids extracted from the biofilm of diatoms and in *A. tepida* endoplasm. Relative abundances (expressed in %) of the eight dominant FAs extracted from the biofilm of diatoms and in *A. tepida* individuals incubated under oxic (B) and anoxic (C) conditions, respectively. White: control specimens; grey: after Day 7 and black: after Day 28. Error bars are ±1 SD ($n=3$).

Under anoxia, the relative variations in the abundance of individual FAs with time were significantly smaller than those observed under oxic conditions (Fig 2.5C). Only the abundance of 14:0 decreased slightly during the experiment, with a trend similar to that observed under oxic conditions. No significant changes ($p>0.05$) were observed in the contents of 16:0, 22:5($n-3$), and 22:6($n-3$) during the experiment. 16:1($n-7$) first increased slightly, then decreased from Day 7 to Day 28 ($p<0.05$). 18:1 abundance first decreased at Day 7 ($p<0.05$), and stabilized ($p>0.05$). 20:4($n-6$) was the only FA that showed a significant, albeit minor increase (from 8.1 ± 0.1 to 10.2 ± 0.4 %; $p<0.05$) along the experiment.

The ^{13}C atomic fraction of FAs ($\delta^{13}\text{C}_{\text{FA}}$ in ‰) are shown in Table 2.3. These ^{13}C -enrichments were significantly higher after Day 7 of incubation ($p<0.05$) under both conditions and in general FAs ^{13}C -enrichments were higher under oxic than anoxic conditions.

Table 2.3: ^{13}C atomic fraction of dominant fatty acids in the cytoplasm of *A. tepida*. ^{13}C atomic fraction ($\delta^{13}\text{C}$ in ‰) of dominant fatty acids in the cytoplasm of *A. tepida* ($n=2$) for oxic and anoxic conditions at Days 7 and 28.

Fatty acid	Control	Oxic		Anoxic	
		Day 7	Day 28	Day 7	Day 28
14:0	1.08 ± 0.01	1.81 ± 0.04	1.89 ± 0.02	1.32 ± 0.07	1.37 ± 0.02
16:0	1.08 ± 0.01	2.07 ± 0.07	2.01 ± 0.11	1.85 ± 0.06	1.92 ± 0.04
16:1	1.08 ± 0.01	2.25 ± 0.04	2.23 ± 0.04	1.40 ± 0.06	1.41 ± 0.02
18:1	1.08 ± 0.01	2.31 ± 0.01	2.39 ± 0.05	1.47 ± 0.10	1.23 ± 0.01
20:4($n-6$)	1.08 ± 0.01	1.77 ± 0.04	1.93 ± 0.04	1.28 ± 0.05	1.33 ± 0.02
20:5($n-3$)	1.08 ± 0.01	2.01 ± 0.04	2.03 ± 0.05	1.33 ± 0.01	1.39 ± 0.02
22:6($n-3$)	1.08 ± 0.01	1.69 ± 0.03	1.72 ± 0.01	1.22 ± 0.01	1.31 ± 0.02
22:5($n-3$)	1.08 ± 0.01	1.74 ± 0.03	1.85 ± 0.01	1.15 ± 0.01	1.18 ± 0.01

3 Discussion

3.1 Survival and growth

No significant difference was observed between the survival rate of fed *A. tepida* specimens incubated for 13 days under oxic and anoxic conditions (2.S1 Fig). This is in line with results of previous laboratory experiments showing that *A. tepida* is capable of surviving under strong hypoxia and anoxia for extended time periods, up to 60 days (Geslin et al., 2014; Nardelli et al., 2014). Growth of *A. tepida* under anoxia was assessed by three different methods: (i) measurement of juvenile shell size before and after incubation (2.S2 Fig), (ii) quantification of the carbonate content in shells of adult specimens, and (iii) shell ^{13}C -enrichment (2.S1 Table). The results consistently showed that on average *A. tepida* grew and added at least one chamber under oxic conditions, whereas only minimal, if any growth took place under anoxia. A previous study using incubation with calcein labeled foraminifera to detect chamber formation showed that among adult *A. tepida* living under anoxic conditions for 60 days, only 5 % were able to add one chamber (Nardelli et al., 2014). These observations clearly indicate that a strong perturbation of normal physiological processes results from a shift to anoxia.

3.2 Feeding and metabolism: bulk data

Under oxic conditions, the TOC and its ^{13}C -fraction increased by almost 100 %, within the first 7 days in fed, adult *A. tepida* (Fig 2.1). Similar TOC values are reported in the literature quantifying the rate of ingestion of diatoms (Linshy et al., 2014), indicating an important role for benthic foraminifera in the organic carbon cycle in shallow, O_2 -rich marine sediments. After Day 7 under oxic conditions, the TOC began to decrease steadily while its ^{13}C -enrichment remained constant (Fig 2.1), consistent with the visual observation that the food source had been exhausted. From this point onward, the TOC values decreased (*i.e.* cells lost weight), as their reserves of organic C (mainly in the form of lipid droplets) were metabolized and respired. This metabolic consumption of organic matter did not change the ^{13}C content of the residual TOC, indicating that no preferential respiration or preservation of organic compounds with different isotopic composition took place.

Under anoxia *A. tepida* ingested ^{13}C -enriched diatom biofilm only during Day 1. During this time, the ^{13}C -enrichment of the TOC increased by about 30 % and the average of TOC content per cell increased from the control value of $0.65 \mu\text{g C} \times \text{ind}^{-1}$ to about $0.9 \mu\text{g C} \times \text{ind}^{-1}$ (Fig 2.1). In contrast to the results from the corresponding oxic experiment, neither the TOC nor its ^{13}C -enrichment changed substantially after Day 1, consistent with the visual observation that feeding stopped, *i.e.* left over biofilm was not further consumed. Furthermore, the TOC per cell did not decrease (Fig 2.1), providing strong indication that metabolic loss of carbon was minimal after Day 1.

Recent studies with ingestion of phytodetritus under strong hypoxia (O_2 levels around 0.02 mL/L) have documented both ingestion and metabolism in species from the Arabian Sea oxygen minimum zones (OMZ) (Enge et al., 2014; Larkin et al., 2014). The fact that foraminifera metabolism seems relative insensitive to hypoxic conditions might be due to their low rate of oxic respiration compared to other benthic meiofauna (Geslin et al., 2011). A picture emerges of benthic foraminifera capable of maintaining an efficient metabolism even under strong hypoxia, while complete anoxia leads to a shutdown of aerobic metabolic processes on a timescale of less than 24 hours.

3.3 Feeding and metabolism: subcellular observations

Key sub-cellular structures of *A. tepida* involved in ingestion and metabolism include the ingested diatoms, residual bodies, and lipid droplets (2.S3 Fig), the latter representing the principal form of carbon storage (Hottinger, 1982; Hottinger and Dreher, 1974; Pawlowski et al., 1995). Fully intact diatoms (*i.e.* with the diatom cell-material still contained in its silica frustule) were directly integrated into the cytoplasm by the foraminifera during the first day under both conditions (Figs 2.2A-C and 2.3A-C), consistent with previous observations of feeding *A. tepida* (Goldstein and Corliss, 1994) and a number of other species (Bé et al., 1977; Goldstein and Corliss, 1994; McEnery and Lee, 1981). Nevertheless, the density in the cytoplasm of ingested diatoms observed in our study was substantially higher than previously reported in the literature, with ca. 30 % of the cytoplasm area occupied by intact diatoms after Day 1 under both conditions. This might be ascribed to the fact that the foraminifera had been fasting during the 6 days between the initial collection on the mudflat and the start of the feeding experiment, thus they grazed quickly on the available biofilm at the beginning of the incubation.

Following the efficient ingestion of intact diatoms during Day 1, the sub-cellular TEM and NanoSIMS observations for oxic and anoxic conditions diverged dramatically (Figs 2.2 and 2.3). Under oxic conditions, the intact diatom frustules were all emptied and their ^{13}C -enriched contents incorporated into other subcellular components before Day 7. On Day 7, the silica frustules had almost entirely disappeared (Figs 2.2G and 2.4A). The process by which the foraminifera break down the frustules remains unknown. Exocytosis of the empty frustules was not observed, nor frustules being degraded.

Part of the organic diatomic material was converted into fatty acids stored in clearly ^{13}C -labeled lipid droplets (Figs 2.2G-I, 2.4C and D). After Day 7, the ^{13}C -labeled diatomic material had become part of the metabolic pathways and ^{13}C -enrichment had spread into most components of the cytoplasm (Figs 2.2I, L, O). Consistent with the observed decrease in TOC after Day 7 (Fig 2.1A), once the entire diatom biofilm had been ingested, the foraminifera began to metabolize their lipid reserves. As a result, lipid droplets had disappeared at Day 28 (Fig 2.4C). In contrast, residual bodies with clear ^{13}C -

enrichment appeared in the cytoplasm at Day 14 (Figs 2.2J, 2.4E and 2.4F). These heterogeneous vacuoles are believed to hold metabolic waste and recycled organelles (Hottinger and Dreher, 1974; Leutenegger, 1977c). The rapid ingestion, catabolism, and anabolism of the ^{13}C -enriched diatom biofilm in *A. tepida* under oxic conditions (Fig 2.2) is consistent with the bulk observations discussed above and the evolution of the fatty acid composition discussed below. The observation of labeled organic lining in 5 of the foraminifera incubated in oxic conditions is likely to be linked with chamber formation, because the organic lining is thought to play a key role in initiating calcite formation (Angell, 1967; Hottinger and Dreher, 1974). Consistent with this, no ^{13}C -labeled organic lining was observed in the specimens from anoxic conditions, which did not grow new chambers.

Under anoxic conditions, the metabolism was very different (Fig 2.3). Following the initial ingestion of diatoms during Day 1, there was substantially less redistribution of ^{13}C -enriched material in the foraminifera cells until the experiment ended. On Day 28, diatoms with their frustules were still present in the cytoplasm with their original content of strongly ^{13}C -labeled material (Figs 2.3M-O). Nevertheless, some early metabolism/redistribution did occur, resulting e.g. in the appearance of ^{13}C -enriched lipid droplets from Day 3 (Fig 2.4C). The density of lipid droplets remained constant after Day 3, consistent with the observation of constant average TOC levels (Fig 2.1A). The formation of lipid droplets earlier in anoxic (Day 3) than in oxic conditions (Day 7) might be attributed to the stressful conditions: faced with a lack of oxygen the foraminifera were first storing carbon in lipid droplets instead of using it for the cell metabolism. A qualitatively similar increase of lipid droplet abundance was observed in *Ammonia beccarii* specimens submitted to stress from Cu contamination (Le Cadre and Debenay, 2006). Such a response does not seem to be specific to foraminifera; it has also been observed in marine dinoflagellates (Prevot and Soyer, 1978). Mildly ^{13}C -enriched residual bodies did not appear until between Day 21 and 28 (Figs 2.3M-O and 2.4E-F).

3.4 Fatty acid composition and synthesis

Fatty acids 14:0, 16:0, 16:1(*n*-7), and specifically the 20:5(*n*-3) (Fig 2.5A, Table 2.2) are biomarkers of marine diatoms (Dunstan et al., 1993; Graeve et al., 1994; Zhukova and Aizdaicher, 1995). These FAs had already been observed in algae feeding experiments with foraminifera under both oxic (Ward et al., 2003) and hypoxic conditions (Larkin et al., 2014; Nomaki et al., 2009). In our study, the observed increase during the first 7 days of 16:0 under oxic conditions and of 16:1(*n*-7) under anoxic conditions is ascribed to the ingestion of diatoms. The decreases of 14:0 under both conditions and of 16:1(*n*-7) under oxic conditions at Day 7 suggest lipolysis and fatty acid catabolism (their β -oxidation to C_2 units). Part of the degradation products were probably used for *de novo* synthesis of long chain fatty acid intermediates for the production of PUFAs, i.e. 20:4(*n*-6), 20:5(*n*-3),

and 22:5(*n*-3) under oxic conditions (Fig 2.5B). Under oxic conditions, the relative abundance of 20:5(*n*-3) first decreased and then increased. This suggests that this PUFA was first consumed (by metabolic breakdown or used for the synthesis of 22:5) and then formed by desaturation and C₂ elongation of short-chain precursors. The relative increase in 20:5(*n*-3) cannot be explained by an ingestion of diatoms, because there were completely ingested after Day 7 under oxic conditions. This supports *de novo* synthesis of eicosapentaenoic acid 20:5(*n*-3) by the foraminifera.

20:4(*n*-6) and 22:5(*n*-3) were present only in small abundances in the diatom biofilm (Fig 2.5A), but in higher concentrations in *A. tepida* cytoplasm under both oxic and anoxic conditions (Figs 2.5B and C and Table 2.2). This can be explained by either a selective uptake of these PUFAs (Ward et al., 2003), or by *de novo* biosynthesis following a pathway similar to that for 20:5(*n*-3). A similar high increase in 20:4(*n*-6) content was observed in other foraminiferal feeding experiment with microalgae (Larkin et al., 2014; Suhr et al., 2008, 2003b; Würzberg et al., 2011). The observed concentration increase, combined with significant ¹³C-enrichment (Figs 2.5B and C and Table 2.2), strongly suggest *de novo* synthesis of this arachidonic acid, as hypothesized in other publications (Larkin et al., 2014; Würzberg et al., 2011).

A. tepida is also able to graze on bacteria (Pascal et al., 2008b). The increase in the relative abundance of 18:1, which is a bacterial biomarker in marine environments (Sargent et al., 1987), during the first 7 days under oxic conditions (Fig 2.5B) suggests that bacteria developed during the beginning of the experiment, assimilating ¹³C by degrading the de-frozen diatom biofilm (Figs 2.5B and Table 2.3). Further support for ingestion of bacteria is provided by the presence of small amounts of other bacterial FAs (15:0, 15:1, 17:0, and 17:1) in the foraminiferal cells (Table 2.2).

Finally, under anoxic conditions, the foraminifera assimilated clearly less ¹³C labeled fatty acids from the diatom biofilm than under oxic conditions (Table 2.3, Figs 2.5B and C), and they produced less new fatty acids. Between Days 7 and 28, only the relative abundances of the FAs 16:1(*n*-7) and 20:4(*n*-6) varied, indicating some, albeit strongly reduced metabolism compared to oxic conditions.

Together, our observations under anoxia indicate that food digestion and metabolic redistribution took place at a much-reduced rate compared to oxic conditions. Nevertheless, anabolic processes did initially take place, conceivably driven by the 'oxic metabolic machinery' still available to the cell during the first hours after establishment of anoxic conditions. The reduced state of metabolism seems consistent with a state of dormancy or quiescence, defined as a suspension of active life, arrested development, and reduced or suspended metabolic activity (Ross and Hallock,

2016), in our case due to the sudden onset of anoxic conditions. Consistent with a state of dormancy/quiescence is the fact that no obvious ultrastructural damage to the cells was observed, indicating that capability to return to a state of normal vitality once oxic conditions are reestablished.

4 Conclusion

Benthic foraminifera *Ammonia tepida* are ubiquitous in coastal marine sediments, where they are often exposed to hypoxia or completely anoxic conditions. In order to survive such anoxic conditions for longer time periods they must either rely on alternative, anaerobic metabolism, which would allow them to produce energy and thus maintain a certain level of activity, or enter a state of dormancy that minimizes energy consumption. With a broad suite of observations we show here that these single cell organisms respond to anoxic conditions by a radical reduction in their heterotrophic metabolism. This, combined with the observation of arrested calcification and the complete absence of physical movements upon exposure to anoxia (movement is restored when oxygen is returned to the environment (Maire et al., 2016)), indicates that these species do not have access to an alternative metabolic mechanism allowing them to maintain, even approximately, their level of physical activity under oxic conditions. Therefore, we propose that, upon exposure to anoxia, the *A. tepida* organism enters into a state of dormancy/quiescence, with strongly reduced metabolic requirements that make them capable of withstanding anoxic conditions for unusually long time intervals (here up to 28 days), compared with other benthic meiofauna.

5 Material and methods

5.1 Experiment I: Survival and growth rate of *A. tepida*

Superficial (top 2 cm) sediment was collected at low tide on January 15, 2013, from the intertidal mudflat of l'Aiguillon Bay (France). Living foraminifera were picked out of sieved sediment of two size fractions: >150 μm (adults) and 100–150 μm (juveniles).

Experiment I took place at the LPG-BIAF laboratory (Angers, France). For determination of the survival rate 300 adult foraminifera were checked for their vitality using 2 criteria: presence of yellow brownish cytoplasm in the shell and detection of movement of the foraminifera (Geslin et al., 2014). For determination of growth rate, 150 juveniles at a growth stage with 8 ± 1 chambers were selected using the same criteria as for adults.

Incubation was carried out in two glass aquaria ($33 \times 21 \times 19 \text{ cm}^3$) containing 10 liters ASW (RedSea Salt, salinity of 35 psu), under oxic and anoxic conditions, respectively. Each aquarium contained eighteen 10 mL glass vials ($h=45 \text{ mm}$, $\phi=22 \text{ mm}$), 15 vials holding 10 adult individuals and 3 vials holding 25 juvenile individuals, with each vial representing a replicate in subsequent calculations. Before the start of the experiment, a thin layer of freeze-dried *Chlorella* algae was added, forming a biofilm on the vial bottom ($14.3 \mu\text{g chlorophyll} \times \text{cm}^{-2}$). Each vial was then covered with a 100 μm mesh net, the aquaria were covered with Plexiglas lids to minimize evaporation and avoid changes in salinity and the lid of the anoxic aquarium was sealed with plastic tape to prevent gas leakage/exchange. Each aquarium was bubbled continuously with air using a standard aquarium pump to maintain oxic conditions, or with a mixture of N_2 and 0.04 % CO_2 (Air liquide, France, 99.999 % N_2 , 99.99 % CO_2) to produce anoxic conditions. Bubbling began immediately after the foraminifera were placed inside. The incubation started on the 12th of February 2013 and lasted 13 days. Oxygen concentrations, temperature, salinity and pH were measured continuously (oxygen and temperature) or at the beginning and end of the experiment (salinity and pH) using dedicated sensors (details in 2.S2 Table). O_2 contents were between 4.0 to 4.5 $\text{mL} \times \text{L}^{-1}$, and below 0.007 $\text{mL} \times \text{L}^{-1}$ (detection limit) in the oxic and anoxic aquaria, respectively. Temperature was between 17.5 and 19.5 $^\circ\text{C}$, salinity $35.2 \pm 0.2 \text{ psu}$ and pH 8.1 ± 0.1 . After 13 days, the incubation was stopped and the vials with the foraminifera taken out of the aquaria.

To determine survival rates, individuals were immediately incubated with 10 μM FDA (fluorescein diacetate) solution (Bernhard et al., 1995). After rinsing, fluorescence of the foraminifera was immediately observed with an epifluorescence stereomicroscope (Olympus SZX16, LPG-BIAF laboratory) equipped with a fluorescent light source (Olympus U-RFL-T). Foraminifera with less than 3

chambers not fluorescing (terminal chambers) were considered to be alive. The average size of all juveniles was measured before (t_0) and after (t_1) the incubation using an automatic particle analyzer (LPG-BIAF laboratory) equipped with an automated incident light microscope system; a Leica CLS100X ring light source mounted on a monocular Leica Z16PO microscope. A camera (SIS CC12) recorded images and the size of individuals was determined with the software analySIS FIVE (SIS/Olympus) (Bollmann et al., 2004). The growth rate (in % size change) was calculated as: $\frac{\text{Size } t_1 - \text{Size } t_0}{\text{Size } t_0} \times 100$.

5.2 Experiment II: Feeding behavior of *A. tepida* under oxic and anoxic conditions

Superficial (top 2 cm) sediment was collected at low tide on March 27, 2014, on the intertidal mudflat of the Bay of Bourgneuf (France). Living foraminifera were picked out from sieved sediment and transported to LGB laboratory (EPFL, Switzerland).

The diatom *Navicula salinicola* (CCAP, strain 1050/10) was grown for one week in F2 medium enriched with 2 mM of ^{13}C -enriched sodium bicarbonate (^{13}C fraction of 99 %, Sigma-Aldrich, Switzerland). The F2 medium was made with non-decarbonated water with an original concentration of ~2 mM sodium bicarbonate. Thus the addition of 2 mM of ^{13}C -enriched sodium bicarbonate resulted in a labeling of roughly 50 % of the dissolved inorganic carbon (DIC). The microalgae were harvested by centrifugation (1500 g, 10 min), washed 3 times with artificial seawater (RedSea Salt, salinity of 35 psu) to remove the excess $\text{NaH}^{13}\text{CO}_3$, and frozen at -20°C until use in the experiment.

Starting on April 2nd, 2014 (six days after collection on the mudflat and one day before the feeding experiment began), living *A. tepida* specimens were selected under a binocular microscope, with the same criteria as in Experiment I. A total of about 6000 individuals were distributed in 93 10 mL glass vials (h=45 mm, ϕ =22 mm), so that each vial contained ca. 65 specimens. 39 vials with foraminifera were placed in each aquarium. Fifteen vials containing foraminifera were used as control material for the subsequent analyses: 3 for TEM-NanoSIMS and total organic carbon (TOC) quantification and stable isotope analysis; 12 for fatty acid analysis. These were placed overnight in ASW (RedSea Salt, salinity of 35 psu) under oxic conditions without feeding and were sampled on Day 1, *i.e.* during the first sampling of foraminifera.

Incubation was performed as in Experiment I in oxic and anoxic aquarium. After 4 hours of bubbling with the mixture of N_2 and 0.04 % CO_2 (Carbagas AG, Switzerland), enough to allow the complete depletion of O_2 in the anoxic aquarium, the experiment started. All the foraminifera were fed by adding ^{13}C -enriched diatoms (ca. 578 mg $\text{C}\times\text{m}^{-2}$) to all vials (*i.e.* in both oxic and anoxic aquaria)

over a timespan of a few minutes. Anoxic and oxic conditions, were maintained from this point onwards. Oxygen concentrations were in the range of 4.1-4.8 mL×L⁻¹ and below 0.007 mL×L⁻¹ in the oxic and anoxic aquaria, respectively. Throughout the experiment, temperature was between 23 and 24 °C, salinity 32 psu and pH 8.3.

For TEM-NanoSIMS and TOC quantification and stable isotope analysis, 3 vials were harvested at 1, 3, 7, 14, and 28 days from each aquarium. In addition, 12 vials were harvested from each aquarium for fatty acid analyses at Day 7 and Day 28, respectively. Immediately upon removal from the aquaria, the foraminifera were incubated for 3 h at room temperature in the dark with FDA to a concentration of 100 µM (Bernhard et al., 1995). Vitality was assessed under an epifluorescent stereomicroscope (Leica M165C equipped with SFL100 LED fluorescence module; GFP green). Only living specimens were selected for further analysis. After rinsing with ASW, individuals for TEM-NanoSIMS analysis were immediately processed, those for TOC and fatty acid analysis were stored in cleaned and pre-heated 5 mL glass vials at -20 °C until required.

5.2.1 TEM and NanoSIMS analysis

After incubation with FDA, specimens were immediately fixed and prepared for TEM imaging using standard procedures (details can be found in S1 Text) and observed with a transmission electron microscope (TEM, Philips 301 CM100, 80 kV) at the Electron Microscopy Platform of the University of Lausanne. Ultra-thin sections observed with TEM were subsequently imaged with a NanoSIMS ion microprobe (Hoppe et al., 2013). Areas of interest for NanoSIMS imaging were selected based on TEM observations permitting direct correlation of ultrastructural (TEM) and isotopic images. Our observations systematically focused on the antepenultimate chamber of the foraminifera, i.e. the third chamber counting from the aperture. NanoSIMS imaging followed established procedures (Kopp et al., 2013, 2015a; Pernice et al., 2012), as detailed in 2.S1 Text. Regions of interest (ROIs) were drawn with the software Look@NanoSIMS (Polerecky et al., 2012) to estimate the percentage of cytoplasmic occupation and to quantify mean ¹³C enrichments of different sub-cellular structures of a given foraminifera. ¹³C enrichments were reported as ¹³C atom fraction in %: $x(^{13}\text{C}) = ^{13}\text{C}/(^{13}\text{C}+^{12}\text{C})\times 100$.

5.2.2 Fatty acids

Foraminifera from oxic and anoxic conditions sampled at Days 7 and 28, respectively, plus a sample of the ¹³C-labeled diatomic biofilm were analyzed for their fatty acids (FAs) composition using procedures adapted from (Spangenberg et al., 2014). Each sample was analyzed in triplicate, and the mean value was used for further calculations. For each analysis, lipids were extracted from 200 water-washed and dried specimens by sonication with mixture of methanol and dichloromethane of

decreasing polarity. An aliquot of internal standard solution of deuterated carboxylic acids was added to permit quantification. The carboxylic acids were obtained by alkaline hydrolysis of the organic extract and were methylated with BF_3/MeOH to obtain fatty acid methyl esters (FAMES). Chemical characterization of the fatty acids (as FAMES) was performed by gas chromatography/mass spectrometry and quantification by gas chromatography/flame ionization detection (details in 2.S2 Text).

5.2.3 Stable isotope analyses by isotope ratio mass spectrometry (IRMS)

Compound specific stable C isotopic composition of fatty acids was measured by gas chromatography/combustion/isotope ratio mass spectrometry. The standard deviation for repeatability of the ^{13}C atomic fraction, $x(^{13}\text{C})_{\text{FA}}$ in %, ranged between ± 0.01 % and ± 0.06 %. The lipid-free foraminifera carbonate shell were analyzed for their ^{13}C atomic fraction, $x(^{13}\text{C})_{\text{car}}$, using a carbonate preparation device (GasBench II, Thermo Fisher Scientific, Bremen, Germany) and isotope ratio mass spectrometry. The measured shell ^{13}C atom fractions, $x(^{13}\text{C})_{\text{car}}$, had a precision of ± 0.01 % (2 SD). The average carbonate content (in $\mu\text{g C} \times \text{ind}^{-1}$) of the shells was determined from the peak area of the major ions, $\pm 0.02 \mu\text{g C} \times \text{ind}^{-1}$ for TOC content. The ^{13}C atom fraction of the total organic matter, $x(^{13}\text{C})_{\text{TOC}}$, of decalcified foraminifera were determined by continuous flow elemental analysis/isotope ratio mass spectrometry. For each analysis, 30 previously decalcified specimens were used. The total organic carbon (TOC) content was determined from the peak area of the major isotopes and expressed in microgram per individual cell ($\mu\text{g C} \times \text{ind}^{-1}$). Reproducibility and accuracy were better than ± 0.01 % for $x(^{13}\text{C})_{\text{TOC}}$ (2 SD) and $\pm 0.02 \mu\text{g C} \times \text{ind}^{-1}$ for TOC content. For each analysis, 30 specimens were used (details in 2.S3 Text).

5.2.4 Statistical analysis

Data were analyzed using the R software. Univariate ANOVA tests were performed to compare the effects of the time and experimental conditions (*i.e.* oxic vs. anoxic). To determine the significance between two time points or two conditions at the same time point, the Tukey *post-hoc* test was carried out following the ANOVA. For the fatty acid abundance data, two-sample *t*-tests were performed to investigate significance of variations between time points for a given condition. Variances of the data were checked with a *F*-test prior the *t*-tests. The used significance level for all the tests was $\alpha = 0.05$.

Access to both sampling sites did not required any specific permissions, and the work did not involve endangered or protected species

Acknowledgements

Florence Manero from the SCIAM platform at the University of Angers (France) is thanked for help with sample treatment and electron microscopy. The electron microscopy platform at the University of Lausanne is thanked for access and technical assistance.

Availability of data and material

The datasets generated and/or analyzed during the current study are available in the LabArchives repository, DOI: 10.6070/H4X0653H.

Supporting information

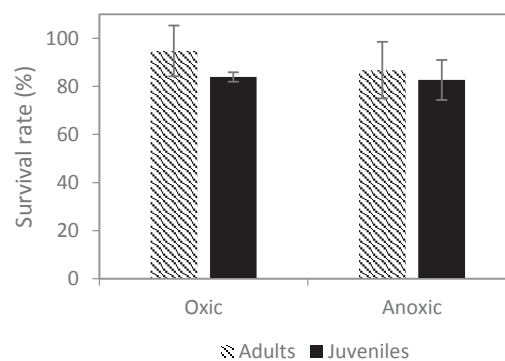


Figure 2.S1: Survival rate Experiment I: Survival rate (%) of adults (striped bars) and juveniles (solid bars) of *A. tepida* incubated for 13 days in oxic and anoxic conditions ($n=10$). Error bars are ± 1 SD.

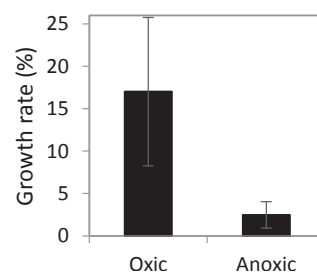


Figure 2.S2: Growth rate Experiment I: Growth rate (%) of juveniles incubated 13 days in oxic and anoxic condition ($n=3$). Error bars are ± 1 SD.

Table 2.S1: Carbonate uptake and shell ^{13}C -enrichment: Carbonate uptake (calculated as the difference of the C_{car} content of the foraminiferal shells of the individuals collected after 28 days and the foraminiferal shells of the control individuals, in $\mu\text{g } C_{\text{car}} \times \text{ind}^{-1}$) and ^{13}C enrichment (calculated as the difference of the $\delta(^{13}\text{C})_{\text{car}}$ values of the foraminiferal shells of the individuals collected after 28 days and the foraminiferal shells of the control individuals, in ‰) of *A. tepida* carbonate shells after 28 days under oxic and anoxic conditions with feeding ($n=3$).

	Oxic	Anoxic
Carbonate uptake ($\mu\text{g } C_{\text{car}} \times \text{ind}^{-1}$)	4.9 ± 1.8	0.2 ± 0.4
$\Delta^{13}\text{C} = (\delta(^{13}\text{C})_{\text{car}})_{\text{sample}} - \delta(^{13}\text{C})_{\text{car}})_{\text{control}} (\text{‰})$	0.05 ± 0.01	0.00 ± 0.01

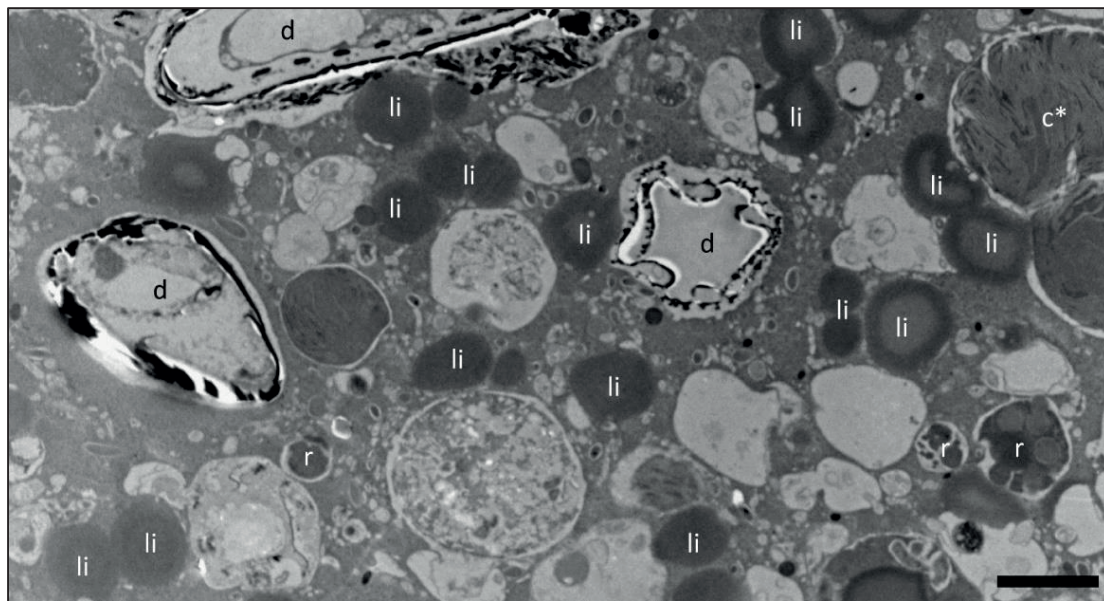


Figure 2.S3: Typical cellular structures of *Ammonia tepida* cytoplasm TEM image of the cytoplasm structures in the antepenultimate chamber of an *A. tepida* specimen collected *in situ*. Lipid droplets (li) are dark, homogenous vesicles with diameters between 1 to 5 μm , no visible membrane surround them. Residual bodies (r) are circular heterogeneous vacuoles with diameters of about 1 to 5 μm and heterogeneous content. Empty diatomic frustules (d) and a chloroplast in degradation (c*) are visible. Scale bar: 2 μm .

Table 2.S2: Sensors used in Experiment I and II

Parameter	Experiment I	Experiment II
Oxygen concentration	Continuously recorded: OX-100, Unisense, Denmark	Continuously recorded: OXROB3 for oxic aquarium and TROXROB3 (PyroScience) for anoxic aquarium
Temperature	Continuously recorded: testo 175 T1	Continuously recorded: TSUB36 , PyroScience
pH	Measured at the beginning and the end of the experiment: pH-500C, Unisense, Denmark	Measured at each sampling time point: Portable pH meter pH 3310, WTW
Salinity	Measured at the beginning and the end of the experiment: Handheld meter Cond 330i, WTW	Measured at each sampling time point: Handheld meter Cond 330i, WTW

Text 2.S1: TEM and NanoSIMS imaging

After incubation with FDA, specimens were rinsed 3 times in ASW (RedSea Salt, salinity: 35 psu), then chemically fixed as follows: fixation for 24 h with a mix of 4 % glutaraldehyde and 2 % paraformaldehyde 0.2 M cacodylate buffer, 0.4 M sucrose and 0.1 M NaCl (pH 7.4, room temperature, then storage at 4 °C). After rinsing, specimens were first decalcified with a solution EDTA 0.1 M, then post-fixed in 2 % osmium tetroxide. After a series of dehydration steps in ethanol (50, 70, 95, and 100 %), samples were embedded into an acrylic resin (LR White Resin Hard Grade). Specimens were cut into 70 nm sections with an ultramicrotome (Reichert Ultracut S) using a diamond knife (Diatome, Ultra, 45°). Sections were placed on electron microscopy copper grids with a formvar-carbon film, then stained for 10 min with 2 % uranyl acetate, rinsed, and observed with a transmission electron microscope (TEM, Philips 301 CM100, 80 kV) at the Electron Microscopy Platform of the University of Lausanne. Ultra-thin sections observed with TEM were subsequently imaged with a NanoSIMS ion microprobe (Hoppe et al., 2013). Areas of interest for NanoSIMS imaging were selected based on TEM observations permitting direct correlation of ultrastructural (TEM) and isotopic images. Our observations systematically focused on the antepenultimate chamber of the foraminifera, *i.e.* the third chamber counting from the aperture.

Prior to NanoSIMS imaging, the TEM grids were coated with 10 nm of gold to prevent charging effects. Images of typically 30×30 μm² with 256×256 pixels were obtained by rastering a 16 keV primary Cs⁺ beam (about 2 pA) focused to a size of 120-150 nm across the sample surface with a dwell-time of 5 milliseconds. Secondary cyanide ions (¹²C¹⁴N⁻ and ¹³C¹⁴N⁻) were simultaneously collected in electron multipliers at a mass resolution (M/ΔM) of about 9000 (Cameca definition), enough to resolve ¹³C¹⁴N⁻ from its ¹²C¹⁵N⁻ interference. Each NanoSIMS image consist of 6 sequential images, drift corrected, and accumulated using the software L'IMAGE (developed by Dr. Larry Nittler, Carnegie Institution of Washington, USA). Carbon isotope ratio images were obtained by taking the ratio between the cumulated ¹³C¹⁴N⁻ and ¹²C¹⁴N⁻ images.

Regions of interest (ROIs) were drawn with the software Look@NanoSIMS (Polerecky et al., 2012) to quantify mean ¹³C enrichments of different sub-cellular structures of a given foraminifera. The average ¹³C enrichment (and its standard deviation) for a given class of ROIs was obtained from images of 3 different foraminifera for each time point. The ROIs were also used to determine the percentage area occupied by a given type of structure in the cytoplasm (the sum of the pixels for a given type of ROI divided by the total number of pixels in the corresponding total images), providing an estimate of the abundance of a structure as a function of time.

Text 2.S2: Detailed protocol of fatty acid analysis

Foraminifera from oxic and anoxic conditions sampled at Days 7 and 28, respectively, plus a sample of the ^{13}C -labeled diatomic biofilm were analyzed for their fatty acids (FAs) composition in the IDYST laboratory at the University of Lausanne using procedures adapted from Spangenberg et al. (2014). Extraction and separation of acid lipids was carried out on three replicates for each time point and on one sample for the biofilm. For each lipid analysis of foraminifera cells, 200 specimens were rinsed with water purified using a Millipore® Direct-Q 3 System (Millipore Corporation, Bedford, MA, USA) to remove attached material from the shell. This material was frozen at $-20\text{ }^{\circ}\text{C}$ for 2 days, freeze-dried for 1 day in a Lyovac GT2 freeze-dryer (SRK System Technik GmbH, Goddelau, Germany) and stored at $-20\text{ }^{\circ}\text{C}$ for lipid extraction. An aliquot of internal standard solution containing a defined amount of deuterated carboxylic acids ($\text{D}_{23}\text{n-C}_{12:0}$, lauric acid, $\text{D}_{39}\text{n-C}_{20:0}$, arachidic acid) was added to each sample, permitting identification and quantification. Lipids were then extracted using sonication in solvents of decreasing polarity (10 min in 2 mL methanol, 10 min in 2 mL methanol/dichloromethane, 1:1, v/v; 2×10 mins in 2 mL dichloromethane). The extracts were combined and the solvent removed via gentle evaporation under a clean nitrogen flow. The carboxylic acids were obtained by hydrolysis with 10 % KOH/MeOH at room temperature for 16 h. The non-saponifiables were separated with hexane. The fraction containing the acid lipids was acidified with 1 N HCl to $\text{pH} < 1$, and the acid lipids extracted with hexane and methylated (boron trifluoride/methanol solution) to provide fatty acid methyl esters (FAMES). The FAMES were stored at $4\text{ }^{\circ}\text{C}$ until analysis. Chemical characterization of FAMES was performed by gas chromatography/mass spectrometry (GC/MS) using an Agilent (Palo Alto, USA) 6890 gas chromatograph connected to an Agilent 5973 mass selective detector operating at 70 eV (source $230\text{ }^{\circ}\text{C}$ and quadrupole $150\text{ }^{\circ}\text{C}$) in the electron ionization mode with emission current 1 mA and multiple ion detection over m/z 45 to 750. Helium was used as carrier gas. The FAMES were analyzed with two different fused silica columns and GC temperature programmed to permit the detection of long chain FAs and good separation of unsaturated FAs: (i) HP-ULTRA 2 (50 m \times 0.32 mm; length \times inner diameter) coated with $0.17\text{ }\mu\text{m}$ 5 % phenylmethylsilicone stationary phase. Samples were injected splitless at $320\text{ }^{\circ}\text{C}$. After an initial period of 2 min at $100\text{ }^{\circ}\text{C}$, the column was heated to $310\text{ }^{\circ}\text{C}$ (held 20 min) at $4\text{ }^{\circ}\text{C}/\text{min}$. (ii) HP-FFAP (50 m \times 0.20 mm; length \times inner diameter) coated with $0.33\text{ }\mu\text{m}$ nitroterephthalic acid modified polyethylene glycol stationary phase. Samples were injected splitless at $200\text{ }^{\circ}\text{C}$. After an initial period of 2 min at $100\text{ }^{\circ}\text{C}$, the column was heated to $240\text{ }^{\circ}\text{C}$ (held 30 min) at $5\text{ }^{\circ}\text{C}/\text{min}$. Compound assignment was based on comparison with standards, GC retention time, and MS fragmentation patterns. FAMES were quantified by gas chromatography with flame ionization detection (GC/FID). An Agilent Technologies (Wilmington, USA) 7890B GC system equipped with a 7693A automated injection system and a flame ionization detector

was used. Gas chromatography/flame ionization detection (GC/FID) analyses were performed using the HP-ULTRA 2 column and same chromatographic conditions as for GC/MS. The concentrations of the FAs were obtained from the GC/FID peak areas and expressed in nanogram per individual cell ($\text{ng} \times \text{ind}^{-1}$). One blank sample was run for every six samples throughout the analytical procedure. The absence of any measurable recovered extract from the blanks indicates that no detectable laboratory contamination was introduced to the foraminifera and biofilm samples during the analytical procedure.

Text 2.S3: Detailed protocol of stable isotope analyses by isotope ratio mass spectrometry (IRMS)

The stable carbon isotope analyses using IRMS were also performed in the Stable isotope laboratory at IDYST. For each time point, 3 replicates were analyzed, except in the case of stable C isotope analysis of individual fatty acids, for which 2 replicates were analyzed.

C-isotope analysis of total organic carbon (TOC).

The ^{13}C atom fraction, $x(^{13}\text{C})$, of the total organic matter of decarbonated living foraminifera were determined by continuous flow elemental analysis/isotope ratio mass spectrometry (EA/IRMS) using flash combustion on a Carlo Erba 1108 elemental analyzer (Fisons Instruments, Milan, Italy) connected via a ConFlow III open split interface to a Delta V Plus isotope ratio mass spectrometer (Thermo Fisher Scientific, Bremen, Germany). For each analysis, 30 specimens were placed into a silver capsule, acidified with 1 drop of 10 vol. % HCl, let to react and dry for 16 h before EA/IRMS analysis. The total organic carbon (TOC) content was determined from the peak area of the major isotopes and expressed in microgram per individual cell ($\mu\text{g C} \times \text{ind}^{-1}$). Reproducibility and accuracy were better than $\pm 0.01\%$ for $x(^{13}\text{C})_{\text{TOC}}$ (2 SD) and $\pm 0.02 \mu\text{g C} \times \text{ind}^{-1}$ for TOC content.

C-isotope analysis of the foraminiferal carbonate shells.

The foraminifera carbonate shell C-isotopic ratio, $x(^{13}\text{C})_{\text{car}}$, was determined using a Thermo Fisher Scientific (Bremen, Germany) carbonate preparation device and GasBench II equipped with a Combi-Pal autosampler (CTC Analytics AG, Zwingen, Switzerland) and coupled to a Delta Plus XL isotope ratio mass spectrometer (both Thermo Fisher Scientific). We analyzed shells recovered after lipid-extraction for fatty acid analysis (see below). In each analysis, 10 lipid-free specimens were placed in a 12 mL vials (LABCO Ltd., Lampeter, UK) and immersed in 5 % sodium hypochlorite (NaOCl) solution for 12 h to remove potentially remaining labile organic compounds, washed with Millipore water, and dried at 40°C . The vials were sealed with septum caps (from LABCO) and placed in an aluminum

heating block at 70 °C for CO₂ extraction by reaction with anhydrous phosphoric acid. The measured shell ¹³C atom fractions, $x(^{13}\text{C})_{\text{car}}$, had a precision of $\pm 0.01\%$ (2 SD). The average carbonate content (in $\mu\text{g C}\times\text{ind}^{-1}$) of the shells was determined from the peak area of the major ions, $\pm 0.02\ \mu\text{g C}\times\text{ind}^{-1}$ for TOC content.

Carbon isotope analysis of individual fatty acids.

Compound specific stable C isotopic composition of fatty acids in living foraminifera incubated under oxic and anoxic conditions, respectively, was measured by gas chromatography/combustion/isotope ratio mass spectrometry (GC/C/IRMS) using an Agilent 6890 GC instrument coupled to a Thermo Fisher Scientific (Bremen, Germany) Delta V Plus isotope ratio mass spectrometer via a combustion interface III under a continuous He flow. GC separation was performed with the same column and chromatographic condition as for GC/FID. Background subtracted stable isotope compositions were first calculated using the Thermo Fisher Scientific ISODAT 2.5 software. For calibration were used the previously determined C isotopic compositions (by EA/IRMS) of the deuterated carboxylic acids added as internal standards. For quality control, the repeatability and intermediate precision of the GC/C/IRMS analysis and the performance of the GC and combustion interface were evaluated every 5 runs by injection of a carefully prepared mixture of FAMES reference materials and duplicate analyses of the foraminifera samples FAME fractions. The standard deviation for repeatability of the ¹³C atomic fraction, $x(^{13}\text{C})_{\text{FA}}$ in %, ranged between $\pm 0.01\%$ and $\pm 0.06\%$.

Chapter 3: Kleptoplasty in benthic foraminifera from photic environments

Chapter 3.1: Ultrastructure and distribution of sequestered chloroplasts in benthic foraminifera from shallow-water (photic) habitats

Chapter 3.1 presents a manuscript submitted to the special issue “Foraminiferal ultrastructures” of the journal *Marine Micropaleontology*, investigating the fine structure of sequestered chloroplasts in different benthic foraminiferal species.

PhD student's contribution: the PhD student collected the samples from the field with TJ only for the species *Haynesina germanica*, *Elphidium williamsoni*, *E. oceanense*, and *Ammonia aomoriensis*; performed TEM analysis of the species mentioned above; interpreted their TEM micrographs with EG, TJ and JMB; discuss the results with all the authors and comment and edit the manuscript written by TJ.

Ultrastructure and distribution of sequestered chloroplasts in benthic foraminifera from shallow-water (photic) habitats

Thierry Jauffrais^{1*}, Charlotte LeKieffre², Karoliina A. Koho³, Masashi Tsuchiya⁴, Magali Schweizer¹,
Joan M. Bernhard⁵, Anders Meibom^{2,6}, Emmanuelle Geslin¹

¹ UMR CNRS 6112 LPG-BIAF, Bio-Indicateurs Actuels et Fossiles, Université d'Angers, 2 Boulevard Lavoisier, 49045 Angers CEDEX 1, France

² Laboratory for Biological Geochemistry, School of Architecture, Civil and Environmental Engineering (ENAC), Ecole Polytechnique Fédérale de Lausanne (EPFL), 1015 Lausanne, Switzerland

³ University of Helsinki, Department of Environmental Sciences, Viikinkaari 1, Helsinki, Finland

⁴ Department of Marine Biodiversity Research, Japan Agency for Marine-Earth Science and Technology, 2-15 Natsushima-cho, Yokosuka, Kanagawa, Japan

⁵ Woods Hole Oceanographic Institution, Geology & Geophysics Department, Woods Hole, MA, USA

⁶ Center for Advanced Surface Analysis, Institute of Earth Sciences, University of Lausanne, Switzerland

*contact: Thierry.jauffrais@univ-angers.fr

Abstract

Maintaining foreign chloroplasts (i.e., those not grown by the host) inside an organism is termed “chloroplast sequestration”, and is known for certain benthic foraminifera. Existing data indicates that sequestered chloroplasts can be intact and functional, but with different retention times depending on foraminiferal species. In the present study, seven species of benthic foraminifera (*Haynesina germanica*, *Elphidium williamsoni*, *E. selseyense*, *E. oceanense*, *E. aff. E. crispum*, *Planoglabratella opercularis* and *Ammonia aomoriensis*) were collected from shallow-water benthic habitats and examined with Transmission Electron Microscopy (TEM) for cellular ultrastructure to ascertain attributes of sequestered chloroplasts. Results indicate that all these foraminiferal taxa actively sequestered chloroplasts but organized them differently within their endoplasm. In some species, the sequestered chloroplasts were evenly distributed throughout the endoplasm (e.g., *H. germanica*, *E. oceanense*, *A. aomoriensis*), whereas other species consistently had plastids distributed close to the external cell membrane (e.g., *Elphidium williamsoni*, *E. selseyense*, *P. opercularis*). Chloroplast degradation also seemed to differ between species, as many degraded plastids were found in *A. aomoriensis* and *E. oceanense* compared to other investigated species. Digestion ability, along with different feeding and sequestration strategies (e.g., diatom frustules only found in *A. aomoriensis*; single to multiple sequestered plastids surrounded per host membrane), may explain the differences in retention time between taxa. Additionally, the organization of the sequestered plastids within the

endoplasm may also suggests behavioral strategies to expose and/or protect the sequestered plastids to/from light and/or to favor gas and/or nutrient exchange with their surrounding habitats.

Key words: Kleptoplasty; foraminifera; chloroplast; TEM; transmission electron microscopy

1 Introduction

Some benthic foraminiferal species have the ability to steal and sequester chloroplasts from their microalgal food sources. These foraminiferal species mainly ingest diatoms (Goldstein et al., 2004; Jauffrais et al., 2017; Knight and Mantoura, 1985; Pillet et al., 2011; Tsuchiya et al., 2015) but have different strategies for sequestering and feeding (Austin et al., 2005; Grzymski et al., 2002; Jauffrais et al., 2016; Lopez, 1979). In some species, the sequestered chloroplasts are degraded within hours, possibly as a result of a digestive process, while in other foraminiferal species the ingested plastids are kept and/or remain functional for weeks to months (Cedhagen, 1991; Correia and Lee, 2000, 2002b, 2002a; Grzymski et al., 2002; Jauffrais et al., 2016; Lee and Lanners, 1988; Lopez, 1979; Tsuchiya et al., 2015). This process, termed “kleptoplasty” (Clark et al., 1990), is observed in benthic foraminifera from different environments: shallow to deep-sea, oxic to anoxic and photic to aphotic habitats (Alexander and Banner, 1984; Bernhard et al., 2000; Bernhard and Alve, 1996; Bernhard and Bowser, 1999; Correia and Lee, 2000; Lee and Lanners, 1988; Lopez, 1979). The photosynthetic function of plastids has been demonstrated in some shallow-water benthic foraminifera (e.g., *Elphidium williamsoni* and *Haynesina germanica* in Cesbron et al., 2017; Jauffrais et al., 2016; Lopez, 1979). Nevertheless, it remains unknown why deep-sea foraminifera sequester chloroplasts as light is absent in their habitat (Bernhard and Bowser, 1999; Grzymski et al., 2002).

In photic shallow-water habitats (e.g., estuaries, bays, lagoons and other intertidal or shallow-water subtidal areas), kleptoplastic benthic foraminiferal species, such as *Haynesina germanica*, *Elphidium williamsoni*, the “*excavatum*” species complex (e.g., *E. oceanense*, *E. selseyense*, see Darling et al. (2016)), or *Ammonia* spp., are often the dominant mudflat foraminiferal taxa (Bouchet et al., 2009; Cesbron et al., 2016; Debenay et al., 2000, 2006; Morvan et al., 2006; Pascal et al., 2009; Thibault de Chanvalon et al., 2015). Their vertical distribution is characterized by a clear maximum density in the surface oxygenated millimeters of the sediment (Alve and Murray, 2001; Bouchet et al., 2009; Cesbron et al., 2016; Thibault de Chanvalon et al., 2015), where light can penetrate (Cartaxana et al., 2011; Kuhl et al., 1994). However, in some kleptoplastic species (e.g., the morphospecies *A. tepida* and *E. excavatum*) sequestered chloroplasts lack photosynthetic activity (Lopez, 1979; Jauffrais et al., 2016), and in many other kleptoplastic species, the photosynthetic activity has not yet been assessed and/or quantified.

Host-kleptoplast interactions (oxygen production, carbon assimilation) play an important role in the physiology and the biogeochemical capabilities of at least some extant kleptoplastic benthic foraminifera. The observed differences in the maintenance of the sequestered chloroplasts suggest there must be substantial differences between kleptoplastic shallow-water foraminiferal species. It is,

therefore, necessary to understand the sequestration mechanism in kleptoplastic foraminifera that have similar food sources and environments, but may have different chloroplast-retention times. In this study, we used Transmission Electron Microscopy (TEM) to document the ultrastructure and cellular organization of different kleptoplastic foraminifera from shallow-water photic habitats to assess chloroplast organization and degradation processes. Furthermore, individuals from the same populations as the ultrastructurally examined specimens have been genetically characterized with DNA barcoding to ascertain their taxonomic identity to ease future comparisons.

2 Material and methods

2.1 Specimen collection and field sample fixations

We examined seven species of shallow-water benthic foraminifera: *Haynesina germanica* (Fig. 3.1.1 and 3.1.2), *Elphidium williamsoni* (Fig. 3.1.3), *Elphidium oceanense* (Fig. 3.1.4), *Elphidium selseyense* (Fig. 3.1.5), *Elphidium* aff. *E. crispum* (Fig. 3.1.6), *Planoglabratella opercularis* (Fig. 3.1.7 and 3.1.8) and *Ammonia aomoriensis* (Fig. 3.1.9 and 3.1.10).

Haynesina germanica (4 specimens observed for ultrastructure), *E. oceanense* (3 specimens observed) and *A. aomoriensis* (3 specimens observed) were collected from the Bourgneuf Bay tidal mudflat (Bay of Biscay, south of the Loire estuary, France), from surface sediments (~ 0-0.5 cm depth) in March 2016. The foraminifera-bearing sediments were fixed in the field immediately after sampling, with a fixative solution containing 4% glutaraldehyde and 2% paraformaldehyde in artificial seawater (Red Sea® salt in MilliQ® water at salinity 35). The samples were then kept at room temperature (18-20°C) for 24 h and subsequently placed at 4°C until further processing.

Haynesina germanica (3 specimens observed) and *E. selseyense* (1 specimen observed) were isolated in February 2016 from two Wadden Sea tidal mudflats: Mokbaai and Cocksdoorp (Texel Island, the Netherlands), respectively. Sediment cores were sliced at 1-cm intervals down to 10-cm depth. The top 1-cm of each sediment core was sieved over a 125-µm screen and foraminifera containing healthy looking protoplasm were picked within 30 h of sampling from the >125-µm fraction. The vitality of all isolated foraminifera was further assessed based on movements as outlined in Koho et al. (2011). Immediately after vitality checks, living specimens were transferred to a fixative solution containing 2% glutaraldehyde and 4% paraformaldehyde in filtered seawater and stored at 4°C. After 24 h, the specimens were transferred into a solution containing 4% paraformaldehyde in filtered seawater and stored at 4°C, where they remained until further processing.

Elphidium williamsoni (5 specimens observed) were collected from surface sediments (0-0.5 cm depth) in May 2016 from a small tidal mudflat in Fiskebäckskil near Kristineberg Marine Research Station (Gullmar Fjord, Sweden). The sediments with foraminifera were fixed and preserved as noted for *H. germanica* from the Bourgneuf Bay tidal mudflat.

Living individuals of *E. aff. E. crispum* (12 specimens observed) and *P. opercularis* (12 specimens observed) were isolated from coralline algae (*Corallina pilulifera*, Rhodophyta) collected from rocky shores of Yugawara (Kanagawa prefecture, Japan). The vitality of all isolated foraminifera was assessed based on pseudopodial extension using an inverted microscope with a phase-contrast apparatus. Living specimens were picked with a fine (soft) needle, fixed for 2 h in 2.5% seawater-buffered glutaraldehyde and then transferred in filtered (0.2 µm) seawater and kept at 4°C until processing.

2.2 Species identifications

Specimens were taxonomically identified based solely on the morphology of the test as revealed with Scanning Electron Microscopy (SEM) or based on both morphology (SEM micrographs) and molecular (DNA barcoding; DNA sequences) tools.

For the Bay of Bourgneuf and the Gullmar Fjord, foraminifera from the same samples as specimens used for the TEM studies were selected for DNA barcoding (Table 3.1.1). Live foraminifera were picked from the sediment, dried on micropalaeontological slides, imaged with an environmental SEM (EVO LS10, ZEISS) and individually extracted for DNA in Deoxycholate (DOC) buffer (e.g., Pawlowski, 2000; Schweizer et al., 2011). For the DNA amplification, a fragment situated at the 3' end of the SSU rDNA was selected because this region is the barcode for foraminifera (Pawlowski and Holzmann, 2014). The primer pairs were s14F3 and J2 for the primary PCR and s14F1 and N6 for the secondary (nested) PCR (Darling et al., 2016; Pawlowski, 2000). Positive PCR reactions gave a fragment of about 500 nucleotides (nt) that was purified and sequenced directly as described in Schweizer et al. (2011). New DNA sequences were deposited in GenBank (accession numbers KY347797-KY347800).

For the Dutch and Japanese specimens, available DNA sequences (Schweizer et al., 2008, 2011; Tsuchiya et al., 2000; Pawlowski and Holzmann, unpublished data) were gathered from GenBank (Table 3.1.1).

The sequences retrieved for the studied specimens (Table 3.1.1) were then compared to published sequences (Darling et al., 2016; Hayward et al., 2004) within an alignment obtained with SeaView (Gouy et al., 2009) to identify them molecularly.

Table 3.1.1: Available DNA sequences for specimens from the same population or the same location as TEM studied specimens. The phylotype names refer to the systems described by Hayward et al. (2004) for *Ammonia* and Darling et al. (2016) for *Elphidium* and *Haynesina*.

Morphospecies	Gene	Phylotype	DNA isolate	Location	Accession number (GenBank)	Reference
<i>Haynesina germanica</i>	SSU	S16	H17-16	Bourgneuf (FR)	KY347799	present study
<i>Haynesina germanica</i>	SSU	S16	6008	Den Oever (NL)	EF534074	Schweizer et al., 2008
<i>Haynesina germanica</i>	SSU	S16	F323	Den Oever (NL)	GQ853557	Schweizer et al., 2011
<i>Elphidium williamsoni</i>	SSU	S1	GF191	Gullmar Fjord (SE)	KY347798	present study
<i>Elphidium oceanense</i>	SSU	S3	Bn130	Bourgneuf (FR)	KY347797	present study
<i>Elphidium selseyense</i>	SSU	S5	1244	Mokbaai (NL)	GQ853558-59	Schweizer et al., 2011
<i>Planoglabratella opercularis</i>	SSU	N/A	N/A	Omaezaki (JP)	Z69614	Pawlowski et al., 1997
<i>Planoglabratella opercularis</i>	ITS	A1	GO17	Ooura Cove, Shimoda (JP)	AF498333	Tsuchiya et al., 2003, 2014
<i>Planoglabratella opercularis</i>	LSU	N/A	GO17	Ooura Cove, Shimoda (JP)	AF194044	Tsuchiya et al., 2000
<i>Ammonia aomoriensis</i>	SSU	T6	H17-34	Bourgneuf (FR)	KY347800	present study

2.3 Ultrastructural observations by TEM

In the laboratory chemically preserved specimens were rinsed in filtered seawater. They were then either decalcified in 0.1 or 0.5 M ethylenediamine tetraacetic acid (EDTA) prepared in distilled water (pH 7.4) and post-fixed with 2% osmium tetroxide (OsO₄) solution prepared in filtered seawater for about 1-2 h, or the reverse (both processes work). Foraminifera were then dehydrated with successive ethanol baths and embedded in resin, either Epon (Epon 812 resin, TAAB) or LR White® (Sigma-Aldrich). Ultra-thin sections (60-70 nm) were then prepared with an ultra-microtome (Reichert Ultracut S, Leica) after staining with uranyl acetate, or with 1% aqueous uranyl acetate and 0.5% lead citrate, and then coated with carbon using a JEE-400 high vacuum evaporator (JEOL Ltd). The ultrathin sections were finally examined with either a JEM-1400 (JEOL Ltd), JEM-1210 (JEOL Ltd) or TECNAI G2 20 (FEI Company) TEM at an acceleration voltage of 80-100kV.

3 Results and discussion

This contribution presents the ultrastructure and cellular distribution of sequestered chloroplasts to highlight differences in chloroplast organization and degradation processes in foraminifera from shallow-water habitats (synopsis in Table 3.1.2). The description and organization of sequestered chloroplasts in foraminifera from deep-sea habitats and of other organelles in benthic foraminifera are described in detail elsewhere in the present special issue (see, Bernhard et Geslin, submitted; and Chapter 1).

3.1 *Haynesina germanica*

Haynesina germanica is relatively easy to recognize morphologically and there is good congruence between morphological and molecular identification (Darling et al., 2016, phylotype S16). Similarly, good agreement existed between the molecular and morphological identification of the specimens collected from the Bourgneuf Bay tidal mudflat (France). Direct molecular identification was not performed on specimens collected from Texel (Mokbaai, NL). However, specimens from a nearby site (Wadden Sea, Den Oever, NL) that were sequenced and identified as phylotype S16 (Schweizer et al., 2011, Table 3.1) bore similar morphology to Mokbaai specimens.

In all four specimens studied with TEM, the sequestered chloroplasts were evenly distributed in each chamber and large vacuoles were also densely and evenly distributed (Fig. 3.1.1B and C and Fig. 3.1.2B). The chloroplasts showed fine structural details and were relatively well preserved in the foraminiferal endoplasm with thylakoids, girdle lamella surrounding each kleptoplast and pyrenoids (Fig. 3.1.1E and F, 3.1.2C and E). The pyrenoids were also well preserved, often transected by a lamella and surrounded by another lamella (Fig. 3.1.1E, F and Fig. 3.1.2C, E). Ideally in *H. germanica*, five membranes are visible around the chloroplast; the four inner membranes are most likely those of the diatom and the fifth and outermost membrane is that of the foraminifer (Goldstein et al., 2004). In the present study, an electron-lucent space was often observed between the chloroplast membranes and the host membrane (Fig. 3.1.1D, E and F, and Fig. 3.1.2E). This electron-lucent space may be an artefact caused by the chemical fixation and embedding procedures.

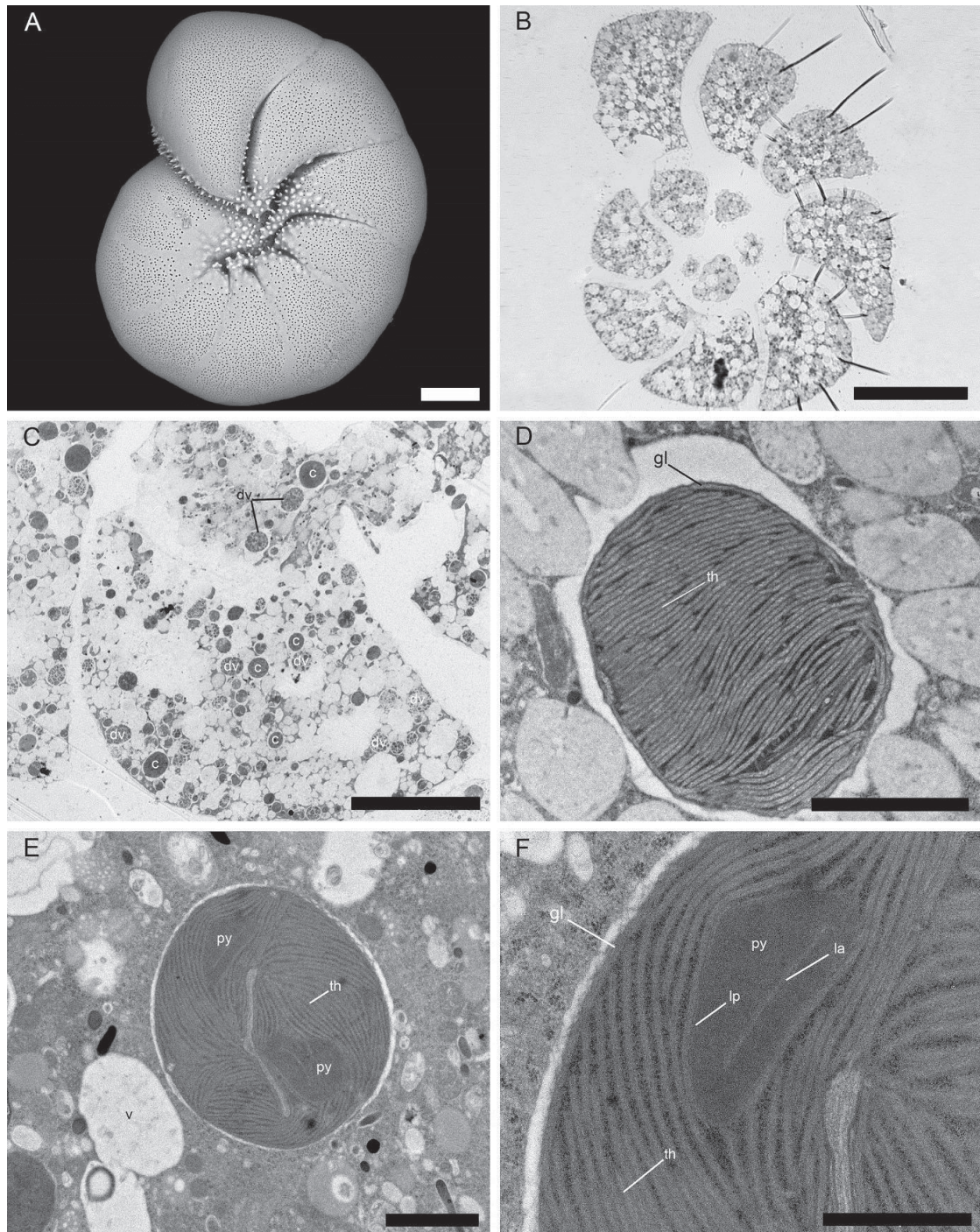


Figure 3.1.1: *Haynesina germanica* (elphidiid phylotype S16) isolated from Bourgneuf Bay (France). A. Scanning electron micrograph. B. Light micrograph of semi-thin section. C-F. TEM micrographs. C. Overview of a chamber showing sequestered chloroplasts (c) and digestive vacuoles (dv) evenly and densely distributed in the endoplasm. D and E. Sequestered chloroplast with thylakoid (th), girdle lamella (gl); pyrenoids (py). F. Higher magnification view of a sequestered chloroplast with the girdle lamella (gl) surrounding the kleptoplast, thylakoids (th), a pyrenoid (py) with a lamella (la) inside and a lamella surrounding the pyrenoid (lp). Scale bars: A, B = 50 µm, C = 20 µm, D = 2 µm, E = 1 µm and F = 0.5 µm.

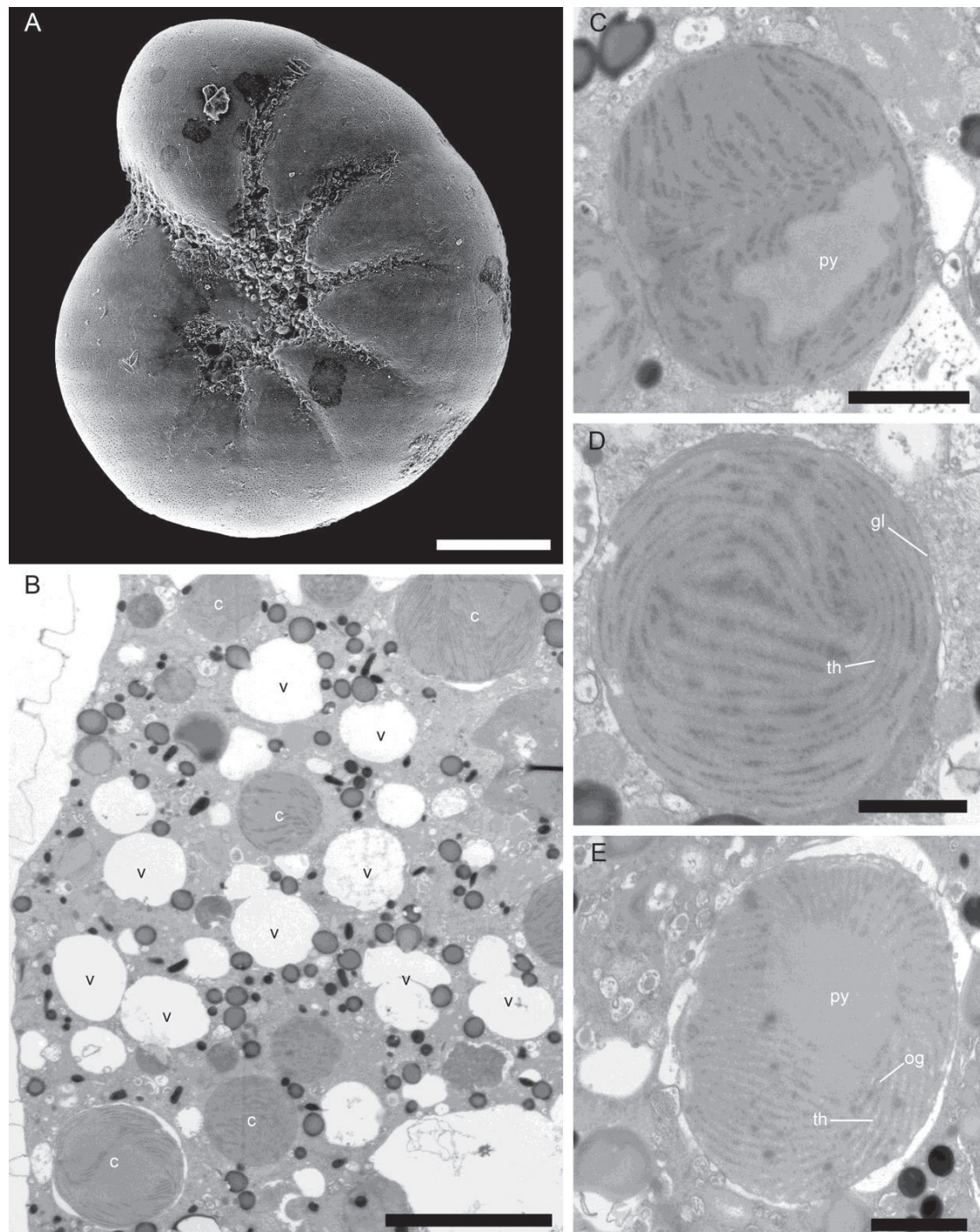


Figure 3.1.2: *Haynesina germanica* (elphidiid phylotype S16) isolated from Wadden Sea (Texel, Netherlands). A. Scanning electron micrograph. B-E. TEM micrographs. B. Overview of a chamber showing sequestered chloroplasts (c) and vacuoles (v) evenly and densely distributed in the endoplasm. C - E. Sequestered chloroplasts with pyrenoid (py), thylakoids (th) and osmiophilic globule (possibly plastoglobules). Scale bars: A= 100 µm, B = 5µm, C and D = 0.5 µm and E = 1µm.

3.2 *Elphidium williamsoni*

The morphospecies *Elphidium williamsoni* has been formally linked to phylotype S1 (Darling et al., 2016) with DNA sequencing of topotypic specimens (Roberts et al., 2016). A specimen from the Gullmar Fjord sample was also sequenced and found to belong to phylotype S1 (Table 3.1), confirming the morphological determination.

Sequestered chloroplasts were abundant and situated just below the cell periphery (Fig. 3.1.3B and C) or close to it (Fig. 3.1.3D). Sequestered chloroplasts were also well preserved with pyrenoid, lamella and thylakoids (Fig. 3.1.3E and F). A degraded sequestered chloroplast at the foraminiferal cell periphery had inter-thylakoid spaces (Fig. 3.1.3C (c*)). As observed in *H. germanica*, the sequestered chloroplasts were surrounded by the host membrane, with electron-lucent spaces between the chloroplasts and the endoplasm of the host (Fig. 3.1.3B to F) that may be an artefact caused by the chemical embedding procedure.

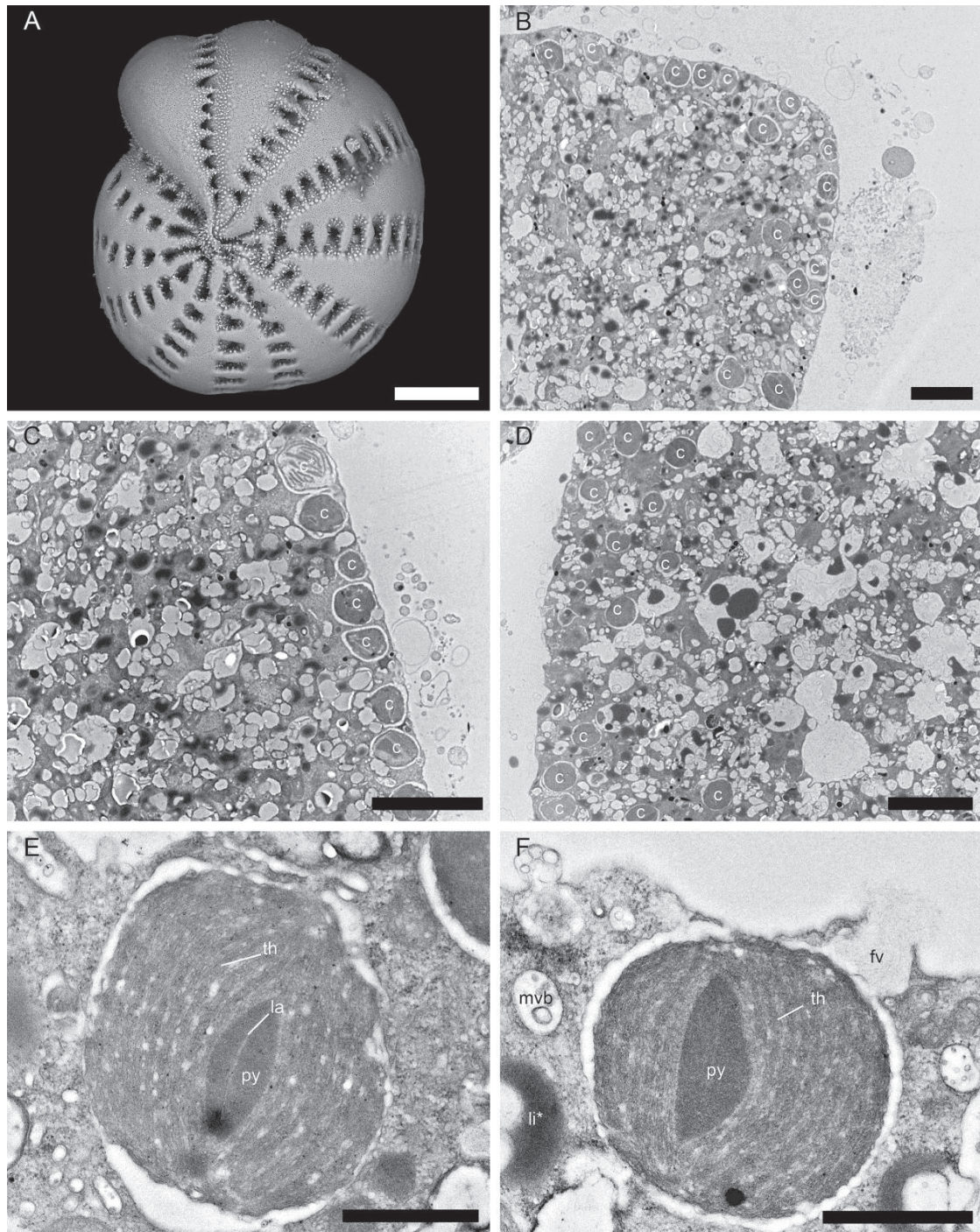


Figure 3.1.3: *Elphidium williamsoni* (elphidiid phylotype S1) isolated from Gullmar fjord (Sweden). A. Scanning electron micrograph. B-F. TEM micrographs. B, C and D. Overviews of different chambers showing intact (c) and degraded (c*) sequestered chloroplasts situated immediately below the host periphery (B and C) or close to it (D). E and F. Sequestered chloroplasts with pyrenoid (py), lamella (la) and thylakoids (th). In F, note the fibrillar vacuole (fv), the multivesicular bodies (mvb) and the degraded lipid droplet (li*) near the sequestered chloroplast. Scale bars: A = 100 μ m, B- D = 5 μ m, and E, F = 1 μ m.

3.3 *Elphidium* “*excavatum*” species complex

Elphidium oceanense and *E. selseyense* belong to the “*excavatum*” species complex as defined by Darling et al. (2016). The morphospecies *Elphidium excavatum* was thought to include a large number of ecophenotypes due to its high morphological diversity. However, recent molecular phylogenetics studies have shown that this morphospecies is actually a species complex, consisting of a group of closely related species (Darling et al., 2016; Pillet et al., 2013; Schweizer et al., 2011). These species are pseudocryptic, meaning that a careful morphological examination of specimens traditionally determined as *E. excavatum* allows classification to one species of the complex (Darling et al., 2016). Presently, four different phylotypes have been identified and linked to previously described morphological forms that were then given species status: S3=*E. oceanense*, S4=*E. clavatum*, S5=*E. selseyense*, S13=*E. lidoense* (Darling et al., 2016).

3.3.1 *Elphidium oceanense*

Specimens collected from the Bourgneuf Bay tidal mudflat, France, were morphologically and molecularly identified as phylotype S3 in Darling et al. (2016). This phylotype is the most common member of the “*excavatum*” species complex in the Bourgneuf Bay tidal mudflat (Schweizer et al., unpublished results and Table 3.1.1).

In *E. oceanense*, sequestered chloroplasts and vacuoles were evenly and densely distributed in the endoplasm (Fig. 3.1.4C, D). The sequestered chloroplasts were in large vacuoles containing numerous plastids and fine materials (Fig. 3.1.4D - F). The plastids often appeared in a degraded state with small circular electron-lucent disruptions of thylakoids and pyrenoids (Fig. 3.1.4E and F). Kleptoplast pyrenoids, lamella and thylakoids remained clearly distinguishable (Fig. 3.1.4E and F).

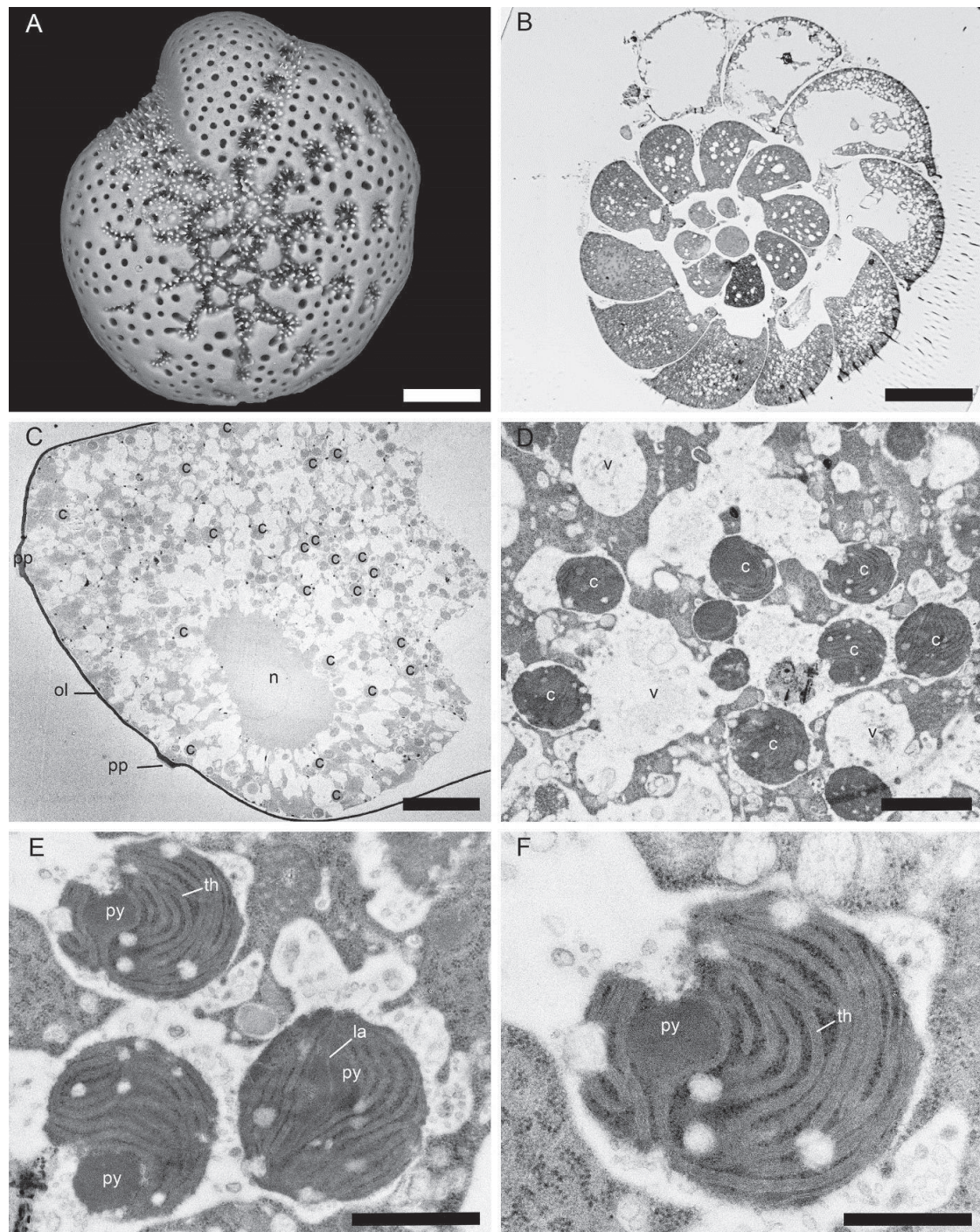


Figure 3.1.4: *Elphidium oceanense* (elphidiid phylotype S3) isolated from Bourgneuf Bay (France). A. Scanning electron micrograph. B. Light micrograph of semi-thin section. C-F. TEM micrographs. C. Overview of a chamber showing sequestered chloroplasts (c) and vacuoles (v) evenly and densely distributed in the endoplasm. Also noted are the nucleus (n), pore plates (pp) and organic lining (ol). D. Chloroplasts (c) often in degradation or perforated in large vacuoles. E and F. Higher magnification views showing chloroplasts, often in degraded state, with pyrenoid (py), lamella (la) and thylakoids (th). Scale bars: A, B = 50 µm, C = 10 µm, D = 2 µm, E = 1 µm and F = 0.5 µm.

3.3.2 *Elphidium selseyense*

The specimens from Cocksdoorp (Wadden Sea) were identified morphologically as *E. selseyense*. This species, which is linked to the phylotype S5 (Darling et al., 2016), was sequenced in 1999 from the same location (Schweizer et al., 2011; Table 3.1.1). *Elphidium selseyense* is known as a widespread and opportunistic species with ecology similar to the other species described above (Darling et al., 2016; Horton and Edwards, 2006; Murray, 1991).

Specimens of *E. selseyense* had many sequestered chloroplasts situated immediately below the host-cell periphery (Fig. 3.1.5B, C and D) and relatively fewer chloroplasts internally in the endoplasm (Fig. 3.1.5B). Sequestered chloroplasts exhibited a girdle lamella, a simple pyrenoid, thylakoids and also osmiophilic globules (Bedoshvili et al., 2009), which could be lipoprotein particles such as plastoglobules as suggested previously by Leutenegger (1977) and Schmaljohann and Röttger (1978).

Despite being phylogenetically closely related (Darling et al. 2016), *E. oceanense* and *E. selseyense* clearly have different chloroplast sequestration strategies. First, the plastids were distributed throughout cytoplasm in *E. oceanense* compared to *E. selseyense*, where the plastids occurred peripherally. Second, the kleptoplasts were relatively degraded in *E. oceanense* and relatively intact in *E. selseyense*. Third, multiple plastids occurred in one vacuole of *E. oceanense* whereas, typically, a single plastid was seen in one vacuole of *E. selseyense*. These differences suggest that, in *E. oceanense*, the kleptoplasts were not functional, whereas, in *E. selseyense* they may still be functional, possibly producing oxygen and assimilating inorganic carbon and nitrogen. Although these two *Elphidium* taxa are within the same species complex as defined by Darling et al. (2016), differences in chloroplast maintenance and distribution reveal that the species differ not only genetically and morphologically, but also physiologically. Such observations emphasize the need to clearly identify individuals within this species complex. These differences within the same species complex also hamper direct comparison with previous studies on *E. excavatum* structures (Correia and Lee, 2000, 2002a, b; Lopez, 1979) where no morphological (SEM images) and/or molecular (sequence) data are available.

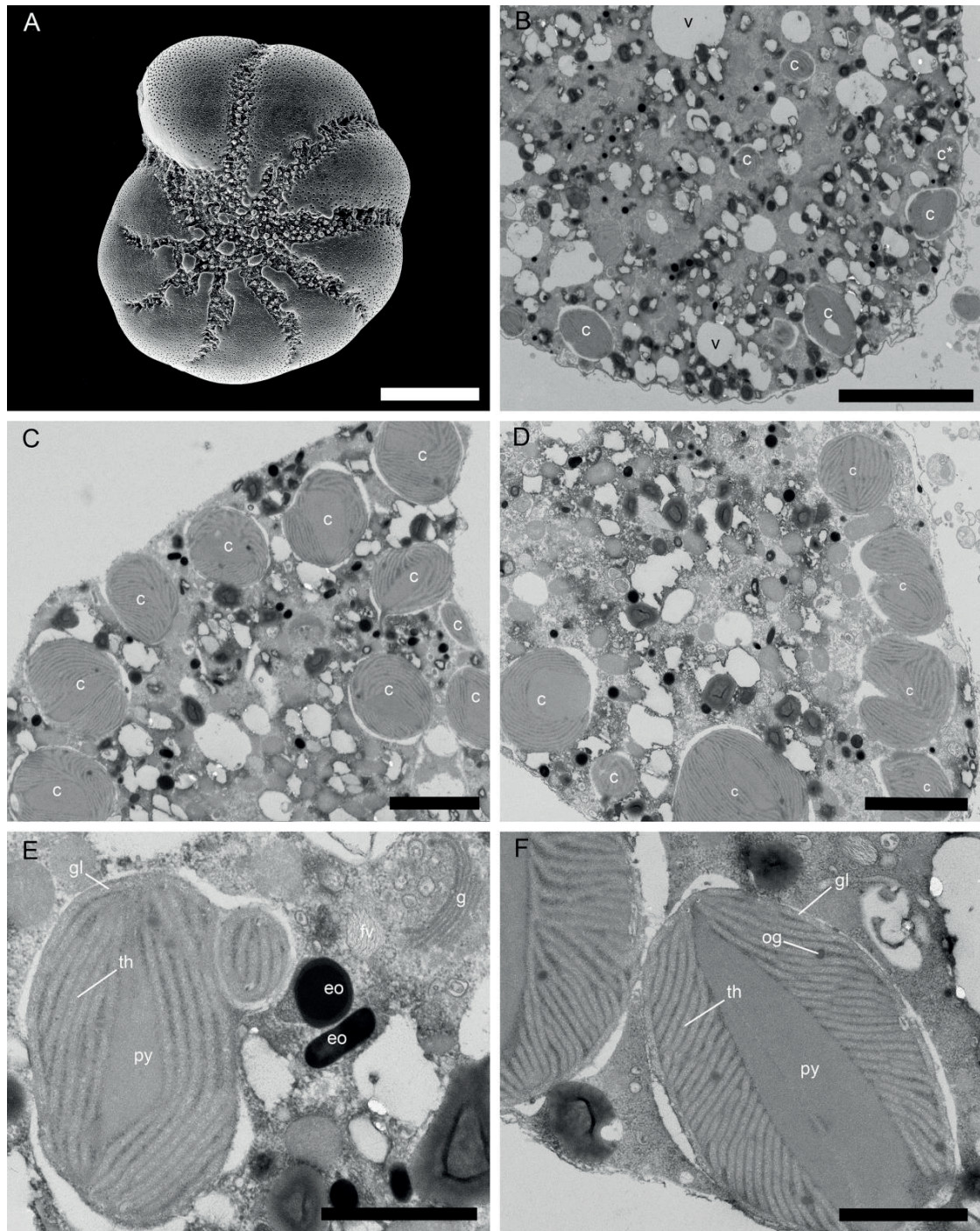


Figure 3.1.5: *Elphidium selseyense* (elphidiid phylotype S5) isolated from Wadden Sea (Texel, Netherlands). A. Scanning electron micrograph. B-F. TEM micrographs. B, C and D. Overview of different chambers showing sequestered chloroplasts (c) situated immediately below the host periphery (B-D) with some internally (B). E and F. Sequestered chloroplasts with a girdle lamella (gl), a simple pyrenoid (py), thylakoids (th) and osmiophilic globules (possibly plastoglobules). In E, note the Golgi apparatus (g) and electron opaque bodies (eo) near the sequestered chloroplast. Scale bars: A = 100 µm, B, C and D = 5 µm, E = 2 µm, and F = 1 µm.

3.4 *Elphidium* aff. *E. crispum*

Specimens of *E. aff. E. crispum* were isolated from intertidal rocky shores of Yugawara (Kanagawa prefecture, Japan) where they are commonly encountered living on coralline algae (Kitazato, 1994). No published sequence data is yet available for this species, but the preliminary sequence differs from the European *E. crispum* (phylotype S11, Darling et al., 2016 and Tsuchiya, unpubl. data), therefore explaining the use of open nomenclature here.

Sequestered chloroplasts were evenly and densely distributed in the endoplasm (Fig. 3.1.6B, C, F). Some organelles such as mitochondria, Golgi apparatus, and peroxisomes were found near the sequestered chloroplasts (Fig. 3.1.6D). The kleptoplasts appear singly in vacuoles and have a girdle lamella, thylakoids, and pyrenoid divided in two by a lamella and the presence of osmiophilic globules (Fig. 3.1.6E and G). Sequestered chloroplasts were noted in different states of degradation (Fig. 3.1.6H).

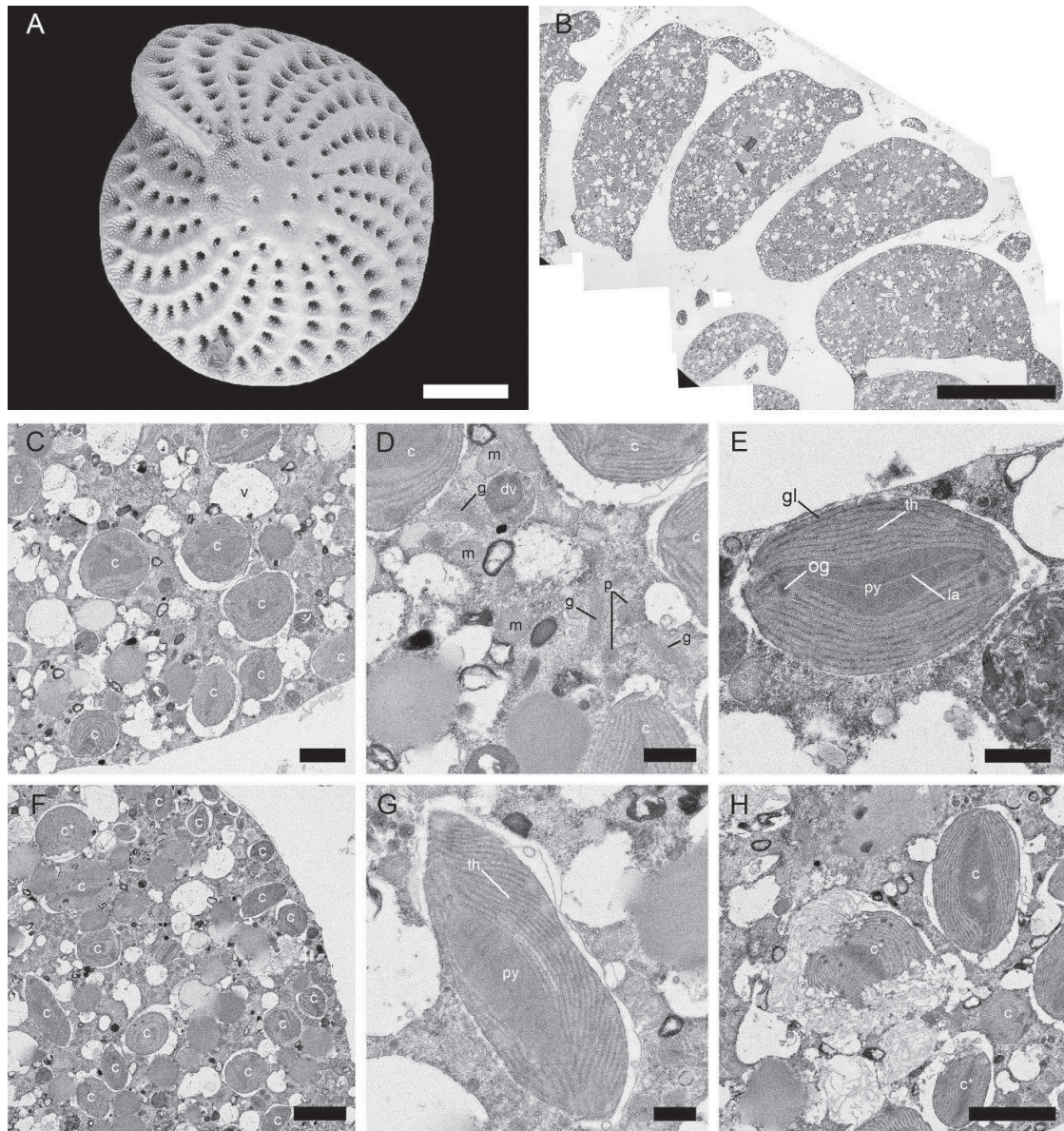


Figure 3.1.6: *Elphidium* aff. *E. crispum* isolated from Yugawara (Kanagawa prefecture, Japan). A. Scanning electron micrograph. B-H. TEM micrographs. B. Overviews showing four different chambers. C and D. Sequestered chloroplasts (c) evenly and densely distributed in the endoplasm of the cell and organization of surrounding organelles (D): mitochondria (m), digestive vacuole (dv), Golgi apparatus (g), peroxisome (p). E. Sequestered chloroplast with a girdle lamella (gl), thylakoids (th), pyrenoid (py) divided in two by a lamella (la) and osmiophilic globules (possibly plastoglobules). F. Sequestered chloroplasts (c) in the endoplasm. G and H. Intact and degraded (c*) sequestered chloroplasts. Scale bars: A = 100μm, B = 50 μm, C = 4 μm, D, E, G = 1 μm, F = 5 μm, and H = 2 μm.

3.5 *Planoglabratella opercularis*

Planoglabratella opercularis is also commonly encountered in the intertidal zone of rocky shores around the Japanese Islands where it lives on thalli of coralline algae (Kitazato, 1988; Tsuchiya et al., 2014). Specimens collected near the TEM-sample collection site have been sequenced previously for the LSU and SSU rDNA (Tsuchiya et al., 2000 see Table 3.1.1) and ITS rDNA sequences (Tsuchiya et al., 2003; Tsuchiya et al., 2014, see Table 3.1.1). Moreover, SSU rDNA sequences of *P. opercularis* from China have now been deposited in GenBank (LN714815-LN714825; Pawlowski and Holzmann, unpublished). The LSU rDNA sequence of a deposited Chinese specimen is identical to LSU sequences of the Japanese *P. opercularis* (Table 3.1.1).

Because *P. opercularis* is trochospiral with an attached mobile mode of life and directly exposed to sunlight, chloroplast distribution and sequestration are discussed in the context of spiral, umbilical and lateral perspectives, respectively (Fig. 3.1.7A-C). Sequestered chloroplasts were situated at the proximity of the foraminifer's spiral surface, close to the pores and pores plates, where they formed a continuous layer of chloroplasts (Fig. 3.1.7B and Fig. 3.1.8A and B). Also, some of the plastids were distributed in the endoplasm but at a lower density (Fig. 3.1.7B, 8E). Surrounding organelles such as mitochondria and Golgi apparatus were also found close to the sequestered chloroplasts (Fig. 3.1.7F). The kleptoplasts were well preserved with thylakoids and a pyrenoid (Fig. 3.1.7C, D and F). Such peripheral distributions suggest active strategies of *P. opercularis* to maximise light acquisition by the kleptoplast, to favor gas (e.g., O₂, CO₂) and/or dissolved nutrient (e.g., nitrogen) exchanges with their surrounding habitats.

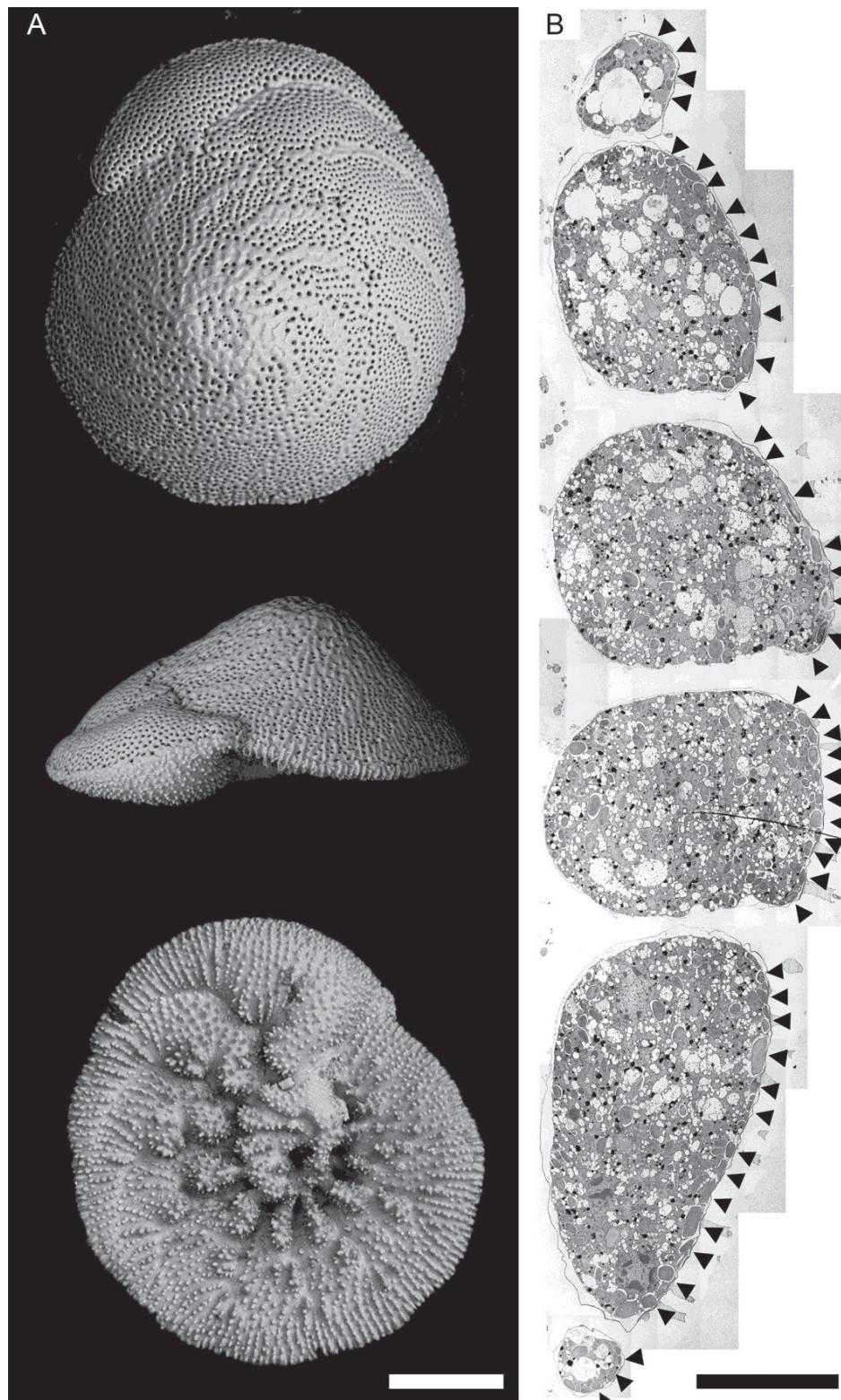


Figure 3.1.7: *Planoglabratella opercularis* isolated from Yugawara (Kanagawa prefecture, Japan). A. Scanning electron micrographs of dorsal (upper), lateral (middle) and ventral (lower) views. B. Transmission electron micrograph montage showing chambers and organization plastids at the cell periphery. Scale bars: A = 100 μm and B = 25 μm .

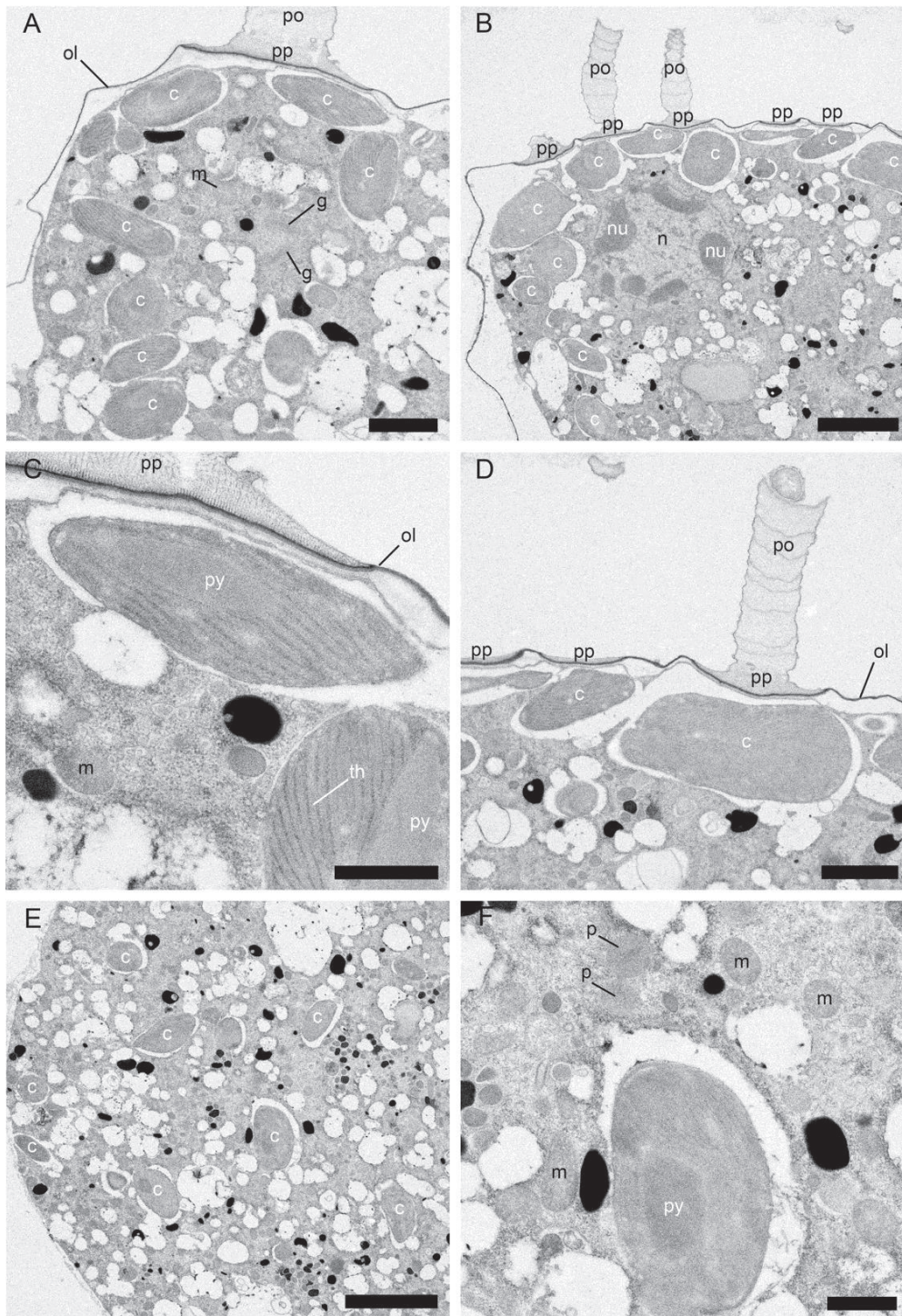


Figure 3.1.8: Transmission electron micrographs of *P. opercularis*. A-B. Organization of the sequestered chloroplasts (c) situated immediately below the host periphery close to the pore plates (pp) as well as in the endoplasm but at a lower density. Note the surrounding organelles: mitochondria (m), Golgi apparatus (g), nucleus (n) and nucleolus (nu), and also the pores (po), pore plates (pp) and the organic lining (ol). C and D. Details of peripheral sequestered chloroplasts showing thylakoids (th) and pyrenoids (py). E and F. Sequestered chloroplasts (E) in the endoplasm with surrounding organelles (F): mitochondria (m), digestive vacuole (dv), Golgi apparatus (g), peroxisome (p). Scale bars: A, D = 2 μm , B = 5 μm , C, E, F = 1 μm .

3.6 *Ammonia aomoriensis*

Ammonia isolated in Bourgneuf Bay tidal mudflat (France) were first identified as the morphospecies *A. tepida* (Jauffrais et al., 2016). This morphospecies, however, is polyphyletic, with morphologically identical specimens belonging to distantly related species genetically (Hayward et al., 2004). Specimens from the same sample as the TEM-studied ones were sequenced (Schweizer et al., unpublished results and Table 3.1.1) and identified as *Ammonia aomoriensis* (phylotype T6, Hayward et al., 2004).

Sequestered chloroplasts were evenly distributed through chambers, along with diatom frustules and large vacuoles (Fig. 3.1.9B). An entire section of a diatom was noted in the endoplasm of one host (Fig. 3.1.9D). In this case, the degradation of the diatom had begun because the diatom cell had shrunk within the frustule, however, the details and the intracellular organization of the diatom remained clearly visible. Two chloroplasts with a simple pyrenoid were observable; they were linked by a bridge of cytoplasm where a nucleus and small vacuoles were also visible. A thin layer of cytoplasm then extended to the ends of the cell surrounding two large vacuoles and mitochondria.

Sequestered chloroplasts of *A. aomoriensis* appeared in different states of degradation (Fig. 3.1.10). In well-preserved sequestered chloroplasts, the pyrenoid was separated by a lamella composed of a thylakoid and surrounded by an electron-lucent lamella (Fig. 3.1.10A). The thylakoids and girdle lamella were also visible (Fig. 3.1.10A and B). In degraded sequestered chloroplasts, the structure of the thylakoids and pyrenoid was disrupted and the lamellae were degraded. These degraded sequestered chloroplasts had inter-thylakoid spaces (Fig. 3.1.10C and D). Their degradation state and the fact that *A. aomoriensis* kleptoplasts are known to quickly become non-functional (Jauffrais et al., 2016) suggest that this species merely feeds on diatoms and does not sequester chloroplasts to perform photosynthesis.

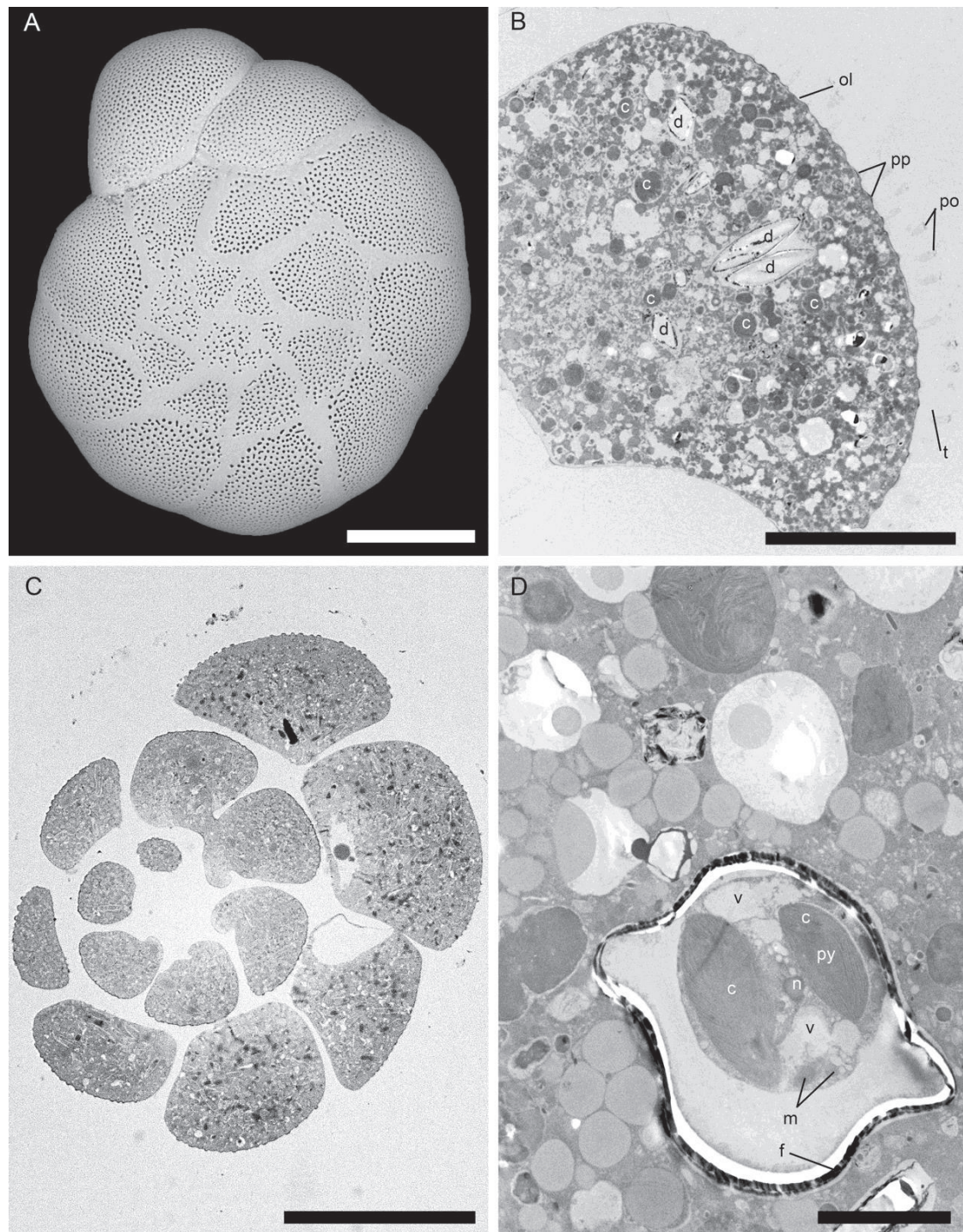


Figure 3.1.9: *Ammonia aomoriensis* (*Ammonia* phylotype T6) from Bourgneuf Bay (France). A. Scanning electron micrograph. B. Transmission electron micrograph overview of a chamber of *Ammonia aomoriensis* showing sequestered chloroplasts (c), empty diatom frustules (d), vacuoles (v), pores (po), pore plates (pp), organic lining (ol) and former location of the test (t). C. Light micrograph of semi-thin section. D. Transmission electron micrograph of a diatom in the endoplasm of the foraminifer, showing diatom organelles: chloroplast (c), nucleus (n), vacuoles (v), mitochondria (m) and frustules (f). Scale bars: A, C = 100 μ m, B = 50 μ m, and D = 5 μ m.

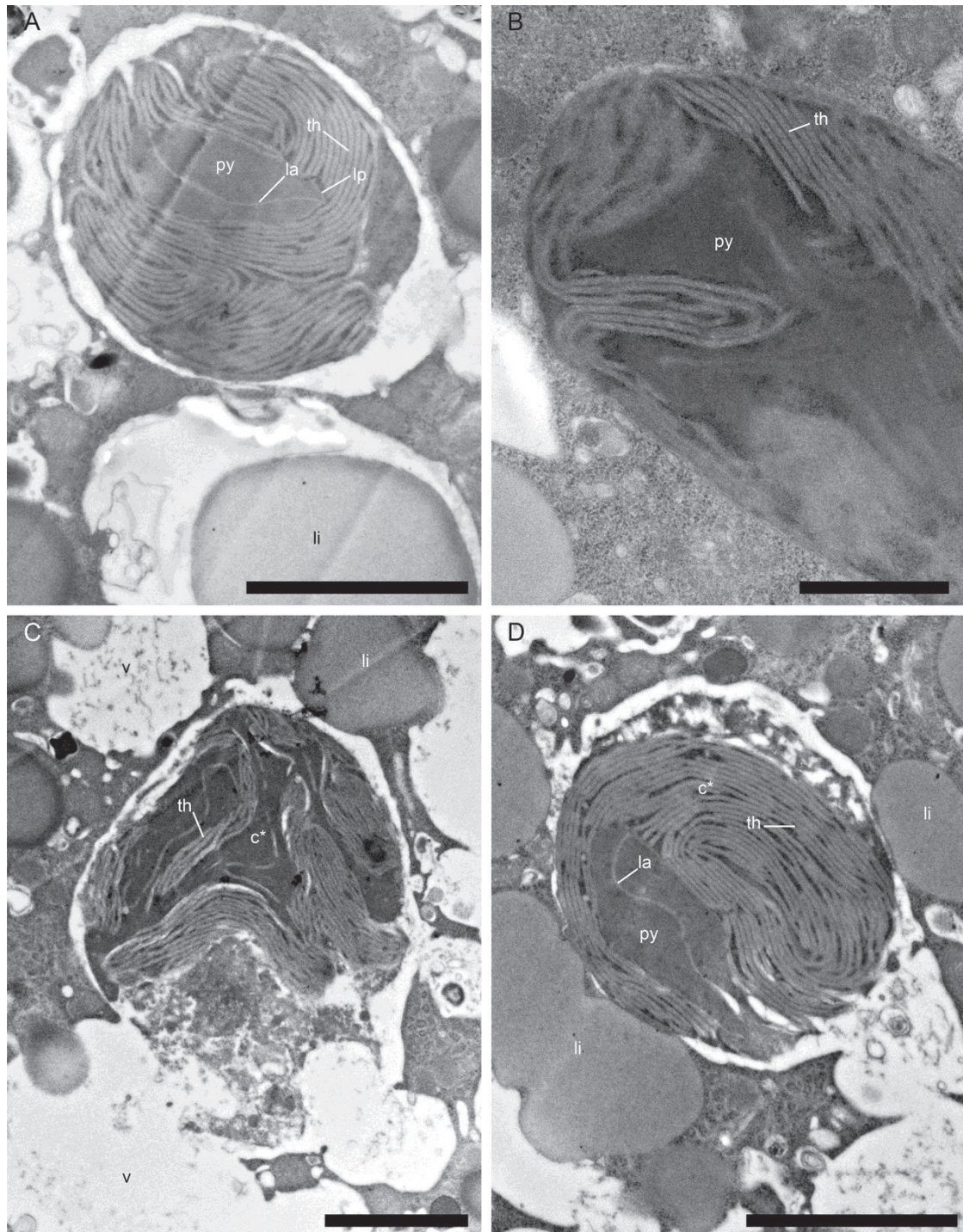


Figure 3.1.10: Transmission electron micrographs of *A. aomoriensis*. A and B. Organization of sequestered chloroplasts showing pyrenoids (py), lamella (la) and lamella surrounding the pyrenoid (lp), thylakoids (th) and girdle lamella (gl). C and D. Sequestered chloroplasts in degradation. Note the lipids (li) in the foraminifer. Scale bars: A, C, D = 2 μ m, B = 1 μ m.

3.7 General discussion

Our findings indicate that all seven foraminiferal taxa studied actively sequester chloroplasts but sequestration strategies differed between species.

First, the structure of the pyrenoid (simple with one transecting lamella surrounded by one membrane), the presence of a girdle lamella, the thylakoids and the absence of starch accumulation, together with published data (ultrastructural, pigment and molecular analyses of the sequestered plastids, Goldstein et al., 2004; Knight and Mantoura, 1985; Pillet et al., 2011, Jauffrais et al. 2016), suggest that the sequestered chloroplasts in all seven species belonged to diatoms.

Second, kleptoplast distributions within the endoplasm differed. In some species, the sequestered chloroplasts were evenly distributed (e.g., *H. germanica*, *E. oceanense* and *A. aomoriensis*), whereas in other species the plastids were located close to the cell periphery (e.g., *E. williamsoni*, *E. selseyense*, *P. opercularis*) and pore-plate complexes (e.g., *P. opercularis*). The differences in the organization of plastids within the endoplasm suggest different behavioral strategies, which expose and/or protect the sequestered plastids to/from light, and can favor gas (e.g., O₂, CO₂) and dissolved nutrient (e.g., ammonium, nitrate) exchange with their surrounding habitats. Peripheral chloroplast distributions might be considered as an active strategy of the foraminifer (e.g., *E. williamsoni*, *E. selseyense*, *P. opercularis*) to maximize light acquisition by kleptoplasts. Whereas, an internal distribution (e.g., *H. germanica*, *E. oceanense* and *A. aomoriensis*) could be considered either as an absence of strategy, as a strategy to protect the sequestered plastids from an excess of light and/or as an alternative strategy to maximize light exposure by continuously moving kleptoplasts in the endoplasm of the cell to modulate light exposure. In any case, the clear difference in the chloroplast organization between two phylogenetically closely related species, *E. oceanense* and *E. selseyense* (Darling et al., 2016), lends a novel (physiological) attribute distinguishing the two species beyond genetics and morphology.

Third, chloroplast degradation time and processes seem to be species specific as many degraded plastids were found in *E. oceanense* and *A. aomoriensis* compared to other species. Furthermore, the presence of numerous degraded chloroplasts in the endoplasm of *A. aomoriensis* and *E. oceanense* is consistent with the absence of photosynthetic activity in both of these species (Jauffrais et al., 2016; Lopez, 1979).

Fourth, ingestion and sequestration strategies also differed among taxa. Diatom frustules were only found in *A. aomoriensis* while other species had isolated plastids lacking frustules. Another distinguishing characteristic could be the number of sequestered plastids (single to multiple)

surrounded by a single host membrane. Such variations may be related to differences in chloroplast maintenance between foraminiferal species.

Acknowledgements

The authors thank Romain Mallet, Florence Manero and Guillaume Mabilieu for their help at the Imaging core facility (SCIAM laboratory) of the University of Angers, and Sophie Quinchard (UMR 6112 LPG-BIAF) for her technical help in molecular identification of the different foraminiferal species. TJ was funded by the “FRESCO” project, a project supported by the Region Pays de Loire and the University of Angers. This work was also supported by a grant no. 200021_149333 from the Swiss National Science Foundation and The Investment in Science Fund at WHOI. Also, KK acknowledges the Academy of Finland (Project numbers: 278827, 283453), Electron Microscopy unit of University of Helsinki and the Netherlands Institute for Sea Research for funding, preparation and assistance with TEM and SEM images, and providing facilities to conduct fieldwork in the Dutch Wadden Sea, respectively. MT thanks Katsuyuki Uematsu and Akihiro Tame (Marine Works Japan, Ltd) for their help with TEM preparations.

Table 3.1.2. Synopsis of the ecology, sequestered plastid abundance, plastid distribution and other specifics for seven species of benthic foraminifera from shallow-water photic habitats.

Foraminiferal species	Ecology	Relative plastid abundance*	Plastid length (maximum dimension)	Plastid distribution	Other specifics
<i>Haynesina germanica</i> (S16)	Tolerant to variations in temperature and salinity, often encountered in Lusitanian and Boreal waters, in shallow intertidal to subtidal habitats (Alve and Murray, 1999; Darling et al., 2016)	Abundant	2-5 µm	Evenly distributed in the endoplasm	Presence of both healthy and degraded sequestered plastids Single plastids surrounded by host membrane
<i>Elphidium williamsoni</i> (S1)	Tolerant to variations in temperature and salinity, commonly encountered in shallow intertidal to subtidal habitats of Lusitanian and Boreal waters (Alve and Murray, 1999; Darling et al., 2016)	Abundant	2-3 µm	Mainly distributed at the periphery of the endoplasm and also globally distributed but at lower density	Single plastids surrounded by host membrane
<i>Elphidium oceanense</i> (S3)	Tolerant to large variations in temperature and salinity, only marginally encountered in shallow intertidal to subtidal Lusitanian and Boreal waters in sediment with high organic content (Alve and Murray, 1999; Darling et al., 2016)	Abundant	1-2 µm	Evenly distributed in the endoplasm	Plastids often appeared degraded with small circular electron-lucent disruption of thylakoids and pyrenoids Numerous sequestered plastids per vacuole
<i>Elphidium selsevense</i> (S5)	Widespread and opportunistic species, tolerant to variations of temperature and salinity in shallow intertidal to subtidal Lusitanian and Boreal waters (Darling et al., 2016; Horton and Edwards, 2006; Murray, 1991)	Abundant	2-3 µm	Mainly distributed at the periphery of the endoplasm and globally but at lower density	Single plastids surrounded by host membrane
<i>Elphidium</i> aff. <i>E. crispum</i>	Commonly encountered in the intertidal zone of rocky shores around the Japanese Islands, living on coralline algae (Kitazato, 1994)	Abundant	4-8 µm	Evenly distributed in the endoplasm	Single plastids surrounded by host membrane
<i>Planoglabratella opercularis</i>	Commonly encountered in the intertidal zone of rocky shores around the Japanese Islands where it lives on thalli of coralline algae (Tsuchiya et al., 2014). It has an attached and mobile form, and graze on epiphytic diatoms (Kitazato 1988)	Abundant	3-5 µm	Situated immediately below the dorsal foraminiferal periphery, close to pores and pores plates, forming a continuous layer of chloroplasts and also globally in the endoplasm but at lower density	One to three plastids surrounded by host membrane
<i>Ammonia aomoriensis</i> (T6)	Typical intertidal species in Europe and East Asia, tolerant to variations of temperature and salinity, found in tidal flats, marshes and brackish lakes (Hayward et al., 2004)	Rare	2-3 µm	Evenly distributed in the endoplasm	Diatom frustules with or without their cellular content Occurrence of both healthy and degraded plastids

* The results of this column are based on visual observations and literature data (Lopez et al., 1979; Correia and Lee, 2002; Goldstein et al., 2004; Cesbron et al. 2017)

Chapter 3.2: Inorganic carbon and nitrogen assimilation by a benthic kleptoplastic foraminifera

Chapter 3.2 presents a manuscript in preparation, assessing the role of kleptoplasts in the carbon and nitrogen metabolism of a shallow water benthic species.

PhD student's contribution: the PhD student collected the samples from the field with MEG and EG, designed the experiment with EG and AM; analyzed the samples with MEG; interpreted the data with MEG, EG, TJ, and AM; performed the statistical analysis; discuss the results with EG, TJ, JMB, BJ and AM and wrote the manuscript with comments and edits from all the authors.

Inorganic carbon and nitrogen assimilation by a benthic kleptoplastic foraminifera

Charlotte LeKieffre¹, Thierry Jauffrais², Emmanuelle Geslin², Bruno Jesus^{3,4}, Joan M. Bernhard⁵, Maria-Evangelia Giovanni¹, Anders Meibom^{1,6}

¹ Laboratory for Biological Geochemistry, School of Architecture, Civil and Environmental Engineering (ENAC), Ecole Polytechnique Fédérale de Lausanne (EPFL), 1015 Lausanne, Switzerland

² UMR CNRS 6112 LPG-BIAF, Bio-Indicateurs Actuels et Fossiles, Université d'Angers, 2 Boulevard Lavoisier, 49045 Angers CEDEX 1, France

³ EA2160, Laboratoire Mer Molécules Santé, Université de Nantes, Nantes, France

⁴ BioISI – Biosystems & Integrative Sciences Institute, Campo Grande University of Lisboa, Faculty of Sciences, Lisboa, Portugal.

⁵ Woods Hole Oceanographic Institution, Department of Geology & Geophysics, Woods Hole, MA, USA

⁶ Center for Advanced Surface Analysis, Institute of Earth Sciences, University of Lausanne, Switzerland

Abstract

Haynesina germanica, a ubiquitous benthic foraminifera in intertidal mudflats, has the remarkable ability to isolate, sequester, and use chloroplasts from microalgae. The functionality of these kleptoplasts has already been demonstrated in terms of photosynthetic efficiency (photosystem II quantum efficiency and oxygen production rates). The objective of this study was to investigate, using correlated TEM and NanoSIMS imaging, the assimilation of inorganic C and N (here ammonium; NH_4^+) in kleptoplastic benthic foraminiferal cells. *H. germanica* specimens were incubated for 20 h in artificial seawater spiked with $\text{H}^{13}\text{CO}_3^-$ and $^{15}\text{NH}_4^+$ during a light/dark cycle. All specimens incorporated ^{13}C into their endoplasm (stored primarily in the form of lipid droplets), fibrillar vesicles, and electron-opaque bodies. A control incubation in darkness resulted in no ^{13}C -uptake. Ammonium assimilation was observed both with and without light. The resulting ^{15}N -enrichments were diffusely distributed throughout the cytoplasm, with higher than average concentrations in fibrillar vesicles, electron-opaque bodies, tubulin paracrystals, bacterial associates, and some kleptoplasts. The latter observation might indicate that the chloroplasts are involved in N assimilation.

Key words: NanoSIMS, ultrastructure, kleptoplast, photosynthesis, ammonium uptake

1 Introduction

Kleptoplasty is defined as the process in which a cell sequesters algal chloroplasts while discarding or digesting other algal components (Clark et al., 1990). This phenomenon is encountered in different organisms, such as sacoglossans (sea slug; e.g., Pelletreau et al., 2011; Rumpho et al., 2001; Serôdio et al., 2014), ciliates (reviewed in Dolan, 1992), dinoflagellates (e.g. Kim et al., 2012; Nagai et al., 2008; Nishitani et al., 2012), and benthic foraminifera (Bernhard and Bowser, 1999). With regard to benthic foraminiferal kleptoplasty, studies have focused on shallow-water species inhabiting photic zones, especially *Haynesina germanica* and *Elphidium* spp. These studies relied on ultrastructural observations and/or genetic analyses, which established the diatom origin of the kleptoplasts, or incubation/starvation experiments to define kleptoplast lifetimes inside foraminiferal cells (Bernhard and Alve, 1996; Cedhagen, 1991; Cevasco et al., 2015; Correia and Lee, 2000, 2002a, 2002b; Lechlitter, 2014; Leutenegger, 1984; Pillet et al., 2011; Pillet and Pawlowski, 2013; Tsuchiya et al., 2015).

Lopez (1979) showed that *H. germanica* and *Elphidium williamsoni* had a net uptake of inorganic carbon (H^{14}CO_3) in light, and experiments with oxygen microelectrodes demonstrated that maximal O_2 production by *H. germanica* depended on light intensity and light history (Cesbron et al., 2017; Jauffrais et al., 2016). A kleptoplastic strategy thus provides these organisms with both carbon and a source of oxygen. Such photosynthetic activity might furthermore contribute to the creation of oxygenated micro-niches in the sediment, which would provide species living in coastal environments that are often subject to hypoxic periods (e.g., *H. germanica*) with a certain ecological advantage (Cesbron et al., 2017; Diaz and Rosenberg, 2008; Middelburg and Levin, 2009; Zhang et al., 2010).

Foraminiferal kleptoplasts might also be involved in uptake of inorganic N. Indeed, diatoms, from which foraminifera sequester their kleptoplasts (e.g. Pillet et al., 2011; Tsuchiya et al., 2015), are able to assimilate ammonium through the chloroplast GS/GOGAT (glutamate synthase and glutamine oxoglutarate aminotransferase) enzymatic pathway (Syrett, 1981; Zehr et al., 1988; Zehr and Falkowski, 1988). Among deep-sea benthic species living in complete darkness and thus unable to perform photosynthesis (Bernhard and Bowser, 1999; Grzymski et al., 2002), *Nonionella stella* maintains kleptoplasts and associated functional enzymatic machinery (including ribulose bis-phosphate carboxylase oxygenase (RuBisCO) and phosphoenol pyruvate carboxylase (PEP carboxylase)) intact for months in the dark after sampling (Grzymski et al., 2002). It was suggested that kleptoplasts in these species are involved in assimilation of inorganic N (Grzymski et al., 2002).

NanoSIMS ultra high-resolution isotopic mapping correlated with TEM imaging and combined with stable isotope labeling experiments is a relatively recent technique (Hoppe et al., 2013) that has already been successfully applied to study assimilation, storage, and transfer of C and N in several

different marine organisms, including foraminifera (Ceh et al., 2013; Clode et al., 2007; Kopp et al., 2013, 2015a; Krupke et al., 2015; LeKieffre et al., 2017; Nomaki et al., 2016; Pernice et al., 2012; Raina et al., 2017). Using this integrative approach, the present study had three objectives: (1) to investigate the role of kleptoplasts in light induced C fixation, (2) to investigate the transfer and distribution of photosynthetically produced organic C into the host; and (3) to investigate the potential role of kleptoplasts in the foraminiferal N metabolism.

2 Material and methods

2.1 Experiment 1: light/dark cycle incubation with $\text{H}^{13}\text{CO}_3^-$ and $^{15}\text{NH}_4^+$

Living foraminifera were collected on April 9, 2015, at low tide on the intertidal mudflat of the Bourgneuf Bay (France, 47°00'59.4"N 2°01'29.8"W). The top centimeter of the sediment was sampled, sieved over a mesh of 150 μm with *in situ* seawater and immediately transported in the dark over ~3 hours to the laboratory.

In the laboratory, healthy living individuals of *H. germanica* were selected under a binocular microscope based on their cytoplasm color (i.e. yellow-brownish material spread through all the chambers of the specimen, except the last chamber). The selected specimens were placed into 5 Petri dishes (5 specimens per Petri dish) filled with artificial seawater (ASW, Red Sea Salt, salinity = 35, pH = 8.0). Four of the Petri dishes contained ASW spiked with 2mM $\text{NaH}^{13}\text{CO}_3$ and 10 μM $^{15}\text{NH}_4\text{Cl}$. The fifth Petri dish was filled with unlabeled artificial seawater; these specimens served as controls for NanoSIMS analysis (see below) and were fixed already at the beginning of the experiment. All other Petri dishes were placed in an incubator (Fytoscope FS130, temperature: 18°C, light intensity: 90 $\mu\text{mol m}^{-2} \text{s}^{-1}$). After 8 h of light incubation they were transferred to dark conditions for another 12 h. The foraminifera remained in the spiked ASW all along the experiment (except the control specimens). Specimens were collected after 4, 8, 12 and 20 hours of incubation (Fig. 3.2.1). Immediately after collection, the foraminifera were chemically fixed.

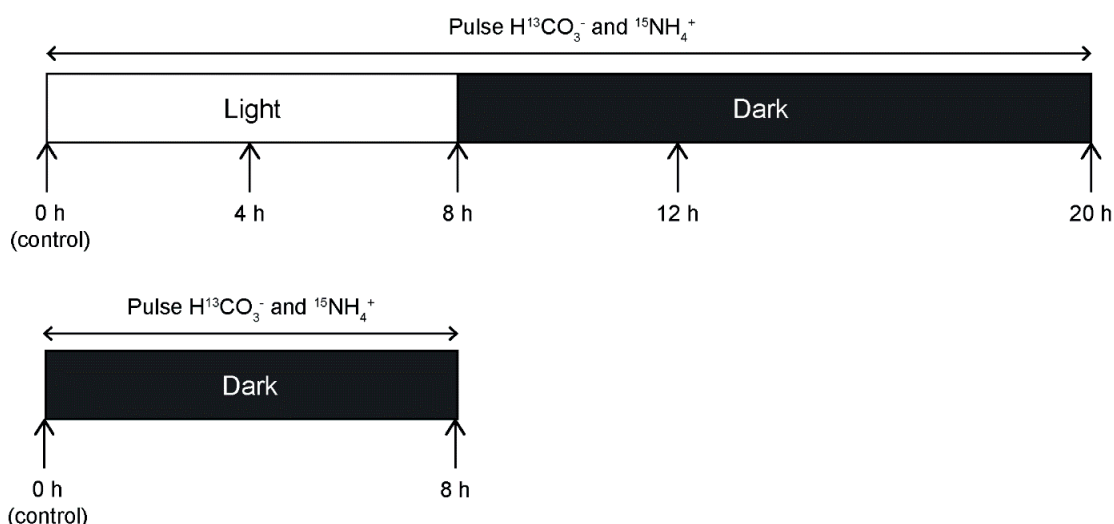


Figure 3.2.1: Schematic of Experiments 1 and 2, exposing *H. germanica* to different light conditions. Three specimens were sampled at each indicated time point. See text for details.

2.2 Experiment 2: Incubation in continuous darkness with $\text{H}^{13}\text{CO}_3^-$ and $^{15}\text{NH}_4^+$

H. germanica specimens were collected on May 16, 2015, at low tide on the intertidal mudflat of the Bourgneuf Bay (France) following the same procedure described above. Five living specimens were selected and placed in a Petri dish with artificial seawater (Red Sea Salt, salinity= 35; pH=8.0) enriched with 2mM $\text{NaH}^{13}\text{CO}_3$ and 10 μM of $^{14}\text{NH}_4\text{Cl}$. They were incubated in continuous darkness for 8 h (Fig. 3.2.1A) and immediately chemically fixed at the end of this incubation. Control samples, which were incubated in normal seawater, were fixed at the beginning of the experiment (Fig. 3.2.1B).

2.3 Preparation for TEM-NanoSIMS studies

Chemical fixation and transmission electron microscopy (TEM) of the foraminifera were performed at the Electron Microscopy Facility of the University of Lausanne (Switzerland). The specimens were chemically fixed following the protocol described in Chapter 1. Briefly, fixation took place at room temperature during 24 h with a mix of 4% glutaraldehyde and 2% paraformaldehyde diluted in 0.1 M cacodylate buffer, 0.4 M sucrose, and 0.1 M NaCl (pH=7.4). After rinsing, specimens were decalcified in two successive baths (1 and 48 h, respectively) with a solution of 0.1 M of EDTA diluted in 0.1 M cacodylate buffer, then post-fixed for 1 h in 2% osmium tetroxide diluted in distilled water. After serial dehydration in ethanol, the samples were embedded into an acrylic resin (LR White). Specimens were cut into 70 nm ultra-thin sections with an ultramicrotome (Reichert ultracut S), placed on carbon-formvar coated copper grids, and post-stained for 10 min with 2% uranyl acetate before observing with the TEM (Philips 301 CM100, 80kV). Only chambers from $n - 3$ to $n - 8$ (n being the youngest chamber next to the aperture) were examined. The integrity of the mitochondria and membranes of all the specimens were checked as recommended by (Nomaki et al., 2016) to ensure the vitality of each studied specimens.

2.4 Stable isotope mapping with NanoSIMS

NanoSIMS analyses were carried out on areas defined on the basis of prior TEM observations. Grids with TEM sections were mounted on 10 mm disks with double sticking Cu-tape and coated with a ca. 10 nm thick gold layer before being imaged with the NanoSIMS (Secondary Ion Mass Spectrometry) 50L ion microprobe to image and quantify the distribution of ^{13}C and ^{15}N enrichment.

Foraminiferal sections were imaged with the NanoSIMS ion microprobe with a 16-keV primary ion beam of Cs^+ focused to a beam spot of around 100-150 nm. The secondary molecular ions $^{12}\text{C}_2^-$, $^{13}\text{C}^{12}\text{C}^-$, $^{12}\text{C}^{14}\text{N}^-$ and $^{12}\text{C}^{15}\text{N}^-$ were collected in electron multipliers detectors at a mass-resolution of about 10000, enough to resolve potential interferences in the mass spectrum (Kopp et al., 2013, 2015a). Isotopic images ranged in size from 15x15 μm to 30x30 μm with 256x256 pixel resolution. For each

image, 6 layers were acquired, drift corrected, and superimposed using the software L'IMAGE (developed by Dr. Larry Nittler, Carnegie Institution of Washington DC, USA). The quantified $^{13}\text{C}/^{12}\text{C}$ and $^{15}\text{N}/^{14}\text{N}$ ratios were obtained as follows:

$$\delta^{13}\text{C} (\text{‰}) = \left(\left(C_{mes}/C_{nat} \right) - 1 \right) \times 10^3$$

$$\delta^{15}\text{N} (\text{‰}) = \left(\left(N_{mes}/N_{nat} \right) - 1 \right) \times 10^3$$

Where C_{mes} is the measured $^{12}\text{C}^{13}\text{C}/^{12}\text{C}_2^-$ ratio of the sample and C_{nat} is the average $^{12}\text{C}^{13}\text{C}/^{12}\text{C}_2^-$ ratio measured in unlabeled samples (control). Similarly, N_{mes} is the measured $^{12}\text{C}^{15}\text{N}/^{12}\text{C}^{14}\text{N}$ ratio of the sample and N_{nat} is the average $^{12}\text{C}^{15}\text{N}/^{12}\text{C}^{14}\text{N}$ ratio measured in non-labelled samples. The software L'IMAGE was used to determine the isotopic enrichment of specific organelles by drawing profiles on the ratio images, which provided $\delta^{13}\text{C}$ and $\delta^{15}\text{N}$ values along the profile (lines were 3 pixels wide). Regions of interest (ROIs) to quantifying the average isotopic enrichment of the cytoplasm were defined from the $^{15}\text{N}/^{14}\text{N}$ and $^{12}\text{C}^{14}\text{N}$ images by drawing 3 circles of about 2 μm in diameter per image avoiding highly ^{15}N -enriched organelles. For each specimen, between one and three NanoSIMS images were analyzed.

2.5 Statistical analysis

For each time point, three specimens were analyzed. Cytoplasm $\delta^{13}\text{C}$ and $\delta^{15}\text{N}$ values were obtained as the average of all corresponding ROIs for each specimen for each time point. The errors bars provided are thus standard deviations representing inter-specimen variability. However, for the statistical analysis, a linear mixed-effects model was made on all the ROIs of the three specimens for each time point (taking into account pseudo-replication effects, i.e. regrouping ROIs from three different specimens into one category), followed by a Tukey multiple comparison test. The statistical analyses were performed with Rstudio software using a significance level set at $\alpha = 0.05$.

3 Results

3.1 TEM observations of the foraminiferal cytoplasm

The cytoplasm of all specimens had well-preserved ultrastructure (Fig. 3.2.2A), as well as intact mitochondria with visible double-membranes and cristae (Fig. 3.2.2B). Numerous small lipids with a waxy appearance, diameter of about 500 nm, and no distinguishable membranes (Fig. 3.2.2C) were observed in the cytoplasm, along with some larger lipid droplets with a size ranging from 1 to 3 μm in diameter. Numerous small oval fibrillar vesicles (ca. 500 nm in length), with the fibrils arranged in parallel, and spherical to oval-shaped electron-opaque bodies (200 – 500 nm) were observed in the cytoplasm (Fig. 3.2.2D, E), along with occasional tubulin paracrystals identifiable due to the regular pattern of their ultrastructure revealed by high-magnification TEM imaging (Fig. 3.2.2F). In all specimens, we observed many small structures (2 to 3 μm in length) variable in shape but mainly ovoid (Fig. 3.2.2A) with the presence of numerous vacuoles within their matrix (Fig. 3.2.2G, H). Henceforth, we refer to these as “multi-vacuolar structures”.

In all observed specimens, TEM images of the endoplasm revealed well-preserved kleptoplasts with visible pyrenoids and thylakoids (Figs. 3.2.2A, 3.2.3, 3.2.4). These kleptoplasts ranged in size from 2 to 10 μm in diameter. Generally, their outlines were circular to oval. They were distributed in the endoplasm with no clear pattern and often surrounded by an electron-lucent space between the kleptoplast membranes and the endoplasm. Some small lipid droplets were adjacent to the kleptoplast periphery. In some cases, lipid droplets were closely associated with kleptoplast membranes (Fig. 3.2.3B).

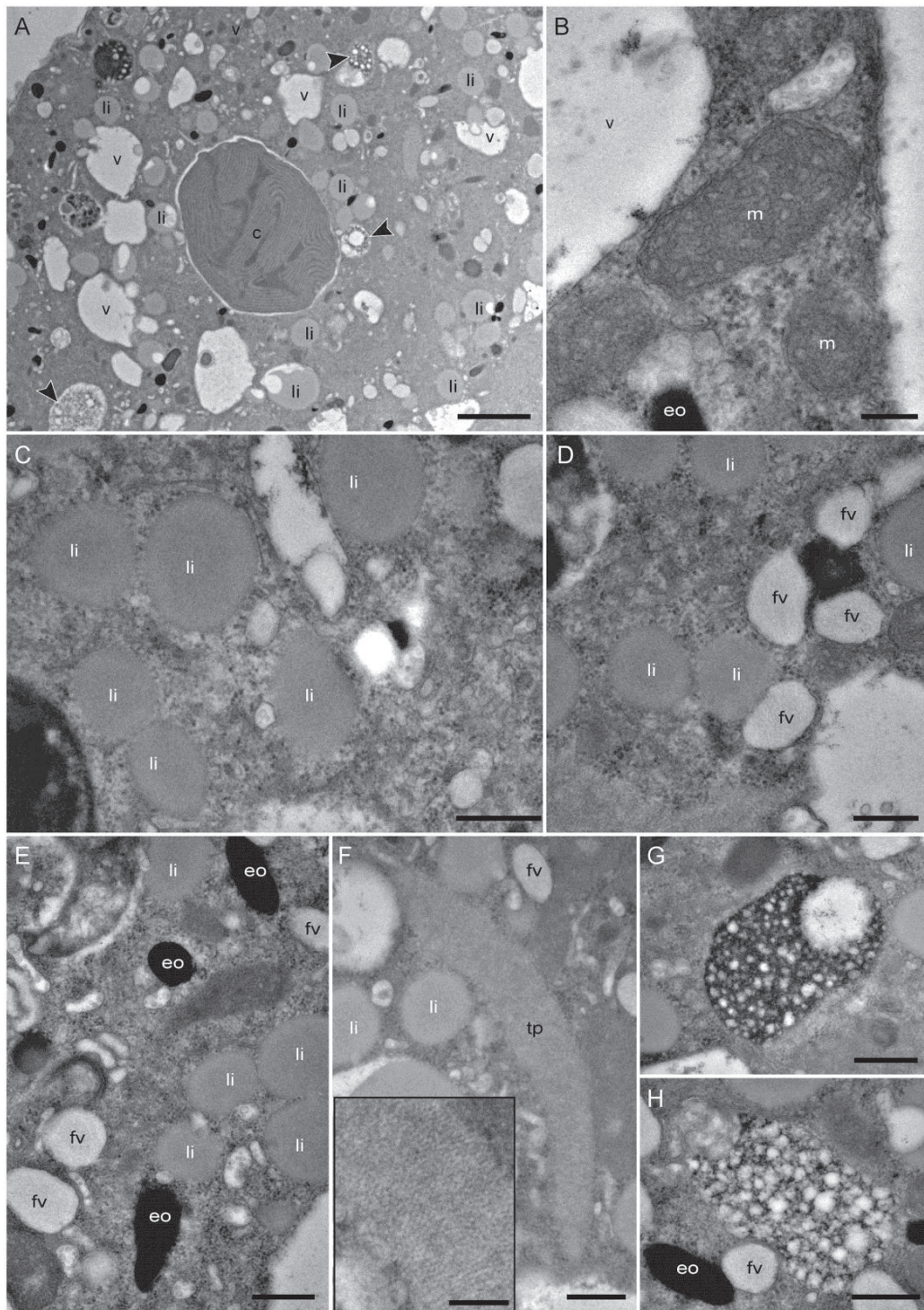


Figure 3.2.2: TEM micrographs of the cytoplasm and organelles of *Haynesina germanica*. A: Aspect of the cytoplasm in a chamber of the penultimate whorl. B: Intact mitochondria with well-defined cristae and intact double-membranes. C: Small lipid droplets. D: Fibrillar vesicles. E: Electron-opaque bodies, F: Tubulin paracrystals; Inset: higher magnification revealing regular pattern of the paracrystal ultrastructural organization. G and H: multi-vacuolar structures. Arrowheads: multi-vacuolar structures; c: chloroplast; eo: electron-opaque bodies, fv: fibrillar vesicles, li: lipid droplets; m: mitochondria, tp: tubulin paracrystals, v: vacuole. Scale bars: A: 2 µm; B, inset F: 200 nm; C, D, E, F, G, H: 500 nm.

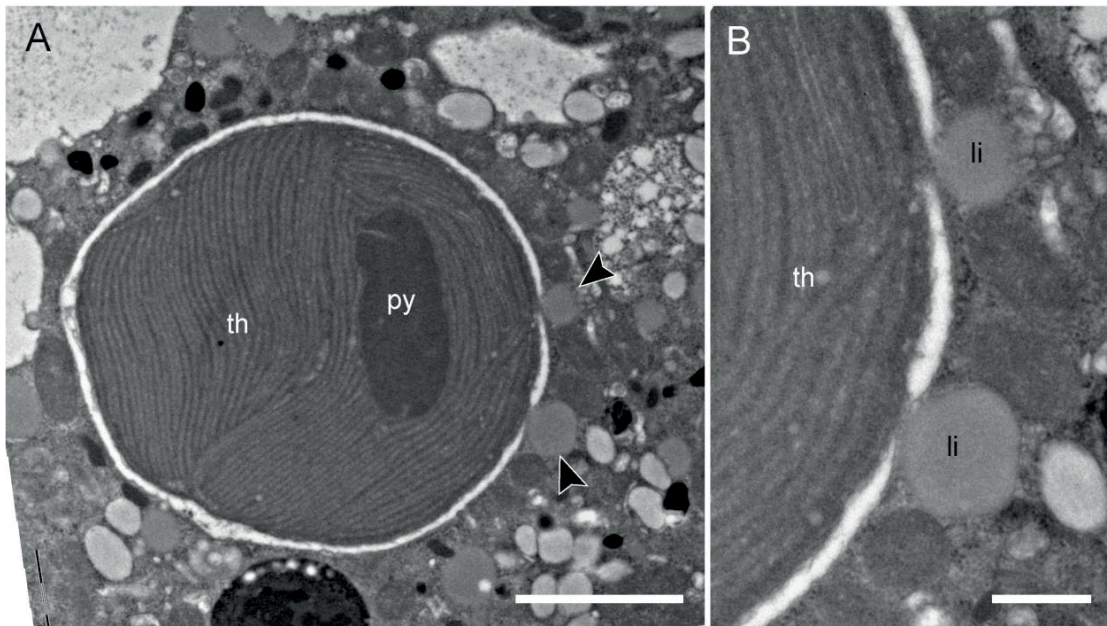


Figure 3.2.3: TEM micrographs of one chloroplast in *Haynesina germanica* cytoplasm. A: Intact pyrenoid and thylakoids. B: Higher magnification image showing two small lipid droplets in contact with the chloroplast membranes. The chloroplast membranes adjacent to the lipid vesicle on the left are disrupted. li: lipid droplets, py: pyrenoid, th: thylakoid. Scale bars: A: 2 μm ; B: 500 nm.

3.2 Uptake of $\text{H}^{13}\text{CO}_3^-$ within the foraminiferal cell.

In Experiment 1, starting with the second time point ($t = 8 \text{ h}$), ^{13}C -enrichments were detected in all specimens. In contrast, only one specimen from the first time point (*i.e.* at 4 h) exhibited ^{13}C -enriched structures, concentrated in fibrillar vesicles and electron opaque bodies (Figs. 3.2.4). Although some lipid droplets were present, they were not enriched at 4 h (Fig. 3.2.4). All specimens collected between 8 and 20 h of incubation exhibited ^{13}C -enrichments in the endoplasm. The signal was concentrated in fibrillar vesicles, electron opaque bodies, and lipids (Figs. 3.2.4, 3.2.5A - C). The cytoplasm itself was significantly more enriched after 8 h of incubation than after 4 h, with averages of $101 \pm 32\%$ and $39 \pm 23\%$, respectively ($p < 0.05$; Fig. 3.2.6). However, the cytoplasmic enrichment did not change statistically between 8 h and 20 h ($p > 0.05$; Fig. 3.2.6). No detectable ^{13}C -enrichments were detected in foraminifera incubated with $\text{H}^{13}\text{CO}_3^-$ in darkness (Experiment 2; Fig. 3.2.7).

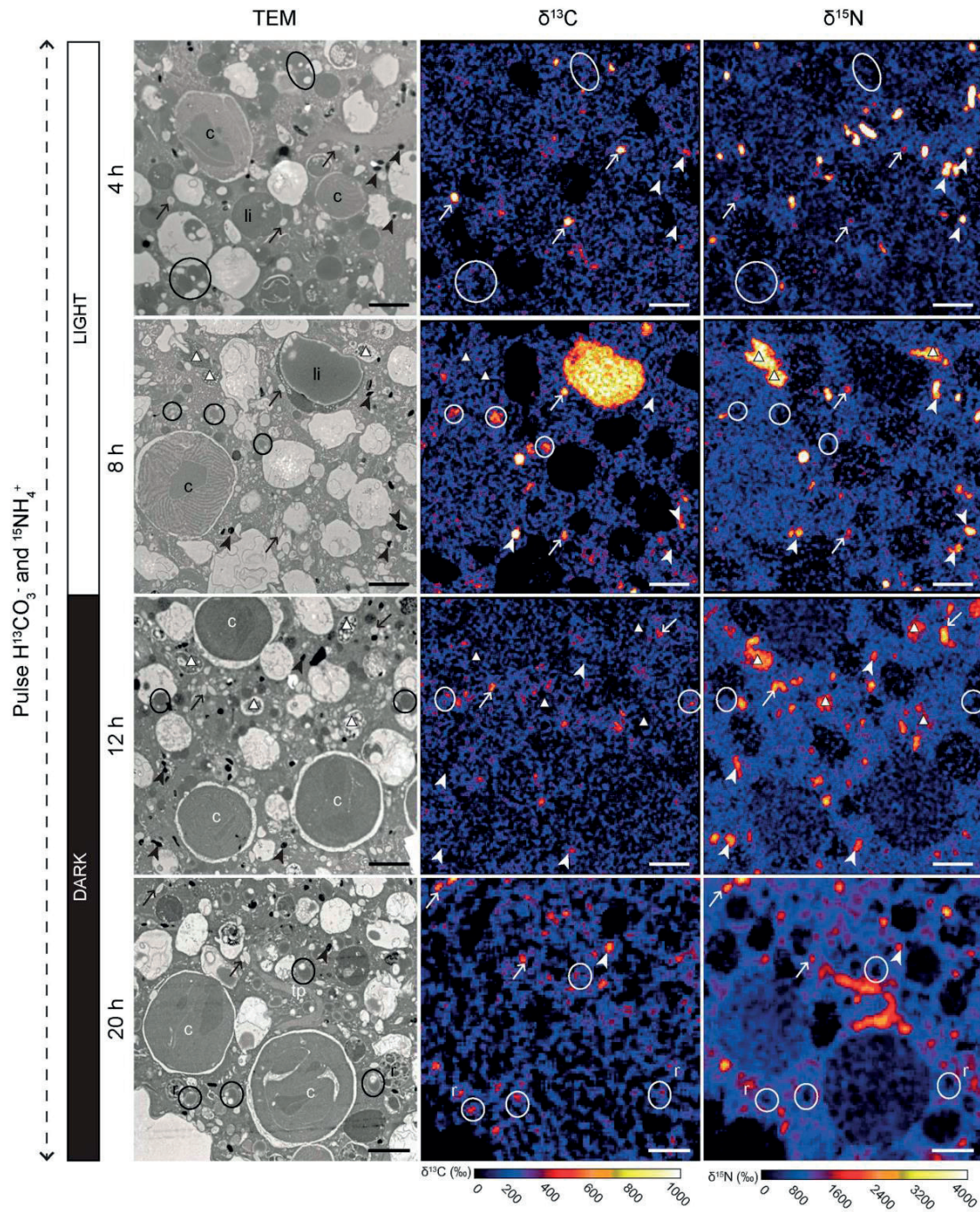


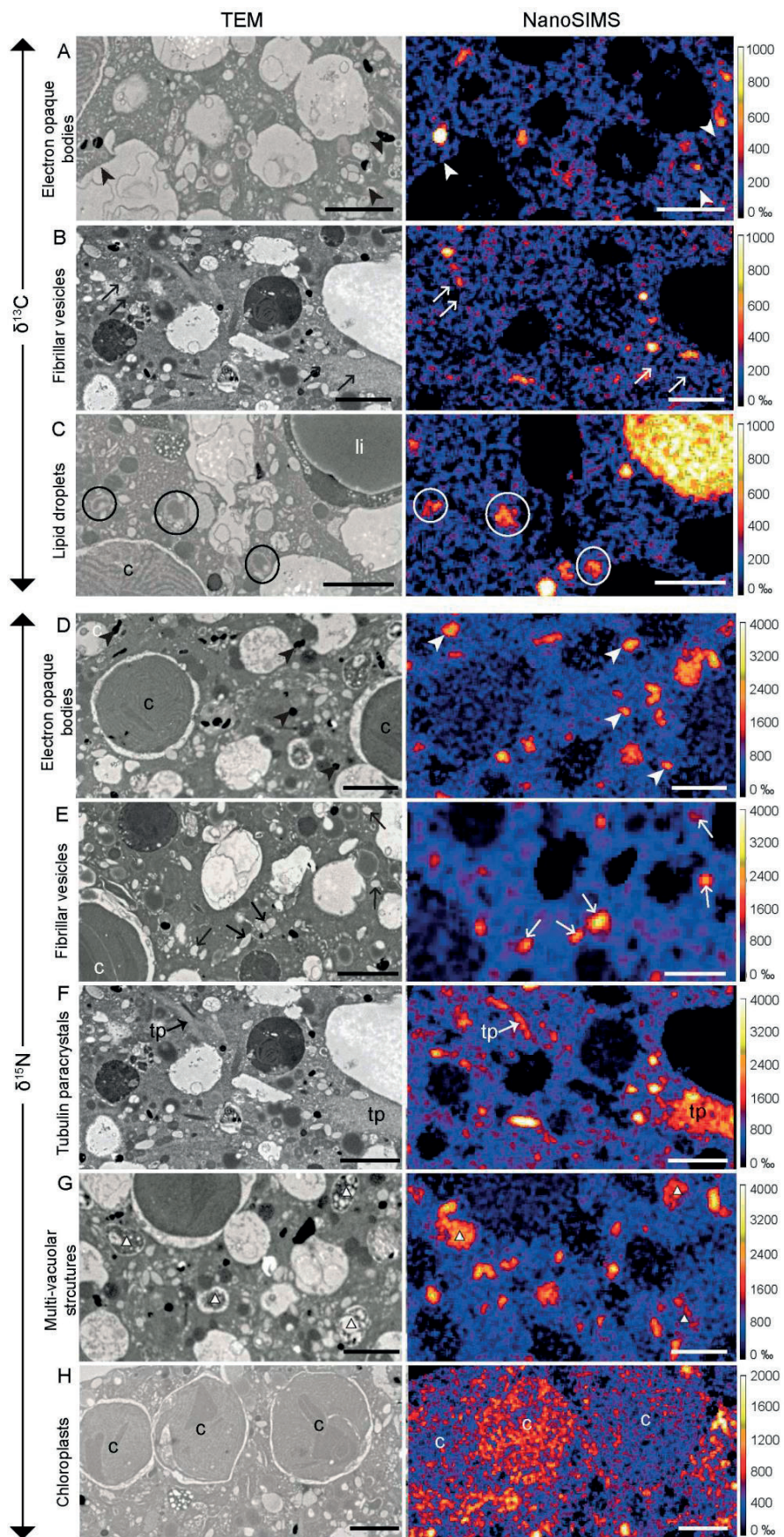
Figure 3.2.4: Time-evolution of ^{13}C and ^{15}N uptake and fate within the cytoplasm of *H. germanica* during Experiment 1 (light/dark incubation with $\text{H}^{13}\text{CO}_3^-$ and $^{15}\text{NH}_4^+$). Left column: TEM micrographs. Middle and right columns: corresponding NanoSIMS $\delta^{13}\text{C}$ and $\delta^{15}\text{N}$ images, respectively, expressed in ‰. Arrows: fibrillar vesicles; arrowheads: electron opaque bodies; circles and li: lipid droplets, white triangles: multi-vacuolar structures; c: chloroplast; re: residual bodies, tp: tubulin paracrystals. Scale bars: 2 μm .

3.3 Uptake of $^{15}\text{NH}_4^+$ in the foraminiferal cell.

All specimens of Experiment 1 exhibited detectable ^{15}N -enrichments. In the cytoplasm of *H. germanica*, ^{15}N -enrichments significantly increased between 4 and 8 h (during the light phase), from 254 ± 88 to 545 ± 140 ‰ ($p < 0.05$), and stabilized between 8 and 20 h ($p > 0.05$), i.e., during the dark phase (Fig. 3.2.6). Similar to the observed ^{13}C -enrichments, the ^{15}N -signal was concentrated in electron-opaque bodies and fibrillar vesicles (Figs. 3.2.4, 3.2.5D and E). However some of organelles were occasionally enriched in ^{15}N but not in ^{13}C . The tubulin paracrystals and the multi-vacuolar structures were also strongly enriched in ^{15}N after 8 h (Figs. 3.2.5F and G, 3.2.6). Kleptoplasts rarely exhibited ^{15}N -enrichments, which were then always moderate to low (Fig. 3.2.5H).

In Experiment 2, after 8h in darkness, the foraminifera had incorporated a much higher concentration of $^{15}\text{NH}_4^+$ (Fig. 3.2.6) compared with Experiment 1 at any given time ($p < 0.05$); the cytoplasmic average ^{15}N -enrichment reached a value of 1096 ± 115 ‰ after 8 h. As in Experiment 1, the ^{15}N isotopic signal was observed most concentrated in electron-opaque bodies, fibrillary vesicles, tubulin paracrystals, in the multi-vacuolar structures as well as in a few kleptoplasts (Fig. 3.2.7).

Figure 3.2.5 (p. 140): Foraminiferal organelles enriched in ^{13}C - and/or ^{15}N -enriched in Experiment 1 at different time points. Left column: TEM micrographs. Right column: corresponding NanoSIMS $\delta^{13}\text{C}$ (for A, B; C) and $\delta^{15}\text{N}$ images (for D, E, F, G, H) expressed in ‰. A, B and C: Organelles enriched in $\delta^{13}\text{C}$; A: electron-opaque bodies (after 8 h of incubation), B: fibrillar vesicles (after 20 h) and C: lipid droplets (after 8 h of incubation). D, E, F, G and H: organelles enriched in $\delta^{15}\text{N}$; D: electron-opaque bodies (after 12 h), E: fibrillar vesicles (after 20 h of incubation), F: tubulin paracrystals (after 18 h of incubation), G: multi-vacuolar structures (after 12 h of incubation) and H: chloroplasts (after 8 h of incubation). Arrowheads: electron-opaque bodies; arrows: fibrillar vesicles; circles and li: lipid droplets; c: chloroplast; white triangles: multi-vacuolar structures; tp: tubulin paracrystals. Scale bars: 2 μm .



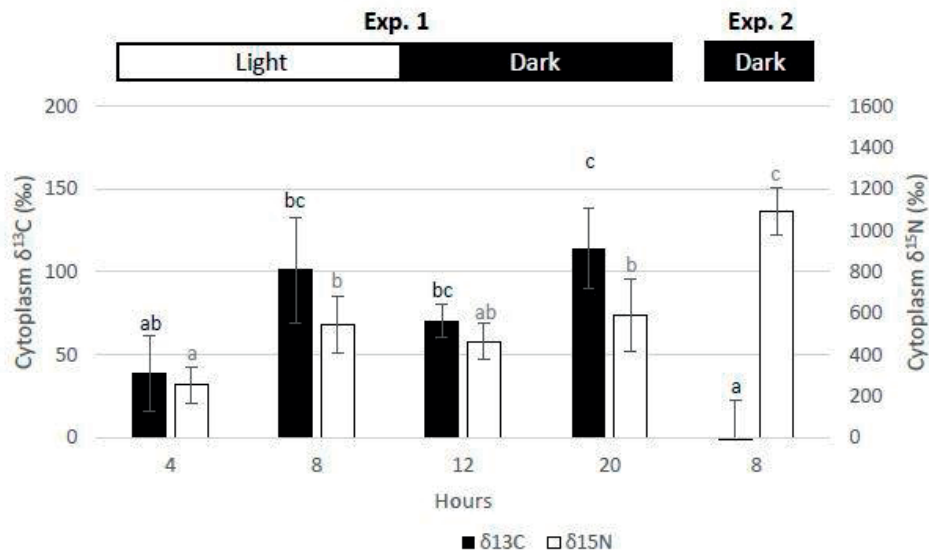


Figure 3.2.6: Average ^{13}C and ^{15}N enrichment of the cytoplasm of *H. germanica* ($n=3$) as a function of time. Error bars represent one standard deviation. Significant differences between time points and Experiment 1 and 2 are indicated in black for ^{13}C -enrichment, and in grey for ^{15}N -enrichment.

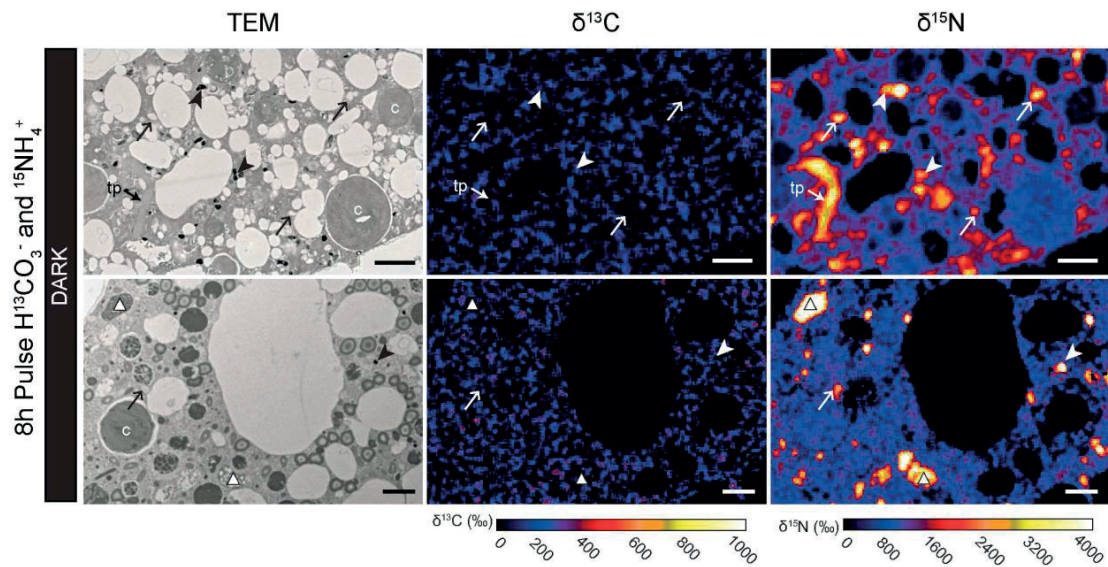


Figure 3.2.7: ^{13}C and ^{15}N uptake and fate within the cytoplasm of *H. germanica* during Experiment 2 (continuous dark incubation with $\text{H}^{13}\text{CO}_3^-$ and $^{15}\text{NH}_4^+$). Left column: TEM micrographs. Middle and right columns: corresponding NanoSIMS $\delta^{13}\text{C}$ and $\delta^{15}\text{N}$ images, respectively, expressed in ‰. Arrows: fibrillar vesicles; arrowheads: electron opaque dense bodies; circles: lipid droplets, white triangles: multi-vacuolar structures; c: chloroplast, tp: tubulin paracrystals. Scale bars: 2 μm .

4 Discussion

4.1 Ultrastructural observations

All specimens exhibited mitochondria with intact cristae and double-membranes indicating that they were alive at the time of fixation (Nomaki et al., 2016). The kleptoplasts observed in our study correspond to the morphological description made in chapter 3.1. for *H. germanica* collected from the Bourgneuf Bay (as in this study) and from the Wadden Sea (Mokbaai, NL). Specimens were well preserved with undamaged thylakoids and pyrenoids. The electron-lucent space that sometimes surrounded the kleptoplasts was also previously described in the chapter 3.1.) and ascribed to a possible fixation artefact. Indeed, an ultrastructural study of algal symbionts within the green ciliate *Paramecium bursaria* showed the same artefact in chemically fixed samples, whereas this artefact was absent in cryo-fixed samples (Song et al., 2017).

4.2 Assimilation of C

The correlated TEM-NanoSIMS observations allowed the visualization of inorganic C uptake ($\text{H}^{13}\text{CO}_3^-$) within foraminiferal cells incubated under a light/dark cycle (Figs. 3.2.4 and 3.2.6). The absence of ^{13}C assimilation in continuous darkness (Experiment 2, Figs 3.2.6 and 3.2.7) and the observed production of O_2 recorded in *H. germanica* in other studies (Cesbron et al., 2017; Jauffrais et al., 2016) strongly suggest that kleptoplasts have a functional Calvin-Benson cycle, resulting in the production and transfer of ^{13}C -photosynthates to the foraminiferal cell. Foraminifera can acquire C by different trophic mechanisms (Goldstein, 1999) but they are not known to actively uptake inorganic C in the absence of either bacterial symbionts or the presence of kleptoplasts. We found no indications of the presence of symbiotic cyanobacteria and, therefore, suggest that the observed incorporation of ^{13}C -bicarbonate is the result of photosynthesis occurring at the kleptoplasts. The absence of ^{13}C -enrichments inside the kleptoplasts (Figs. 3.2.4 and 3.2.5) can be attributed either to the fact that the ^{13}C -photosynthates are 1) transported away from the kleptoplasts immediately, 2) lost during sample fixation/dehydration/embedding, and/or 3) that the resin infiltration during the sample preparation has a diluting effect and bring the kleptoplast ^{13}C -enrichment below the detection limit of the NanoSIMS. In previous NanoSIMS studies of autotrophic ^{13}C -exchanges in the symbiotic association between dinoflagellates and corals, ^{13}C -enrichments in dinoflagellate chloroplasts were much lower than in other sub-cellular organelles, such as algal starch grains (Kopp et al., 2015a). In our study we have not yet seen any evidence of dividing kleptoplasts; this could explain the absence of ^{13}C -labeling in kleptoplasts as no ^{13}C would be incorporated in their structure during the experiment.

The numerous multi-vacuolar structures observed in *H. germanica* (Fig 3.2.2A, G, H) are similar to the bacteria observed in another benthic species, *Globocassidulina* cf. *G. bitor* (Bernhard, 1993). The presence of numerous such vacuoles within prokaryotic cells has already been described and linked to different biological functions like buoyancy (gas vacuoles) in planktonic bacteria or nitrate vacuoles in filamentous sulfur bacteria (e.g., Jørgensen and Gallardo, 1999; Walsby, 1972). Thus these structures could potentially be interpreted as endosymbionts, eventually photosynthetic. However they were not labeled in ^{13}C (Fig. 3.2.5G). Different NanoSIMS studies looking at ^{13}C -bicarbonate assimilation in cyanobacteria or anaerobic photosynthetic bacteria showed a strong bacterial ^{13}C -enrichment (e.g. Behrens et al., 2008; Finzi-Hart et al., 2009; Musat et al., 2008). Therefore we can conclude that even if the multi-vacuolar structures observed in our study are bacteria, the absence of ^{13}C in their cells is a solid argument to prove that they are not photosynthetic, and that thus they could not play any role in the inorganic ^{13}C assimilation.

Carbon was assimilated during the light phase, transferred to the foraminiferal cell, and accumulated in specific organelles: electron-opaque bodies, fibrillar vesicles, and lipid droplets. Lipid droplets are indeed the main C storage form in foraminifera. A similar accumulation process/sequence has been observed in symbiotic planktonic foraminifera *Orbulina universa*, where photosynthesis led to an assimilation of inorganic C ($\text{H}^{13}\text{CO}_3^-$) stored in the form of lipid droplets (Chapter 4).

In kleptoplastic sea slugs (e.g., *Elysia chlorotica*), lipid droplets observed in the animal tissue were argued to result from the exudation of lipids from the plastids because their fatty acids had a large proportion of algal-derived eicosapentaenoic acid (20:5) (Pelletreau et al., 2014). However, the authors could not conclude whether the plastids transferred directly via triacylglycerols (TAGs) or free fatty acids which will be further transformed by the host to enter lipid droplets. The *de novo* production of triacylglycerol by chloroplasts in marine algae has been demonstrated (Fan et al., 2011; Merchant et al., 2012). Furthermore, *de novo* fatty acid synthesis is known to occur in plant cell chloroplasts (Ohlrogge et al., 1979), followed by a transfer in the form of free fatty acids to the cytosol (Koo et al., 2004). Additional transfer of soluble molecules such as maltose or glucose across the chloroplast membranes through transporters also takes place in plant cells (e.g. Weber, 2004). In the present study the close association observed between kleptoplast membranes and small lipid droplets (Fig. 3.2.3) could indicate a potential transfer of C via the exudation of small lipid droplets from the kleptoplast to *H. germanica* cell, although the detailed mechanisms by which the fatty acids would cross the kleptoplast membranes remain unknown. Unfortunately the distribution of soluble molecules cannot be investigated with the NanoSIMS because the sample preparation protocol causes near complete loss of such components.

4.3 Assimilation of N

Teugels *et al.* (2008) reported that ammonium assimilation by the kleptoplastic sacoglossan *Elysia viridis* was significantly higher under the light condition than in darkness, consistent with the glutamine oxoglutarate aminotransferase (GOGAT) enzyme requiring electron donors (e.g., reduced ferredoxin formed in the photosynthetic electron transport) (Grossman and Takahashi, 2001). Furthermore, the glutamate synthase (GS) metabolic reaction is ATP-dependent, and gene expression of some key enzymes (GS and GOGAT) is light regulated (Grossman and Takahashi, 2001). In corals, symbiotic dinoflagellate GS/GOGAT enzymes is thought to be the main ammonium assimilation pathway (Anderson and Burris, 1987; Kopp *et al.*, 2013; Pernice *et al.*, 2012; Rahav *et al.*, 1989). Furthermore, cnidarian cells are also known to produce cytosol glutamate dehydrogenase (GDH) (Rahav *et al.*, 1989; Wang and Douglas, 1998; Yellowlees *et al.*, 1994). This enzyme has a dual function: 1) it converts glutamate to α -ketoglutarate and ammonium, which is subsequently assimilated in the chloroplasts via the GOGAT pathway (Teugels *et al.* 2008), 2) it also catalyzes the opposite reaction, i.e. the amination of the α -ketoglutarate to produce the amino acid glutamate (Srivastava and Singh, 1987).

In our study, the observation of ^{15}N -labeled kleptoplasts in *H. germanica* seems consistent with a GS/GOGAT kleptoplastic pathway for ammonium assimilation (Fig. 3.2.5H). However, the uptake of ^{15}N -ammonium was higher after 8 h of incubation in total darkness (Experiment 2) than in Experiment 1 (light-dark cycle) (Fig. 3.2.6). And the same organelles (fibrillar vesicles, electron-opaque bodies and multi-vacuolar structures) were found to be ^{15}N -enriched. This higher uptake in darkness than under light is not coherent with the light regulation of the GS/GOGAT enzymatic machinery (Grossman and Takahashi, 2001). Ammonium incorporation might thus also take place by another N-assimilation pathway in foraminifera, for example through the glutamine dehydrogenase (GDH) pathway in mitochondria.

Ammonium is known to be a suitable N source for many marine prokaryotes (e.g. Tupas and Koike, 1991; Wheeler and Kirchman, 1986; Zehr and Ward, 2002). Thus if the multi-vacuolar structures, abundant in all *H. germanica* specimens (Fig 3.2.2A, G, H) are endosymbionts (see above) they would be expected to incorporate $^{15}\text{NH}_4^+$, as it is indeed observed (Fig. 3.2.5G). They could thus constitute another putative nitrogen assimilation pathway for the benthic foraminifera *H. germanica*. However we cannot conclude in our study about the symbiotic nature of these putative prokaryotes in *H. germanica*, nor about their role in foraminiferal N metabolism.

4.4 Advantages of a mixotrophic strategy

A comparative study of organic C (algae) uptake through feeding between the two dominant foraminiferal species inhabiting mudflats, the akleptoplastic *Ammonia* sp. and kleptoplastic *H. germanica*, showed a higher uptake rate for the former (Wukovits et al., 2016). Our results highlight that *H. germanica* can fix inorganic carbon. Therefore, unlike *Ammonia* sp., *H. germanica* does not rely solely on food to meet its C requirements. The mixotrophic feeding strategy of *H. germanica* might give a competitive advantage and allow it to become dominant in the foraminiferal assemblage in these environments (e.g. Cesbron et al., 2016; Debenay et al., 2006; Mojtahid et al., 2016). Also, whether *H. germanica* assimilates nitrogen through the kleptoplasts, potential endosymbionts or by another pathway specific to foraminifera, our observations demonstrate that it is capable of using inorganic N as a nutrient source. Further investigation is required to quantify this uptake and elucidate the role of this benthic foraminifera in the N cycle; especially since *H. germanica* thrives in coastal ecosystems that are subject to increasing eutrophication (Diaz and Rosenberg, 2008; Zhang et al., 2010).

5 Conclusion

Our study shows inorganic C is assimilated, most likely via the kleptoplasts in *Haynesina germanica*. The absence of ^{13}C assimilation in darkness combined with previous studies documenting O_2 production in light strongly suggest photosynthesis as the process dominating inorganic C-assimilation. Subsequently, photosynthates are transferred to the foraminiferal cell and utilized in the general metabolism. The observation of small lipid droplets attached to the kleptoplast membranes might suggest a transfer of C from the kleptoplasts to the foraminiferal cell in the form of lipids. However, the detailed mechanism(s) involved in this transfer remains unknown. The kleptoplasts might also provide the added value of furnishing additional N sources to foraminiferal metabolic pathways via their GS-GOGAT enzymes. However, ammonium assimilation was even more efficient in darkness, requiring the existence of other N-assimilation pathways (e.g., in mitochondria).

Acknowledgements:

The electron microscopy platform at the University of Lausanne (Switzerland) is acknowledged for technical assistance.

Funding sources:

This work was supported by the Swiss National Science Foundation (grant no. 200021_149333) and was part of the CNRS EC2CO-Lefe project ForChlo. It was also supported by the Region Pays de la Loire (Post-doc position of TJ, on Fresco projects) as well as the WHOI Robert W. Morse Chair for Excellence in Oceanography and The Investment in Science Fund at WHOI.

Supporting information

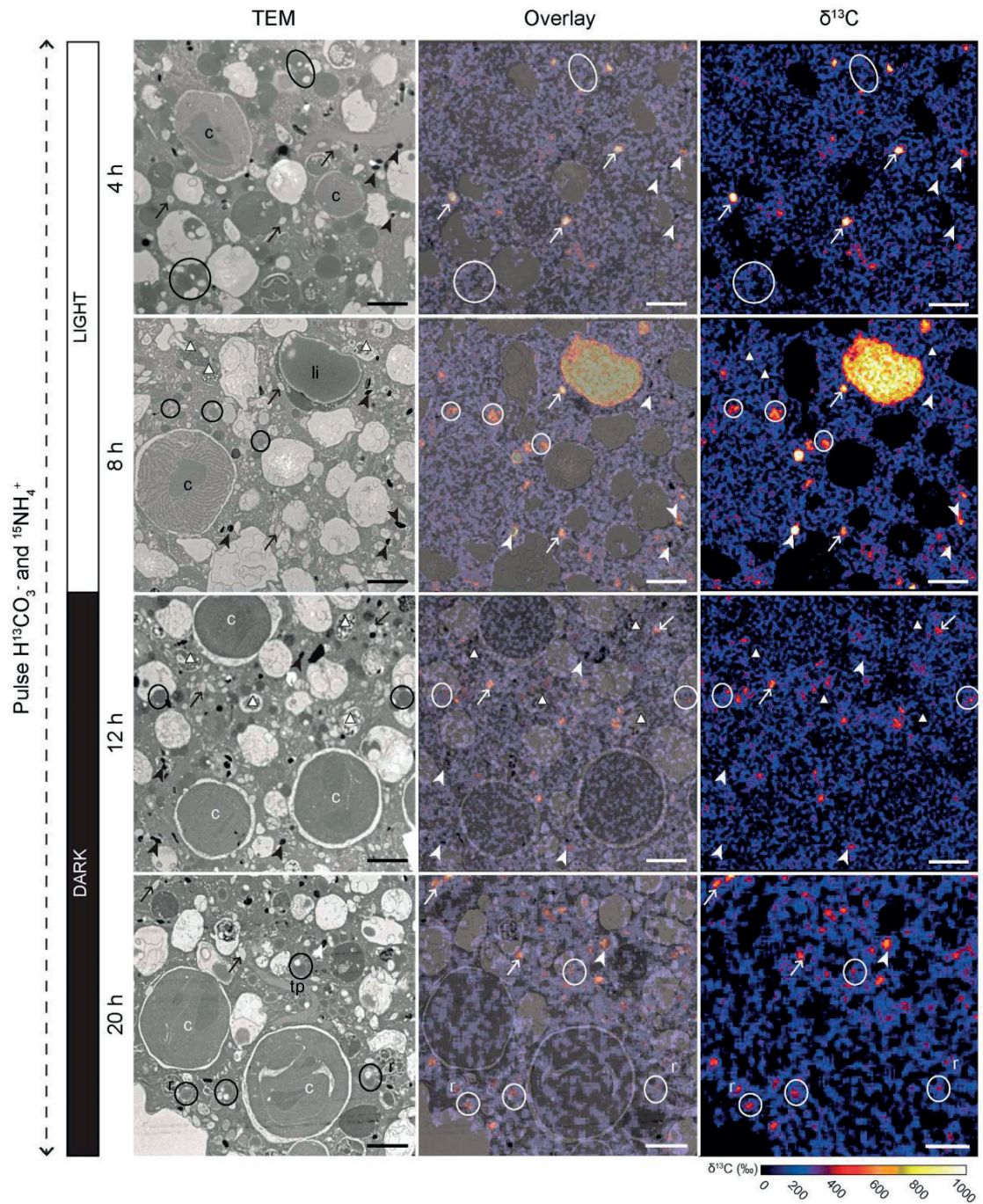


Figure 3.2.S1: Time-evolution of ^{13}C uptake and fate within the cytoplasm of *H. germanica* during Experiment 1 (light/dark incubation with $\text{H}^{13}\text{CO}_3^-$ and $^{15}\text{NH}_4^+$). Left column: TEM micrographs. Right columns: corresponding NanoSIMS $\delta^{13}\text{C}$ images expressed in ‰. Central column: overlay between TEM and NanoSIMS images. Arrows: fibrillar vesicles; arrowheads: electron opaque bodies; circles: small lipid droplets, white triangles: multi-vacuolar structures; c: chloroplast; li: large lipid droplets; re: residual bodies, tp: tubulin paracrystals. Scale bars: 2 μm .

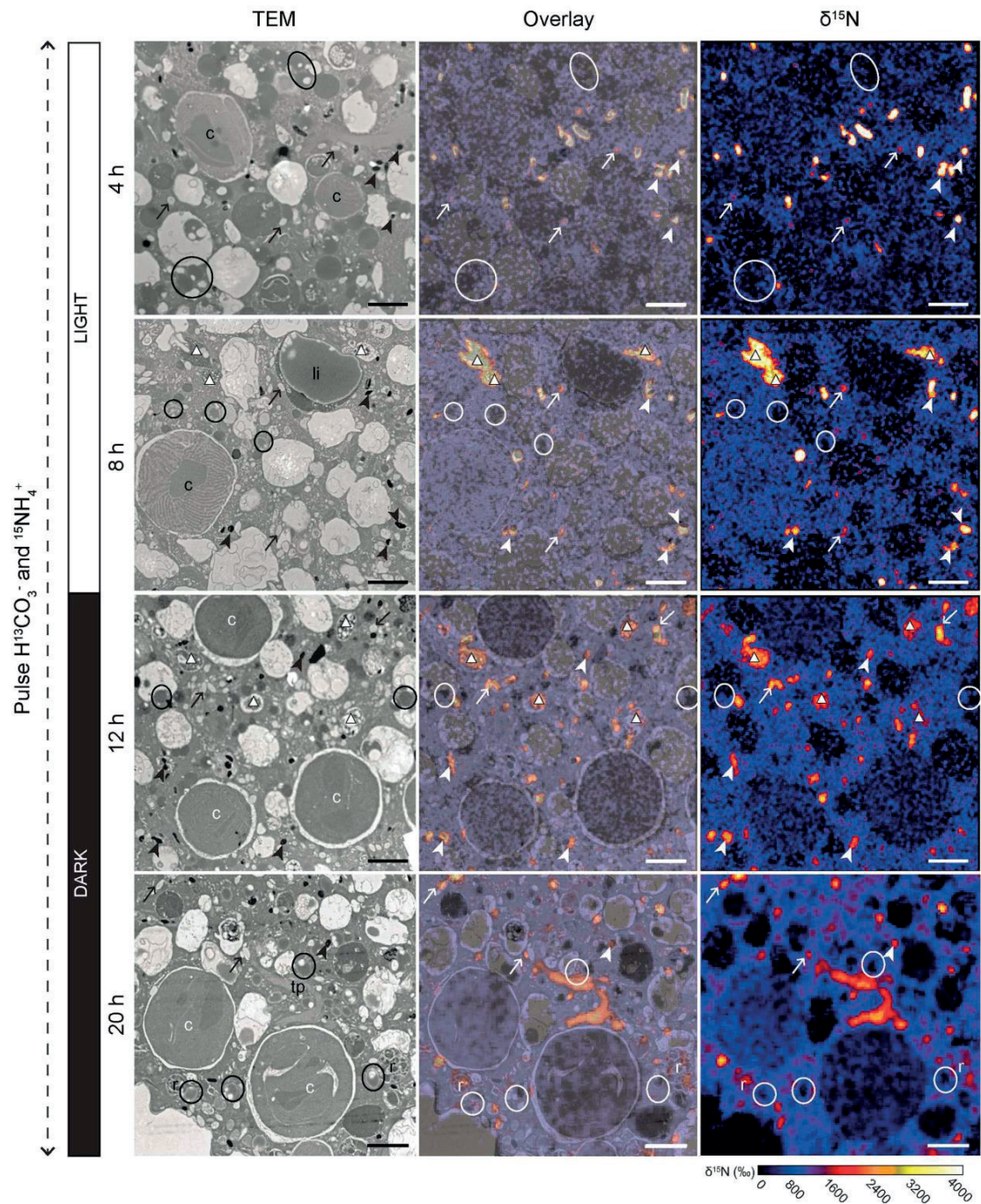


Figure 3.2.S2: Time-evolution of ^{15}N uptake and transfer within the cytoplasm of *H. germanica* during Experiment 1 (light/dark incubation with $\text{H}^{13}\text{CO}_3^-$ and $^{15}\text{NH}_4^+$). Left column: TEM micrographs. Right columns: corresponding NanoSIMS $\delta^{15}\text{N}$ images expressed in ‰. Central column: overlay between TEM and NanoSIMS images. Arrows: fibrillar vesicles; arrowheads: electron opaque bodies; circles: small lipid droplets, white triangles: multi-vacuolar structures; c: chloroplast; li: large lipid droplets; re: residual bodies, tp: tubulin paracrystals. Scale bars: 2 μm .

Chapter 3.3: Carbon, ammonium and sulfate uptake by benthic foraminifera: A comparison between kleptoplastic and non-kleptoplastic species from a photic environment

This chapter presents the result of a preliminary experiment investigating the inorganic carbon, ammonium and sulfate assimilation by a kleptoplastic foraminiferal species. The species chosen is *Elphidium williamsoni*, a benthic species inhabiting coastal ecosystems and thus inhabiting photic environments. In order to better understand the role of the kleptoplasts in the metabolic pathways, the results obtained for *Elphidium williamsoni* were compared to another species: the non kleptoplastic *Ammonia cf. tepida*. As it is emphasized in the discussion, this study will be completed by a second series of experiments to clarify the foraminiferal metabolic pathways unravel by this first TEM-NanoSIMS study.

PhD student's contribution: the PhD student collected the samples from the field with TJ and OM; designed the experiment with EG, TJ and AM; analyzed the samples for TEM and NanoSIMS imaging; interpreted the data with TJ and EG, and wrote this manuscript with edit and comments from EG, TJ and AM. TJ performed the O₂ (respiration rate) measurements. This experiment will later be completed with complementary analysis, thus the manuscript was not edited and commented yet by all co-authors.

Carbon, ammonium and sulfate uptake by benthic foraminifera: A comparison between kleptoplastic and non-kleptoplastic species from a photic environment

Charlotte LeKieffre¹, Thierry Jauffrais², Joan M. Bernhard³, Bruno Jesus^{4,5}, Helena L. Filipsson⁶, Olivier Maire^{7,8}, Anders Meibom^{1,9}, Emmanuelle Geslin²

¹ Laboratory for Biological Geochemistry, School of Architecture, Civil and Environmental Engineering (ENAC), Ecole Polytechnique Fédérale de Lausanne (EPFL), 1015 Lausanne, Switzerland

² UMR CNRS 6112 LPG, Bio-Indicateurs Actuels et Fossiles, Université d'Angers, 2 Boulevard Lavoisier, 49045 Angers CEDEX 1, France

³ Woods Hole Oceanographic Institution, Geology & Geophysics Department, Woods Hole, MA, USA

⁴ EA2160, Laboratoire Mer Molécules Santé, Université de Nantes, Nantes, France

⁵ BioISI – Biosystems & Integrative Sciences Institute, Campo Grande University of Lisboa, Faculty of Sciences, Lisboa, Portugal.

⁶ Department of Geology, Lund University, Sölvegatan 12, SE-223 62 Lund, Sweden

⁷ Univ. Bordeaux, EPOC, UMR 5805, F-33400 Talence, France

⁸ CNRS, EPOC, UMR 5805, F-33400 Talence, France

⁹ Center for Advanced Surface Analysis, Institute of Earth Sciences, University of Lausanne, Switzerland

1 Introduction

As kleptoplasty in benthic foraminifera was already described in the two previous chapters, this introduction will focus on carbon, nitrogen and sulfur metabolism in kleptoplastic and non kleptoplastic foraminifera.

To our knowledge, only four studies have investigated the chloroplast functionality in foraminifera inhabiting photic areas. One study examined the functionality of the xanthophyll cycle in *H. germanica* (Jauffrais et al., 2017), two studies measured the O₂ production by sequestered chloroplasts in *H. germanica*: using oxygen microelectrodes they recorded values from about 200 to 1000 pmol O₂ cell⁻¹ d⁻¹ (Cesbron et al., 2017; Jauffrais et al., 2016). A fourth study estimated the production of photosynthates by incubating foraminifera with H¹⁴CO₃ (Lopez, 1979). With this method kleptoplastic foraminifera were shown to assimilate inorganic carbon only under light incubation (i.e. no assimilation was observed under darkness). In addition, this uptake was proportional to the foraminiferal chlorophyll content.

In Chapter 3.2 it was shown that kleptoplastic *H. germanica* assimilate inorganic ¹³C-bicarbonate, most likely through photosynthesis. The resulting photosynthates are transferred to the foraminiferal cell to be stored, primarily in lipid droplets, or used in the cell metabolism. *H. germanica* is therefore mixotroph (Cesbron et al., 2017). It can obtain nutrients through both heterotrophy (i.e.

feeding) and autotrophy (photosynthesis). This gives a major advantage to this species over non-kleptoplastic and other meiofaunal species in its environment. The first objective of this new experiment is to investigate whether or not similar C assimilation and transfer happens in another kleptoplastic species, *E. williamsoni*, and if intracellular pathways appear similar.

Non-symbiotic algal cells, including diatoms from which the foraminifera are obtaining the chloroplasts (Correia and Lee, 2002a; Grzyski et al., 2002; Lechlitter, 2014; Pillet et al., 2011; Tsuchiya et al., 2015), uptake inorganic N (i.e., ammonium, nitrite, or nitrate) from their surrounding environment and assimilate it via the GS/GOGAT (glutamate synthase and glutamine oxoglutarate aminotransferase) enzymatic machinery of the chloroplast to form amino acids (Syrett, 1981; Zehr et al., 1988; Zehr and Falkowski, 1988). A role for the kleptoplasts in foraminiferal N metabolism was first suggested in the case of foraminifera inhabiting aphotic environments, in order to explain the presence of kleptoplasts despite the absence of light and thus photosynthesis (Bernhard and Bowser, 1999; Grzyski et al., 2002). In Chapter 3.2 it was shown that, in addition to inorganic C assimilation, *H. germanica* is capable of assimilating ^{15}N -ammonium. However, it was not possible to determine the role of the kleptoplasts in this assimilation. The second objective of this new experiment will be to clarify the role of kleptoplasts in foraminiferal N metabolism by comparing ^{15}N -assimilation and intracellular dynamics between a kleptoplastic and a non-kleptoplastic species.

Finally, this study investigates potential differences in sulfate assimilation between and kleptoplastic and a non-kleptoplastic species. Chloroplasts play many roles in algal cells, besides C and potential N assimilation they can also assimilate sulfate and use it to form sulfated amino acids (like cysteine) and sulfolipids, which are essential components of thylakoids and chloroplast membranes (Benning and Garavito, 2008; Giordano et al., 2008; Giordano and Raven, 2014; Takahashi et al., 2011). Diatoms in particular are known to exhibit sulfo-lipid concentrations higher than in other algae or plants (Goss and Wilhelm, 2009; Vieler et al., 2007). The third objective of this work is therefore to investigate potential difference in the sulfate metabolism between kleptoplast and non-kleptoplast foraminiferal species.

If kleptoplasts play a role in foraminiferal inorganic nitrogen and sulfur assimilation, it would provide the foraminifera with a great advantage. As for C, they could rely on nutrient source other than heterotrophic feeding, by meeting their nutrient requirements in N and S through an additional autotrophic mechanism.

In this chapter, using the approach of stable isotopic labeling experiments together with correlated TEM-NanoSIMS imaging and respiration rate measurements, we will investigate and compare the C, N and S metabolisms of two species: the kleptoplastic *E. williamsoni*, and the non-

kleptoplastic *Ammonia* cf. *tepida*. We have three main objectives: (1) to compare the fate of inorganic C assimilated by *E. williamsoni* and another kleptoplastic species *H. germanica* (Chapter 3.2); (2) to assess whether or not the kleptoplasts are playing any role in the foraminiferal N metabolism by comparing a kleptoplastic and a non-kleptoplastic species; and (3) to investigate their potential role in foraminiferal S metabolism.

2 Material and methods

2.1 Sampling and incubation in light condition with $\text{H}^{13}\text{CO}_3^-$, $^{15}\text{NH}_4^+$ and $^{34}\text{SO}_4^{2-}$

Living foraminifera were collected on the May 9, 2016, at low tide on an intertidal mudflat located next to Fiskebäckskil harbor in the Gullmar fjord (Sweden; 58.240768 N, 11.460901 E). The top 5 millimeters of the sediment were sampled and immediately transported in the dark to the laboratory.

The incubation was carried out at the Kristineberg Sven Lovén Center for Marine Infrastructure (Sweden) the day after collection. In the laboratory, the sediment was sieved on a 300 μm mesh with natural surface sea water directly pumped from the fjord. Only the fraction $>300 \mu\text{m}$ was used. Living individuals of the foraminiferal species *Elphidium williamsoni* and *Ammonia* cf. *tepida* were selected under a binocular based on the color of their cytoplasm (yellow-brownish material spread through all the chambers of the specimen (except the last chamber) the day before the experiment and let overnight in Petri-dish filled with seawater to check their vitality. Ten specimens per species were selected and placed into new plastic Petri dishes (1 species per Petri dish and 5 specimens per species). Two Petri dishes were filled with artificial seawater (Red Sea Salt, salinity = 34) spiked with 2 mM $\text{NaH}^{13}\text{CO}_3$, 10 μM $^{15}\text{NH}_4\text{Cl}$, and 25mM $\text{Na}^{34}\text{SO}_4$ (Cambridge isotope Inc.); the other two were filled with natural seawater. The specimens incubated with natural seawater were used as control for NanoSIMS analysis; see below. The incubation was carried in a cold room at 10°C with a light source set at 90 $\mu\text{mol photon m}^{-2} \text{s}^{-1}$. After 20 h of incubation with light the foraminifera were immediately chemically fixed by transferring them individually to microtubes filled with fixative solution.

2.2 Preparation for TEM-NanoSIMS studies

Chemical fixation and transmission electron microscopy (TEM) of the foraminifera were performed at the Electron Microscopy Facility of the University of Lausanne (Switzerland).

The specimens were chemically fixed following the protocol described in previous chapters. Briefly, they were fixed at room temperature for 24 h with a mix of glutaraldehyde 4 % and paraformaldehyde 2 % diluted in cacodylate buffer 0.2 M, sucrose 0.4 M and NaCl 0.1 M (pH = 7.4). After rinsing, specimens were decalcified in two successive baths (1 and 48 h) with a solution of 0.1 M of EDTA diluted in cacodylate buffer 0.1M, then post-fixed for 1 h in osmium tetroxide 2 % diluted in distilled water. After a series of dehydration in ethanol, the samples were embedded into an acrylic resin (LR White). Specimens were cut into 70 nm ultra-thin sections with an ultramicrotome (Reichert ultracut S). Sections were placed on carbon-formvar coated copper grids and post-stained 10 min with uranyl acetate 2 % before TEM observations (Philips 301 CM100, 80kV). The study focused on

chambers located between $n - 3$ to $n - 8$ (n being the youngest chamber next to the aperture). The integrity of the mitochondria and the membranes of all the specimens were checked by TEM observations as described by (Nomaki et al., 2016) to ensure the vitality of the studied specimens.

2.3 Stable isotope mapping with NanoSIMS

Sample sections were mounted on 10 mm aluminum disks with double sticking Cu-tape and coated with a ca. 10 nm thick gold layer before being imaged with a NanoSIMS (Secondary Ion Mass Spectrometry) 50L ion microprobe to image and quantify the distribution of ^{13}C , ^{15}N and ^{34}S enrichment (Hoppe et al., 2013). NanoSIMS analyses were carried out on the areas of interest chosen from TEM images.

Foraminifera sections were imaged with the NanoSIMS ion microprobe with a 16-keV primary ion beams of Cs^+ , focused to a spotsize of about 150 nm. Secondary molecular ions $^{12}\text{C}_2^-$, $^{13}\text{C}^{12}\text{C}^-$, $^{12}\text{C}^{14}\text{N}^-$ and $^{12}\text{C}^{15}\text{N}^-$, $^{32}\text{S}^-$ and $^{34}\text{S}^-$ were collected in electron multipliers detectors. Isotopic images ranging in size from $15 \times 15 \mu\text{m}$ to $30 \times 30 \mu\text{m}$ with 256×256 pixels resolution were obtained. For each image 6 layers were acquired, drift corrected, and accumulated using the software L'IMAGE (developed by Dr. Larry Nittler, Carnegie Institution of Washington, USA). The quantified $^{13}\text{C}/^{12}\text{C}$ ratio distribution was obtained by the ratio of $^{12}\text{C}^{13}\text{C}^-$ with the $^{12}\text{C}_2^-$, the $^{15}\text{N}/^{14}\text{N}$ ratio distribution was obtained by the ratio of $^{12}\text{C}^{15}\text{N}^-$ with the $^{12}\text{C}^{14}\text{N}^-$ and the $^{34}\text{S}/^{32}\text{S}$ by the ratio of $^{34}\text{S}^-$ with $^{32}\text{S}^-$ as follows:

$$\delta^{13}\text{C} (\text{‰}) = \left(\left(C_{mes} / C_{nat} \right) - 1 \right) \times 10^3$$

$$\delta^{15}\text{N} (\text{‰}) = \left(\left(N_{mes} / N_{nat} \right) - 1 \right) \times 10^3$$

$$\delta^{34}\text{S} (\text{‰}) = \left(\left(S_{mes} / S_{nat} \right) - 1 \right) \times 10^3$$

Where C_{mes} is the measured $^{12}\text{C}^{13}\text{C}^- / ^{12}\text{C}_2^-$ ratio and C_{nat} is the average natural $^{12}\text{C}^{13}\text{C}^- / ^{12}\text{C}_2^-$ ratio measured in unlabeled samples (control). Similarly, N_{mes} and S_{mes} are the $^{12}\text{C}^{15}\text{N}^- / ^{12}\text{C}^{14}\text{N}^-$ and $^{34}\text{S}^- / ^{32}\text{S}^-$ ratios measured and N_{nat} and S_{nat} are the corresponding natural ratios measured in non-labelled samples.

2.4 Respiration rates

An oxygen microelectrode $50 \mu\text{m}$ Clark (OXI50 - Unisense, Denmark) was used to measure the oxygen flux (Revsbech 1989) around *E. williamsoni*. The microelectrode was calibrated using ASW

saturated in oxygen (100%) and a solution of sodium ascorbate for anoxic conditions (0.1 M). The oxygen respiration rates were measured as described in Høglund et al. (2008) and Geslin et al. (2011). Measurements were done in glass micro-tube with an inner diameter of 1 mm. The tube was pasted to a small vial, filled with artificial seawater (salinity = 34). The vial was then placed in a thermo-regulated aquarium at 10°C. Each measure was carried out on seven specimens placed at the bottom of the glass micro-tube. The experiment was repeated three times with different specimens each time. Measurements registered oxygen micro-profiles on total period of 4 hours: 90 min of light, followed by 120 min of night and 30 min of light again with a light intensity set at 300 $\mu\text{mol m}^{-2} \text{s}^{-1}$ for the light phases. Oxygen micro-profiles were made at a distance of 200 μm to 1100 μm away from the specimens to avoid oxygen turbulences around foraminifera, in steps of 50 μm (Geslin et al 2011). The first law of Fick was applied to calculate the oxygen flux (J):

$$J = -D \times \left(\frac{dC}{dx} \right)$$

Where D is the O_2 diffusion coefficient ($\text{cm}^2 \text{s}^{-1}$) at 10°C and salinity of 34 (Li and Gregory 1974), and dC/dx the O_2 concentration gradient ($\text{pmol O}_2 \text{cm}^{-1}$). The O_2 concentration gradients were calculated using the O_2 profiles and the R^2 of the regression line to determine the best gradient. Oxygen consumption was calculated as the product of O_2 fluxes by the surface area of the micro-tube and subsequently divided by the number of specimens in order obtain the cell specific rate ($\text{pmol O}_2 \text{cell}^{-1} \text{d}^{-1}$) (Geslin et al 2011).

3 Results

3.1 Ultrastructural observations

The TEM observations of *Ammonia cf. tepida* and *E. williamsoni* cytoplasm revealed ultrastructural differences. *E. williamsoni* cytoplasm was shown to harbor many kleptoplasts mainly present at the cell periphery, although some could be found within the cytoplasm (Fig. 3.3.1 A, B). All kleptoplasts were surrounded by a host membrane, with an electron-lucent space between the plast and the foraminiferal cytoplasm (Fig. 3.3.1 B, C). Most of the kleptoplasts were intact with fine-structural features discernable: the thylakoids, the pyrenoids and their transecting lamella (Fig. 3.3.1 C). In some of the kleptoplasts lipid inclusions, interpreted as plastoglobuli, were observed (Fig. 3.3.1 C). *E. williamsoni* cytoplasm also contained numerous unknown vesicles that were called “thick membrane vesicles”, these vesicles have the same size and shape than the fibrillar vesicles but they lack the fibrils and possess a thick membrane (Fig. 3.3.1 D, E). They were abundant in *E. williamsoni* but absent from *Ammonia cf. tepida* cytoplasm.

Ammonia cf. tepida cytoplasm did not exhibit any intact kleptoplasts (Fig. 3.3.2 A). Lipid droplets were observed in both species but were bigger in *Ammonia cf. tepida* with a diameter of 2 – 5 μm (Fig 3.3.2 B) versus ca. 1 μm in *E. williamsoni* (Fig. 3.3.1 D). Unlike *E. williamsoni*, *Ammonia cf. tepida* exhibited some residual bodies throughout its cytoplasm (Fig. 3.3.2 A). The residual bodies are circular vacuoles with a diameter of about 2 to 5 μm , containing heterogeneous material.

Fibrillar vesicles (small oval vesicles of about 500 nm in length containing fibrils) and electron-opaque bodies (200 to 500 nm inclusions) were abundant in both species (Figs. 3.3.1 D, E and 3.3.2 B, C). Finally intact mitochondria with clearly distinguishable double membrane and crests were observed in all the specimens of both species, indicating their vitality at the time of fixation (i.e. after the incubation).

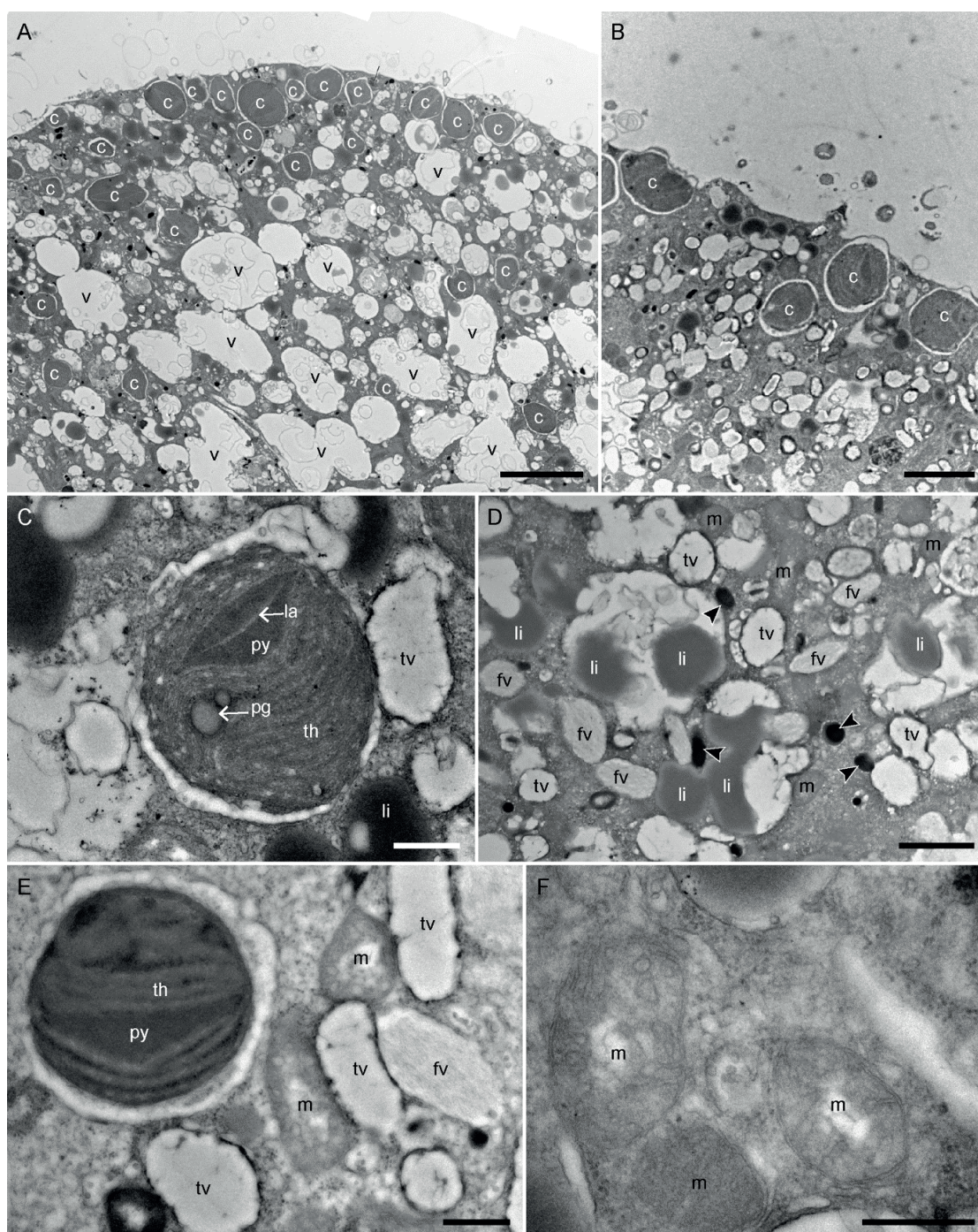


Figure 3.3.1: TEM micrographs of the cytoplasm of *Elphidium williamsoni*. A: Global view of the cytoplasm with numerous vacuoles and kleptoplasts. The kleptoplasts are distributed throughout the whole chamber but are mainly concentrated along the external wall. B: Kleptoplasts distributed along the external wall. C: Detailed structure of a kleptoplast. D: Higher magnification image of the cytoplasm with lipid droplets, mitochondria, electron-opaque bodies, fibrillar vesicles and thick-membrane vesicles. E: Structure of the fibrillar and the thick-membrane vesicles. F: Mitochondria with visible intact cristae and double membrane. Arrowheads: electron-opaque bodies, c: chloroplasts, fv: fibrillar vesicles, la: chloroplast lamella, li: lipid droplets, m: mitochondria, pg: plastoglobuli, py: chloroplast pyrenoid, th: chloroplast thylakoids, tv: thick-membrane vesicles, v: vacuoles. A = 5 μm ; B = 2 μm ; C, E and F = 500 nm; D = 1 μm .

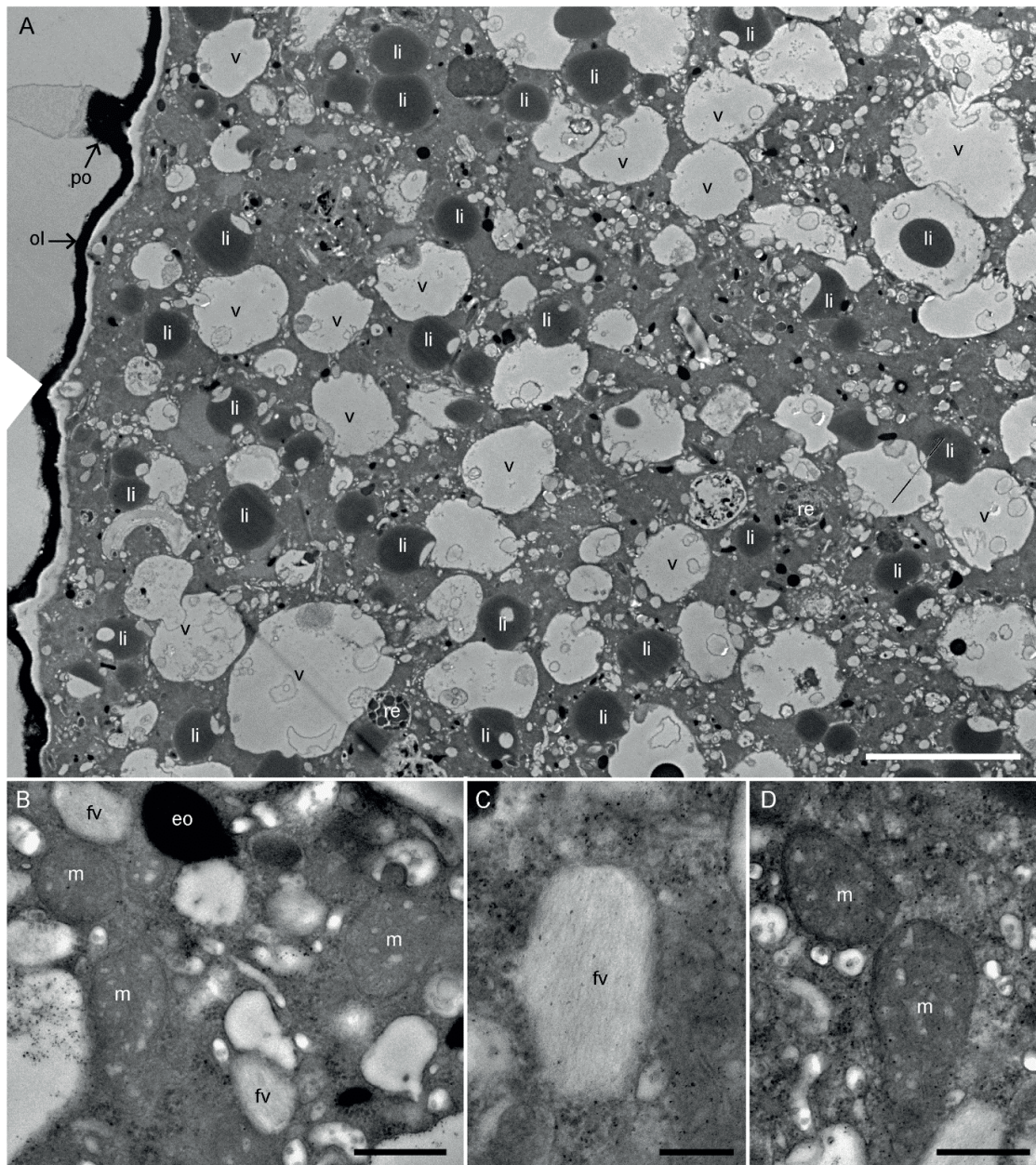


Figure 3.3.2: TEM micrographs of the cytoplasm of *Ammonia cf. tepida*. A: Global view of the cytoplasm with numerous lipid droplets, vacuoles and a few residual bodies. B: Higher magnification image of mitochondria, electron-opaque bodies and fibrillar vesicles. C: Detail structure of a fibrillar vesicle, fibrils are organized in parallel. D: Mitochondria with visible intact cristae and double membrane. eo: electron-opaque bodies, fv: fibrillar vesicles, li: lipid droplets, m: mitochondria, ol: organic lining, po: pore, re: residual bodies, v: vacuoles. A = 5 μ m; B, D = 500nm; C = 200 nm.

3.2 Inorganic carbon, ammonium and sulfate uptake and transfer within the foraminiferal cell

All the specimens of *E. williamsoni* showed ^{13}C -enrichment structures in their cytoplasm after 20 h incubation under light with $\text{H}^{13}\text{CO}_3^-$. Some fibrillar vesicles, electron-opaque bodies, along with a few thick-membrane vesicles and other small structures with unknown functions (< 500 nm of diameter) were found to be slightly enriched in ^{13}C (~ 300 ‰; Fig. 3.3.3 A). No lipid droplets nor kleptoplasts were enriched. No ^{13}C -enrichment was found in *Ammonia cf. tepida* cytoplasm.

After 20 h of incubation the cytoplasmic background of all the analyzed specimens of both *E. williamsoni* and *A. tepida* was slightly enriched in ^{15}N by ~ 1500 to 3000 ‰ (Figs. 3.3.3 and 3.3.4). Most of the electron opaque bodies and a few fibrillar vesicles were ^{15}N -enriched in both species, with the addition of a few thick membrane vesicles in *E. williamsoni* cytoplasm.

Finally both *E. williamsoni* and *A. tepida* exhibited structures enriched in ^{34}S , including some fibrillar vesicles plus a number of undescribed structures (Figs. 3.3.3 and 3.3.4). In addition, a few ^{34}S -enriched thick-membrane vesicles were observed in *E. williamsoni* cytoplasm. The electron opaque bodies were not ^{34}S enriched in none of the species.

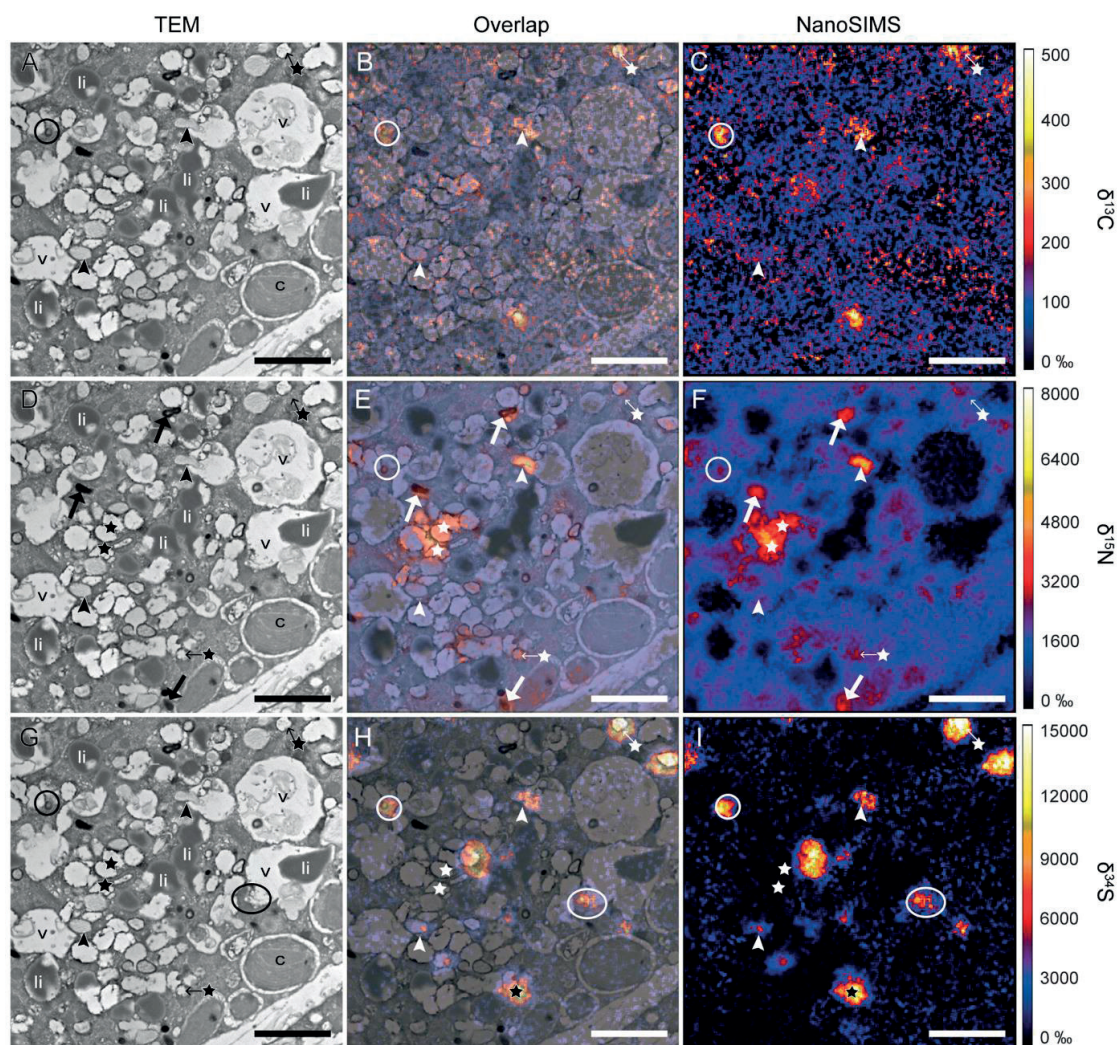


Figure 3.3.3: ^{13}C , ^{15}N and ^{34}S cellular localization in the cytoplasm of *Elphidium williamsoni* after 20 h of incubation in light with $\text{H}^{13}\text{CO}_3^-$ (A, B, C), $^{15}\text{NH}_4^+$ (D, E, F) and $^{34}\text{SO}_4^{2-}$ (G, H, I). Left column: TEM micrographs; central column: overlap of the TEM and NanoSIMS images; right column: corresponding NanoSIMS $\delta^{13}\text{C}$, $\delta^{15}\text{N}$ and $\delta^{34}\text{S}$ images (with scales expressed in ‰). Arrows: electron-opaque bodies; arrowheads: fibrillar vesicles; circles: unidentified isotopically enriched structures; stars: thick-membrane vesicles; c: chloroplasts, li: lipid droplets, v: vacuoles. Scale bars: 2 μm .

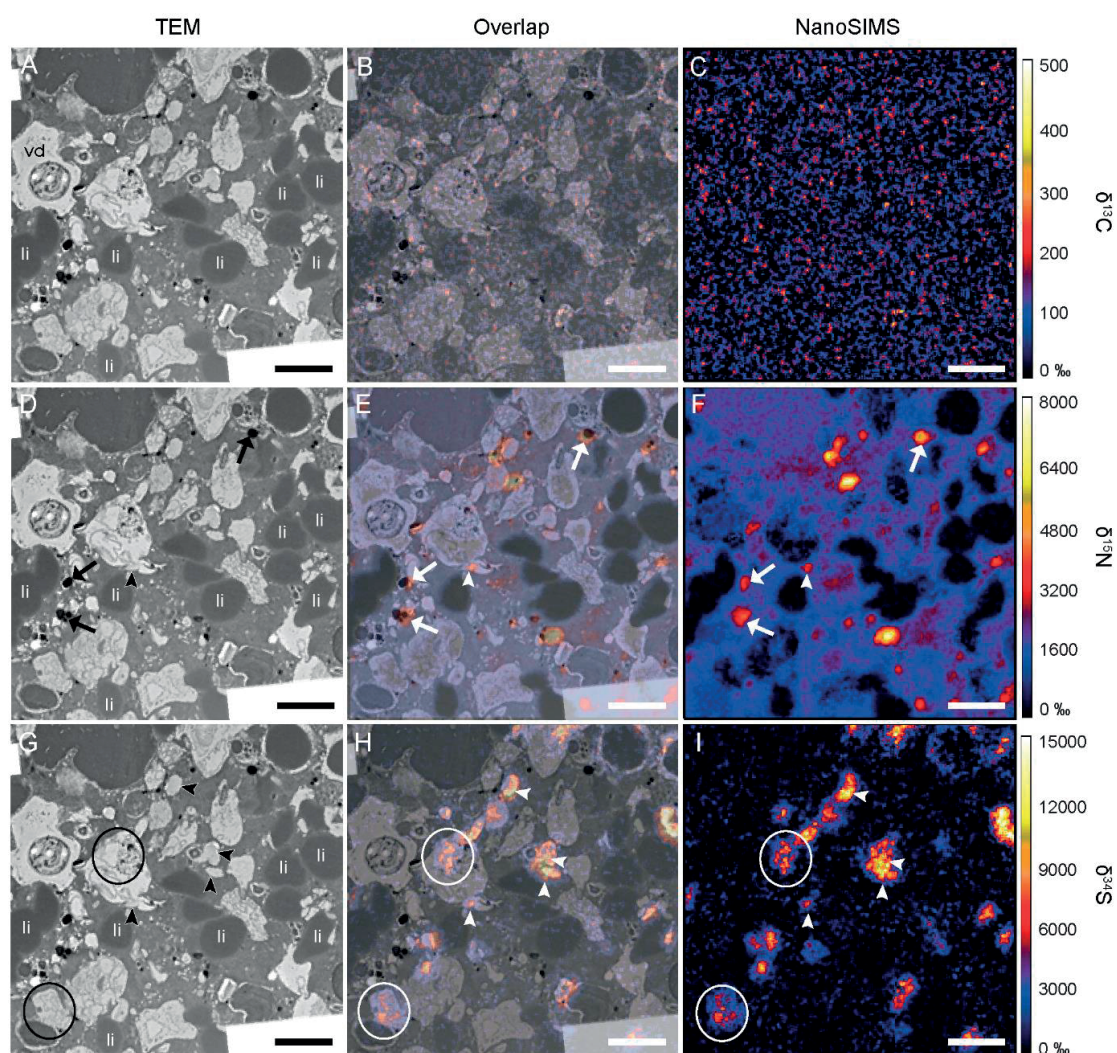


Figure 3.3.4: ^{13}C , ^{15}N and ^{34}S cellular localization in the cytoplasm of *Ammonia cf. tepida* after 20 h of incubation in light with $\text{H}^{13}\text{CO}_3^-$ (A, B, C), $^{15}\text{NH}_4^+$ (D, E, F) and $^{34}\text{SO}_4^{2-}$ (G, H, I). Left column: TEM micrographs; central column: overlap of the TEM and NanoSIMS images; right column: corresponding NanoSIMS $\delta^{13}\text{C}$, $\delta^{15}\text{N}$ and $\delta^{34}\text{S}$ images (with scales expressed in ‰). Arrows: electron-opaque bodies; arrowheads: fibrillar vesicles; circles: unidentified isotopically enriched structures; li: lipid droplets, vd: degradation vacuole. Scale bars: 2 μm .

3.3 Respiration rates

The O_2 production/consumption rates represent the respiration/photosynthesis dynamics of the kleptoplast foraminifera (Fig. 3.3.5). Positive value signify that the O_2 production by photosynthesis exceed the O_2 consumption by respiration (i.e. a positive value shows net photosynthesis). Negative values signify that respiration exceeds photosynthetic O_2 production.

The three repetitions of *E. williamsoni* respiration rates showed similar profiles: oxygen production during the light and oxygen consumption during dark phase (Fig. 3.3.5). During the first light phase the foraminifera produced up to $\sim 7600 \text{ pmol } O_2 \text{ day}^{-1} \text{ cell}^{-1}$. Rapidly after the switch to dark conditions the oxygen dynamics passed from a net O_2 production to respiration. The consumption rates reaching values of -4000 to $-6000 \text{ pmol } O_2 \text{ day}^{-1} \text{ cell}^{-1}$ after 30 to 60 minutes in darkness. After the switch to the second light phase, the oxygen dynamics rapidly changed to oxygen production again, reaching values of 2000 to $6000 \text{ pmol } O_2 \text{ day}^{-1} \text{ cell}^{-1}$ after about 30 minutes of light.

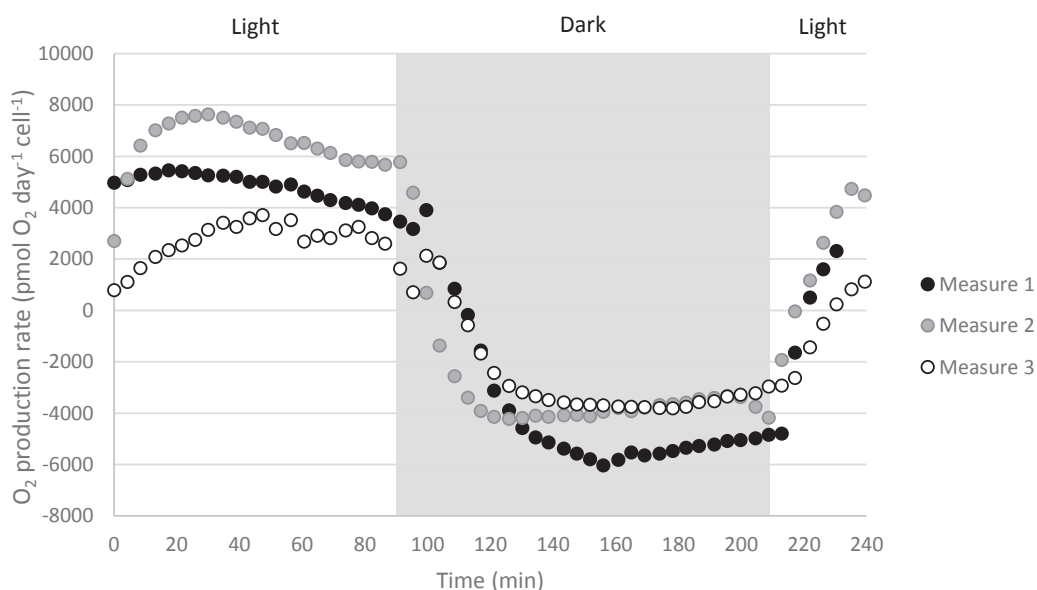


Figure 3.3.5: Oxygen production/consumption profiles for *E. williamsoni* over time, under dark and light conditions. Measures were realized on seven specimens, and normalized to one specimen to obtain cell specific rate expressed in $\text{pmol } O_2 \text{ cell}^{-1} \text{ d}^{-1}$.

4 Discussion

4.1 Ammonium and sulfate assimilation

A key result of this experiment is the observed assimilation by *Ammonia* cf. *tepida* of ammonium and sulfate. This is to our knowledge the first record of the ability of a non-symbiotic foraminifer to directly assimilate ammonium from its environment. *Ammonia* cf. *tepida* is not considered as a true kleptoplastic species (Jauffrais et al., 2016), and although one study mentions the presence of bacterial endosymbionts in *Ammonia* cf. *tepida* from Nojima bay (Japan) (Nomaki et al., 2014), we did not find any evidence of such symbionts in our study of specimens from the Gullmar fjord or from the Bourgneuf bay (France) (chapter 2).

One study already observed an assimilation of ^{34}S within the cell of a non kleptoplastic species, *Ammonia* sp. sampled in the Nojima bay (Japan) (Nomaki et al., 2016). However in their experiment they incubated foraminifera into sediment, and placed the sediment into seawater spiked with $^{34}\text{SO}_4^{2-}$. TEM observations revealed the presence of potential endosymbionts within the foraminiferal cells. It is therefore conceivable that the ^{34}S -sulfate were first assimilated by prokaryotes (in the sediment or endosymbionts) before being incorporated in another organic or inorganic S-form by foraminifera.

Other example of inorganic N assimilation can be found in the literature in non-photosynthetic protists (e.g. Kamp et al., 2015). For example there are evidence of nitrate respiration in the freshwater ciliate *Loxodes* via dissimilatory nitrate reductase in the absence of oxygen (Finlay et al., 1983; Finlay, 1985). Some foraminifera are also able to store intracellular nitrate pool, used for complete denitrification in the absence of oxygen (Kamp et al., 2015; Risgaard-Petersen et al., 2006). The study of Nomaki et al. (2016) also showed ^{15}N -nitrate assimilation. But again, foraminifera were incubated into sediment in seawater spiked with $^{15}\text{NO}_3^-$, thus ^{15}N -nitrate might have been processed by prokaryotes prior assimilation by foraminifera.

Assimilation of sulfate in non-photosynthetic organisms was already observed in yeasts, fungi and some protists: these organisms possess functional metabolic pathways to uptake and activate sulfate, reduce the sulfate (SO_4^{2-}) into sulfite (SO_3^{2-}) and produce the amino acid cysteine and others sulfated compounds (such as glutathione and phytochelatins) (review in Mendoza-Cózatl et al., 2005). In the photosynthetic protist *Euglena gracilis* and in algal and plant cells, some of the enzymes involved in these processes have different isoforms and can be found both into chloroplasts, mitochondria, and cytosol, respectively (review in Mendoza-Cózatl et al., 2005 and Shibagaki and Grossman, 2008; see also Li et al., 1991). It seems possible that foraminifera also possess these enzymes in their cytosol.

Assimilation of $^{15}\text{NH}_4^+$ and $^{34}\text{SO}_4^{2-}$ was also observed in the kleptoplastic species *E. williamsoni*. However, the capacity of non-kleptoplastic foraminifera to assimilate inorganic compounds directly makes the assimilation pathway in kleptoplastic foraminifera less straight forward to study. In our study we cannot conclude if the kleptoplasts play any role in ammonium or sulfate assimilation in *E. williamsoni*, although since the sequestered chloroplasts have been shown to have functional photosynthetic machinery, they are likely to have retained enzymes associated with nitrogen and sulfur metabolisms. It is also possible that the kleptoplastic foraminifera use both kleptoplastic and cytoplasmic pathways to meet their nutrient requirements, which would allow them to use a wider range of nutrient sources, thereby making them more competitive in their environment. At this point an analysis of the metabolites labeled in ^{15}N or ^{34}S produced by the foraminifera (amino acids and sulfolipids especially) seems essential to gain insights in the metabolic pathways involved.

4.2 Photosynthesis and inorganic carbon uptake

The O_2 measurements in microenvironment around *E. williamsoni* revealed functional photosynthetic O_2 production by the kleptoplasts (Fig. 3.3.5). The recorded values for net photosynthesis (i.e. total photosynthesis – foraminiferal respiration) are higher than previously measured values for the kleptoplastic species *Haynesina germanica*: up to $\sim 7600 \text{ O}_2 \text{ day}^{-1} \text{ cell}^{-1}$ versus $200\text{--}1000 \text{ pmol O}_2 \text{ day}^{-1} \text{ cell}^{-1}$ for *E. williamsoni* and *H. germanica* in the work of (Cesbron et al., 2017; Jauffrais et al., 2016), respectively. Lopez (1979) demonstrated the correlation between C uptake and chlorophyll content in *H. germanica* and *E. williamsoni*, and showed a chlorophyll content four times superior in the latter. Similarly the O_2 production might be correlated to chlorophyll content, explaining the higher O_2 production rate in *E. williamsoni* compared to *H. germanica*.

In another study, bulk analysis on *E. williamsoni* revealed active ^{14}C assimilation within their cell when incubated under light with $\text{H}^{14}\text{CO}_3^-$: up to $2.3 \times 10^{-3} \text{ mg C mg}^{-1} \text{ h}^{-1}$, five times more than in *H. germanica* (Lopez, 1979). In the same study the absence of ^{14}C -uptake in darkness and the correlation between net ^{14}C -uptake and the foraminiferal chlorophyll content strongly suggest an inorganic C assimilation via photosynthetic kleptoplastic pathway. But in our study, the NanoSIMS observations showed only a weak inorganic ^{13}C assimilation within cells of *E. williamsoni*: after the 20 h incubation with $\text{H}^{13}\text{CO}_3^-$ only a few foraminiferal organelles were found to be slightly ^{13}C -enriched, in addition no ^{13}C -accumulation in lipid droplets was observed. This last finding is discrepant with the observations

made in the previous chapter with the species *H. germanica*, in which most of the ^{13}C -signal was found to be stored in foraminiferal lipid droplets. The main hypothesis to explain the weak ^{13}C -enrichment within *E. williamsoni* is that C might be primarily as a soluble compound, which was washed out during the sample preparation procedures. This could explain why we found so little ^{13}C enrichment in the cytoplasm compared to *H. germanica* even though both oxygen production and carbon assimilation in *E. williamsoni* were higher than in *H. germanica* (Cesbron et al., 2017; Jauffrais et al., 2016; Lopez, 1979). A bulk analysis carried out after a similar incubation would allow us to confirm this hypothesis. It might also be interesting to look more closely at the lipid inclusions in the kleptoplasts (i.e. the potential plastoglobuli) to investigate potential ^{13}C -enrichments. Unfortunately during this first experiment no kleptoplasts with such structures was analyzed with NanoSIMS.

Ammonia cf. tepida sampled from another location, but belonging to the same phylotype (Magali Schweizer, pers. com.) was shown to have strongly reduced photosynthetic capacity compared to the kleptoplastic species *H. germanica* (Jauffrais et al., 2016). In their O_2 measurement in *Ammonia cf. tepida* microenvironment, Jauffrais et al. (2016) measured lower respiration rate under light than under dark at the beginning of their incubation and attributed it to a low O_2 production under light. *Ammonia cf. tepida* performed photosynthesis for a short time (less than 24 h) presumably with the chloroplasts of the diatoms ingested within its cytoplasm, but it is not able to maintain these chloroplasts within their cell for longer time periods. Indeed, *Ammonia cf. tepida* ingests full diatoms in its cytoplasm (see chapter 2) with intact chloroplasts that perform photosynthesis during a few hours after ingestion. The observation of some chloroplasts and diatoms in degradation in its cytoplasm support this hypothesis (chapter 3.1). This might explain the low O_2 production recorded in Jauffrais et al. (2016) experiment at the beginning of their incubation. However, our NanoSIMS data show that this weak activity of chloroplasts from freshly digested diatoms is not enough to fix inorganic carbon, as no ^{13}C enrichment was found in *Ammonia cf. tepida* cell.

4.3 Kleptoplast ultrastructure and cellular distribution

The particular kleptoplast distribution at the cell periphery (Fig. 3.1.1A, B) was already observed in *E. williamsoni* as well as *E. selseyense (excavatum)* and *Planoglabratella opercularis*. However, in other kleptoplastic species, such as e.g. *H. germanica*, kleptoplasts are distributed throughout the entire cytoplasm (Lopez, 1979; chapters 3.1 and 3.2). These differences in the kleptoplast organization suggest different strategies among kleptoplastic foraminifera (Jauffrais et al.,

2016). It could explain the difference in photosynthesis efficiency between *H. germanica* and *E. williamsoni*: the peripheral distribution observed in the latter might be interpreted as a strategy to maximize light acquisition by kleptoplasts, or to favor gas exchanges with the foraminiferal environment through pores (see chapter 3.1).

The description of sequestered kleptoplasts in *E. williamsoni* in this study corresponds to the description found in the literature: well preserved with distinguishable central pyrenoids crossed by a lamella, intact thylakoids; and a girdle lamella surrounding the entire chloroplast (Lopez, 1979; chapter 3.1). Although these authors did not mention the presence of lipid inclusion in the kleptoplasts, small lipid inclusions, interpreted here as potential plastoglobuli, could be seen on their micrographs, as well as in our observations. The electron-lucent space surrounding the kleptoplasts was also noted in both studies and similarly interpreted as an artifact due to fixation. This seems likely as the kleptoplasts observed in *H. germanica* after cryo-fixation did not present any electro-lucent space around them (Goldstein et al., 2004). The same was noted in a comparative study between standard fixation and cryo-fixation: this electron-lucent space was present only around the algal symbionts of a *Paramecium* fixed following traditional protocol, while in cryo-fixed samples there was no space between the symbionts and the host cytoplasm (Song et al., 2017).

4.4 Specific organelles isotopically enriched

Fibrillar bodies and electron opaque bodies are common organelles in benthic foraminifera (chapter 1). Fibrillar bodies were found labeled in *Ammonia cf. tepida* (^{15}N and ^{34}S) and in the kleptoplastic *E. williamsoni* (^{13}C , ^{15}N , and ^{34}S). This is consistent with the previous experiment with the kleptoplastic *H. germanica* where a similar incubation with $^{15}\text{NH}_4^+$ and $\text{H}^{13}\text{CO}_3^-$ also lead to their enrichment (chapter 3.2). The absence of ^{13}C -enrichment in *Ammonia cf. tepida* can be explained by the absence of inorganic C uptake within its cytoplasm. Fibrillar bodies are thought to be involved in the transport of GAGs (glycosaminoglycans, sulfated amino-polysaccharides) (Langer, 1992). Thus an enrichment in ^{13}C , ^{15}N and ^{34}S is expected, given that the foraminifera is able to assimilate the isotopic sources provided.

The electron opaque bodies were only enriched in ^{15}N in both species. In another experiment with the species *Ammonia* sp. incubated in sediment placed under dysoxic conditions with $^{15}\text{NO}_3^-$ and $^{34}\text{SO}_4^{2-}$, these organelles (referred as “dense bodies”) were also ^{15}N and ^{34}S enriched. The absence of ^{34}S in electron opaque bodies in our study is therefore surprising.

4.5 Trophic mechanism impacts on cellular ultrastructure

A difference in the lipid size was noted between the two studied species, with lipid droplets two to five times bigger in *Ammonia cf. tepida* than in *E. williamsoni*. In addition, unlike *E. williamsoni*, *Ammonia cf. tepida* possess numerous residual bodies, a feature that was already observed in another ultrastructural study (chapter 2). These differences might be attributed to different feeding strategies. The residual bodies are thought to be vacuoles containing all the non-digestible detritus of the cell (review in chapter 1). As *Ammonia cf. tepida* does not possess assimilate nutrients through kleptoplasts or any other symbionts (at least in the specimens collected in our study), it relies only on feeding (heterotrophy) to obtain its carbon compounds. This species is known to actively graze on microphytobenthos (Pascal et al., 2008b, 2008a). In chapter 2 we saw that the microalgae material is digested within the cell, and that the C is either stored in lipid droplets or directly used in the foraminiferal metabolism. The carbon extracted from the microalgae is then ultimately found in the residual bodies, where it could have arrived either as a non-digestible component of the microalgae or after autophagocytosis of a foraminiferal organelle constructed with microalgal carbon. In *E. williamsoni* the absence of residual bodies and the smaller lipid droplets suggest another type of trophic mechanism: its mixotrophy strategy provided by its photosynthetic kleptoplasts allows it to rely on another carbon source than feeding. The assimilation of inorganic carbon via the kleptoplasts might be sufficient to maintain its metabolic activity. Thus *E. williamsoni* might not need to graze on biofilm, and therefore form less or no residual bodies. This alternative pathway could as well result in the formation of smaller lipid droplets. Similarly, in a feeding experiment with algae, the kleptoplastic species *H. germanica* was shown to have an organic C uptake ten times inferior to *Ammonia cf. tepida* (Wukovits et al., 2016). The author explained it as the preference for *H. germanica* for another type of food, but we suggest that, as in our study, this would rather be explained by the mixotrophy strategy of this kleptoplastic species.

5 Conclusion

We show here the first evidence of direct inorganic nitrogen and sulfate assimilation by a non kleptoplastic (and non-symbiotic) foraminiferal species. This new process should be quantified to assess more precisely the foraminiferal contributions to the nitrogen and sulfate geochemical cycles. It also emphasizes the need for more research to unravel the role played by the sequestered chloroplasts in kleptoplastic species. Which pathways do the foraminifera species use to meet their nutrient and sulfate requirements: assimilation of inorganic compounds via (1) the kleptoplasts, (2)

the foraminifera's own metabolism (3) through feeding, or (4) through all of these pathways? Analyses of specific metabolite (amino acids, sulfolipids and intermediate molecules in the nitrogen and sulfate metabolic pathways) are underway to better understand the metabolic pathways taking place in the foraminiferal cell.

These first results also highlight the diversity of metabolism within kleptoplastic species. *E. williamsoni* showed a photosynthetic rate higher than other kleptoplastic species, which is in agreement with the data from literature. But while another species, *H. germanica*, was shown to store a large part of the photosynthetically acquired carbon in lipid droplets, no carbon translocation to the lipid fraction was seen in *E. williamsoni*, and only a slight ^{13}C -enrichment could be detected. To understand these differences in the metabolism more experiments are needed. We plan to perform experiments in which a similar incubation scheme followed by TEM-NanoSIMS analysis will be carried out, coupled with a bulk analysis of the cell to investigate the soluble carbon ^{13}C enrichment. Mass spectrometry analysis of targeted metabolites, such as carbon compounds (fatty acids, sugars), amino acids, or sulfated compounds should also be performed.

Chapter 4: Assimilation and translocation of carbon between photosynthetic symbiotic dinoflagellates and their planktonic foraminifera host

The Chapter 4 presents a manuscript in preparation investigating carbon assimilation by symbiotic dinoflagellates, and carbon translocation between the symbionts and the foraminiferal host cell.

PhD student's contribution: the PhD student designed the Experiment with HJ and AM; analyzed the samples; interpreted the data with HJ and AM; performed the statistical analysis; discuss the results with HS, EG, AR, JF, and AM and wrote the manuscript with comments and edits from all the authors.

Assimilation and translocation of carbon between photosynthetic symbiotic dinoflagellates and their planktonic foraminifera host

Charlotte Le Kieffre¹, Howard J. Spero², Ann D. Russell², Jennifer S. Fehrenbacher^{2,3}, Emmanuelle Geslin⁴, Anders Meibom^{1,5}

¹ Laboratory for Biological Geochemistry, School of Architecture, Civil and Environmental Engineering (ENAC), Ecole Polytechnique Fédérale de Lausanne (EPFL), Switzerland.

² Department of Earth and Planetary Sciences, University of California Davis, Davis, CA 95616, USA.

³ College of Earth, Ocean, and Atmospheric Sciences, Oregon State University, Corvallis, OR 97331, USA.

⁴ UMR CNRS 6112 - LPG-BIAF, Université d'Angers, 49045 Angers Cedex, France.

⁵ Center for Advanced Surface Analysis, Institute of Earth Sciences, University of Lausanne, Switzerland.

Abstract

Some planktonic species inhabiting the surface waters of oligotrophic environments are in symbiosis with dinoflagellate microalgae, which can assimilate C through photosynthesis. However, the nature and dynamics of C photosynthate translocation to the foraminiferal host cell, and related benefits for the dinoflagellates in this symbiotic association, are poorly documented and understood. We performed pulse-chase experiments with ¹³C-enriched dissolved inorganic carbon, combined with TEM and quantitative NanoSIMS isotopic imaging to visualize photosynthetic C assimilation by individual symbiotic dinoflagellates and subsequent translocation to their *Orbulina universa* host in waters north of Santa Catalina Island (California, USA). Although the dinoflagellate population is known to migrate out into the ectoplasm around the spines during the day, our observations show that a small fraction remains inside the host cell at all times. At night all dinoflagellates from the spine-ectoplasm region migrate back into the foraminiferal cell, probably controlled by a need to replenish P- and N-nutrients to support mitosis. All symbionts, whether outside or inside the foraminifera cell, effectively assimilate C into starch nodules through photosynthesis during the day, and transfer it to the foraminiferal cell, where it is stored primarily in the form of lipid droplets. The mechanism of translocation is not clear, but transfer of individual free fatty acids through the symbiosome membrane and/or exocytosis of lipid droplets from the symbiosome might be involved. During the nighttime, respiration strongly reduces the abundance of starch in dinoflagellates, but translocation of lipids to the host continues.

Key-words: Dinoflagellate symbiosis, photosynthesis, carbon translocation, NanoSIMS, TEM, *Orbulina universa*, planktonic foraminifera

1 Introduction

The intracellular association between photosynthetic algae and foraminifera has been recorded in numerous studies of large benthic (e.g. Lee, 1983 and Leutenegger, 1984) and planktonic species (Anderson and Bé, 1976b; Bé et al., 1977; Lee et al., 1965; Rhumbler, 1911; Spero, 1987; Spero and Parker, 1985), and the symbiotic nature of this relationship confirmed by the effects of the symbionts on host metabolism and growth. For example, in large benthic foraminifera, such as *Heterostegina depressa*, *Amphistegina lessonii*, and *Archaias angulatus*, the symbionts were shown to enhance growth rate (Duguay and Taylor, 1978; Lee and Zucker, 1969; Röttger and Berger, 1972). In a planktonic species, *Globigerinoides sacculifer*, dinoflagellate symbiont photosynthetic rates have been demonstrated to strongly effect final shell size; furthermore, elimination of symbionts resulted in earlier gametogenesis and reduced lifespan (Bé et al., 1982). Studies with micro-sensors have shown significant changes in oxygen production in planktonic *O. universa* correlated with variations in light level, demonstrating the effect of symbiotic dinoflagellate photosynthesis on the host cell microenvironment (Köhler-Rink and Kühl, 2005; Rink et al., 1998). In the symbiotic planktonic species *G. sacculifer*, longer survival rates have been recorded in unfed specimens exposed to high light levels (= elevated photosynthetic rates) in comparison with unfed specimens kept under low light conditions (Caron et al., 1981), suggesting that the dinoflagellates are needed to provide photosynthates to the foraminiferal host cell. To date, however, no studies have documented the timing, extent and distribution of translocated organic C photosynthates between symbiotic dinoflagellates and their foraminiferal host cell.

The NanoSIMS ion microprobe technique permits subcellular, quantitative isotopic imaging of biological tissue, directly correlated with TEM ultrastructural imaging. Combined with isotopic pulse-chase labeling experiments, this has allowed metabolic pathways to be studied at the sub-cellular level in other symbiotic marine organisms, such as corals or phytoplankton (Ceh et al., 2013; Clode et al., 2007; Kopp et al., 2013, 2015b, 2015a; Krupke et al., 2015; Pernice et al., 2012). Two recent studies have applied NanoSIMS in studies of foraminifera metabolism (LeKieffre et al., 2017; Nomaki et al., 2016). Here, we present data from a suite of stable isotope pulse-chase labeling experiment on planktonic foraminifera *Orbulina universa* specimens using ^{13}C -enriched dissolved inorganic carbon (DIC; $\text{H}^{13}\text{CO}_3^-$) in combination with correlated TEM and NanoSIMS imaging. The main objective was to visualize and quantify incorporation and turnover of inorganic C by the dinoflagellates, as well as translocation of photosynthates to their host, with high temporal resolution (hours to days) across a full diurnal cycle.

2 Material and Methods

2.1 Collection of the foraminifera

Specimens of *Orbulina universa* were hand-collected by SCUBA divers from surface waters, 1 to 2 km north of Santa Catalina Island (California, USA) on August 4, 2014. The specimens were collected individually in glass jars and transported within 1 h to the laboratory at the University of Southern California Wrigley Marine Science Center. Each individual was then transferred with a glass pipette to a clean glass jar containing 0.8 μm filtrated sea water and maintained at 22°C. Light micrographs were taken of living specimens, both in light and after acclimation of the specimens to dark, using a Nikon TMS inverted microscope.

2.2 Experiment: incubation with $\text{NaH}^{13}\text{CO}_3$ during a light-dark cycle

Approximately one day after collection, 24 pre-sphere (trochospiral test) *O. universa* were selected and fed a one-day-old *Artemia salina* brine shrimp nauplius; this feeding took place 4 h prior to the ^{13}C -incubation experiment. On August 5, at 13:00 local time (i.e. corresponding to maximum symbiont photosynthetic rate (Spero and Parker, 1985), 21 fed specimens were transferred into 22 ml scintillation vials (one specimen per vial), filled with 0.8 μm filtered seawater (pH: 8.2), which had been spiked by the addition of 2 mM $\text{NaH}^{13}\text{CO}_3$ (^{13}C fraction of 99 %, Cambridge Isotopes Laboratory Inc.). The addition of 2 mM of ^{13}C -enriched sodium bicarbonate resulted in a final dissolved inorganic carbon concentration of $\sim 4\text{mM}$ and a DIC $^{13}\text{C}/^{12}\text{C}$ ratio ≈ 0.45 ; i.e. extremely ^{13}C -enriched compared to natural DIC ($^{13}\text{C}/^{12}\text{C} \approx 0.01$). The capped vials were then immersed into seawater at 22°C under artificial light (Sylvania F24T12 'Cool White' fluorescent lights), with a minimum intensity of $350 \mu\text{Einsteins m}^{-2} \text{sec}^{-1}$ which is the P_{max} light saturation threshold for symbiont photosynthesis in this species (Rink et al., 1998; Spero and Parker, 1985). Three individuals were maintained in non-spiked, filtrated seawater under identical conditions to serve as control specimens. After 6 h, the isotopic incubation was terminated and a chase phase began by transferring foraminifera to new vials filled with ambient 0.8 μm filtrated seawater with normal seawater $\delta^{13}\text{C}_{\text{DIC}}$ and a DIC concentration of ca. 2mM. Specimens were transferred through an intermediate wash vial in order to avoid increasing the $\delta^{13}\text{C}_{\text{DIC}}$ of the chase solution. These vials were then placed in the dark for 12 h at 22°C. Finally the vials were moved back into the light for an additional 12 h period. During this 30 h experiment, three specimens were removed for TEM fixation at the following time points: 45 min, 2, 6, 7, 12, 18 and 30 h, as indicated in Fig. 4.1.

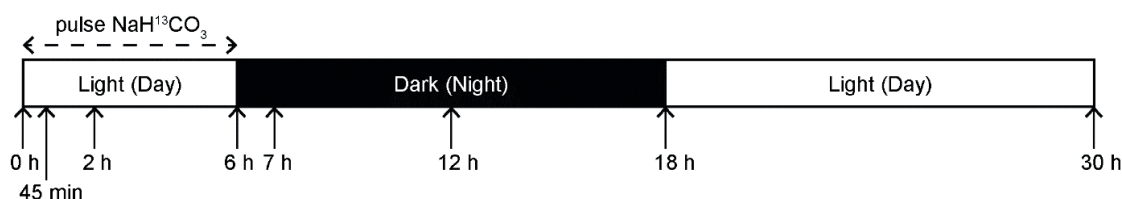


Figure 4.1: The *O. universa* incubation experiment time line. Three specimens were sampled at each time point indicated with arrows. Details in the text.

2.3 TEM – NanoSIMS sample preparation

At each sampling time point, the culled *O. universa* were individually transferred into 0.5 mL micro-centrifuge tubes containing filtered seawater with 4% glutaraldehyde and 2% paraformaldehyde, (pH = 8.1) and fixed for 24 h at room temperature. The fixative solution was then replaced by a solution of 2% glutaraldehyde in filtrated seawater for transport to the Electron Microscopy Facility, University of Lausanne, Switzerland. During this transport phase, the majority of spines were broken and most of the reticulopods and symbiotic microalgae attached to the spines were lost, preserving only a thin layer of ectoplasmic matrix outside the test (see below). These specimens were rinsed in artificial sea water (RedSea Salt, 34 psu), then post-fixed with a solution of 2% OsO₄ diluted in distilled water for 1 h. After thorough rinsing with distilled water, all specimens were embedded in 3% Agar (Sigma-Aldrich, type VII-A, low gelling temperature), following the procedure described by (Spero, 1988). This step protected the fixed foraminifera during the decalcification and dehydration steps, and preserved the natural positioning of the symbiotic dinoflagellates that were present at the base of the broken spines on the outer shell surface. The agar-embedded foraminifera were then decalcified in two successive baths (1 h and 48 h, respectively) of EDTA 0.1 M diluted in distilled water, followed by a dehydration series of increasing ethanol concentrations (50, 70, 95, and 100 %). Samples were prepared for TEM at room temperature using a sequential LR White resin impregnation of a 1:1 resin / ethanol 100 % mixture for 1 h, followed by pure resin for 8 h. Finally, all specimens were placed in a third bath of pure resin for 3 h and then allowed to cure in solid resin at 70°C for 8 h. Specimens were sliced with an ultramicrotome (Reichert Ultracut S) equipped with a diamond knife (Diatome Ultra, 45°) into semi-thin (500 nm) and ultra-thin (70 nm) sections. Semi-thin sections were stained with a mix of toluidine blue and basic fuchsin prior to observation under a light microscope. The ultra-thin sections were placed on formvar-carbon coated copper grids, stained with 2% uranyl acetate for 10 min and observed with a transmission electron microscope (TEM, Philips 301 CM100, 80 kV). Areas of interest for NanoSIMS imaging were selected from TEM images and analyzed based on the procedure described in (LeKieffre et al., 2017).

Following TEM imaging, the same ultrathin sections were coated with gold prior to imaging with a Cameca NanoSIMS 50L ion microprobe (Hoppe et al., 2013). NanoSIMS images were obtained by bombarding thin sections with a beam of Cs^+ focused to a spot size of ~ 150 nm (beam current ~ 2 pA) and counting $^{12}\text{C}^{12}\text{C}^-$, $^{13}\text{C}^{12}\text{C}^-$ and $^{12}\text{C}^{14}\text{N}^-$ ions in electron multipliers at a mass resolution of about 8.000, enough to resolve potential interferences in the mass spectrum. NanoSIMS images were drift-corrected and ^{13}C enrichments obtained by forming the ratio $^{12}\text{C}^{13}\text{C}^-/^{12}\text{C}_2^-$, reported in the delta-notation, i.e. in per mil (‰) deviation from a standard $^{13}\text{C}/^{12}\text{C}$ ratio:

$$\delta^{13}\text{C}(\text{‰}) = \left(\frac{C_{\text{meas}}}{C_{\text{nat}}} - 1 \right) * 1000$$

where C_{meas} is the $^{13}\text{C}/^{12}\text{C}$ ratio measured in the samples, and C_{nat} is the $^{13}\text{C}/^{12}\text{C}$ ratio measured in an isotopically normal control sample, prepared and handled in an identical manner.

Analysis of the NanoSIMS images was carried out as described in (LeKieffre et al., 2017). Briefly, TEM images were aligned with NanoSIMS $^{12}\text{C}^{14}\text{N}^-$ images using the software Look@NanoSIMS (Polerecky et al., 2012), which permitted an accurate drawing of the regions of interest (ROIs) corresponding to different organelles (dinoflagellate starch grains, foraminiferal lipid droplets, and fibrillar bodies). For each type of organelle and each time point, the average ^{13}C -enrichment (and its standard deviation) was calculated based on 3 replicate foraminifera (except for the 6 h and 30 h time points, where only 2 replicates were available). The ROIs drawn on TEM images were also used to assess the relative abundance (in %) of starch grains in the dinoflagellate cytoplasm, determined simply as the number of pixels occupied by starch grains divided by the total number of pixels covering cytoplasm, providing an estimate of the relative abundance of the starch grains in a cross-section as a function of time.

2.4 Statistical analysis

Starch abundances in dinoflagellates, as well as starch and lipid $\delta^{13}\text{C}$, were obtained by calculating the average of ROIs within each specimen and then calculating the average of the three specimens for each time point. Thus, the errors bars shown are standard deviations representing the inter-specimen variability (i.e. $n = 3$ specimens). However, statistical analysis was also carried out on the total set of ROIs for each time point using a linear mixed-effects model (taking into account pseudo-replication effects), followed by a Tukey multiple comparison test. Comparisons of relative starch abundance and $\delta^{13}\text{C}$ in dinoflagellate endoplasm or matrix were performed with a t-test for each time point. All statistical analysis were performed with the Rstudio software (RStudio Team, 2016) with the significance level set to $\alpha = 0.05$.

3 Results

Specimens in Fig. 4.2 are *O. universa* with a spherical test surrounding the inner multi-chambered trochospiral test. The partitioned distribution of the cytoplasm (endoplasm vs. ectoplasm) can be seen in the semi-thin section images (Fig. 4.2C-D). The trochospiral test chambers are filled with foraminifera endoplasm, while the space between these chambers and the *O. universa* sphere appears void of material because this region was filled with seawater (washed away and replaced by resin during fixation process) and strands of rhizopodia. We refer to the space between the trochospiral and spherical chambers as the 'internal matrix', in order to distinguish it from the 'external matrix', defined here as the ectoplasm outside the spherical chamber (Fig. 4.2C- D). For specimens that did not produce a spherical test prior to fixation, this distinction is simply made between endoplasm and ectoplasmic matrix outside the trochospiral test.

3.1 Dinoflagellate migration in and out of the foraminiferal endoplasm

As reported previously (Hemleben et al., 1985), we observe a strong day-night migration pattern in the symbiotic dinoflagellates. In light, the majority of symbiotic algae are found on the spine surfaces surrounding the foraminifera test, i.e. in the external matrix (Fig. 4.2A, C). However, a small subset of the dinoflagellate population is systematically observed in the internal matrix and endoplasm (Fig. 4.2C, E). In contrast, symbionts are rarely observed outside the endoplasm during the night (Fig. 4.2B, D). TEM and light micrographs of individuals fixed during day and night, respectively, demonstrate a permanent, albeit strongly fluctuating population of dinoflagellates in the endoplasm (Fig. 4.2E, F).

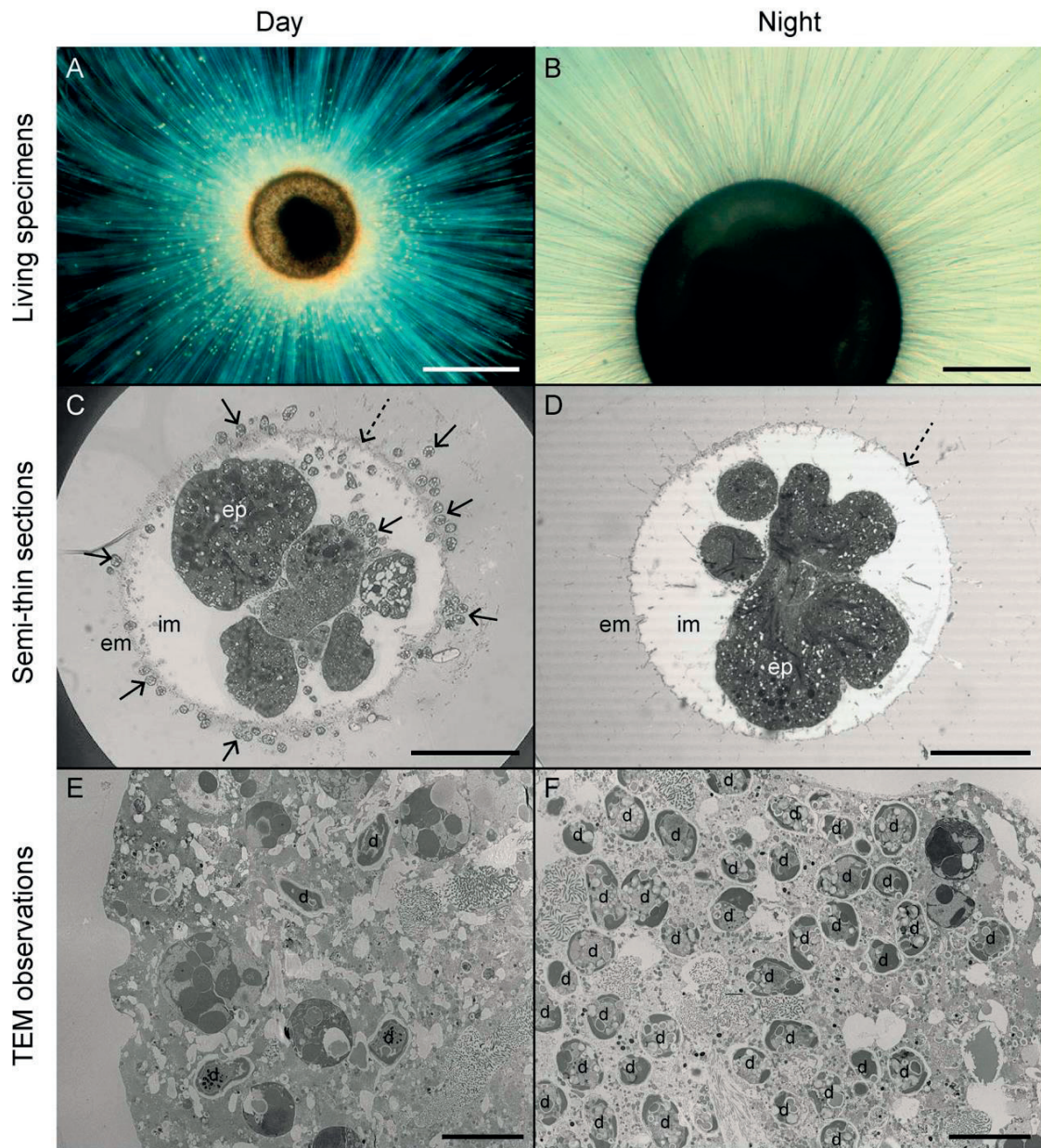


Figure 4.2: *Orbulina universa* during day (left column) and night (right column). Light microscopy pictures of living specimens of (A, B) and semi-thin sections (500 nm) (C, D), and TEM micrographs of the cytoplasm displaying representative dinoflagellate densities within *O. universa* endoplasm (E, F). During the day, the majority of the symbionts are outside the spherical test on the spines (yellow dots in A), with a few symbionts still residing in the internal matrix (im) (C), and even fewer residing in the endoplasm (ep) (D). During the night, all symbionts migrate into the endoplasm (ep). Dotted arrows point to the position of the decalcified spherical test. Dinoflagellates are indicated with solid arrows or labeled 'd'. Scale bars: A = 500 μm ; B, C and D = 200 μm ; E and F = 10 μm .

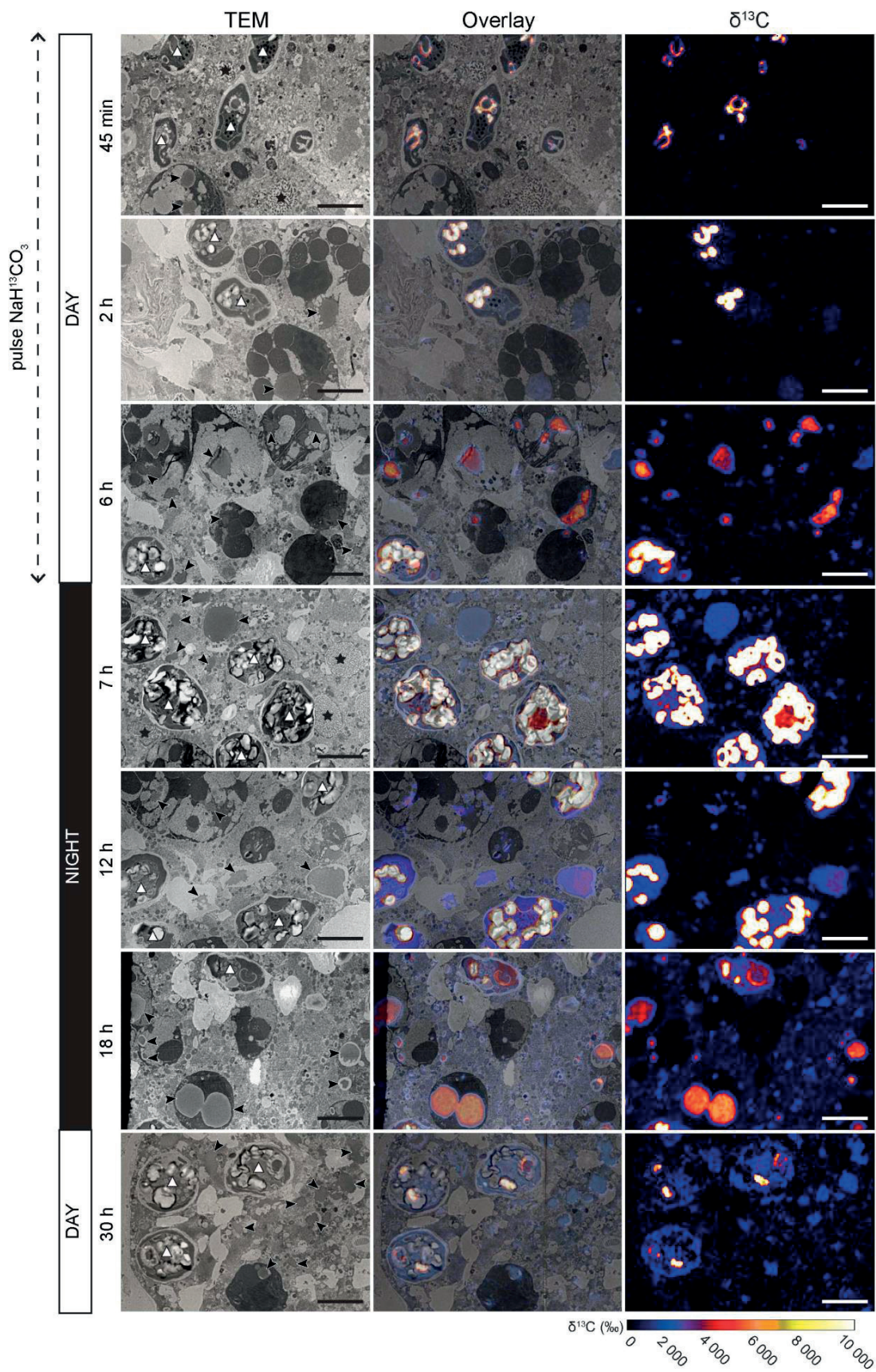
3.2 Carbon uptake and storage by the symbiotic dinoflagellates

Starch ^{13}C -enrichment appears initially on the pyrenoid surfaces, and then in starch grains accumulating in the dinoflagellate cytosol (Fig. 4.3). The relative starch abundance inside dinoflagellates (in % of total cytoplasm area) varied strongly throughout a diurnal cycle (Figs. 4.3, 4.4A – C). TEM micrographs of dinoflagellates fixed at the end of the first light phase (i.e. after 6 h) showed numerous starch grains (Fig. 4.4A) while at the end of the first night cycle, TEM micrographs revealed nearly starch free dinoflagellates (Fig. 4.4B). The relative abundance of starch grains in dinoflagellates (expressed in percentage of the area occupied by starch grains within dinoflagellates) significantly increased from $\sim 11\%$ after 45 min to $\sim 43\%$ after 6 h of incubation in the light ($p < 0.05$; Fig. 4.4C). During the subsequent 12 h dark phase, the abundance of starch steadily decreases to $\sim 7\%$ ($p < 0.05$) of the area within the symbionts. During the second light phase (from 18 h to 30 h), the starch abundance again increased to an average of $\sim 41\%$ ($p < 0.05$; Fig. 4.4C) of the symbiont cytosol area.

Starch ^{13}C -enrichment is observed after only 45 min of incubation with ^{13}C -labeled bicarbonate (Fig. 4.3; 45 min). Rapidly thereafter, i.e. already at 2 h, ^{13}C -enrichment is observed in starch grains throughout the dinoflagellate cells. Mean starch $\delta^{13}\text{C}$ values significantly increased from $\sim 3400\text{‰}$ to $\sim 13200\text{‰}$ during the light phase ($p < 0.05$; Fig. 4.4D). In the following dark chase phase, dinoflagellate starch ^{13}C -enrichment remained essentially constant ($p > 0.05$), although displaying a tendency to decrease towards the end of the night. During the subsequent light chase phase ($t = 18\text{ h}$ to 30 h), unlabeled starch accumulated (Fig. 4.4C) and the average dinoflagellate starch ^{13}C -enrichment decreased to $\sim 1200\text{‰}$ ($p < 0.05$; Fig. 4.4D).

A comparison of the relative abundances and isotopic composition of starch in dinoflagellate cells occupying the host endoplasm vs. the internal/external matrix (or ectoplasm in pre-sphere specimens) can only be made during periods of illumination (e.g. $T = 45\text{ min}$, 2 h , 6 h , and 30 h), (Fig. 4.4C, D) because dinoflagellates were not found outside the endoplasm during the night. At these time points, the relative abundance and ^{13}C -enrichment of starch within dinoflagellates did not vary significantly ($p > 0.05$) between these two host cell environments (Fig. 4.4C, D).

Figure 4.3 (p. 183): Time-evolution of starch production and ^{13}C incorporation by the symbiotic dinoflagellates in *Orbulina universa* endoplasm during the pulse phase of the experiment (45 mins, 2 h, 6 h), followed by a chase including night conditions (7 h, 12 h, 18 h), and a second light cycle (until 30 h). Left column: TEM micrographs of *O. universa* endoplasm with symbiotic dinoflagellates Right column: corresponding NanoSIMS images of $^{13}\text{C}/^{12}\text{C}$ distributions (expressed as $\delta^{13}\text{C}$ in ‰). Central column: overlay of the TEM and NanoSIMS images. Black arrowheads: foraminiferal endoplasmic lipid droplets; white triangles symbiotic dinoflagellates; black stars: fibrillar bodies. White objects in NanoSIMS images are accumulated starch in the symbionts, with ^{13}C -enrichments above the imposed 10.000 ‰ upper color scale limit. Scale bars: 5 μm .



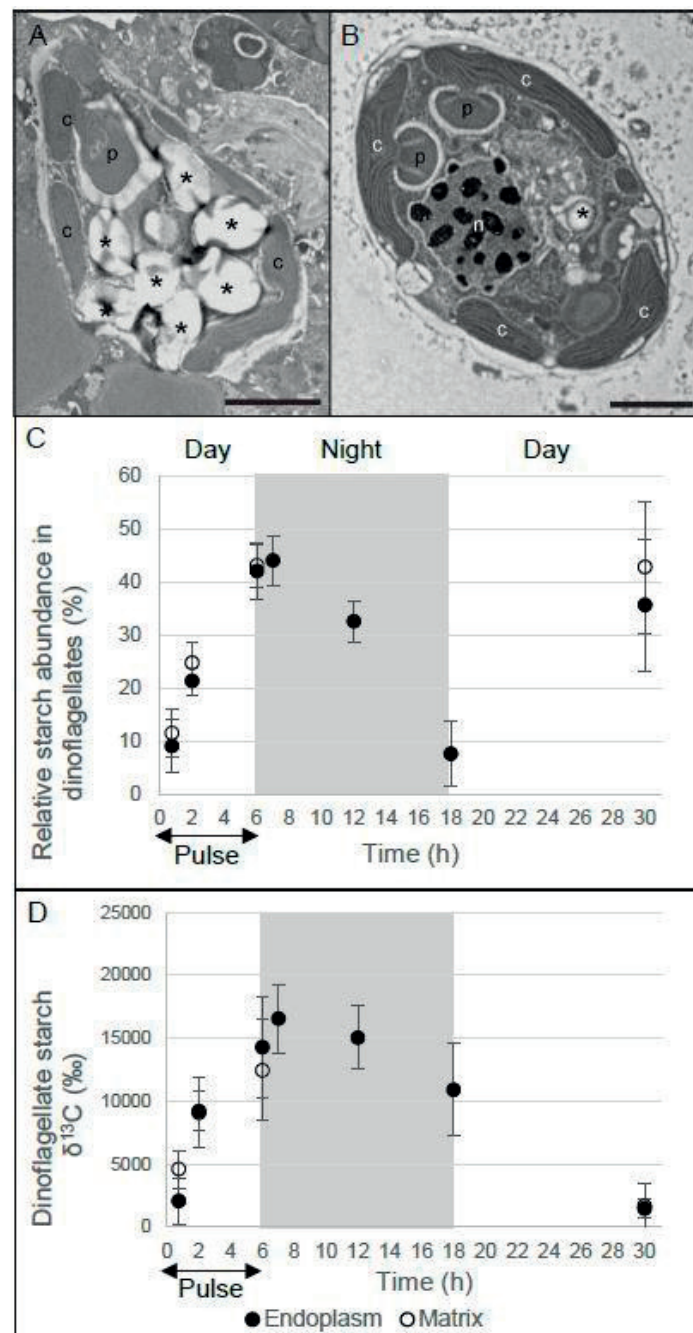


Figure 4.4: Dinoflagellate starch grain abundance and their ^{13}C -enrichments. A and B: TEM micrographs of dinoflagellates in the endoplasm of *O. universa* illustrating the difference in their starch grain content between the end of the day (A) and after 12 h in darkness (B). Asterisks: dinoflagellate starch grains, c: dinoflagellate chloroplasts, n: dinoflagellate nucleus, p: pyrenoids. Scale bars: 2 μm . C: The relative abundance of starch grains in dinoflagellates (in % of total cytoplasm area). D: Average starch ^{13}C -enrichments. A distinction is made between starch from dinoflagellates present in the endoplasm (black circles) or in the internal/ectoplasmic matrix (white circles) of *O. universa*. Error bars: ± 1 SD ($n = 3$ specimens).

3.3 Transfer of carbon to the foraminiferal host cell

The first evidence of translocation of ^{13}C -enriched photosynthates from symbiont to foraminifera host appears as ^{13}C -labeled lipid droplets, already after 45 minutes (Figs. 4.3 and 4.5). Osmiophilic lipid droplets in the foraminifera host display a steady increase in $\delta^{13}\text{C}$ during the pulse phase, from $\sim 100\text{‰}$ after 45 min to $\sim 1300\text{‰}$ at 6 h ($p < 0.05$; Fig. 4.5). Lipid $\delta^{13}\text{C}$ values then remained essentially constant during the dark chase phase, before decreasing to $\sim 450\text{‰}$ at the end of the second light phase ($p < 0.05$; Fig. 4.5).

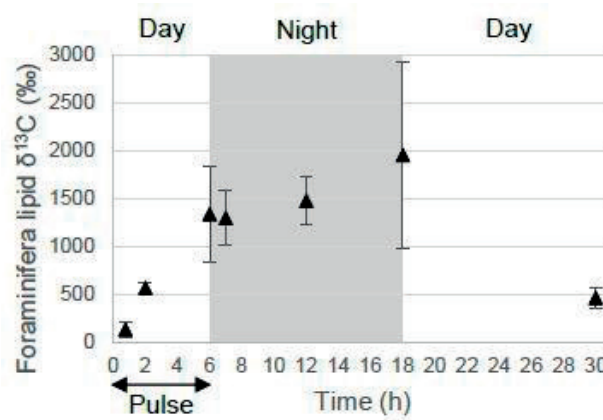


Figure 4.5: Average ^{13}C -enrichment in *O. universa* lipid droplets in the endoplasm as a function of time. Error bars: ± 1 SD ($n = 3$ specimens).

During the initial 18 h of the experiment, the foraminiferal endoplasm ‘background’ displayed a slow heterogeneous increase in ^{13}C that was particularly evident at the end of the night chase (i.e. at 18 h; Fig. 4.3). Higher magnification TEM and NanoSIMS images of specimens fixed during the dark phase reveal small (0.2 to $1\text{ }\mu\text{m}$) ^{13}C -enriched lipid droplets within the cytoplasm of the dinoflagellate and foraminiferal host cells (Fig. 4.6A). These lipids are often observed in direct contact with the symbiosome membrane surrounding the dinoflagellate and are either inside (Fig. 4.6A, C, D, E) or external (Fig. 4.6B, D) to the symbiont cell. Higher magnification TEM and NanoSIMS images also reveal small (200 to 500 nm diameter), spherical to irregularly shaped electron-opaque structures enriched in ^{13}C and distributed evenly throughout the foraminiferal endoplasm (Fig. 4.7A, B). The nature and function of these structures are unknown. Some fibrillar bodies (Lee et al., 1965) exhibit high $\delta^{13}\text{C}$ values, whereas adjacent fibrillar bodies are not significantly enriched in ^{13}C (Fig. 4.7C, D).

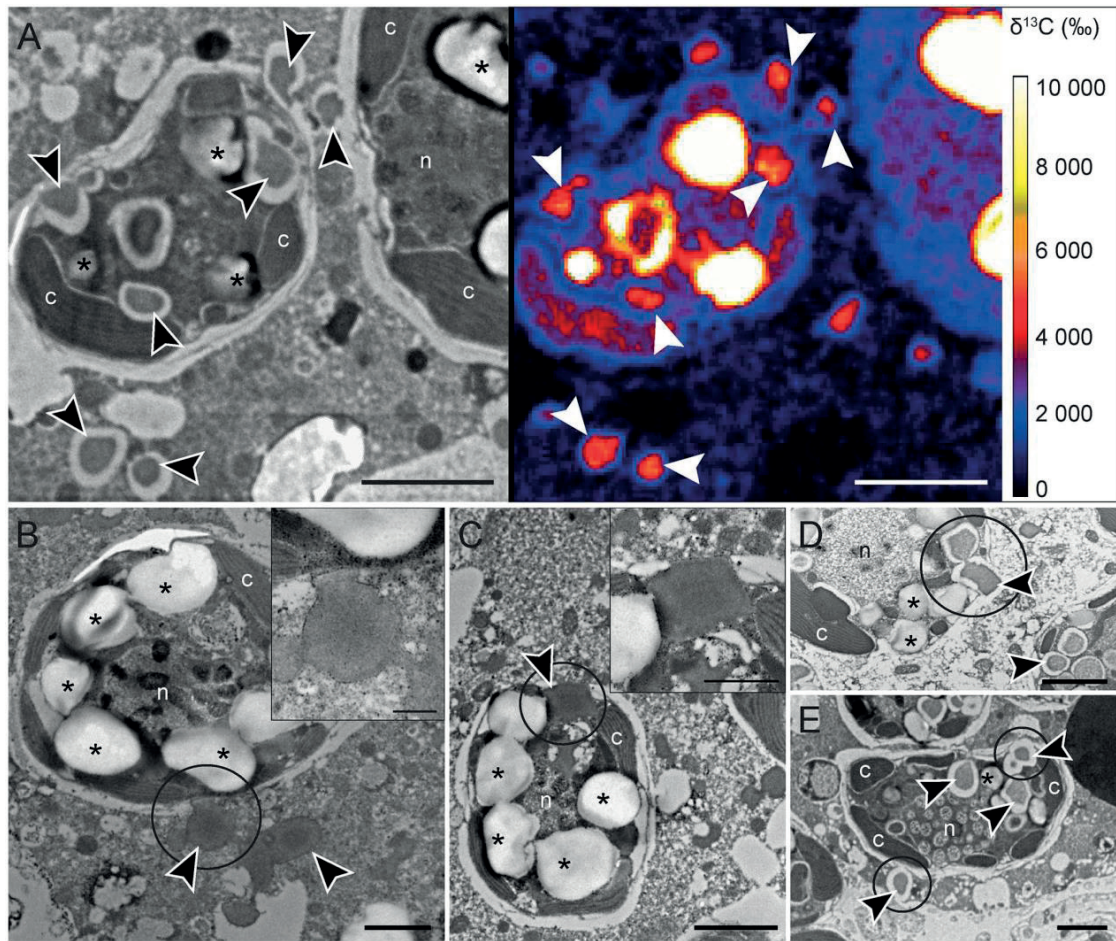


Figure 4.6: Translocation of ^{13}C -enriched lipids from the symbiotic dinoflagellates to *Orbulina universa* endoplasm. A: TEM micrograph and corresponding NanoSIMS image showing the ^{13}C -enrichment of the lipid droplets observed within a dinoflagellate and within the foraminiferal endoplasm. B, C, D and E: TEM micrographs of dinoflagellates in *O. universa* endoplasm during the night phase ($t = 12$ or 18 h). Circles are drawn around potential lipid transfer areas from the dinoflagellate to the foraminiferal endoplasm, i.e. lipid droplets in very close proximity/in direct contact with the symbiosome. In some specimens lipid droplets have a void around the lipid core, which is likely an artifact of the fixation process. Arrowheads: lipid droplets, asterisks: dinoflagellate starch grains, c: dinoflagellate chloroplasts, n: dinoflagellate nucleus. Scale bars: A, C, D, E = $2\ \mu\text{m}$; B, inset D = $1\ \mu\text{m}$; inset B = $500\ \text{nm}$.

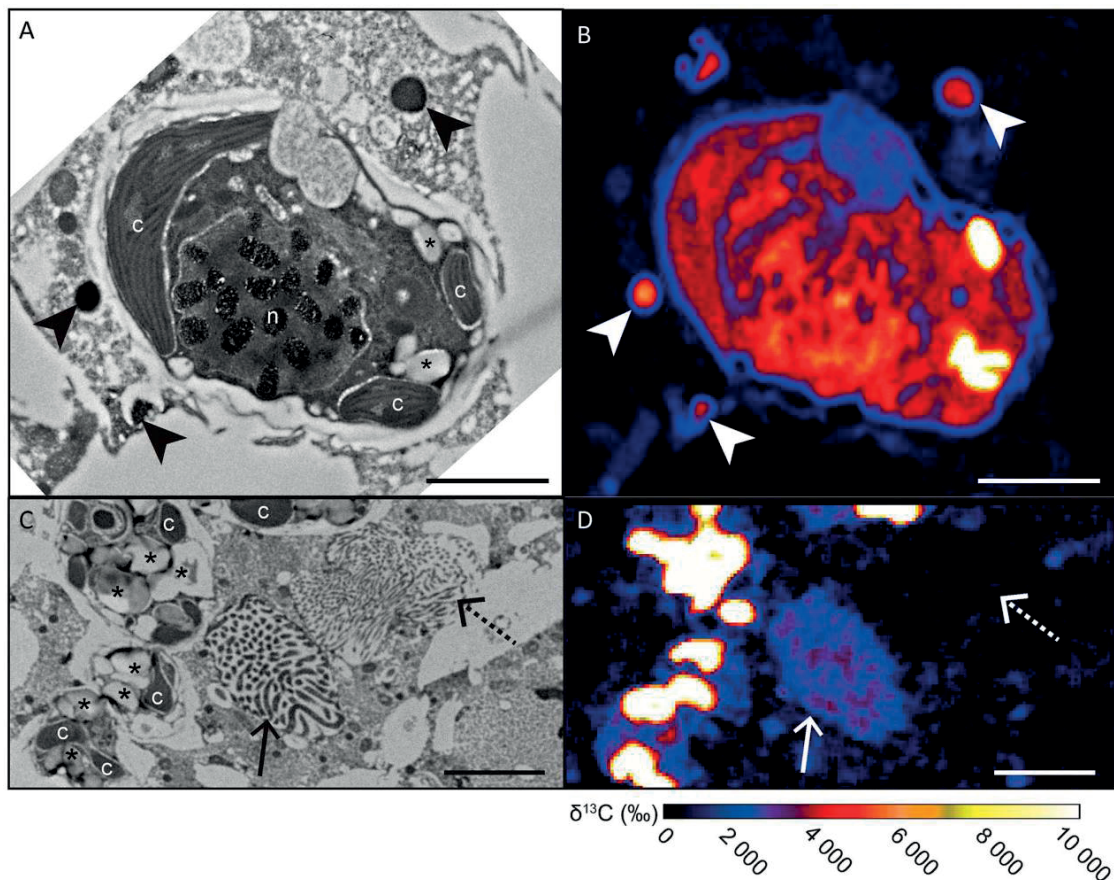


Figure 4.7: ^{13}C -enriched small electron-opaque and fibrillar bodies. Left: TEM micrograph. Right: corresponding NanoSIMS image. A and B: ^{13}C -enriched electron opaque bodies surrounding a symbiotic dinoflagellate. Adjacent fibrillar bodies in the endoplasm of *O. universa* endoplasm at 12 h of incubation (i.e. after 6 h in light with ^{13}C -enriched bicarbonate and 6 h in dark with normal seawater). One is ^{13}C -enriched (solid arrow) while the other is not (dotted arrow). Arrowheads: electron-opaque bodies; arrows: fibrillar bodies; asterisks: dinoflagellate starch grains, c: dinoflagellate chloroplasts, n: dinoflagellate nucleus. Scale bars: A, B = 2 μm ; C, D = 5 μm .

3.4 Dinoflagellate cell division within the foraminiferal host cell

Dinoflagellates undergoing mitosis, identified by the appearance of two nuclei containing condensed chromosomes, are observed in the endoplasm of all specimens fixed in the middle of the night phase (Fig. 4.8A). A few dividing symbiont are also seen in foraminifera fixed at T=18h at the end of the night phase. Symbiont cell division was not observed at other times in the diurnal cycle. Before division initiated, ^{13}C -enrichment was concentrated in starch grains (Fig. 4.8B, C). At the end of the night phase, after a fraction of the dinoflagellates had divided, the ^{13}C -signal was distributed more evenly throughout the dinoflagellate cytoplasm including ^{13}C -enrichment of the nucleus and chloroplasts (Fig. 4.8D, E), indicating the utilization of C fixed the previous day for cell division and cell growth.

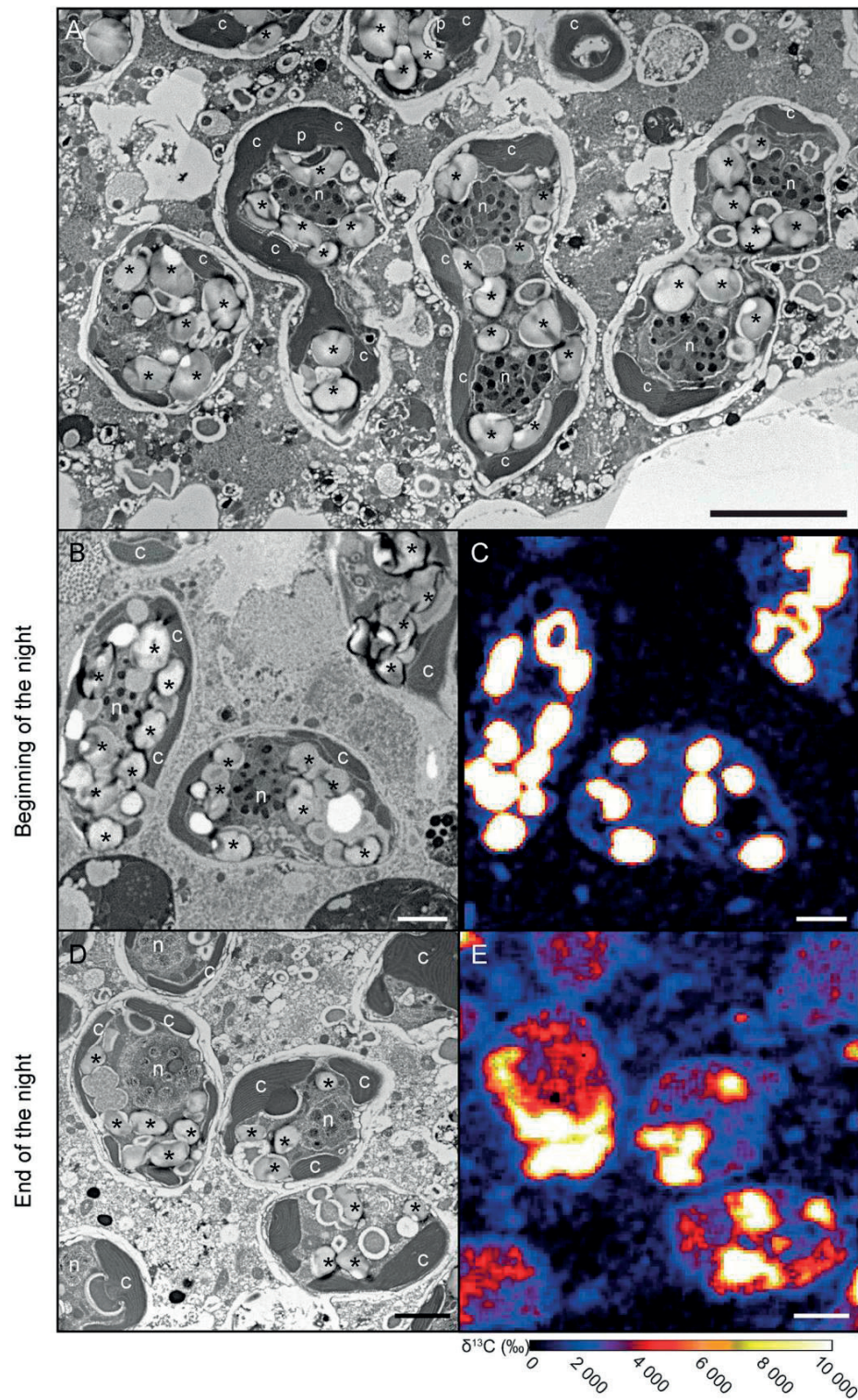


Figure 4.8: Dinoflagellate mitosis. A: TEM micrograph of three dinoflagellate symbionts undergoing mitosis in the *O. universa* endoplasm at 12 h (i.e. middle of the night phase; cf. Fig. 1). TEM micrographs (B and D) and corresponding NanoSIMS ^{13}C -enrichment images of dinoflagellates in *O. universa* endoplasm at the beginning of the night (C) and at end of the night (E), respectively. c: dinoflagellate chloroplasts, n: dinoflagellate nucleus, p: dinoflagellate pyrenoids, asterisks: dinoflagellate starch grains. Scale bars: A = 5 μm ; B, C, D and E = 2 μm .

4 Discussion

4.1 Diurnal patterns of symbiont distribution

As previously documented in other symbiotic planktonic species (Anderson and Bé, 1976b; Bé and Hutson, 1977) and in *O. universa* (Bé et al., 1977; Spero, 1987), the dinoflagellate symbionts migrate up and down the foraminiferal spines, synchronized with the day-night cycle (Fig. 4.2). At the onset of night conditions, the symbiotic dinoflagellates migrated down the spines and passed through the juvenile chamber apertures where each dinoflagellate became encapsulated inside a vacuole in the endoplasm, as also shown by (Spero, 1987). However, this process was not completely reversed during the day. Rather, we observe a small subpopulation of symbionts within the endoplasm of *O. universa* during the day. (Anderson and Bé, 1976b) suggested that such sequestration within the endoplasm could enhance transfer of photosynthates. However, the transfer rate of ^{13}C from the dinoflagellates to *O. universa* lipid droplets was not observed to be faster during the night (Fig. 4.5). These observations, combined with the measurement of ^{13}C -signal in foraminiferal organelles already after 45 min of incubation in light (Fig. 4.3). The majority of the dinoflagellates were on the spines during the day to benefit from light and performing photosynthesis. But the transfer of photosynthates to the foraminiferal cell occurred throughout the diurnal cycle, suggesting that a fraction of the dinoflagellates is continuously residing inside the endoplasm.

4.2 Dinoflagellate mitosis and photosynthesis: role of the foraminifera?

In the middle of the night (i.e. after 12 h of incubation) dinoflagellates were commonly observed in the process of undergoing mitosis (Fig. 4.8). The division of chrysophyte symbionts within the endoplasm of the planktonic species *Globigerinella siphonifera* was previously documented and the foraminiferal endoplasm suggested to be the most favorable environment for survival and growth of the microalgae (Faber et al., 1988). The foraminifera provides a protective environment and could potentially also provide extra nutrients needed by the microalgae, such as N and P that they obtain through prey capture (Jørgensen et al., 1985). The symbiotic dinoflagellates of the pelagic cnidarian *Mastigias* sp. also undergo mitosis at night when the host is visiting a nutrient-rich chemocline lower in the water column (Wilkerson et al., 1983). A study made on diatoms and dinoflagellates in culture showed that a pulse of nutrients can induce cell division of the microalgae (Doyle and Poore, 1974). In addition, Yoder et al. (1982) demonstrated that in the diatom *Thalassiosira weissflogii*, mitosis was stimulated by a pulse of nitrate, and became asynchronous when the nitrate was supplied continuously. In large benthic foraminifera the feeding of foraminifera was shown to increase symbiont productivity (Lee and Bock, 1976; Lee and Zucker, 1969), which might be driven by host nutrient

acquisition through prey ingestion. Because *O. universa* typically inhabits low nutrient environments (Spero and Parker, 1985) it might be necessary for the symbiotic dinoflagellates to be supplied with an environment rich in N and P nutrients to stimulate mitosis (Uhle et al., 1999). This role could be investigated with prey capture experiments. Indeed, *O. universa* would be well suited for such experiments because it is mixotrophic (Bé et al., 1977).

Another advantageous role for the foraminifera to enhance symbiont success is providing the dinoflagellates with a concentrated source of CO₂ in the photosynthesizing microenvironment. In our study, starch accumulating in the dinoflagellates during the second light phase (i.e. during the chase phase without ¹³C-labeled added inorganic carbon) was still slightly enriched in ¹³C (Figs. 4.3 and 4.4). There can be several reasons for this enrichment. First, the original label was not completely rinsed from the foraminifera during the chase phase. While we cannot eliminate this possibility, we find it unlikely given the multiple rinses used to eliminate this contamination. Second, we observed a large amount of variability among specimens where some *O. universa* individuals analyzed after 18 h at the end of the night phase still contained ¹³C-enriched starch grains within the dinoflagellates (Figs. 4.3 and 4.4) which would represent a form of carbohydrate contamination at T=30h. Finally, ¹³C-labeled C that was fixed during the first light phase and translocated to the foraminifera host from T=6h to T=18h is being metabolized and ¹³C-enriched CO₂ is being released from the cell. Or the slight enrichment observed at the end of the second light phase could result from the respiration of the foraminifera of its ¹³C-enriched lipid stocks, thereby providing recycled inorganic ¹³C to the dinoflagellate photosynthetic system which would be then be available for incorporation into starch grains. Although in our study it was not possible to measure the $\delta^{13}\text{C}_{\text{DIC}}$ in the foraminiferal microenvironment during the chase period, it seems inevitable that the foraminifera respire and release remineralized ¹³C-enriched CO₂ to the surrounding aqueous environment. Microsensor measurements of oxygen in the *O. universa* microenvironment highlighted this possibility as *O. universa* respiration corresponds to ca. 48 % of the dinoflagellate gross photosynthesis (Rink et al., 1998). For the same species a time-lag in CO₂ concentration changes was recorded in the foraminiferal microenvironment after a switch from light to dark conditions and vice-versa, while the O₂ concentrations immediately changed due to photosynthesis (Köhler-Rink and Kühl, 2005). Besides rates of O₂ release by the symbionts were much higher than their CO₂ uptake. This was interpreted as the consequence of an internal CO₂ supply mechanism, the foraminifera provide CO₂ to the symbionts via their respiration, thus symbionts take less CO₂ from their environment.

4.3 Photosynthate assimilation and turnover in the symbiotic dinoflagellates

Consistent with previous work (Spero 1987), the incorporation of ^{13}C into starch on the dinoflagellate pyrenoid surfaces was evident after only 45 min into the ^{13}C pulse (Fig. 4.3) and likely starts as soon as the symbiont is exposed to light, judging from the observed enrichment levels (Fig. 4.4D). Initially, we observe ^{13}C -enrichments in starch on the pyrenoid surfaces and in starch grains accumulating in the dinoflagellate cytosol. These observations indicate that the dinoflagellates rapidly transfer starch from the pyrenoid surface to the cytosol during the initial 6 h pulse/light period (Fig. 4.3). A similar carbon storage pathway was reported for the symbiotic dinoflagellate *Symbiodinium* spp. in corals during a comparable pulse-chase experiment (Kopp et al., 2015a).

The abundance of starch grains in the cytosol increased throughout the light pulse phase, followed by a steady decrease during the night (Fig. 4.4C), due to dinoflagellate respiration, cell division (as indicated by ^{13}C redistribution to other dinoflagellate organelles following mitosis; Fig. 4.8E), as well as photosynthate translocation to the host (Figs. 4.3, 4.5 and 4.6). These carbon pathways for the photosynthetically assimilated carbon seem similar to those reported for symbiotic corals (Kopp et al., 2015a). Starch, the most abundant C storage form in plant cells, consist of amylopectin and amylose synthesized from the simple hexose glucose (supplied by photosynthetic C fixation), and its degradation results mainly in the formation of glucose and maltose which can be further processed in other C compounds (e.g. Preiss, 1982; Smith et al., 1997; Zeeman et al., 2010). In symbiotic dinoflagellates, starch is also the main form of C storage (although lipid droplets can also be seen (Dodge and Crawford, 1971; Taylor, 1968). Its degradation into simple hexoses and their reprocessing might provide C for both the algae and foraminiferal cell metabolism as was suggested in the coral-dinoflagellate symbiosis (Kopp et al., 2015a).

The efficiency of the *O. universa* dinoflagellate photosynthetic system to fix C was previously demonstrated by oxygen flux measurements using microsenors (Jørgensen et al., 1985; Köhler-Rink and Kühl, 2005; Rink et al., 1998). Based on a ^{14}C pulse chase experiment and an estimate of foraminiferal C content, Caron et al. (1995) calculated a daily symbiont carbon production rate equivalent to 39 % of the total organic carbon weight of the foraminifera (host + symbiont complex). By comparing the respiration rate of dinoflagellates with the respiration rate of *O. universa*, Lombard et al. (2009) suggested that C is assimilated in excess by the foraminifera (i.e. the amount of organic matter produced and translocated by photosynthetic symbionts exceeds what is needed for host and symbiont growth) and that excess C could be released into the environment, potentially under the form of amino acids to attract prey.

4.4 Photosynthate translocation and fate inside the host cell

After 45 minutes of incubation, we observed ^{13}C -enriched lipid droplets within the foraminiferal endoplasm (Fig. 4.3), which indicates rapid translocation of ^{13}C -photosynthates from the dinoflagellate to the foraminiferal host cell. Fast C transfer was also observed in a coral symbiotic system where ^{13}C -enriched host lipids were observed after only 15 minutes (Kopp et al., 2015a). The continuous increase of lipid ^{13}C -enrichment during the first 18 hours of these experiments (Fig. 4.5) indicates photosynthate C is moving between the dinoflagellates and foraminiferal host continuously. In addition to the presence of lipid in the endoplasm we also see a gradual increase in ^{13}C -label in all foraminiferal endoplasm compartments indicating the foraminifera is utilizing the assimilated photosynthate carbon for its metabolic needs.

Small lipid droplets similar in appearance were observed both in the dinoflagellates and the foraminiferal endoplasm (Fig. 4.6). The presence of lipid droplets in the dinoflagellates was previously documented in both *O. universa* symbionts (Siano et al., 2010) and in free swimming dinoflagellates (Dodge and Crawford, 1971). In our study it is noteworthy that these lipid droplets were often seen in close proximity to the dinoflagellate vacuolar membrane (Fig. 4.6). These images could suggest a translocation of photosynthate carbon from the symbiotic dinoflagellate to the host foraminiferal cell either as a direct cross membrane transfer by lipid exudation or solubilization of the lipids into free fatty acids in the dinoflagellate to pass the membrane, and an immediate recombination on the other side in the foraminiferal cell.

Several studies have reported that fatty acid production of triacylglycerols (TAGs) in marine algae chloroplasts initiates in the chloroplasts prior to export from the algal cell (Fan et al., 2011; Merchant et al., 2012). Incubation of the coral *Pocillopora capitata* with ^{14}C -acetate suggests the coral first assimilates acetate and subsequently transfers carbon to the dinoflagellates where it is then converted into fatty acids prior to transferring the synthesized lipids back to the host cell (Patton et al., 1977). Although the C-integration pathway is different than in our experiment where inorganic carbon assimilation occurs in the symbionts, it attests to the direct transfer of fatty acids between the symbionts and the host cell. The same incubation protocol applied to the sea anemone *Condylactis gigantea* led to similar ^{14}C incorporation in host lipid droplets (Kellogg and Patton, 1983). The same exudation process was observed in isolated dinoflagellates from the corals *Stylophora pistillata* and *Seriatopora hystrix*, where the coral lipid droplets were also observed adjacent to the algal membrane (Patton and Burris, 1983). However no lipid exudation was observed in the dinoflagellates from the coral *Millepora exesa* and the giant clam *Tridacna* sp., which suggests that this phenomenon may not be universal or might be seasonal. Besides the exudation of lipid droplets, carbon transfer could occur

as free fatty acid transfer as it was suggested between symbiotic dinoflagellates and clams (Johnston et al., 1995). In Johnston et al. (1985), a $\delta^{13}\text{C}$ comparison of the fatty acids found in the clam tissue *versus* the dinoflagellates suggests a direct translocation of palmitic and 16:1 ω 7 acids.

Transfer of other carbon compounds between symbiotic dinoflagellates and host cells has been proposed such as glycerol and soluble molecules such as glucose, malate, citrate, glycolate, succinate or amino acids (Hofmann and Kremer, 1981; Trench, 1971, 1979). In corals, ciliates and sponges, symbiotic green algae chlorellae are known to release maltose, as well as other soluble compounds like glucose (Cernichiari et al., 1969; Muscatine et al., 1967). However, the studies discussed above quantified compounds released in culture medium by isolated symbiotic microalgae. A more recent study performed on different dinoflagellate-bearing symbiotic cnidarians suggests that glycerol translocation, which was thought to be one of the main carbon transport forms, is a stress response of the symbiotic algae after being separated from their natural host cell environment (Burriesci et al., 2012). These authors separated the symbiotic algae from their host after exposure to ^{13}C -bicarbonate and found that glucose might be the main metabolite that is transferred between symbionts and host cells.

In the symbiotic radiolarian *Collosphaera huxleyi*, as well as in the coral *Heteroxenia fuscescens*, a large proportion of the transferred carbon found in the host cell is thought to involve a glycerol transfer step prior to the production of lipids (e.g., wax, fatty acids and triglycerides) (Anderson et al., 1983; Schlichter et al., 1983). In *H. fuscescens*, Schlichter et al. (1983) reported a rapid conversion of soluble compounds into lipids in both symbiont and host cells, and attributed this to the better energy storage yield conferred by the lipogenesis over a carbohydrate storage. The reprocessing of C-soluble compounds was also shown in the coral *Acropora* cf. *scandens* where labeled ^{14}C -glycerol and ^{14}C -glucose were rapidly converted to lipid. After 60 min of incubation, ~30 % of the ^{14}C fraction was found in the lipophilic fraction (Schmitz and Kremer, 1977). However the authors could not conclude whether the reprocessing of the photosynthates occurs in the symbionts or the host.

Whatever the metabolite transferred, it is likely that these transfers of soluble compounds also happen in the symbiosis between dinoflagellates and *O. universa*. Unfortunately the method used here does not allow the detection of soluble compounds. If glycerol, hexoses or amino acids were present in the *O. universa* symbiotic system, then we would have lost evidence of this step during the rinse phase of sample preparation. Only ^{13}C stored in lipid or fixed carbohydrates could be detected in our study. Transfer lipid or soluble forms are not mutually exclusive and might be concomitant in the symbiosis between dinoflagellate and foraminiferal cells. In cnidarians these processes are controlled by the host through the expression of specific molecules to stimulate or inhibit the release of

photosynthates from the algae (review in Yellowlees et al., 2008). Thus depending on the environmental conditions and the host metabolic state, the host could modulate this transfer and preferentially trigger the translocation of lipids or soluble compounds. The different transfer pathways may lead to different carbon uses in the host cell such as storage in lipid droplets or direct use in various metabolic pathways.

The small ^{13}C -enriched opaque structures observed in the foraminiferal endoplasm (Fig. 4.7) could correspond to the electron opaque bodies described in benthic foraminifera (see chapter 1) and seen on the TEM micrographs of planktonic species in several previous publications (Anderson and Bé, 1976b; Hemleben et al., 1989). These structures, also called “electron dense bodies”, were found to contain nitrogen and significantly more sulfur than other organelles (Nomaki et al., 2016).

The fibrillar bodies (Fig. 4.7) observed in the *O. universa* endoplasm and internal matrix are organelles specific to the planktonic foraminifera. They were previously described in many TEM studies from different planktonic species (Anderson and Bé, 1976b, 1976c; Hansen, 1975; Lee et al., 1965; Spero, 1988). Variation in the ^{13}C -enrichment of the fibrillar bodies reflects their time of formation before or during the pulse and/or chase phases of our experiment. Based on cytological staining, (Lee et al., 1965) identified the protein nature of the fibrillar bodies (called vesicular system). The role of these organelles remains unknown although Hansen (1975) speculated that they could serve an ion exchange function and were important for buoyancy. Later Spero (1988) suggested the fibrillar bodies are integrally involved in biomineralization, chamber formation and Ca storage.

Despite speculation by Hansen that the fibrillar bodies are related to buoyancy, the production of ^{13}C -lipid in *O. universa* raises the intriguing possibility that lipid production is integrally related to the buoyancy mechanism in this and perhaps other species of planktonic foraminifera. (Spero, 1988) noted that the majority of *O. universa* specimens produce a spherical chamber at night when the symbionts are sequestered within the endoplasm. The production of such a large test, coupled with chamber thickening during calcification, means the foraminifera must have evolved a mechanism to rapidly generate positive buoyancy in order to counter the density increase of the organism that is associated with calcification. We hypothesize that lipid production associated with carbon translocation plays a significant role in buoyancy. Furbish and Arnold (1997) and Kucera (2007) also point to low density lipids or gasses as a source of negative buoyancy to offset the negative buoyancy of the shell calcite. Such a function for lipids could provide a rationale for the foraminifera system to vary the type of carbon translocated between symbiont and host cell to lipid vs soluble carbon as discussed earlier.

5 Conclusion

The symbiotic dinoflagellates transfer their photosynthates to the foraminiferal cell continuously, throughout the day-night cycle. Thus their massive migration along the spines to enter the foraminiferal endoplasm at night might have another reason than to enhance this transfer. The NanoSIMS data bring the evidence of an efficient dinoflagellate photosynthesis and a rapid translocation of the carbon to the foraminiferal cell as it has been documented in the coral system. We cannot conclude here about the detailed metabolic mechanism concerning the photosynthates transfer from the dinoflagellate to the host cell. From our data and literature it seems that this transfer could happen either whether under the form of small lipid droplets transferred directly exudate the algal and symbiosome membranes; or under the form of free lipophilic fatty acids soluble crossing the membranes; or under hydrophilic forms such as glycerol or other hexoses which would be later reprocessed into lipids; all pathways might be concomitant. The carbon translocated to the foraminiferal cell is then either stored by the foraminifera in lipid droplets or directly used for its metabolism. Finally our data do not allow us to conclude about the possibility of the dinoflagellate to use the CO₂ respired by the foraminifera, also this seems really likely as it would provide them a substantial source of inorganic carbon to maintain their high photosynthetic rate.

Acknowledgements:

The electron microscopy platform at the University of Lausanne (Switzerland) is thanked for help and access to the equipment. The technical assistant from the Wrigley marine Institute and the divers are thanked.

Funding sources:

This work was supported by the Swiss National Science Foundation (grant no. 200021_149333).

General discussion and perspectives

In this thesis work NanoSIMS analysis correlated with TEM observations was used to investigate foraminiferal metabolism and physiological processes. Incubation with stable isotopes were done to follow the assimilation and fate within the cell of different organic and inorganic compounds. First, detailed ultrastructural description of the organelles encountered in foraminiferal cell were made to facilitate the interpretation of NanoSIMS-TEM results. This thesis work then focused on three different physiological functions in benthic and planktonic foraminifera: (1) dormancy in response to anoxia, (2) kleptoplasty (chloroplasts sequestration) in benthic foraminifera from both photic environments, and (3) symbiosis of photosynthetic microalgae with planktonic foraminifera. The main results are discussed below, after a short discussion of the main analytical method used in this work.

1 NanoSIMS advantages and limitations

NanoSIMS has proven to be a powerful analytical tool to study foraminiferal metabolism. Its high spatial resolution enabled us to follow precisely the assimilation of isotopically labeled compounds within the cell and even within sub-cellular compartments; albeit the specific chemical nature of these compounds cannot be determined from NanoSIMS analysis. In correlation with transmission electron microscopy (TEM) the NanoSIMS is ideal to identify the labeled structures and characterize more precisely the transfers and exchanges that take place between organelles and/or between symbionts/kleptoplasts and the foraminiferal cell. In addition to the high spatial resolution provided by TEM-NanoSIMS correlation, the use of time-series experiments enables the visualization of the dynamics of these exchanges and the time scale of the metabolic processes could thus be determined and compared for different conditions or experiments. And finally, although it cannot be used to precisely quantify the uptake of a compound, NanoSIMS imaging yields quantitative information that can be used as relative concentrations to compare assimilation from one cell type/compartment to another.

However, it is important to keep in mind that bias due to the sample preparation preclude estimates of net uptake of any labeled compounds (Musat et al., 2014, Nomaki et al., submitted), or precisely compare isotopic enrichment values with values obtained with different methods. To obtain this kind of data complementary analysis are needed, such as bulk isotopic measurement (as it was done in chapter 2 to calculate the net uptake of an inorganic compounds).

One of the major problems encountered in the NanoSIMS work presented in this thesis is the loss of soluble components during the sample preparation. Indeed, if isotopically labeled soluble compounds are produced by the studied organisms, they could not be detected by NanoSIMS analysis. This could be avoided with the use of cryofixation processes. Cryofixation of foraminifera was already done (Goldstein et al., 2004; Goldstein and Richardson, 2002), but never in combination with any other analytical technique. The soluble compounds could also be analyzed by different techniques, such as those employed to study metabolomics. For example in the chapter 2, the use of GC-MS for fatty acids analysis brought valuable additional information about the feeding metabolic processes under oxic or anoxic conditions, respectively. Some of the studies presented in this thesis work will be completed by new experiments with NanoSIMS combined with metabolomics approaches to further understand the foraminiferal metabolic functions (see below). Many different combination of NanoSIMS with other analytical methods (energy- dispersive X-rays (EDS), time-of-flight secondary ion mass spectrometry (ToF-SIMS), nuclear magnetic resonance (NMR), liquid chromatography-mass spectrometry (LC-MS), epifluorescence, fluorescent hybridization in-situ (FISH) or diverse biochemical analysis) can be found in literature (Jiang et al., 2016; Krueger et al., 2017; Nomaki et al., 2016; Perfumo et al., 2014; Raina et al., 2017), and could be applied to foraminiferal cell analysis.

2 Ultrastructure of benthic foraminiferal cells

As it was emphasized in the introduction, there was a need to systematically gather information about “small” benthic foraminiferal ultrastructure, which was missing from the literature. Especially because the main analytical tool in this study is the NanoSIMS use in combination with TEM, a strong background knowledge of the foraminiferal cell ultrastructure was required. The first chapter of this thesis thus presented an inventory of the organelles observed in benthic foraminiferal cell based both on the review of the literature and novel TEM observations on nine different species inhabiting different environments.

Organelles can be classified into three categories: (1) common organelles with known functions observed in all foraminiferal species, also observed in most eukaryotic cells; (2) organelles recurrent in all foraminiferal species, with no similarities to any structures observed in other taxa; and (3) organelles observed only in some specific species, likely linked to a special metabolism. This work particularly highlighted the variability among species. For example, in the first category, although these common organelles (i.e. nucleus, mitochondria, endoplasmic reticulum, Golgi apparatus or peroxisomes) were observed in all foraminiferal cells, their aspect can differ between species. In

addition, the endoplasm aspect can differ greatly between species, probably due to different metabolism. For example, the large vacuoles mainly observed in denitrifying species are thought to harbor nitrate intracellular pool. Structures linked to feeding metabolism will vary depending on the diet or trophic mechanism. A systematic study of foraminiferal ultrastructure thus permits to gain insights into the metabolic mechanisms exhibited by the different species. The review of functions and roles of the organelles involved in trophic mechanisms was of fundamental for the rest of this thesis work. Indeed, the following chapters all discussed feeding strategies in foraminifera, whether for grazing on algal biofilm or mixotrophy strategies brought by symbionts.

Finally this work also emphasized the need for further research. As it could be seen, TEM observations alone are not sufficient to unravel the role and function of most of the organelles observed in foraminiferal cytoplasm. Complementary techniques, such as the NanoSIMS, are necessary to link ultrastructure to metabolic pathways and physiological functions.

3 Dormancy in response to anoxia

Among the different adaptations proposed for foraminiferal survival to anoxia (including symbiosis with prokaryotes, kleptoplasts, ultrastructural adaptations) only denitrification was proven, by the foraminifera itself or through symbiosis with denitrifying prokaryotes (Bernhard et al., 2012a, 2012b; Risgaard-Petersen et al., 2006). Denitrification performed by foraminifera may play an important role in nitrogen geochemical cycle depending on the environment (Høgslund et al., 2008; Piña-Ochoa et al., 2010a). But although this alternative anaerobic metabolism is widespread, not all foraminifera possess it (Piña-Ochoa et al., 2010a). The case of *Ammonia cf tepida* is interesting: this shallow benthic species is one of the most abundant species in intertidal environments. It is able to survive long laboratory incubation under anoxia (Nardelli et al., 2014) and is found *in situ* deep in the sediment column where no oxygen can be found (Thibault de Chanvalon et al., 2015) where they are brought by macrofaunal bioturbation (Maire et al., 2016). The feeding experiment carried out under both oxic and anoxic conditions presented in chapter 2 shows that the *Ammonia cf tepida* trophic mechanism is strongly affected by the lack of oxygen. Although they survived 28 days under anoxia, we observed a drastic reduction of their physiological functions: they stopped their heterotrophic metabolism after 24 h and they could not grow (i.e. they did not calcify during the experiment). All these observations indicate that *Ammonia cf tepida* lacks any alternative anaerobic metabolism which could provide them energy to maintain the level of activity they have under oxic conditions. Thus we suggested that it enters dormancy to withstand long anoxic conditions, with strongly reduced

metabolic activity. This strategy is in agreement with previous findings of species exhibiting lower intracellular ATP concentrations when incubated in anoxia (Bernhard and Alve, 1996). This dormancy strategy might thus be found in other foraminiferal species, and be more widespread than previously acknowledged (Ross and Hallock, 2016).

In oxic conditions, benthic foraminifera are thought to play a significant role in the carbon processing in the sediment, due to their rapid uptake of phytodetritus (Gooday et al., 1990, 1992, Moodley et al., 2000, 2002; Nomaki et al., 2006; Woulds et al., 2007). This is particularly true in intertidal mudflats, where foraminifera have been shown to account for up to 7% of the organic matter that is remineralized into the sediment (Cesbron et al., 2016). However, we showed here that under anoxic conditions, some species are able to remain dormant; suggesting their role might be negligible compared to that of other benthic components such as bacteria. However, to validate this hypothesis, the occurrence of dormancy in foraminifera need to be more thoroughly investigated, to determine how widespread this metabolic response is to anoxic conditions. This will be a particularly important consideration for species inhabiting coastal ecosystems, as these are more frequently subjected to low O₂ events (Diaz and Rosenberg, 2008; Helly and Levin, 2004; Rabalais et al., 2010). Foraminifera have been shown to be among the most resistant species to anoxia compared to the rest of the meiofauna and the macrofauna (Gooday et al., 2000; Levin et al., 2009; Moodley et al., 1997). Denitrification and dormancy are two metabolisms that can explain this tolerance. But the metabolism of many species have not been assessed yet and there may be other anaerobic metabolisms in foraminifera that remain to be discovered.

4 Kleptoplasty in coastal benthic foraminifera

Sequestration of chloroplasts in foraminifera inhabiting photic environments present two main advantages due to photosynthesis: (1) the production of oxygen within the cell (Cesbron et al., 2017; Jauffrais et al., 2016), and (2) the uptake of inorganic carbon via the Benson-Calvin cycle, its assimilation into organic compounds, and transfer to the foraminiferal cell (Lopez, 1979, chapter 3.2). The latter might represent an advantage by avoiding competition for resources with other heterotrophic organisms.

Chapter 3.1 first showed that among the different species harboring kleptoplasts, different sequestration pattern are represented. Some species, like *Ammonia* cf. *tepida*, are not true kleptoplastic, the few kleptoplasts they possess are mostly in a degradation state. In addition, their

kleptoplasts are known to be non-functional (Jauffrais et al., 2016; chapter 3.3). We here confirm the hypothesis first speculated by Jauffrais et al. (2016), that the presence of sequestered chloroplasts in these species might likely result from a transitional state of algae digestion, i.e. foraminifera feed on diatoms that they digest within the cell, and the chloroplasts are among the last organelles to be degraded (chapter 1, data not shown), thus remaining temporary in the foraminiferal cytoplasm. Other species, such as *Elphidium williamsoni* and *Haynesina germanica* are known to be true kleptoplastic species, harboring functional kleptoplasts (Cesbron et al., 2017; Jauffrais et al., 2016, 2017; Lopez, 1979). This was confirmed in this thesis with the measurement of photosynthetic oxygen production in *E. williamsoni* and inorganic carbon assimilation and transfer to the foraminiferal cell in both species (chapters 3.2. and 3.3). However, the kleptoplastic strategies differ between species. On one hand, *H. germanica* have kleptoplasts distributed within its entire endoplasm, and the carbon coming from photosynthetic carbon assimilation was mainly found stored in lipid droplets (chapters 3.1 and 3.2). In this species, the carbon is thought to be transfer, at least partially, in the form of lipid droplets directly exudated into the foraminiferal host cell. On the other hand, *E. williamsoni* seems to display a particular kleptoplast distribution along the cell periphery, suggesting a strategy to either expose or protect sequestered chloroplasts from light, or favor gas exchanges with the surrounding environment (chapter 3.1). In addition this species exhibited a different carbon metabolism than *H. germanica*: the carbon assimilated by the kleptoplasts was not found in foraminiferal lipid droplets (chapter 3.3). Only a light ^{13}C -enrichment was detected in the cytoplasm. One of the most probable explanation is that the inorganic carbon is assimilated into soluble compounds instead of fatty acids (Fig. 5.1). These compounds would be lost during the sample preparation, and thus not detected by NanoSIMS analysis. To answer this question, new experiments with bulk ^{13}C enrichment measures as well as metabolomics to determine the ^{13}C -labeled compounds (similar analysis then the fatty acid analysis done in chapter 2) are necessary.

The studies presented in the chapters 3.2 and 3.3 show an unclear scheme for inorganic nitrogen and sulfur assimilation in kleptoplast benthic foraminifera (Fig. 5.1). Both the kleptoplastic species *E. williamsoni* and *H. germanica* were shown to assimilate ^{15}N -ammonium and ^{34}S -sulfate. But we showed for the first time that a non-kleptoplastic species, *Ammonia* cf. *tepida*, is also able to actively assimilating labeled ^{15}N -ammonium and ^{34}S sulfate. This result emphasizes the need for more research to determine the role (if any) played by kleptoplasts in these metabolic processes. In algae, chloroplasts are known to play a role in sulfur and nitrogen metabolism: assimilation of inorganic S and N was shown and resulted in the incorporation of these elements into various organic compounds such as amino acids or phospholipids (Benning and Garavito, 2008; Giordano et al., 2008; Giordano and

Raven, 2014; Syrett, 1981; Takahashi et al., 2011; Zehr et al., 1988; Zehr and Falkowski, 1988). This might also be the case in kleptoplastic foraminifera.

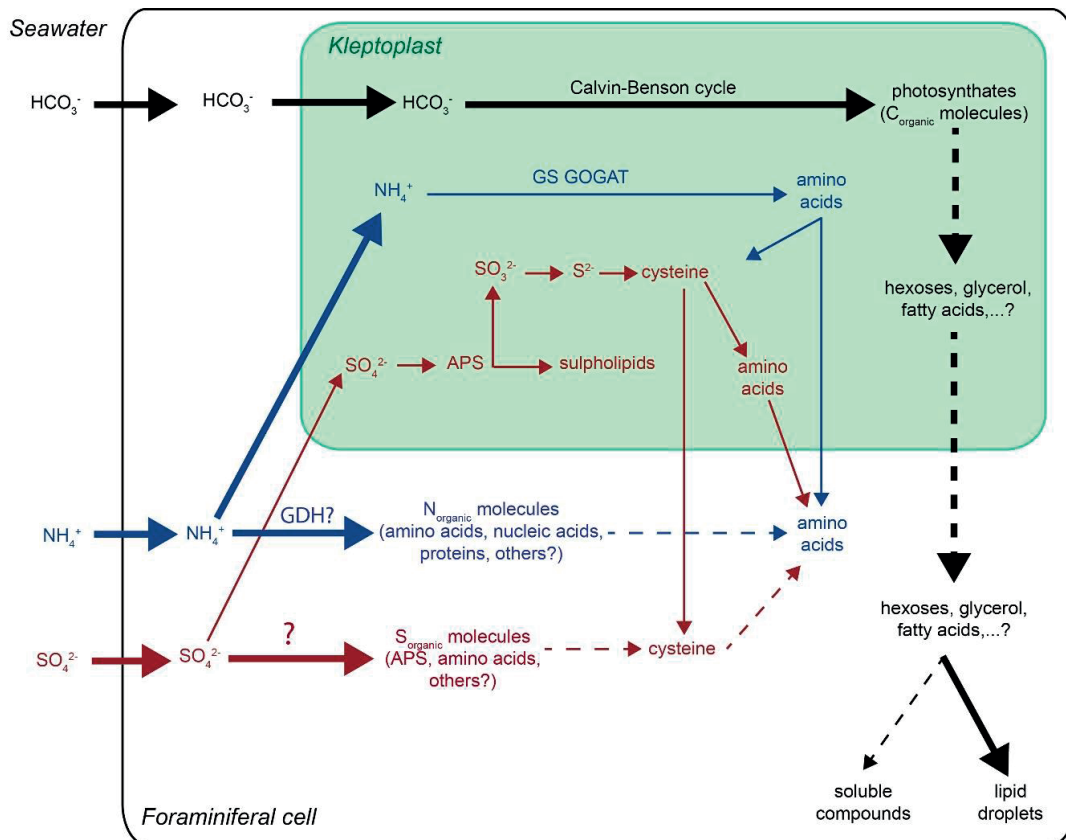


Fig. 5.1: Schematic representation of the C, N and S assimilation pathways in kleptoplastic foraminiferal cell. C, N and S pathways are represented in black, blue and red, respectively. The thick arrows represent pathways demonstrated in this thesis work in the chapters 3.2 and 3.3. The thick dotted arrows represent pathways identified in this thesis but for which the nature of the compounds remain unknown. The thin arrows represent pathways hypothesized at the beginning of the work (see figure 1.5 in the literature review), that have not been proved yet, but are still suspected to happen. And the dotted thin arrows represent new hypotheses made thanks to the result obtained in this thesis. APS: adenosine 5-phosphosulphate, GDH: glutamate dehydrogenase, GOGAT: glutamine oxoglutarate aminotransferase, GS: glutamate synthase. Modified from Giordano and Raven (2014), Pyke (2009) and Takahashi et al (2011).

So there are still a lot of questions unanswered (Fig. 5.1). For example, what is the main form of carbon transfer between kleptoplasts and foraminifera cytoplasm? We suggested in *H. germanica* that this happened by lipid droplets exudation; but due to the sample preparation for TEM-NanoSIMS analysis, soluble compounds were lost and their transfer could not be assessed (see section 1). Also,

in *E. williamsoni*, where does the photosynthetically assimilated carbon go in the foraminiferal cell? And what are the preferential pathways used by kleptoplastic species to meet their nitrogen and sulfur requirements: assimilation of inorganic compounds via the kleptoplasts and/or via the foraminifera's own metabolism? And does it vary according to environmental conditions (e.g. light, oxygen concentration)? In an attempt to answer these questions, additional experiments will be done. New incubations with labeled isotopes will be conducted, and NanoSIMS analysis will be combined with other analytical techniques. The analysis of specific metabolite (sugars, fatty acids, amino acids, sulfolipids, etc.) concentration and isotopic enrichment should be done to better understand the metabolic pathways happening in the foraminiferal cell, kleptoplastic or not.

Finally, the probably most interesting study to be made is the quantification of inorganic ammonium and sulfate uptake. These results would be very interesting as they could help to assess the role played by foraminifera in the geochemical cycles of their environments. In particular, foraminifera were not known until now to actively assimilate ammonium and sulfate, and even if it was suspected in kleptoplastic foraminifera (Grzyski et al., 2002), their role in nitrogen and sulfur cycles might have been totally underestimated.

5 Carbon metabolism in symbiotic planktonic foraminifera

Symbionts associated to planktonic foraminifera include mainly dinoflagellates (Anderson and Lee, 1991; Hemleben et al., 1989). One of the most studied species is *Orbulina universa*, in symbiosis with the photosynthetic dinoflagellate *Pelagodinium béii* (previously known as *Gymnodinium béii*, Siano et al., 2010). In the chapter 4 we investigated the carbon metabolism in this foraminiferal species, i.e. the inorganic carbon assimilation by the symbionts and its subsequent transfer to the foraminiferal host cell.

One of the remarkable features of *O. universa* is the migration of the symbionts along its spines. Previously this was thought to follow a strict diurnal cycle: all the symbionts on the spines during day, and within the foraminiferal endoplasm at night (Bé et al., 1977; Spero, 1987). However we showed that there is a permanent pool of dinoflagellates inside the foraminiferal endoplasm, even during the day. This allows the transfer of carbon between the symbionts and the host cell to happen at any time. At night all the dinoflagellates were migrating inside the foraminiferal endoplasm, where they underwent division. It is possible that the foraminifer triggers the dinoflagellate mitosis by

providing it with nutrients (potentially nitrogen or phosphorus) (Jørgensen et al., 1985; Uhle et al., 1999), but the experiment done did not allow us to confirm this assumption.

The NanoSIMS analysis of assimilation of ^{13}C -bicarbonate and ^{13}C fate within the cells demonstrated an efficient dinoflagellate assimilation of carbon, which is then either stored into starch grains, respired, or translocated to the foraminiferal cell. The carbon translocated to the foraminiferal cell is then either stored by the foraminifera in lipid droplets or directly used for its metabolism. The nature of this transfer to the foraminiferal host cell remains unknown, although our observations gave insights of the existence of a transfer under a lipid form; either lipid droplet exudation, or direct transfer of free fatty acids across the dinoflagellate and symbiosome membranes. As for the benthic kleptoplast foraminifera we cannot exclude a concomitant transfer under a soluble form. This would be likely as it was shown to take place in other symbiosis, including symbiosis between dinoflagellates and marine organisms (cnidarians mostly), with transfer of glycerol, glucose and other hexoses, or amino acids (Burriesci et al., 2012; Trench, 1979; Yellowlees et al., 2008).

Again here the analysis of the isotopically enriched metabolites would be necessary to fully understand the carbon exchanges between symbionts and foraminiferal cell. In addition the nitrogen and phosphorus metabolisms would be very interesting to look at, especially to test the assumption of the foraminifera providing nutrients to trigger dinoflagellate division at night.

6 Conclusion

In this work we showed that NanoSIMS is a well-adapted analytical technique to look at foraminiferal metabolism. It allowed to visualize the extreme variability of metabolic pathways in the frame of different physiological functions among different species, or even within a single species exposed to different environmental conditions. But while certain questions were answered, many others were raised by the obtained results. Indeed, TEM-NanoSIMS technique apply to foraminifera enabled the discovery of several metabolic mechanisms ignored in foraminifera (in particular ammonium assimilation by foraminifera), and these results pose a many new questions that need to be addressed to better understand the foraminiferal metabolic processes, and their role in their ecosystems.

References

- A -

- Alexander, S.P., Banner, F.T., 1984. The functional relationship between skeleton and cytoplasm in *Haynesina germanica* (Ehrenberg). J. Foraminifer. Res. 14, 159–170. doi:10.2113/gsjfr.14.3.159
- Alexander, S.P., Delaca, T.E., 1987. Feeding adaptations of the foraminiferan *Cibicides refulgens* living epizoically and parasitically on the antarctic scallop *Adamussium colbecki*. Biol. Bull. 173, 136–159. doi:10.2307/1541868
- Alve, E., Murray, J.W., 2001. Temporal variability in vertical distributions of live (stained) intertidal foraminifera, Southern England. J. Foraminifer. Res. 31, 12–24. doi:10.2113/0310012
- Anderson, O.R., Bé, A.W.H., 1978. Recent advances in foraminiferal fine structure research. Foraminifera 3, 121–202.
- Anderson, O.R., Bé, A.W.H., 1976a. A cytochemical fine structure study of a phagotrophy in a planktonic foraminifer, *Hastigerina pelagica* (d'Orbigny). Biol. Bull. 151, 437–449.
- Anderson, O.R., Bé, A.W.H., 1976b. The ultrastructure of a planktonic foraminifer, *Globigerinoides sacculifer* (Brady), and its symbiotic dinoflagellates. J. Foraminifer. Res. 6, 1–21. doi:10.2113/gsjfr.6.1.1
- Anderson, O.R., Bé, A.W.H., 1976c. The ultrastructure of a planktonic foraminifer, *Globigerinoides sacculifer* (Brady), and its symbiotic dinoflagellates. J. Foraminifer. Res. 6, 1–21. doi:10.2113/gsjfr.6.1.1
- Anderson, O.R., Lee, J.J., 1991. Cytology and fine structure, in: Lee, J.J., Anderson, O.R. (Eds.), Biology of Foraminifera. Academic Press, London, pp. 7–40.
- Anderson, O.R., Spindler, M., Bé, A.W.H., Hemleben, C., 1979. Trophic activity of planktonic foraminifera. J. Mar. Biol. Assoc. U. K. 59, 791–799.
- Anderson, O.R., Swanberg, N.R., Bennett, P., 1983. Assimilation of symbiont-derived photosynthates in some solitary and colonial radiolaria. Mar. Biol. 77, 265–269.
- Anderson, O.R., Tuntivate-Choy, S., 1984. Cytochemical evidence for peroxisomes in planktonic foraminifera. J. Foraminifer. Res. 14, 203–205. doi:10.2113/gsjfr.14.3.203
- Anderson, S.L., Burris, J.E., 1987. Role of glutamine synthetase in ammonia assimilation by symbiotic marine dinoflagellates (zooxanthellae). Mar. Biol. 94, 451–458.
- Angell, R.W., 1967. The test structure and composition of the foraminifer *Rosalina floridana*. J. Protozool. 14, 299–307.
- Arnold, A.J., Parker, W.C., 1999. Biogeography of planktonic foraminifera, in: Sen Gupta, B.K. (Ed.), Modern Foraminifera. Springer-Verlag New-York, pp. 103–122.
- Arnold, Z.M., 1984. The gamontic karyology of the saccamminid foraminifer *Psammophaga simplora*. J. Foraminifer. Res. 14, 171–186. doi:10.2113/gsjfr.14.3.171

References

- Arnold, Z.M., 1982. *Psammophaga simplora* n. gen., n. sp., a polygenomic Californian saccamminid. J. Foraminifer. Res. 12, 72–78. doi:10.2113/gsjfr.12.1.72
- Austin, H.A., Austin, W.E.N., Paterson, D.M., 2005. Extracellular cracking and content removal of the benthic diatom *Pleurosigma angulatum* (Quekett) by the benthic foraminifera *Haynesina germanica* (Ehrenberg). Mar. Micropaleontol. 57, 68–73. doi:10.1016/j.marmicro.2005.07.002
- B -
- Bé, A.W., Anderson, O.R., 1976. Gametogenesis in planktonic foraminifera. Science 192, 890–892. doi:10.1126/science.946914
- Bé, A.W.H., Anderson, O.R., Faber, W.W., Jr., Caron, D.A., 1983. Sequence of morphological and cytoplasmic changes during gametogenesis in the planktonic foraminifer *Globigerinoides sacculifer* (Brady). Micropaleontology 29, 310–325. doi:10.2307/1485737
- Bé, A.W.H., Hemleben, C., Anderson, O.R., Spindler, M., 1980. Pore structures in planktonic foraminifera. J. Foraminifer. Res. 10, 117–128. doi:10.2113/gsjfr.10.2.117
- Bé, A.W.H., Hemleben, C., Anderson, O.R., Spindler, M., Hacunda, J., Tuntivate-Choy, S., Be, A.W.H., 1977. Laboratory and Field Observations of Living Planktonic Foraminifera. Micropaleontology 23, 155. doi:10.2307/1485330
- Bé, A.W.H., Hutson, W.H., 1977. Ecology of Planktonic Foraminifera and Biogeographic Patterns of Life and Fossil Assemblages in the Indian Ocean. Micropaleontology 23, 369. doi:10.2307/1485406
- Bé, A.W.H., Spero, H.J., Anderson, O.R., 1982. Effects of symbiont elimination and reinfection on the life processes of the planktonic foraminifer *Globigerinoides sacculifer*. Mar. Biol. 70, 73–86. doi:10.1007/BF00397298
- Beauchamp, R.O., Bus, J.S., Popp, J.A., Boreiko, C.J., Andjelkovich, D.A., Leber, P., 1984. A critical review of the literature on hydrogen sulfide toxicity. CRC Crit. Rev. Toxicol. 13, 25–97. doi:10.3109/10408448409029321
- Bedoshvili, Y.D., Popkova, T.P., Likhoshway, Y.V., 2009. Chloroplast structure of diatoms of different classes. Cell Tissue Biol. 3, 297–310. doi:10.1134/S1990519X09030122
- Behrens, S., Losekann, T., Pett-Ridge, J., Weber, P.K., Ng, W.-O., Stevenson, B.S., Hutcheon, I.D., Relman, D.A., Spormann, A.M., 2008. Linking microbial phylogeny to metabolic activity at the single-cell level by using enhanced element labeling-catalyzed reporter deposition fluorescence *in situ* hybridization (EL-FISH) and NanoSIMS. Appl. Environ. Microbiol. 74, 3143–3150. doi:10.1128/AEM.00191-08
- Benning, C., Garavito, R.M., 2008. Sulfolipid biosynthesis and function in plants, in: Hell, R., Dahl, C., Knaff, D., Leustek, T. (Eds.), Sulfur Metabolism in Phototrophic Organisms, Advances in Photosynthesis and Respiration. Springer, Dordrecht, The Netherlands, pp. 185–200.
- Bernhard, J.M., 2003. Potential symbionts in bathyal foraminifera. Science 299, 861–861.
- Bernhard, J.M., 1993. Experimental and field evidence of Antarctic foraminiferal tolerance to anoxia and hydrogen sulfide. Mar. Micropaleontol. 20, 203–213. doi:10.1016/0377-8398(93)90033-T

References

- Bernhard, J.M., Alve, E., 1996. Survival, ATP pool, and ultrastructural characterization of benthic foraminifera from Drammensfjord (Norway): response to anoxia. *Mar. Micropaleontol.* 28, 5–17.
- Bernhard, J.M., Bowser, S.S., 2008. Peroxisome proliferation in foraminifera inhabiting the chemocline: an adaptation to reactive oxygen species exposure? *J. Eukaryot. Microbiol.* 55, 135–144. doi:10.1111/j.1550-7408.2008.00318.x
- Bernhard, J.M., Bowser, S.S., 1999. Benthic foraminifera of dysoxic sediments: chloroplast sequestration and functional morphology. *Earth-Sci. Rev.* 46, 149–165. doi:10.1016/S0012-8252(99)00017-3
- Bernhard, J.M., Buck, K.R., Barry, J.P., 2001. Monterey Bay cold-seep biota: Assemblages, abundance, and ultrastructure of living foraminifera. *Deep Sea Res. Part Oceanogr. Res. Pap.* 48, 2233–2249.
- Bernhard, J.M., Buck, K.R., Farmer, M.A., Bowser, S.S., 2000. The Santa Barbara Basin in a symbiosis oasis. *Nature* 403, 77–80.
- Bernhard, J.M., Casciotti, K.L., McIlvin, M.R., Beaudoin, D.J., Visscher, P.T., Edgcomb, V.P., 2012a. Potential importance of physiologically diverse benthic foraminifera in sedimentary nitrate storage and respiration. *J. Geophys. Res.* 117. doi:10.1029/2012JG001949
- Bernhard, J.M., Edgcomb, V.P., Casciotti, K.L., McIlvin, M.R., Beaudoin, D.J., 2012b. Denitrification likely catalyzed by endobionts in an allogromiid foraminifer. *ISME J.* 6, 951–960. doi:10.1038/ismej.2011.171
- Bernhard, J.M., Geslin, E. Review of small benthic foraminifera ultrastructure. *Mar. Micropaleontol.* Special issue "Foraminiferal ultrastructure". Submitted.
- Bernhard, J.M., Goldstein, S.T., Bowser, S.S., 2010a. An ectobiont-bearing foraminiferan, *Bolivina pacifica*, that inhabits microxic pore waters: cell-biological and paleoceanographic insights. *Environ. Microbiol.* 12, 2107–2119. doi:10.1111/j.1462-2920.2009.02073.x
- Bernhard, J.M., Gupta, B.K.S., 2003. Foraminifera of oxygen-depleted environments, in: *Modern Foraminifera*. Springer Netherlands, pp. 201–216.
- Bernhard, J.M., Habura, A., Bowser, S.S., 2006. An endobiont-bearing allogromiid from the Santa Barbara Basin: Implications for the early diversification of foraminifera. *J. Geophys. Res. Biogeosciences* 111, G03002. doi:10.1029/2005JG000158
- Bernhard, J.M., Martin, J.B., Rathburn, A.E., 2010b. Combined carbonate carbon isotopic and cellular ultrastructural studies of individual benthic foraminifera: Toward an understanding of apparent disequilibrium in hydrocarbon seeps. *Paleoceanography* 25. doi:10.1029/2010PA001930
- Bernhard, J.M., Newkirk, S.G., Bowser, S.S., 1995. Towards a non-terminal viability assay for foraminiferan Protists. *J. Eukaryot. Microbiol.* 42, 357–367. doi:10.1111/j.1550-7408.1995.tb01594.x
- Bernhard, J.M., Reimers, C.E., 1991. Benthic foraminiferal population fluctuations related to anoxia: Santa Barbara Basin. *Biogeochemistry* 15, 127–149. doi:10.1007/BF00003221

References

- Bernhard, J.M., Richardson, E.A., 2014. FLEC-TEM: using microscopy to correlate ultrastructure with life position of infaunal foraminifera, in: Kitazato, H., Bernhard, J.M. (Eds.), *Approaches to Study Living Foraminifera*, Environmental Science and Engineering. Springer Japan, pp. 103–113. doi:10.1007/978-4-431-54388-6_7
- Bernhard, J.M., Sen Gupta, B.K., 1999. Foraminifera of oxygen-depleted environments, in: Sen Gupta, B.K. (Ed.), *Modern Foraminifera*. Kluwer Academic Publishers, Dordrecht, The Netherlands, pp. 201–216.
- Bernhard, J.M., Tsuchiya, M., Nomaki, H. Ultrastructural observations on prokaryotic associates of benthic foraminifera: food, mutualistic symbionts or parasites? *Mar. Micropaleontol.* Special issue "Foraminiferal ultrastructure". Submitted.
- Berthold, W.-U., 1976. Test morphology and morphogenesis in *Patellina corrugata* Williamson, Foraminiferida. *J. Foraminifer. Res.* 6, 167–185. doi:10.2113/gsjfr.6.3.167
- Bianchi, T.S., Johansson, B., Elmgren, R., 2000. Breakdown of phytoplankton pigments in Baltic sediments: effects of anoxia and loss of deposit-feeding macrofauna. *J. Exp. Mar. Biol. Ecol.* 251, 161–183.
- Bird, C., Darling, K.F., Russell, A.D., Davis, C.V., Fehrenbacher, J., Free, A., Wyman, M., Ngwenya, B.T., 2017. Cyanobacterial endobionts within a major marine planktonic calcifier (*Globigerina bulloides*, Foraminifera) revealed by 16S rRNA metabarcoding. *Biogeosciences* 14, 901–920. doi:10.5194/bg-14-901-2017
- Bollmann, J., Quinn, P.S., Vela, M., Brabec, B., Brechner, S., Cortés, M.Y., Hilbrecht, H., Schmidt, D.N., Schiebel, R., Thierstein, H.R., 2004. Automated particle analysis: calcareous microfossils, in: *Image Analysis, Sediments and Paleoenvironments*. Springer, pp. 229–252.
- Boltovskoy, E., Wright, R.C., 1976. *Recent foraminifera*. Springer Netherlands.
- Bouchet, V.M.P., Sauriau, P.-G., Debenay, J.-P., Mermillod-Blondin, F., Schmidt, S., Amiard, J.-C., Dupas, B., 2009. Influence of the mode of macrofauna-mediated bioturbation on the vertical distribution of living benthic foraminifera: First insight from axial tomodesitometry. *J. Exp. Mar. Biol. Ecol.* 371, 20–33. doi:10.1016/j.jembe.2008.12.012
- Bowser, S.S., Alexander, S.P., Stockton, W.L., Delaca, T.E., 1992. Extracellular matrix augments mechanical properties of pseudopodia in the carnivorous foraminiferan *Astrammmina rara*: role in prey capture. *J. Protozool.* 39, 724–732.
- Bowser, S.S., Travis, J.L., 2000. Methods for structural studies of reticulopodia, the vital foraminiferal "soft part". *Micropaleontology* 46, 47–56.
- Boxer, S.G., Kraft, M.L., Weber, P.K., 2009. Advances in Imaging Secondary Ion Mass Spectrometry for Biological Samples. *Annu. Rev. Biophys.* 38, 53–74. doi:10.1146/annurev.biophys.050708.133634
- Buchanan, J.B., Hedley, R.H., 1960. A contribution to the biology of *Astrorhiza limicola* (Foraminifera). *J. Mar. Biol. Assoc. U. K.* 39, 549. doi:10.1017/S0025315400013540
- Buck, K., Bernhard, J., 2004. Protistan-prokaryotic symbioses in deep-sea sulfidic sediments, in: Seckbach, J. (Ed.), *Symbiosis, Mechanisms and Model Systems, Cellular Origin, Life in Extreme Habitats and Astrobiology*. pp. 507–517.

Burriesci, M.S., Raab, T.K., Pringle, J.R., 2012. Evidence that glucose is the major transferred metabolite in dinoflagellate–cnidarian symbiosis. *J. Exp. Biol.* 215, 3467–3477. doi:10.1242/jeb.070946

- C -

Caron, D.A., Bé, A.W., Anderson, O.R., 1981. Effects of variations in light intensity on life processes of the planktonic foraminifer *Globigerinoides sacculifer* in laboratory culture. *J. Mar. Biol. Assoc. U. K.* 62, 435–451.

Caron, D.A., Michaels, A.F., Swanberg, N.R., Howse, F.A., 1995. Primary productivity by symbiont-bearing planktonic sarcodines (Acantharia, Radiolaria, Foraminifera) in surface waters near Bermuda. *J. Plankton Res.* 17, 103–129.

Cartaxana, P., Ruivo, M., Hubas, C., Davidson, I., Serôdio, J., Jesus, B., 2011. Physiological versus behavioral photoprotection in intertidal epipelagic and epipsammic benthic diatom communities. *J. Exp. Mar. Biol. Ecol.* 405, 120–127. doi:10.1016/j.jembe.2011.05.027

Caulle, C., Koho, K.A., Mojtahid, M., Reichart, G.-J., Jorissen, F.J., others, 2014. Live (Rose Bengal stained) foraminiferal faunas from the northern Arabian Sea: faunal succession within and below the OMZ. *Biogeosciences* 11, 1155–1175.

Cedhagen, T., 1994. Taxonomy and biology of *Hyrrokin sarcophaga* gen. et sp. n., a parasitic foraminiferan (Rosalinidae). *Sarsia* 79, 65–82.

Cedhagen, T., 1991. Retention of chloroplasts and bathymetric distribution in the Sublittoral Foraminiferan *Nonionellina labradorica*. *Ophelia* 33, 17–30. doi:10.1080/00785326.1991.10429739

Ceh, J., Kilburn, M.R., Cliff, J.B., Raina, J.-B., van Keulen, M., Bourne, D.G., 2013. Nutrient cycling in early coral life stages: *Pocillopora damicornis* larvae provide their algal symbiont (Symbiodinium) with nitrogen acquired from bacterial associates. *Ecol. Evol.* 3, 2393–2400. doi:10.1002/ece3.642

Cernichiari, E., Muscatine, L., Smith, D.C., 1969. Maltose excretion by the symbiotic algae of *Hydra viridis*. *Proc. R. Soc. Lond. B Biol. Sci.* 173, 557–576. doi:10.1098/rspb.1969.0077

Cesbron, F., Geslin, E., Jorissen, F.J., Delgard, M.L., Charrieau, L., Deflandre, B., Jézéquel, D., Anschutz, P., Metzger, E., 2016. Vertical distribution and respiration rates of benthic foraminifera: contribution to aerobic remineralization in intertidal mudflats covered by *Zostera noltei* meadows. *Estuar. Coast. Shelf Sci.* 179, 23–38.

Cesbron, F., Geslin, E., Le Kieffre, C., Jauffrais, T., Nardelli, M.P., Langlet, D., Mabilieu, G., Jorissen, F.J., Jézéquel, D., Metzger, E., 2017. Sequestered chloroplasts in the benthic foraminifer *Haynesina germanica*: cellular organization, oxygen fluxes and potential ecological implications. *J. Foraminif. Res.* 47, 268–278.

Cevasco, M.E., Lechlitter, S.M., Mosier, A.E., Perez, J., 2015. Initial observations of kleptoplasty in the foraminifera of coastal South Carolina. *Southeast. Nat.* 14, 361–372. doi:10.1656/058.014.0216

Clark, K.B., Jensen, K.R., Stirts, H.M., 1990. Survey for functional kleptoplasty among west Atlantic *Ascoglossa* (=Sacoglossa) (Mollusca: Opisthobranchia). *The Veliger* 33, 339–345.

- Clode, P.L., Stern, R.A., Marshall, A.T., 2007. Subcellular imaging of isotopically labeled carbon compounds in a biological sample by ion microprobe (NanoSIMS). *Microsc. Res. Tech.* 70, 220–229. doi:10.1002/jemt.20409
- Collen, J.D., 1998. *Metarotaliella tuvaluensis* sp. nov. from Funafuti Atoll, western Pacific Ocean: relationship to miliolid foraminifera. *J. Foraminif. Res.* 28, 66–75.
- Correia, M.J., Lee, J.J., 2002a. Fine structure of the plastids retained by the foraminifer *Elphidium excavatum* (Terquem). *Symbiosis* 32, 15–26.
- Correia, M.J., Lee, J.J., 2002b. How long do the plastids retained by *Elphidium excavatum* (Terquem) last in their host? *Symbiosis* 32, 27–37.
- Correia, M.J., Lee, J.J., 2000. Chloroplast retention by *Elphidium excavatum* (Terquem). Is it a selective process? *Symbiosis* 29, 343–355.

- D -

- Dahlgren, L., 1967. On the ultrastructure of the gamontic nucleus and the adjacent cytoplasm of the monothalamous foraminifer *Ovammia opaca*. *Dahlgren Zool Bidr. Upps.* 37, 77–112.
- Dahlgren, L., 1964. On nuclear cytology and reproduction in the monothalamous foraminifer *Ovammia opaca* Dahlgren. *Zool. Bidr. Fraan Upps.* 36, 315–334.
- Darling, K.F., Schweizer, M., Knudsen, K.L., Evans, K.M., Bird, C., Roberts, A., Filipsson, H.L., Kim, J.-H., Gudmundsson, G., Wade, C.M., Sayer, M.D.J., Austin, W.E.N., 2016. The genetic diversity, phylogeography and morphology of Elphidiidae (Foraminifera) in the Northeast Atlantic. *Mar. Micropaleontol.* 129, 1–23. doi:10.1016/j.marmicro.2016.09.001
- De Duve, C., Baudhuin, P., 1966. Peroxisomes (microbodies and related particles). *Physiol. Rev.* 46, 323–357.
- Debenay, J.-P., Bicchì, E., Goubert, E., Armynot du Châtelet, E., 2006. Spatio-temporal distribution of benthic foraminifera in relation to estuarine dynamics (Vie estuary, Vendée, W France). *Estuar. Coast. Shelf Sci.* 67, 181–197. doi:10.1016/j.ecss.2005.11.014
- Debenay, J.-P., Guillou, J.-J., Redois, F., Geslin, E., 2000. Distribution trends of foraminiferal assemblages in paralic environments, in: Martin, R.E. (Ed.), *Environmental Micropaleontology*. Springer US, pp. 39–67.
- DeLaca, T.E., 1982. Use of dissolved amino acids by the foraminifer *Notodendrodes antarctikos*. *Am. Zool.* 22, 683–690.
- DeLaca, T.E., Karl, D.M., Lipps, J.H., 1981. Direct use of dissolved organic carbon by agglutinated benthic foraminifera. *Nature* 289, 287–289. doi:10.1038/289287a0
- Diaz, R.J., Rosenberg, R., 2008. Spreading dead zones and consequences for marine ecosystems. *Science* 321, 926–929. doi:10.1126/science.1156401
- Dodge, J.D., 1974. A redescription of the dinoflagellate *Gymnodinium simplex* with the aid of electron microscopy. *J. Mar. Biol. Assoc. U. K.* 54, 171–177.
- Dodge, J.D., Crawford, R.M., 1971. A fine-structural survey of dinoflagellate pyrenoids and food-reserves. *Bot. J. Linn. Soc.* 64, 105–115.

References

- Dolan, J., 1992. Mixotrophy in ciliates : a review of chlorella symbiosis and chloroplast retention. *Mar. Microb. Food Webs* 6, 115–132.
- Doyle, R.W., Poore, R.V., 1974. Nutrient competition and division synchrony in phytoplankton. *J. Exp. Mar. Biol. Ecol.* 14, 201–210. doi:10.1016/0022-0981(74)90001-X
- Duguay, L.E., Taylor, D.L., 1978. Primary production and calcification by the soritid foraminifer *Archais angulatus* (Fichtel & Moll). *J. Eukaryot. Microbiol.* 25, 356–361.
- Dunstan, G., Volkman, J., Barrett, S., Leroi, J.-M., Jeffrey, S.W., 1993. Essential polyunsaturated fatty acids from 14 species of diatom (Bacillariophyceae). *Phytochemistry* 35, 155–161. doi:10.1016/S0031-9422(00)90525-9
- Dupuy, C., Rossignol, L., Geslin, E., Pascal, P.-Y., 2010. Predation of mudflat meio-macrofaunal metazoans by a calcareous foraminifer, *Ammonia tepida* (Cushman, 1926). *J. Foraminifer. Res.* 40, 305–312.

- E -

- Enge, A.J., Witte, U., Kucera, M., Heinz, P., 2014. Uptake of phytodetritus by benthic foraminifera under oxygen depletion at the Indian margin (Arabian Sea). *Biogeosciences* 11, 2017–2026. doi:10.5194/bg-11-2017-2014
- Esteban, G.F., Finlay, B.J., Clarke, K.J., 2009. Sequestered organelles sustain aerobic microbial life in anoxic environments. *Environ. Microbiol.* 11, 544–550. doi:10.1111/j.1462-2920.2008.01797.x

- F -

- Faber, W.W., Anderson, O.R., Caron, D.A., 1989. Algal-foraminiferal symbiosis in the planktonic foraminifer *Globigerinella aequilateralis*; II, Effects of two symbiont species on foraminiferal growth and longevity. *J. Foraminifer. Res.* 19, 185–193. doi:10.2113/gsjfr.19.3.185
- Faber, W.W., Anderson, O.R., Lindsey, J.L., Caron, D.A., 1988. Algal-foraminiferal symbiosis in the planktonic foraminifer *Globigerinella aequilateralis*; I, Occurrence and stability of two mutually exclusive chrysophyte endosymbionts and their ultrastructure. *J. Foraminifer. Res.* 18, 334–343. doi:10.2113/gsjfr.18.4.334
- Fan, J., Andre, C., Xu, C., 2011. A chloroplast pathway for the de novo biosynthesis of triacylglycerol in *Chlamydomonas reinhardtii*. *FEBS Lett.* 585, 1985–1991. doi:10.1016/j.febslet.2011.05.018
- Farquhar, M.G., Palade, G.E., 1998. The Golgi apparatus: 100 years of progress and controversy. *Trends Cell Biol.* 8, 2–10.
- Febvre-Chevalier, C., 1971. Constitution ultrastructurale de *Globigerina bulloides* d'Orbigny, 1826 (Rhizopoda-Foraminifera). *Protistologica* 7, 311–324.
- Filipsson, H.L., Nordberg, K., 2004. Climate variations, an overlooked factor influencing the recent marine environment. An example from Gullmar Fjord, Sweden, illustrated by benthic foraminifera and hydrographic data. *Estuaries* 27, 867–881.

References

- Finlay, B.J., 1985. Nitrate respiration by Protozoa (*Loxodes* spp.) in the hypolimnetic nitrite maximum of a productive freshwater pond. *Freshw. Biol.* 15, 333–346. doi:10.1111/j.1365-2427.1985.tb00205.x
- Finlay, B.J., Span, A.S.W., Harman, J.M.P., 1983. Nitrate respiration in primitive eukaryotes. *Nature* 303, 333–336. doi:10.1038/303333a0
- Finzi-Hart, J.A., Pett-Ridge, J., Weber, P.K., Popa, R., Fallon, S.J., Gunderson, T., Hutcheon, I.D., Nealson, K.H., Capone, D.G., 2009. Fixation and fate of C and N in the cyanobacterium *Trichodesmium* using nanometer-scale secondary ion mass spectrometry. *Proc. Natl. Acad. Sci.* 106, 6345–6350.
- Freiwald, A., Schönfeld, J., 1996. Substrate pitting and boring pattern of *Hyrrokkin sarcophaga* Cedhagen, 1994 (Foraminifera) in a modern deep-water coral reef mound. *Mar. Micropaleontol.* 28, 199–207. doi:10.1016/0377-8398(96)00002-3
- Frontalini, F., Curzi, D., Cesarini, E., Canonico, B., Giordano, F.M., Matteis, R.D., Bernhard, J.M., Pieretti, N., Gu, B., Eskelsen, J.R., Jubb, A.M., Zhao, L., Pierce, E.M., Gobbi, P., Papa, S., Coccioni, R., 2016. Mercury-pollution induction of intracellular lipid accumulation and lysosomal compartment amplification in the benthic foraminifer *Ammonia parkinsoniana*. *PLOS ONE* 11, e0162401. doi:10.1371/journal.pone.0162401
- Frontalini, F., Curzi, D., Giordano, F.M., Bernhard, J.M., Falcieri, E., Coccioni, R., 2015. Effects of lead pollution on *Ammonia parkinsoniana* (foraminifera): ultrastructural and microanalytical approaches. *Eur. J. Histochem.* 59, 2460. doi:10.4081/ejh.2015.2460
- Frontalini, F., Nardelli, P. Benthic foraminiferal ultrastructural degradation induced by heavy metals. *Mar. Micropaleontol.* Special issue "Foraminiferal ultrastructure". In press.
- Furbish, D.J., Arnold, A.J., 1997. Hydrodynamic strategies in the morphological evolution of spinose planktonic foraminifera. *Geol. Soc. Am. Bull.* 109, 1055–1072.

- G -

- Gastrich, M.D., 1987. Ultrastructure of a new intracellular symbiotic alga found within planktonic foraminifera. *J. Phycol.* 23, 623–632. doi:10.1111/j.1529-8817.1987.tb04215.x
- Geslin, E., Barras, C., Langlet, D., Nardelli, M.P., Kim, J.-H., Bonnin, J., Metzger, E., Jorissen, F.J., 2014. Survival, reproduction and calcification of three benthic foraminiferal species in response to experimentally induced hypoxia, in: Kitazato, H., M. Bernhard, J. (Eds.), *Approaches to Study Living Foraminifera*. Springer Japan, Tokyo, pp. 163–193.
- Geslin, E., Heinz, P., Jorissen, F., Hemleben, C., 2004. Migratory responses of deep-sea benthic foraminifera to variable oxygen conditions: laboratory investigations. *Mar. Micropaleontol.* 53, 227–243. doi:10.1016/j.marmicro.2004.05.010
- Geslin, E., Risgaard-Petersen, N., Lombard, F., Metzger, E., Langlet, D., Jorissen, F., 2011. Oxygen respiration rates of benthic foraminifera as measured with oxygen microsensors. *J. Exp. Mar. Biol. Ecol.* 396, 108–114. doi:10.1016/j.jembe.2010.10.011
- Gibson, G.D., Toews, D.P., Bleakney, J.S., 1986. Oxygen production and consumption in the Sacoglossan (=Ascoglossan) *Elysia chlorotica*. *The Veliger* 28, 397–400.

References

- Giordano, M., Norici, A., Ratti, S., Raven, J.A., 2008. Role of sulfur for algae: Acquisition, metabolism, ecology and evolution, in: Hell, R., Dahl, C., Knaff, D., Leustek, T. (Eds.), *Sulfur Metabolism in Phototrophic Organisms, Advances in Photosynthesis and Respiration*. Springer, Dordrecht, The Netherlands, pp. 397–415.
- Giordano, M., Raven, J.A., 2014. Nitrogen and sulfur assimilation in plants and algae. *Aquat. Bot., SPECIAL ISSUE: In Honour of George Bowes: Linking Terrestrial and Aquatic Botany* 118, 45–61. doi:10.1016/j.aquabot.2014.06.012
- Giraudeau, J., 1993. Planktonic foraminiferal assemblages in surface sediments from the southwest African continental margin. *Mar. Geol.* 110, 47–62.
- Glud, R.N., Thamdrup, B., Stahl, H., Wenzhoefer, F., Glud, A., Nomaki, H., Oguri, K., Revsbech, N.P., Kitazato, H., 2009. Nitrogen cycling in a deep ocean margin sediment (Sagami Bay, Japan). *Limnol Ocean.* 54, 723–734.
- Goldstein, S.T., 1999. Foraminifera: a biological overview, in: Sen Gupta, B.K. (Ed.), *Modern Foraminifera*. Springer-Verlag New-York, pp. 37–55.
- Goldstein, S.T., 1997. Gametogenesis and the antiquity of reproductive pattern in the Foraminiferida. *J. Foraminifer. Res.* 27, 319–328. doi:10.2113/gsjfr.27.4.319
- Goldstein, S.T., 1988. On the life cycle of *Saccamina alba* Hedley, 1962. *J. Foraminifer. Res.* 18, 311–325. doi:10.2113/gsjfr.18.4.311
- Goldstein, S.T., Barker, W.W., 1988. Test ultrastructure and taphonomy of the monothalamous agglutinated foraminifer *Cribothalammina*, n. gen., *alba* (Heron-Allen and Earland). *J. Foraminifer. Res.* 18, 130–136.
- Goldstein, S.T., Bernhard, J.M., Richardson, E.A., 2004. Chloroplast sequestration in the foraminifer *Haynesina germanica*: Application of high pressure freezing and freeze substitution. *Microsc. Microanal.* 10, 1458–1459. doi:10.1017/S1431927604885891
- Goldstein, S.T., Corliss, B.H., 1994. Deposit feeding in selected deep-sea and shallow-water benthic foraminifera. *Deep Sea Res. Part I* 41, 229–241. doi:10.1016/0967-0637(94)90001-9
- Goldstein, S.T., Moodley, L., 1993. Gametogenesis and the life cycle of the foraminifer *Ammonia beccarii* (Linne) forma *Tepida* (Cushman). *J. Foraminifer. Res.* 23, 213–220. doi:10.2113/gsjfr.23.4.213
- Goldstein, S.T., Richardson, E.A., 2002. Comparison of test and cell body ultrastructure in three modern allogromiid foraminifera: Application of high pressure freezing and freeze substitution. *J. Foraminifer. Res.* 32, 375–383. doi:10.2113/0320375
- Gooday, A.J., Bernhard, J.M., Levin, L.A., Suhr, S.B., 2000. Foraminifera in the Arabian Sea oxygen minimum zone and other oxygen-deficient settings: taxonomic composition, diversity, and relation to metazoan faunas. *Deep Sea Res. Part II Top. Stud. Oceanogr.* 47, 25–54.
- Gooday, A.J., Levin, L.A., Linke, P., Heeger, T., 1992. The role of benthic foraminifera in deep-sea food webs and carbon cycling, in: Rowe, G.T., Pariente, V. (Eds.), *Deep-Sea Food Chains and the Global Carbon Cycle*. Springer Netherlands, pp. 63–91.

References

- Gooday, A.J., Nomaki, H., Kitazato, H., 2008. Modern deep-sea benthic foraminifera: a brief review of their morphology-based biodiversity and trophic diversity. *Geol. Soc. Lond. Spec. Publ.* 303, 97–119. doi:10.1144/SP303.8
- Gooday, A.J., Turley, C.M., Allen, J.A., 1990. Responses by benthic organisms to inputs of organic material to the ocean floor: A review [and discussion]. *Philos. Trans. R. Soc. Lond. Math. Phys. Eng. Sci.* 331, 119–138. doi:10.1098/rsta.1990.0060
- Goss, R., Wilhelm, C., 2009. Lipids in algae, lichens and mosses, in: Wada, H., Murata, N. (Eds.), *Lipids in Photosynthesis, Advances in Photosynthesis and Respiration*. Springer Netherlands, pp. 117–137. doi:10.1007/978-90-481-2863-1_6
- Gouy, M., Guindon, S., Gascuel, O., 2009. SeaView version 4: a multiplatform graphical user interface for sequence alignment and phylogenetic tree building. *Mol. Biol. Evol.* 27, 221–224.
- Graeve, M., Kattner, G., Hagen, W., 1994. Diet-induced changes in the fatty acid composition of Arctic herbivorous copepods: Experimental evidence of trophic markers. *J. Exp. Mar. Biol. Ecol.* 182, 97–110. doi:10.1016/0022-0981(94)90213-5
- Green, B.J., Li, W.-Y., Manhart, J.R., Fox, T.C., Summer, E.J., Kennedy, R.A., Pierce, S.K., Rumpho, M.E., 2000. Mollusc-algal chloroplast endosymbiosis. photosynthesis, thylakoid protein maintenance, and chloroplast gene expression continue for many months in the absence of the algal nucleus. *Plant Physiol.* 124, 331–342. doi:10.1104/pp.124.1.331
- Grossman, A., Takahashi, H., 2001. Macronutrient utilization by photosynthetic eukaryotes and the fabric of interactions. *Annu. Rev. Plant Physiol. Plant Mol. Biol.* 52, 163–210. doi:10.1146/annurev.arplant.52.1.163
- Grzymski, J., Schofield, O.M., Falkowski, P.G., Bernhard, J.M., 2002. The function of plastids in the deep-sea benthic foraminifer, *Nonionella stella*. *Limnol. Oceanogr.* 47, 1569–1580.

- H -

- Hallock, P., Talge, H.K., 1994. A predatory foraminifer, *Floresina amphiphaga*, n. sp., from the Florida Keys. *J. Foraminifer. Res.* 24, 210–213.
- Hansen, H.J., 1975. On feeding and supposed buoyancy mechanism in four recent globigerinid foraminifera from the Gulf of Elat, Israel. *Rev. Espanola Micropaleontol.* 7, 325–337.
- Hayward, B.W., Holzmann, M., Grenfell, H.R., Pawlowski, J., Triggs, C.M., 2004. Morphological distinction of molecular types in *Ammonia* – towards a taxonomic revision of the world's most commonly misidentified foraminifera. *Mar. Micropaleontol.* 50, 237–271. doi:10.1016/S0377-8398(03)00074-4
- Heeger, T., 1988. Virus-like particles and cytopathological effects in *Elphidium excavatum clavatum*, a benthic foraminiferan. *Dis. Aquat. Organ.* 4, 233–236.
- Heinz, P., Geslin, E., 2012. Ecological and biological response of benthic foraminifera under oxygen-depleted conditions: evidence from laboratory approaches, in: Altenbach, A.V., Bernhard, J.M., Seckbach, J. (Eds.), *Anoxia*. Springer, pp. 287–303.

References

- Heinz, P., Hemleben, C., Kitazato, H., 2002. Time-response of cultured deep-sea benthic foraminifera to different algal diets. *Deep Sea Res. Part Oceanogr. Res. Pap.* 49, 517–537.
- Helly, J.J., Levin, L.A., 2004. Global distribution of naturally occurring marine hypoxia on continental margins. *Deep Sea Res. Part Oceanogr. Res. Pap.* 51, 1159–1168.
- Hemleben, C., Spindler, M., 1983. Recent advances in research on living planktonic foraminifera. *Utrecht Micropaleontol Bull* 30, 141–170.
- Hemleben, C., Spindler, M., Anderson, O.R., 1989. *Modern Planktonic Foraminifera*. Springer Verlag New-York.
- Hemleben, C., Spindler, M., Breiting, I., Deuser, W.G., 1985. Field and laboratory studies on the ontogeny and ecology of some globorotaliid species from the Sargasso Sea off Bermuda. *J. Foraminifer. Res.* 15, 254–272. doi:10.2113/gsjfr.15.4.254
- Herrmann, A.M., Ritz, K., Nunan, N., Clode, P.L., Pett-Ridge, J., Kilburn, M.R., Murphy, D.V., O'Donnell, A.G., Stockdale, E.A., 2007. Nano-scale secondary ion mass spectrometry — A new analytical tool in biogeochemistry and soil ecology: A review article. *Soil Biol. Biochem.* 39, 1835–1850. doi:10.1016/j.soilbio.2007.03.011
- Hofmann, D.K., Kremer, B.P., 1981. Carbon metabolism and strobilation in *Cassiopea andromedea* (Cnidaria: Scyphozoa): Significance of endosymbiotic dinoflagellates. *Mar. Biol.* 65, 25–33. doi:10.1007/BF00397064
- Høgslund, S., Revsbech, N.P., Cedhagen, T., Nielsen, L.P., Gallardo, V.A., 2008. Denitrification, nitrate turnover, and aerobic respiration by benthic foraminiferans in the oxygen minimum zone off Chile. *J. Exp. Mar. Biol. Ecol.* 359, 85–91. doi:10.1016/j.jembe.2008.02.015
- Hoppe, P., Cohen, S., Meibom, A., 2013. NanoSIMS: Technical aspects and applications in cosmochemistry and biological geochemistry. *Geostand. Geoanalytical Res.* 37, 111–154. doi:10.1111/j.1751-908X.2013.00239.x
- Hottinger, L., 1982. Larger foraminifera, giant cells with a historical background. *Naturwissenschaften* 69, 361–371. doi:10.1007/BF00396687
- Hottinger, L., Dreher, D., 1974. Differentiation of protoplasm in Nummulitidae (foraminifera) from Elat, Red Sea. *Mar. Biol.* 25, 41–61.

- J -

- Jauffrais, T., Jesus, B., Méléder, V., Geslin, E., 2017. Functional xanthophyll cycle and pigment content of a kleptoplastic benthic foraminifer: *Haynesina germanica*. *PLOS ONE* 12, e0172678. doi:10.1371/journal.pone.0172678
- Jauffrais, T., Jesus, B., Metzger, E., Mouget, J.-L., Jorissen, F., Geslin, E., 2016. Effect of light on photosynthetic efficiency of sequestered chloroplasts in intertidal benthic foraminifera (*Haynesina germanica* and *Ammonia tepida*). *Biogeosciences* 13, 2715–2726. doi:10.5194/bg-13-2715-2016

References

- Jiang, H., Kilburn, M.R., Decelle, J., Musat, N., 2016. NanoSIMS chemical imaging combined with correlative microscopy for biological sample analysis. *Curr. Opin. Biotechnol.* 41, 130–135. doi:10.1016/j.copbio.2016.06.006
- Johnston, M., Yellowlees, D., Gilmour, I., 1995. Carbon isotopic analysis of the free fatty acids in a tridacnid-algal symbiosis: Interpretation and implications for the symbiotic association. *Proc. R. Soc. Lond. B Biol. Sci.* 260, 293–297. doi:10.1098/rspb.1995.0094
- Jørgensen, B.B., Erez, J., Revsbech, P., Cohen, Y., 1985. Symbiotic photosynthesis in a planktonic foraminiferan, *Globigerinoides sacculifer* (Brady), studied with microelectrodes1: Symbiotic photosynthesis. *Limnol. Oceanogr.* 30, 1253–1267. doi:10.4319/lo.1985.30.6.1253
- Jørgensen, B.B., Gallardo, V.A., 1999. *Thioploca* spp.: filamentous sulfur bacteria with nitrate vacuoles. *FEMS Microbiol. Ecol.* 28, 301–313. doi:https://doi.org/10.1111/j.1574-6941.1999.tb00585.x
- Jorissen, F.J., 1999. Benthic foraminiferal microhabitats below the sediment-water interface, in: Sen Gupta, B.K. (Ed.), *Modern Foraminifera*. Springer, pp. 161–179.
- Josefson, A.B., Widbom, B., 1988. Differential response of benthic macrofauna and meiofauna to hypoxia in the Gullmar Fjord basin. *Mar. Biol.* 100, 31–40. doi:10.1007/BF00392952
- K -
- Kamp, A., Høgslund, S., Risgaard-Petersen, N., Stief, P., 2015. Nitrate storage and dissimilatory nitrate reduction by eukaryotic microbes. *Front. Microbiol.* 6, 1492. doi:10.3389/fmicb.2015.01492
- Kellogg, R.B., Patton, J.S., 1983. Lipid droplets, medium of energy exchange in the symbiotic anemone *Condylactis gigantea*: a model coral polyp. *Mar. Biol.* 75, 137–149. doi:10.1007/BF00405996
- Kilburn, M.R., Jones, D.L., Clode, P.L., Cliff, J.B., Stockdale, E.A., Herrmann, A.M., Murphy, D.V., 2010. Application of nanoscale secondary ion mass spectrometry to plant cell research. *Plant Signal. Behav.* 5, 760–762. doi:10.4161/psb.5.6.11775
- Kim, M., Kim, S., Yih, W., Park, M.G., 2012. The marine dinoflagellate genus *Dinophysis* can retain plastids of multiple algal origins at the same time. *Harmful Algae* 13, 105–111. doi:10.1016/j.hal.2011.10.010
- Kitazato, H., Ohga, T., 1995. Seasonal changes in deep-sea benthic foraminiferal populations: results of long-term observations at Sagami Bay, Japan. *Biogeochem. Process. Ocean Flux West. Pac.* 331–342.
- Knight, R., Mantoura, R.F.C., 1985. Chlorophyll and carotenoid pigments in Foraminifera and their symbiotic algae: analysis by high performance liquid chromatography. *Mar. Ecol. Prog. Ser.* 23.
- Köhler-Rink, S., Kühl, M., 2005. The chemical microenvironment of the symbiotic planktonic foraminifer *Orbulina universa*. *Mar. Biol. Res.* 1, 68–78. doi:10.1080/17451000510019015
- Koho, K., LeKieffre, C., Nomaki, H., Salonen, I., Geslin, E., Mabilieu, G., Sjøgaard Jensen, L. H., Reichart, G.-J. Ultrastructural features of foraminifera *Ammonia* spp. (tepidal morphocomplex) in anoxic conditions: field and laboratory observations. *Mar. Micropaleontol. Special issue "Foraminiferal ultrastructure"*. In press.

References

- Koho, K.A., Piña-Ochoa, E., 2012. Benthic foraminifera: inhabitants of low-oxygen environments, in: Altenbach, A.V., Bernhard, J.M., Seckbach, J. (Eds.), *Anoxia: Evidence for Eukaryote Survival and Paleontological Strategies*. Springer Netherlands, 21, pp. 249–286.
- Koho, K.A., Piña-Ochoa, E., Geslin, E., Risgaard-Petersen, N., 2011. Vertical migration, nitrate uptake and denitrification: survival mechanisms of foraminifers (*Globobulimina turgida*) under low oxygen conditions: Survival mechanisms of foraminifers. *FEMS Microbiol. Ecol.* 75, 273–283. doi:10.1111/j.1574-6941.2010.01010.x
- Koo, A.J.K., Ohlrogge, J.B., Pollard, M., 2004. On the export of fatty acids from the chloroplast. *J. Biol. Chem.* 279, 16101–16110. doi:10.1074/jbc.M311305200
- Kopp, C., Domart-Coulon, I., Escrig, S., Humbel, B.M., Hignette, M., Meibom, A., 2015a. Subcellular investigation of photosynthesis-driven carbon assimilation in the symbiotic reef coral *Pocillopora damicornis*. *mBio* 6, e02299-14. doi:10.1128/mBio.02299-14
- Kopp, C., Pernice, M., Domart-Coulon, I., Djediat, C., Spangenberg, J.E., Alexander, D.T.L., Hignette, M., Meziane, T., Meibom, A., 2013. Highly dynamic cellular-level response of symbiotic coral to a sudden increase in snvironmental nitrogen. *mBio* 4, e00052-13. doi:10.1128/mBio.00052-13
- Kopp, C., Wisztorski, M., Revel, J., Mehiri, M., Dani, V., Capron, L., Carette, D., Fournier, I., Massi, L., Mouajjah, D., Pagnotta, S., Priouzeau, F., Salzert, M., Meibom, A., Sabourault, C., 2015b. MALDI-MS and NanoSIMS imaging techniques to study cnidarian–dinoflagellate symbioses. *Zoology* 118, 125–131. doi:10.1016/j.zool.2014.06.006
- Krueger, T., Horwitz, N., Bodin, J., Giovani, M.-E., Escrig, S., Meibom, A., Fine, M., 2017. Common reef-building coral in the Northern Red Sea resistant to elevated temperature and acidification. *Open Sci.* 4, 170038. doi:10.1098/rsos.170038
- Krupke, A., Mohr, W., LaRoche, J., Fuchs, B.M., Amann, R.I., Kuypers, M.M., 2015. The effect of nutrients on carbon and nitrogen fixation by the UCYN-A–haptophyte symbiosis. *ISME J.* 9, 1635–1647. doi:10.1038/ismej.2014.253
- Kucera, M., 2007. Planktonic foraminifera as tracers of past oceanic environments, in: Hillaire-Marcel, C., de Vernal, A. (Eds.), *Developments in Marine Geology 1, Proxies in Late Cenozoic Paleoceanography*. the Netherlands, pp. 213–262.
- Kuhl, M., Lassen, C., Jørgensen, B.B., 1994. Light penetration and light-intensity in sandy marine-sediments measured with irradiance and scalar irradiance Fiberoptic microprobes Rid A-1977-2009. *Mar. Ecol. - Prog. Ser.* 105, 139–148.

- L -

- Langer, M.R., 1992. Biosynthesis of glycosaminoglycans in foraminifera: A review. *Mar. Micropaleontol.* 19, 245–255. doi:10.1016/0377-8398(92)90031-E
- Langezaal, A.M., Jannink, N.T., Pierson, E.S., van der Zwaan, G.J., 2005. Foraminiferal selectivity towards bacteria: an experimental approach using a cell-permeant stain. *J. Sea Res.* 54, 256–275. doi:10.1016/j.seares.2005.06.004

References

- Langlet, D., Baal, C., Geslin, E., Metzger, E., Zuschin, M., Riedel, B., Risgaard-Petersen, N., Stachowitsch, M., Jorissen, F.J., 2014. Foraminiferal species responses to *in situ*, experimentally induced anoxia in the Adriatic Sea. *Biogeosciences* 11, 1775–1797. doi:10.5194/bg-11-1775-2014
- Langlet, D., Geslin, E., Baal, C., Metzger, E., Lejzerowicz, F., Riedel, B., Zuschin, M., Pawlowski, J., Stachowitsch, M., Jorissen, F.J., 2013. Foraminiferal survival after long-term *in situ* experimentally induced anoxia. *Biogeosciences* 10, 7463–7480. doi:10.5194/bg-10-7463-2013
- Larkin, K.E., Gooday, A.J., Woulds, C., Jeffreys, R.M., Schwartz, M., Cowie, G., Whitcraft, C., Levin, L., Dick, J.R., Pond, D.W., 2014. Uptake of algal carbon and the likely synthesis of an “essential” fatty acid by *Uvigerina* ex. gr. *semiornata* (Foraminifera) within the Pakistan margin oxygen minimum zone: evidence from fatty acid biomarker and ¹³C tracer experiments. *Biogeosciences* 11, 3729–3738. doi:10.5194/bg-11-3729-2014
- Le Cadre, V., Debenay, J.-P., 2006. Morphological and cytological responses of *Ammonia* (foraminifera) to copper contamination: Implication for the use of foraminifera as bioindicators of pollution. *Environ. Pollut.* 143, 304–317. doi:10.1016/j.envpol.2005.11.033
- Le Calvez, J., 1947. *Entosolenia marginata*, foraminifere apogamique extoparasite d'un autre foraminifere *Discorbis vilardeboanus*. *Académie Sci. Paris Comptes Rendus* 224, 1448–1450.
- Lea, D.W., 1999. Trace elements in foraminiferal calcite, in: Sen Gupta, B.K. (Ed.), *Modern Foraminifera*. Springer-Verlag New-York, pp. 259–277.
- Leadbeater, B., Dodge, J.D., 1966. The fine structure of *Woloszynskia micra* Sp.Nov., a new marine dinoflagellate. *Br. Phycol. Bull.* 3, 1–17. doi:10.1080/00071616600650011
- Lechene, C., Hillion, F., McMahon, G., Benson, D., Kleinfeld, A.M., Kampf, J.P., Distel, D., Luyten, Y., Bonventre, J., Hentschel, D., Park, K.M., Ito, S., Schwartz, M., Benichou, G., Slodzian, G., 2006. High-resolution quantitative imaging of mammalian and bacterial cells using stable isotope mass spectrometry. *J. Biol.* 5, 20. doi:10.1186/jbiol42
- Lechliter, S., 2014. Preliminary study of kleptoplasty in foraminifera of South Carolina. *Bridges* 8, 44.
- Lee, J.J., 1983. Perspective on algal endosymbionts in larger foraminifera. *Int. Rev. Cytol.* 14, 49–77.
- Lee, J.J., Bock, W.D., 1976. The importance of feeding in two species of Soritid foraminifera with algal symbionts. *Bull. Mar. Sci.* 26, 530–537.
- Lee, J.J., Erez, J., Ter Kuile, B., Lagziel, A., Burgos, S., 1988. Feeding rates of two species of larger Foraminifera *Amphistegina lobifera* and *Amphisorus hemprichii*, from the Gulf of Eilat (red Sea). *Symbiosis* 5, 61–102.
- Lee, J.J., Freudenthal, H.D., Kossoy, V., Bé, A., 1965. Cytological observations on two planktonic foraminifera, *Globigerina bulloides* d'Orbigny, 1826, and *Globigerinoides ruber* (d'Orbigny, 1839) Cushman, 1927. *J. Protozool.* 12, 531–542. doi:10.1111/j.1550-7408.1965.tb03253.x
- Lee, J.J., Lanners, E., 1988. The retention of chloroplasts by the foraminifer *Elphidium crispum*. *Symbiosis* 5, 45–59.
- Lee, J.J., McEnery, M., Pierce, S., Freudenthal, H.D., Muller, W.A., 1966. Tracer experiments in feeding littoral foraminifera. *J. Protozool.* 13, 659–670.

- Lee, J.J., McEnery, M.E., Kahn, E.G., Schuster, F.L., 1979. Symbiosis and the Evolution of Larger Foraminifera. *Micropaleontology* 25, 118–140. doi:10.2307/1485262
- Lee, J.J., McEnery, M.E., Koestler, R.L., Lee, M.J., Reidy, J., Shilo, M., 1983. Experimental studies of symbiont persistence in *Amphistegina lessonii*, a diatom-bearing species of larger foraminifera from the Red Sea, in: Schenk, H.E.A., Schwemmler, E. (Eds.), *Endocytobiology II*. Berlin, pp. 487–514.
- Lee, J.J., Muller, W.A., 1973. Trophic dynamics and niches of salt marsh foraminifera. *Am. Zool.* 13, 215–223.
- Lee, J.J., Zucker, W., 1969. Algal flagellate symbiosis in the foraminifer *Archaias*. *J. Protozool.* 16, 71–81. doi:10.1111/j.1550-7408.1969.tb02235.x
- LeKieffre, C., Spangenberg, J.E., Mabilieu, G., Escrig, S., Meibom, A., Geslin, E., 2017. Surviving anoxia in marine sediments: The metabolic response of ubiquitous benthic foraminifera (*Ammonia tepida*). *PLoS ONE* 12, e0177604. doi:10.1371/journal.pone.0177604
- Leutenegger, S., 1984. Symbiosis in benthic foraminifera; specificity and host adaptations. *J. Foraminifer. Res.* 14, 16–35.
- Leutenegger, S., 1983. Specific host-symbiont relationship in larger foraminifera. *Micropaleontology* 29, 111–125. doi:10.2307/1485562
- Leutenegger, S., 1977a. Ultrastructure and motility of dinophyceans symbiotic with larger, imperforated foraminifera. *Mar. Biol.* 44, 157–164. doi:10.1007/BF00386955
- Leutenegger, S., 1977b. Reproduction cycles of larger foraminifera and depth distribution of generations. *Utrecht Micropaleontol. Bull.* 15, 27–34.
- Leutenegger, S., 1977c. Ultrastructure de foraminifères perforés et imperforés ainsi que de leurs symbiontes. *Cah. Micropaléontologie* 3, 1–52.
- Leutenegger, S., 1977d. Symbiosis between larger foraminifera and unicellular algae in the Gulf of Elat. *Utrecht Micropaleontol Bull* 1, 241–244.
- Leutenegger, S., Hansen, H.J., 1979. Ultrastructural and radiotracer studies of pore function in foraminifera. *Mar. Biol.* 54, 11–16.
- Levin, L.A., Ekau, W., Gooday, A.J., Jorissen, F., Middelburg, J.J., Naqvi, S.W.A., Neira, C., Rabalais, N.N., Zhang, J., others, 2009. Effects of natural and human-induced hypoxia on coastal benthos. *Biogeosciences* 6, 2063–2098.
- Levinton, J.S., 1979. Deposit-feeders, their resources, and the study of resource limitation, in: Livingston, R.J. (Ed.), *Ecological Processes in Coastal and Marine Systems*, Marine Science. Springer US, pp. 117–141. doi:10.1007/978-1-4615-9146-7_7
- Li, J., Saidha, T., Schiff, J.A., 1991. Purification and properties of two forms of ATP sulfurylase from *Euglena*. *Biochim. Biophys. Acta BBA - Protein Struct. Mol. Enzymol.* 1078, 68–76. doi:10.1016/0167-4838(91)90094-G
- Linshy, V.N., Nigam, R., Heinz, P., 2014. Response of shallow water benthic foraminifera to a ¹³C-labeled food pulse in the laboratory, in: Kitazato, H., Bernhard, J.M. (Eds.), *Approaches to Study Living Foraminifera*. Springer Japan, Tokyo, pp. 115–131.

References

- Lipps, J.H., 1983. Biotic interactions in benthic foraminifera, in: Tevesz, M.J.S., McCall, P.L. (Eds.), *Biotic Interactions in Recent and Fossil Benthic Communities*. Springer, pp. 331–376.
- Lombard, F., Erez, J., Michel, E., Labeyrie, L., 2009. Temperature effect on respiration and photosynthesis of the symbiont-bearing planktonic foraminifera *Globigerinoides ruber*, *Orbulina universa*, and *Globigerinella siphonifera*. *Limnol. Oceanogr.* 54, 210.
- Lopez, E., 1979. Algal chloroplasts in the protoplasm of three species of benthic foraminifera: taxonomic affinity, viability and persistence. *Mar. Biol.* 53, 201–211. doi:10.1007/BF00952427
- M -
- Maire, O., Barras, C., Gestin, T., Nardelli, M.-P., Romero-Ramirez, A., Duchêne, J.-C., Geslin, E., 2016. How does macrofaunal bioturbation influence the vertical distribution of living benthic foraminifera? *Mar. Ecol. Prog. Ser.* 561, 83–97.
- Mallon, J., Glock, N., Schönfeld, J., 2012. The response of benthic foraminifera to low-oxygen conditions of the Peruvian oxygen minimum zone, in: Altenbach, A.V., Bernhard, J.M., Seckbach, J. (Eds.), *Anoxia: Evidence for Eukaryote Survival and Paleontological Strategies*. Springer Netherlands, pp. 305–322.
- Martin, J.B., Bernhard, J.M., Curtis, J., Rathburn, A.E., 2010. Combined carbonate carbon isotopic and cellular ultrastructural studies of individual benthic foraminifera: Method description. *Paleoceanography* 25, PA2211. doi:10.1029/2009PA001846
- McEnergy, M.E., Lee, J.J., 1981. Cytological and fine structural studies of three species of symbiont-bearing larger foraminifera from the Red Sea. *Micropaleontology* 27, 71–83. doi:10.2307/1485378
- McEnergy, M.E., Lee, J.J., 1976. *Allogromia laticollaris*: a foraminiferan with an unusual apogamic metagenic life cycle. *J. Protozool.* 23, 94–108.
- McMahon, G., Glassner, B.J., Lechene, C.P., 2006. Quantitative imaging of cells with multi-isotope imaging mass spectrometry (MIMS)—Nanoautography with stable isotope tracers. *Appl. Surf. Sci., Proceedings of the Fifteenth International Conference on Secondary Ion Mass Spectrometry, SIMS XV* Proceedings of the Fifteenth International Conference on Secondary Ion Mass Spectrometry, 252, 6895–6906. doi:10.1016/j.apsusc.2006.02.170
- Mendoza-Cózatl, D., Loza-Tavera, H., Hernández-Navarro, A., Moreno-Sánchez, R., 2005. Sulfur assimilation and glutathione metabolism under cadmium stress in yeast, protists and plants. *FEMS Microbiol. Rev.* 29, 653–671. doi:10.1016/j.femsre.2004.09.004
- Merchant, S.S., Kropat, J., Liu, B., Shaw, J., Warakanont, J., 2012. TAG, You're it! *Chlamydomonas* as a reference organism for understanding algal triacylglycerol accumulation. *Curr. Opin. Biotechnol., Energy biotechnology • Environmental biotechnology* 23, 352–363. doi:10.1016/j.copbio.2011.12.001
- Middelburg, J.J., Levin, L.A., 2009. Coastal hypoxia and sediment biogeochemistry. *Biogeosciences* 6, 1273–1293.
- Mojtahid, M., Geslin, E., Coynel, A., Gorse, L., Vella, C., Davranche, A., Zozzolo, L., Blanchet, L., Bénéteau, E., Maillet, G., 2016. Spatial distribution of living (Rose Bengal stained) benthic

- foraminifera in the Loire estuary (western France). *J. Sea Res., Recent and past sedimentary, biogeochemical and benthic ecosystem evolution of the Loire Estuary (Western France)* 118, 1–16. doi:10.1016/j.seares.2016.02.003
- Mojtahid, M., Zubkov, M.V., Hartmann, M., Gooday, A.J., 2011. Grazing of intertidal benthic foraminifera on bacteria: Assessment using pulse-chase radiotracing. *J. Exp. Mar. Biol. Ecol.* 399, 25–34. doi:10.1016/j.jembe.2011.01.011
- Montagna, P.A., 1995. Rates of metazoan meiofaunal microbivory: a review. *Vie Milieu* 45, 1–10.
- Moodley, L., Boschker, H.T., Middelburg, J.J., Pel, R., Herman, P.M., De Deckere, E., Heip, C.H., 2000. Ecological significance of benthic foraminifera: ^{13}C labelling experiments. *Mar. Ecol.-Prog. Ser.* 202, 289–295.
- Moodley, L., Middelburg, J.J., Boschker, H.T., Duineveld, G., Pel, R., Herman, P.M., Heip, C.H., 2002. Bacteria and Foraminifera: key players in a short-term deep-sea benthic response to phytodetritus. *Mar. Ecol. Prog. Ser.* 236.
- Moodley, L., Steyaert, M., Epping, E., Middelburg, J.J., Vincx, M., van Avesaath, P., Moens, T., Soetaert, K., 2008. Biomass-specific respiration rates of benthic meiofauna: Demonstrating a novel oxygen micro-respiration system. *J. Exp. Mar. Biol. Ecol.* 357, 41–47. doi:10.1016/j.jembe.2007.12.025
- Moodley, L., Van der Zwaan, G.J., Herman, P.M.J., Kempers, L., Van Breugel, P., 1997. Differential response of benthic meiofauna to anoxia with special reference to Foraminifera (Protista: Sarcodina). *Mar. Ecol. Prog. Ser.* 158.
- Moore, K.L., Lombi, E., Zhao, F.-J., Grovenor, C.R.M., 2012. Elemental imaging at the nanoscale: NanoSIMS and complementary techniques for element localisation in plants. *Anal. Bioanal. Chem.* 402, 3263–3273. doi:10.1007/s00216-011-5484-3
- Morvan, J., Debenay, J.-P., Jorissen, F., Redois, F., Bénéteau, E., Delplancke, M., Amato, A.-S., 2006. Patchiness and life cycle of intertidal foraminifera: Implication for environmental and paleoenvironmental interpretation. *Mar. Micropaleontol., Foraminifera and Environmental Micropaleontology* 61, 131–154. doi:10.1016/j.marmicro.2006.05.009
- Morvan, J., Le Cadre, V., Jorissen, F., Debenay, J.-P., 2004. Foraminifera as potential bio-indicators of the “Erika” oil spill in the Bay of Bourgneuf: field and experimental studies. *Aquat. Living Resour.* 17, 317–322.
- Muller, W.A., 1975. Competition for food and other niche-related studies of three species of salt-marsh foraminifera. *Mar. Biol.* 31, 339–351. doi:10.1007/BF00392091
- Müller-Merz, E., Lee, J.J., 1976. Symbiosis in the Larger Foraminiferan *Sorites marginalis* (with Notes on *Archaias* spp.). *J. Protozool.* 23, 390–396. doi:10.1111/j.1550-7408.1976.tb03793.x
- Murray, J.W., 2006. Ecology and applications of benthic foraminifera, Cambridge. ed.
- Musat, N., Halm, H., Winterholler, B., Hoppe, P., Peduzzi, S., Hillion, F., Horreard, F., Amann, R., Jørgensen, B.B., Kuypers, M.M., 2008. A single-cell view on the ecophysiology of anaerobic phototrophic bacteria. *Proc. Natl. Acad. Sci.* 105, 17861–17866.
- Musat, N., Stryhanyuk, H., Bombach, P., Adrian, L., Audinot, J.-N., Richnow, H.H., 2014. The effect of FISH and CARD-FISH on the isotopic composition of ^{13}C - and ^{15}N -labeled *Pseudomonas putida*

References

- cells measured by nanoSIMS. *Syst. Appl. Microbiol.* 37, 267–276. doi:10.1016/j.syapm.2014.02.002
- Muscatine, L., Karakashian, S.J., Karakashian, M.W., 1967. Soluble extracellular products of algae symbiotic with a ciliate, a sponge and a mutant hydra. *Comp. Biochem. Physiol.* 20, 1–12. doi:10.1016/0010-406X(67)90720-7
- N -
- Nagai, S., Nitshitani, G., Tomaru, Y., Sakiyama, S., Kamiyama, T., 2008. Predation by the toxic dinoflagellate *Dinophys fortii* on the ciliate *Myrionecta rubra* and observation of sequestration of ciliate chloroplasts. *J. Phycol.* 44, 909–922. doi:10.1111/j.1529-8817.2008.00544.x
- Nardelli, M.P., Barras, C., Metzger, E., Mouret, A., Filipsson, H.L., Jorissen, F., Geslin, E., 2014. Experimental evidence for foraminiferal calcification under anoxia. *Biogeosciences* 11, 4029–4038. doi:10.5194/bg-11-4029-2014
- Nass, M.M., Nass, S., 1963. Intramitochondrial fibers with DNA characteristics I. Fixation and electron staining reactions. *J. Cell Biol.* 19, 593–611.
- Nishitani, G., Nagai, S., Hayakawa, S., Kosaka, Y., Sakurada, K., Kamiyama, T., Gojobori, T., 2012. Multiple plastids collected by the dinoflagellate *Dinophysis mitra* through kleptoplastidy. *Appl. Environ. Microbiol.* 78, 813–821. doi:10.1128/AEM.06544-11
- Nomaki, H., Bernhard, J.M., Ishida, A., Tsuchiya, M., Uematsu, K., Tame, A., Kitahashi, T., Takahata, N., Sano, Y., Toyofuku, T., 2016. Intracellular isotope localization in *Ammonia* sp. (Foraminifera) of oxygen-depleted environments: Results of nitrate and sulfate labeling experiments. *Front. Microbiol.* 163. doi:10.3389/fmicb.2016.00163
- Nomaki, H., Chikaraishi, Y., Tsuchiya, M., Toyofuku, T., Ohkouchi, N., Uematsu, K., Tame, A., Kitazato, H., 2014. Nitrate uptake by foraminifera and use in conjunction with endobionts under anoxic conditions. *Limnol. Oceanogr.* 59, 1879–1888. doi:10.4319/lo.2014.59.6.1879
- Nomaki, H., Heinz, P., Hemleben, C., Kitazato, H., 2005a. Behavior and response of deep-sea benthic foraminifera to freshly supplied organic matter: A laboratory feeding experiment in microcosm environments. *J. Foraminif. Res.* 35, 103–113. doi:10.2113/35.2.103
- Nomaki, H., Heinz, P., Nakatsuka, T., Shimanaga, M., Kitazato, H., 2005b. Species-specific ingestion of organic carbon by deep-sea benthic foraminifera and meiobenthos: *in situ* tracer experiments. *Limnol. Oceanogr.* 50, 134–146.
- Nomaki, H., Heinz, P., Nakatsuka, T., Shimanaga, M., Ohkouchi, N., Ogawa, N.O., Kogure, K., Ikemoto, E., Kitazato, H., 2006. Different ingestion patterns of ¹³C-labeled bacteria and algae by deep-sea benthic foraminifera. *Mar. Ecol. Prog. Ser.* 310, 95–108.
- Nomaki, H., LeKieffre, C., Escrig, S., Meibom, A., Yagyuo, S., Richardson, E.A., Matsuzaki, T., Murayama, M., Geslin, E., Bernhard, J.M., submitted. Innovative TEM-coupled approaches to study foraminiferal cells. *Mar. Mic. Special issue: Foraminiferal Ultrastructure*.
- Nomaki, H., Ogawa, N., Ohkouchi, N., Suga, H., Toyofuku, T., Shimanaga, M., Nakatsuka, T., Kitazato, H., 2008. Benthic foraminifera as trophic links between phytodetritus and benthic metazoans:

References

- carbon and nitrogen isotopic evidence. *Mar. Ecol. Prog. Ser.* 357, 153–164. doi:10.3354/meps07309
- Nomaki, H., Ohkouchi, N., Heinz, P., Suga, H., Chikaraishi, Y., Ogawa, N.O., Matsumoto, K., Kitazato, H., 2009. Degradation of algal lipids by deep-sea benthic foraminifera: An *in situ* tracer experiment. *Deep Sea Res. Part Oceanogr. Res. Pap.* 56, 1488–1503. doi:10.1016/j.dsr.2009.04.013
- Nordberg, K., Gustafsson, M., Krantz, A.-L., 2000. Decreasing oxygen concentrations in the Gullmar Fjord, Sweden, as confirmed by benthic foraminifera, and the possible association with NAO. *J. Mar. Syst.* 23, 303–316. doi:10.1016/S0924-7963(99)00067-6
- Nyholm, K.-G., 1957. Orientation and binding power of recent monothalamous foraminifera in soft sediments. *Micropaleontology* 3, 75–76. doi:10.2307/1484335
- Nyholm, K.G., Nyholm, P.G., 1975. Ultrastructure of monothalamous foraminifera. *Zoon* 3, 141–150.
- O -
- Ohlrogge, J.B., Kuhn, D.N., Stumpf, P.K., 1979. Subcellular localization of acyl carrier protein in leaf protoplasts of *Spinacia oleracea*. *Proc. Natl. Acad. Sci.* 76, 1194–1198.
- P -
- Pascal, P.-Y., Dupuy, C., Richard, P., Haubois, A.-G., Niquil, N., 2008a. Influence of environment factors on bacterial ingestion rate of the deposit-feeder *Hydrobia ulvae* and comparison with meiofauna. *J. Sea Res.* 60, 151–156. doi:10.1016/j.seares.2008.05.003
- Pascal, P.-Y., Dupuy, C., Richard, P., Mallet, C., du Chatelet, E.A., Niquil, N., 2009. Seasonal variation in consumption of benthic bacteria by meio- and macrofauna in an intertidal mudflat. *Limnol. Oceanogr.* 54, 1048.
- Pascal, P.-Y., Dupuy, C., Richard, P., Niquil, N., 2008b. Bacterivory in the common foraminifer *Ammonia tepida*: Isotope tracer experiment and the controlling factors. *J. Exp. Mar. Biol. Ecol.* 359, 55–61. doi:10.1016/j.jembe.2008.02.018
- Patton, J.S., Abraham, S., Benson, A.A., 1977. Lipogenesis in the intact coral *Pocillopora capitata* and its isolated zooxanthellae: Evidence for a light-driven carbon cycle between symbiont and host. *Mar. Biol.* 44, 235–247. doi:10.1007/BF00387705
- Patton, J.S., Burris, J.E., 1983. Lipid synthesis and extrusion by freshly isolated zooxanthellae (symbiotic algae). *Mar. Biol.* 75, 131–136. doi:10.1007/BF00405995
- Pawlowski, J., 2000. Introduction to the molecular systematics of foraminifera. *Micropaleontology* 46, 1–12.
- Pawlowski, J., 1989. Association of foraminifera with the alga Enteromorpha. *Rev. Paléobiol.* 8, 73–75.
- Pawlowski, J., Bolivar, I., Fahrni, J.F., de Vargas, C., Gouy, M., Zaninetti, L., 1997. Extreme differences in rates of molecular evolution of foraminifera revealed by comparison of ribosomal DNA sequences and the fossil record. *Mol. Biol. Evol.* 14, 498–505.

References

- Pawlowski, J., Holzmann, M., 2014. A plea for DNA barcoding of foraminifera. *J. Foraminif. Res.* 44, 62–67. doi:10.2113/gsjfr.44.1.62
- Pawlowski, J., Lee, J.J., 1992. The life cycle of *Rotaliella elatiana* n. sp.: a tiny macroalgavorous foraminifer from the Gulf of Elat. *J. Protozool.* 39, 131–143.
- Pawlowski, J., Swiderski, Z., Lee, J.J., 1995. Observations on the ultrastructure and reproduction of *Trochammina* sp. (Foraminiferida), in: *Proceedings of the Fourth International Workshop on Agglutinated Foraminifera*, Krak'ow, Poland, September 12-19, 1993. p. 233.
- Pelletreau, K.N., Bhattacharya, D., Price, D.C., Worful, J.M., Moustafa, A., Rumpho, M.E., 2011. Sea slug kleptoplasty and plastid maintenance in a metazoan. *Plant Physiol.* 155, 1561–1565. doi:10.1104/pp.111.174078
- Pelletreau, K.N., Weber, A.P.M., Weber, K.L., Rumpho, M.E., 2014. Lipid accumulation during the establishment of kleptoplasty in *Elysia chlorotica*. *PLOS ONE* 9, e97477. doi:10.1371/journal.pone.0097477
- Perfumo, A., Elsaesser, A., Littmann, S., Foster, R.A., Kuypers, M.M.M., Cockell, C.S., Kminek, G., 2014. Epifluorescence, SEM, TEM and nanoSIMS image analysis of the cold phenotype of *Clostridium psychrophilum* at subzero temperatures. *FEMS Microbiol. Ecol.* 90, 869–882. doi:10.1111/1574-6941.12443
- Pernice, M., Meibom, A., Van Den Heuvel, A., Kopp, C., Domart-Coulon, I., Hoegh-Guldberg, O., Dove, S., 2012. A single-cell view of ammonium assimilation in coral–dinoflagellate symbiosis. *ISME J.* 6, 1314–1324.
- Pillet, L., de Vargas, C., Pawlowski, J., 2011. Molecular identification of sequestered diatom chloroplasts and kleptoplastidy in foraminifera. *Protist* 162, 394–404. doi:10.1016/j.protis.2010.10.001
- Pillet, L., Pawlowski, J., 2013. Transcriptome analysis of foraminiferan *Elphidium margaritaceum* questions the role of gene transfer in kleptoplastidy. *Mol. Biol. Evol.* 30, 66–69. doi:10.1093/molbev/mss226
- Piña-Ochoa, E., Hogslund, S., Geslin, E., Cedhagen, T., Revsbech, N.P., Nielsen, L.P., Schweizer, M., Jorissen, F., Rysgaard, S., Risgaard-Petersen, N., 2010a. Widespread occurrence of nitrate storage and denitrification among Foraminifera and Gromiida. *Proc. Natl. Acad. Sci.* 107, 1148–1153. doi:10.1073/pnas.0908440107
- Piña-Ochoa, E., Koho, K., Geslin, E., Risgaard-Petersen, N., 2010b. Survival and life strategy of the foraminiferan *Globobulimina turgida* through nitrate storage and denitrification. *Mar. Ecol. Prog. Ser.* 417, 39–49. doi:10.3354/meps08805
- Polerecky, L., Adam, B., Milucka, J., Musat, N., Vagner, T., Kuypers, M.M.M., 2012. Look@NanoSIMS – a tool for the analysis of nanoSIMS data in environmental microbiology. *Environ. Microbiol.* 14, 1009–1023. doi:10.1111/j.1462-2920.2011.02681.x
- Preiss, J., 1982. Regulation of the biosynthesis and degradation of starch. *Annu. Rev. Plant Physiol.* 33, 431–454.

References

- Prevot, P., Soyer, M.O., 1978. Action du cadmium sur un Dinoflagellé libre: *Prorocentrum micans* E.: croissance, absorption du cadmium et modifications cellulaires. CR Acad Sci Paris 287, 833–836.
- Pucci, F., Geslin, E., Barras, C., Morigi, C., Sabbatini, A., Negri, A., Jorissen, F.J., 2009. Survival of benthic foraminifera under hypoxic conditions: Results of an experimental study using the CellTracker Green method. Mar. Pollut. Bull. 59, 336–351. doi:10.1016/j.marpolbul.2009.08.015
- Pyke, K., 2009. Plastid metabolism, in: Plastid Biology. Cambridge University Press, Cambridge, United Kingdom, pp. 130–152.

- R -

- Rabalais, N.N., Diaz, R.J., Levin, L.A., Turner, R.E., Gilbert, D., Zhang, J., 2010. Dynamics and distribution of natural and human-caused hypoxia. Biogeosciences 7, 585–619.
- Rahav, O., Dubinsky, Z., Achituv, Y., Falkowski, P.G., 1989. Ammonium metabolism in the zooxanthellate coral, *Stylophora pistillata*. Proc. R. Soc. Lond. B Biol. Sci. 236, 325–337.
- Raikov, I.B., Karajan, B.P., Mikhalevitch, V.I., 1998. Ultrastructure of the gamont shell and nucleus in the polythalamous foraminifer *Elphidium ponticum*. Eur. J. Protistol. 34, 153–161.
- Raina, J.-B., Clode, P.L., Cheong, S., Bougoure, J., Kilburn, M.R., Reeder, A., Forêt, S., Stat, M., Beltran, V., Thomas-Hall, P., Tapiolas, D., Motti, C.M., Gong, B., Pernice, M., Marjo, C.E., Seymour, J.R., Willis, B.L., Bourne, D.G., 2017. Subcellular tracking reveals the location of dimethylsulfoniopropionate in microalgae and visualises its uptake by marine bacteria. eLife 6, e23008. doi:10.7554/eLife.23008
- Raven, J.A., Walker, D.I., Jensen, K.R., Handley, L.L., Scrimgeour, C.M., McInroy, S.G., 2001. What fraction of the organic carbon in sacoglossans is obtained from photosynthesis by kleptoplastids? An investigation using the natural abundance of stable carbon isotopes. Mar. Biol. 138, 537–545. doi:10.1007/s002270000488
- Reiffenstein, R.J., Hulbert, W.C., Roth, S.H., 1992. Toxicology of hydrogen sulfide. Annu. Rev. Pharmacol. Toxicol. 32, 109–134.
- Rhumbler, L., 1911. Die Foraminiferen (Thalamophoren) der Plankton-Expedition, Teil 1: Die allgemeinen Organisationsverhältnisse der Foraminiferen. Plankton Exped. Humboldt-Stift. Ergeben 3.
- Rink, S., Kühl, M., Bijma, J., Spero, H.J., 1998. Microsensor studies of photosynthesis and respiration in the symbiotic foraminifer *Orbulina universa*. Mar. Biol. 131, 583–595.
- Risgaard-Petersen, N., Langezaal, A.M., Ingvardsen, S., Schmid, M.C., Jetten, M.S.M., Op den Camp, H.J.M., Derksen, J.W.M., Piña-Ochoa, E., Eriksson, S.P., Peter Nielsen, L., Peter Revsbech, N., Cedhagen, T., van der Zwaan, G.J., 2006. Evidence for complete denitrification in a benthic foraminifer. Nature 443, 93–96. doi:10.1038/nature05070
- Rohling, E.J., Cooke, S., 1999. Stable oxygen and carbon isotopes in foraminiferal carbonate shells, in: Sen Gupta, B.K. (Ed.), Modern Foraminifera. Springer-Verlag New-York, pp. 239–258.

References

- Ross, B.J., Hallock, P., 2016. Dormancy in the Foraminifera: A review. *J. Foraminifer. Res.* 46, 358–368. doi:10.2113/gsjfr.46.4.358
- Röttger, R., Berger, W.H., 1972. Benthic Foraminifera: morphology and growth in clone cultures of *Heterostegina depressa*. *Mar. Biol.* 15, 89–94.
- RStudio Team, 2016. RStudio: Integrated Development for R. RStudio Inc., Boston, MA.
- Rumpho, M.E., Summer, E.J., Green, B.J., Fox, T.C., Manhart, J.R., 2001. Mollusc/algal chloroplast symbiosis: how can isolated chloroplasts continue to function for months in the cytosol of a sea slug in the absence of an algal nucleus? *Zoology* 104, 303–312. doi:10.1078/0944-2006-00036
- Rumpho, M.E., Summer, E.J., Manhart, J.R., 2000. Solar-powered sea slugs. *Mollusc/algal chloroplast symbiosis. Plant Physiol.* 123, 29–38.
- S -
- Sargent, J.R., Parkes, R.J., Mueller-Harvey, I., Henderson, R.J., 1987. Lipid biomarkers in marine ecology. *Microbes Sea* 119–138.
- Schlichter, D., Svoboda, A., Kremer, B.P., 1983. Functional autotrophy of *Heteroxenia fuscescens* (Anthozoa: Alcyonaria): carbon assimilation and translocation of photosynthates from symbionts to host. *Mar. Biol.* 78, 29–38. doi:10.1007/BF00392968
- Schmaljohann, R., Röttger, R., 1978. The ultrastructure and taxonomic identity of the symbiotic algae of *Heterostegina Depressa* (Foraminifera: Nummulitidae). *J. Mar. Biol. Assoc. U. K.* 58, 227–237. doi:10.1017/S0025315400024516
- Schmitz, K., Kremer, B.P., 1977. Carbon fixation and analysis of assimilates in a coral-dinoflagellate symbiosis. *Mar. Biol.* 42, 305–313. doi:10.1007/BF00402192
- Schwab, D., 1977. Light and electron microscopic investigations on monothalamous foraminifer *Boderia albicollaris* n. sp. *J. Foraminifer. Res.* 7, 188–195. doi:10.2113/gsjfr.7.3.188
- Schwab, D., 1976. Gametogenesis in *Allogromia laticollaris*. *J. Foraminifer. Res.* 6, 251–257. doi:10.2113/gsjfr.6.4.251
- Schwab, D., Schwab-Stey, H., 1979. Plate-shaped nuclear pole bodies in the monothalamous foraminifer *Kibisidytes* sp. *Protoplasma* 98, 355–361. doi:10.1007/BF01676566
- Schweizer, M., Fontaine, D., Pawlowski, J., 2011. Phylogenetic position of two Patagonian Cibicididae (Rotaliida, Foraminifera): *Cibicidoides dispars* (d'Orbigny, 1839) and *Cibicidoides variabilis* (d'Orbigny, 1826). *Rev. Micropaléontologie* 54, 175–182. doi:10.1016/j.revmic.2011.03.002
- Schweizer, M., Pawlowski, J., Kouwenhoven, T.J., Guiard, J., van der Zwaan, B., 2008. Molecular phylogeny of Rotaliida (Foraminifera) based on complete small subunit rDNA sequences. *Mar. Micropaleontol.* 66, 233–246. doi:10.1016/j.marmicro.2007.10.003
- Sen Gupta, B.K., Aharon, P., 1994. Benthic foraminifera of bathyal hydrocarbon vents of the Gulf of Mexico: Initial report on communities and stable isotopes. *Geo-Mar. Lett.* 14, 88–96.

- Sen Gupta, B.K., Platon, E., Bernhard, J.M., Aharon, P., 1997. Foraminiferal colonization of hydrocarbon-seep bacterial mats and underlying sediment, Gulf of Mexico slope. *J. Foraminif. Res.* 27, 292–300.
- Serôdio, J., Cruz, S., Cartaxana, P., Calado, R., 2014. Photophysiology of kleptoplasts: photosynthetic use of light by chloroplasts living in animal cells. *Phil Trans R Soc B* 369, 20130242. doi:10.1098/rstb.2013.0242
- Shibagaki, N., Grossman, A., 2008. The state of sulfur metabolism in algae: From ecology to genomics, in: Hell, R., Dahl, C., Knaff, D., Leustek, T. (Eds.), *Sulfur Metabolism in Phototrophic Organisms, Advances in Photosynthesis and Respiration*. Springer, Dordrecht, The Netherlands, pp. 231–267.
- Siano, R., Montresor, M., Probert, I., Not, F., de Vargas, C., 2010. *Pelagodinium* gen. nov. and *P. béii* comb. nov., a Dinoflagellate Symbiont of Planktonic Foraminifera. *Protist* 161, 385–399. doi:10.1016/j.protis.2010.01.002
- Smith, A.M., Denyer, K., Martin, C., 1997. The synthesis of the starch granule. *Annu. Rev. Plant Biol.* 48, 67–87.
- Snider, L.J., Burnett, B.R., Hessler, R.R., 1984. The composition and distribution of meiofauna and nanobiota in a central North Pacific deep-sea area. *Deep Sea Res. Part Oceanogr. Res. Pap.* 31, 1225–1249. doi:10.1016/0198-0149(84)90059-1
- Song, C., Murata, K., Suzuki, T., 2017. Intracellular symbiosis of algae with possible involvement of mitochondrial dynamics. *Sci. Rep.* 7. doi:10.1038/s41598-017-01331-0
- Spangenberg, J.E., Ferrer, M., Jacomet, S., Bleicher, N., Schibler, J., 2014. Molecular and isotopic characterization of lipids staining bone and antler tools in the Late Neolithic settlement, Zurich Opera Parking, Switzerland. *Org. Geochem.* 69, 11–25.
- Spero, H.J., 1988. Ultrastructural examination of chamber morphogenesis and biomineralization in the planktonic foraminifer *Orbulina universa*. *Mar. Biol.* 99, 9–20. doi:10.1007/BF00644972
- Spero, H.J., 1987. Symbiosis in the planktonic foraminifer, *Orbulina universa*, and the isolation of its symbiotic dinoflagellate, *Gymnodinium béii* sp. nov. *J. Phycol.* 23, 307–317.
- Spero, H.J., Parker, S.L., 1985. Photosynthesis in the symbiotic planktonic foraminifer *Orbulina universa*, and its potential contribution to oceanic primary productivity. *J. Foraminif. Res.* 15, 273–281.
- Spindler, M., Anderson, O.R., Hemleben, C., Bé, A.W.H., 1978. Light and electron microscopic observations of gametogenesis in *Hastigerina pelagica* (Foraminifera). *J. Protozool.* 25, 427–433. doi:10.1111/j.1550-7408.1978.tb04164.x
- Spindler, M., Hemleben, C., 1982. Formation and possible function of annulate lamellae in a planktic foraminifer. *J. Ultrastruct. Res.* 81, 341–350. doi:10.1016/S0022-5320(82)90062-4
- Srivastava, H.S., Singh, R.P., 1987. Role and regulation of L-glutamate dehydrogenase activity in higher plants. *Phytochemistry* 26, 597–610. doi:10.1016/S0031-9422(00)84749-4
- Stachowitsch, M., 1991. Anoxia in the Northern Adriatic Sea: rapid death, slow recovery. *Geol. Soc. Lond. Spec. Publ.* 58, 119–129.

References

- Staehelin, L.A., Moore, I., 1995. The plant Golgi apparatus: structure, functional organization and trafficking mechanisms. *Annu. Rev. Plant Biol.* 46, 261–288.
- Suhr, S., Alexander, S., Gooday, A., Pond, D., Bowser, S., 2008. Trophic modes of large Antarctic Foraminifera: roles of carnivory, omnivory, and detritivory. *Mar. Ecol. Prog. Ser.* 371, 155–164. doi:10.3354/meps07693
- Suhr, S.B., Pond, D.W., Gooday, A.J., Smith, C.R., 2003a. Selective feeding by benthic foraminifera on phytodetritus on the western Antarctic Peninsula shelf: evidence from fatty acid biomarker analysis. *Mar. Ecol. Prog. Ser.* 262, 153–162.
- Suhr, S.B., Pond, D.W., Gooday, A.J., Smith, C.R., 2003b. Selective feeding by benthic foraminifera on phytodetritus on the western Antarctic Peninsula shelf: evidence from fatty acid biomarker analysis. *Mar. Ecol. Prog. Ser.* 262, 153–162.
- Syrett, P.J., 1981. Nitrogen metabolism of microalgae. *Can. Bull. Fish. Aquat. Sci.*

- T -

- Takahashi, H., Kopriva, S., Giordano, M., Saito, K., Hell, R., 2011. Sulfur assimilation in photosynthetic organisms: Molecular functions and regulations of transporters and assimilatory enzymes. *Annu. Rev. Plant Biol.* 62, 157–184. doi:10.1146/annurev-arplant-042110-103921
- Taylor, D.L., 1971. Photosynthesis of symbiotic chloroplasts in *Tridachia crispata* (Bérgh). *Comp. Biochem. Physiol. A Physiol.* 38, 233–236. doi:10.1016/0300-9629(71)90111-3
- Taylor, D.L., 1968. *In situ* studies on the cytochemistry and ultrastructure of a symbiotic marine dinoflagellate. *J. Mar. Biol. Assoc. U. K.* 48, 349–366. doi:10.1017/S0025315400034548
- ter Kuile, B., 1991. Mechanisms for calcification and carbon cycling in algal symbiont-bearing foraminifera, in: Lee, J.J., Anderson, O.R. (Eds.), *Biology of Foraminifera*. Academic Press, London, pp. 73–90.
- ter Kuile, B., Erez, J., 1984. *In situ* growth rate experiments on the symbiont-bearing foraminifera *Amphistegina lobifera* and *Amphisorus hemprichii*. *J. Foraminifer. Res.* 14, 262–276. doi:10.2113/gsjfr.14.4.262
- Teugels, B., Bouillon, S., Veuger, B., Middelburg, J., Koedam, N., 2008. Kleptoplasts mediate nitrogen acquisition in the sea slug *Elysia viridis*. *Aquat. Biol.* 4, 15–21. doi:10.3354/ab00092
- Thibault de Chanvalon, A., Metzger, E., Mouret, A., Cesbron, F., Knoery, J., Rozuel, E., Launeau, P., Nardelli, M.P., Jorissen, F.J., Geslin, E., 2015. Two-dimensional distribution of living benthic foraminifera in anoxic sediment layers of an estuarine mudflat (Loire estuary, France). *Biogeosciences* 12, 6219–6234. doi:10.5194/bg-12-6219-2015
- Todd, R., 1965. A new Rosalina (foraminifera) parasitic on a bivalve. *Deep Sea Res. Oceanogr. Abstr.* 12, 831–837. doi:10.1016/0011-7471(65)90806-5
- Tolderlund, D.S., others, 1971. Distribution and ecology of living planktonic foraminifera in surface waters of the Atlantic and Indian Oceans. *Micropaleontol. Oceans Camb. Univ. Press N. Y.* 105–149.

References

- Travis, J.L., Allen, R.D., 1981. Studies on the motility of the foraminifera. I. Ultrastructure of the reticulopodial network of *Allogromia laticollaris* (Arnold). J. Cell Biol. 90, 211–221. doi:10.1083/jcb.90.1.211
- Travis, J.L., Bowser, S.S., 1991. The motility of foraminifera, in: Lee, J.J., Anderson, O.R. (Eds.), Biology of Foraminifera. Academic Press, London, pp. 91–155.
- Trench, R.K., 1979. The cell biology of plant-animal symbiosis. Annu. Rev. Plant Physiol. 30, 485–531.
- Trench, R.K., 1971. The physiology and biochemistry of Zooxanthellae symbiotic with marine coelenterates. II. Liberation of fixed ^{14}C by Zooxanthellae *in vitro*. Proc. R. Soc. Lond. B Biol. Sci. 177, 237–250.
- Tsuchiya, M., Kitazato, H., Pawlowski, J., 2003. Analysis of internal transcribed spacer of ribosomal DNA reveals cryptic speciation in *Planoglabratella opercularis*. J. Foraminifer. Res. 33, 285–293. doi:10.2113/0330285
- Tsuchiya, M., Kitazato, H., Pawlowski, J., 2000. Phylogenetic relationships among species of Glabratellidae (Foraminifera) inferred from ribosomal DNA sequences: Comparison with morphological and reproductive data. Micropaleontology 46, 13–20.
- Tsuchiya, M., Takahara, K., Aizawa, M., Suzuki-Kanesaki, H., Toyofuku, T., Kitazato, H., 2014. How has foraminiferal genetic diversity developed? A case study of *Planoglabratella opercularis* and the species concept inferred from its ecology, distribution, genetics, and breeding behavior, in: Kitazato, H., Bernhard, J.M. (Eds.), Approaches to Study Living Foraminifera, Environmental Science and Engineering. Springer, Tokyo, pp. 133–162. doi:10.1007/978-4-431-54388-6_9
- Tsuchiya, M., Toyofuku, T., Uematsu, K., Brüchert, V., Collen, J., Yamamoto, H., Kitazato, H., 2015. Cytologic and Genetic Characteristics of Endobiotic Bacteria and Kleptoplasts of *Virgulinema fragilis* (Foraminifera). J. Eukaryot. Microbiol. n/a-n/a. doi:10.1111/jeu.12200
- Tupas, L., Koike, I., 1991. Simultaneous uptake and regeneration of ammonium by mixed assemblages of heterotrophic marine bacteria. Mar Ecol Prog Ser 70, 273–282.
- Tyystjärvi, E., Aro, E.M., 1996. The rate constant of photoinhibition, measured in lincomycin-treated leaves, is directly proportional to light intensity. Proc. Natl. Acad. Sci. 93, 2213–2218.

- U -

- Uhle, M.E., Spero, H.J., Lea, D.W., Ruddiman, W.F., Engel, M.H., 1999. The fate of nitrogen in the Orbulina universa foraminifera–symbiont system determined by nitrogen isotope analyses of shell-bound organic matter. Limnol Ocean. 44, 1968–1977.

- V -

- Vertel, B.M., Walters, L.M., Mills, D., 1992. Subcompartments of the endoplasmic reticulum, in: Seminars in Cell Biology. Elsevier, pp. 325–341.

References

Vieler, A., Wilhelm, C., Goss, R., Süß, R., Schiller, J., 2007. The lipid composition of the unicellular green alga *Chlamydomonas reinhardtii* and the diatom *Cyclotella meneghiniana* investigated by MALDI-TOF MS and TLC. Chem. Phys. Lipids 150, 143–155. doi:10.1016/j.chemphyslip.2007.06.224

- W -

- Walsby, A.E., 1972. Structure and function of gas vacuoles. Bacteriol. Rev. 36, 1–32.
- Wang, J., Douglas, A.E., 1998. Nitrogen recycling or nitrogen conservation in an alga-invertebrate symbiosis? J. Exp. Biol. 201, 2445–2453.
- Ward, J.N., Pond, D.W., Murray, J.W., 2003. Feeding of benthic foraminifera on diatoms and sewage-derived organic matter: an experimental application of lipid biomarker techniques. Mar. Environ. Res. 56, 515–530. doi:10.1016/S0141-1136(03)00040-0
- Weber, A.P., 2004. Solute transporters as connecting elements between cytosol and plastid stroma. Curr. Opin. Plant Biol. 7, 247–253. doi:10.1016/j.pbi.2004.03.008
- Wetzel, M.A., Fleeger, J.W., Powers, S.P., 2001. Effects of hypoxia and anoxia on meiofauna: A review with new data from the Gulf of Mexico, in: Rabalais, N.N., Turner, R.E. (Eds.), Coastal Hypoxia: Consequences for Living Resources and Ecosystems. pp. 165–184.
- Wheeler, P.A., Kirchman, D.L., 1986. Utilization of inorganic and organic nitrogen by bacteria in marine systems. Limnol. Oceanogr. 31, 998–1009. doi:10.4319/lo.1986.31.5.0998
- Wilkerson, F.P., Muller, G., Muscatine, P.L., 1983. Temporal patterns of cell division in natural populations of endosymbiotic algae. Limnol. Oceanogr. 28, 1009–1014.
- Woulds, C., Cowie, G.L., Levin, L.A., Andersson, J.H., Middelburg, J.J., Vandewiele, S., Lamont, P.A., Larkin, K.E., Gooday, A.J., Schumacher, S., 2007. Oxygen as a control on sea floor biological communities and their roles in sedimentary carbon cycling. Limnol. Oceanogr. 52, 1698–1709.
- Wukovits, J., Enge, A.J., Wanek, W., Watzka, M., Heinz, P., 2016. Effect of increased temperature on carbon and nitrogen uptake of two intertidal foraminifera *Ammonia tepida* and *Haynesina germanica*. Biogeosciences Discuss. 1–25. doi:10.5194/bg-2016-509
- Würzberg, L., Peters, J., Brandt, A., 2011. Fatty acid patterns of Southern Ocean shelf and deep sea peracarid crustaceans and a possible food source, foraminiferans. Deep Sea Res. Part II Top. Stud. Oceanogr. 58, 2027–2035. doi:10.1016/j.dsr2.2011.05.013

- Y -

- Yamaguchi, K., Mayfield, S.P., Sugita, M., 2005. Transcriptional and translational regulation of photosystem II gene expression, in: Wydrzynski, T.J., Satoh, K., Freeman, J.A. (Eds.), Photosystem II, Advances in Photosynthesis and Respiration. Springer Netherlands, pp. 649–668. doi:10.1007/1-4020-4254-X_29
- Yellowlees, D., Rees, T.A.V., Fitt, W.K., 1994. Effect of ammonium-supplemented seawater on glutamine synthetase and glutamate dehydrogenase activities in host tissue and zooxanthellae

References


- of *Pocillopora damicornis* and on ammonium uptake rates of the zooxanthellae. *Pac. Sci.* 48, 291–295.
- Yellowlees, D., Rees, T.A.V., Leggat, W., 2008. Metabolic interactions between algal symbionts and invertebrate hosts. *Plant Cell Environ.* 31, 679–694. doi:10.1111/j.1365-3040.2008.01802.x
- Yoder, J.A., Martin, J., Nill, A., 1982. Cell division periodicity and the nitrate environment of a marine diatom. *Limnol. Oceanogr.* 27, 352–357. doi:10.4319/lo.1982.27.2.0352
- Z -
- Zeeman, S.C., Kossmann, J., Smith, A.M., 2010. Starch: its metabolism, evolution, and biotechnological modification in plants. *Annu. Rev. Plant Biol.* 61, 209–234. doi:10.1146/annurev-arplant-042809-112301
- Zehr, J.P., Falkowski, P.G., 1988. Pathway of Ammonium Assimilation in a Marine Diatom Determined with the Radiotracer ^{13}N . *J. Phycol.* 24, 588–591. doi:10.1111/j.1529-8817.1988.tb04267.x
- Zehr, J.P., Falkowski, P.G., Fowler, J., Capone, D.G., 1988. Coupling between ammonium uptake and incorporation in a marine diatom: experiments with the short-lived radioisotope ^{13}N . *Limnol. Oceanogr.* 33, 518–527.
- Zehr, J.P., Ward, B.B., 2002. Nitrogen cycling in the ocean: New perspectives on processes and paradigms. *Appl. Environ. Microbiol.* 68, 1015–1024. doi:10.1128/AEM.68.3.1015-1024.2002
- Zhang, J., Gilbert, D., Gooday, A., Levin, L., Naqvi, S.W.A., Middelburg, J.J., Scranton, M., Ekau, W., Pena, A., Dewitte, B., others, 2010. Natural and human-induced hypoxia and consequences for coastal areas: synthesis and future development. *Biogeosciences* 7, 1443–1467.
- Zhukova, N.V., Aizdaicher, N.A., 1995. Fatty acid composition of 15 species of marine microalgae. *Phytochemistry* 39, 351–356. doi:10.1016/0031-9422(94)00913-E

Curriculum vitae

PERSONAL INFORMATION

Charlotte LeKieffre

 Ecole Polytechnique Federale de Lausanne, Switzerland

 +41 (0) 791920331 / +33 (0) 681490848

 charlotte.lekieffre@epfl.ch

 https://www.researchgate.net/profile/Emma_Gibbin

Date of birth: 19/12/1990 | Nationality: French

Languages: French (mother tongue), English (fluent), German (basic)

EDUCATION

09/2013 – 08/2017

Doctoral Assistant in Marine Biology

Laboratory of Biological Geochemistry, EPFL, Lausanne, Switzerland

Thesis title: TEM-NanoSIMS investigation of foraminiferal metabolism

09/2012 – 06/2013

2nd year of Master of Science, Ecology of coastal and continental wetlands

University of Angers, France

Master thesis in the LPG-BIAF laboratory, University of Angers, France

Dissertation title: Anaerobic metabolism of two benthic foraminiferal species, TEM analysis of their ultrastructure

09/2011 – 06/2012

1st year of Master of Science, Ecology-Environment

University of Angers, France

Master thesis in the LIENSs laboratory, University of La Rochelle, France

Dissertation title: Vertical distribution of the benthic meiofauna and trophic interactions with the bacterial community

09/2010 – 06/2012

Bachelor of Science, Plant biology

University of Angers, France

09/2008 – 06/2010

Technical university degree in biological and biochemical analysis

Technical university institute, University of Angers, France

Internship in the EA 921: SONAS (substances from natural origin and structural analogs), University of Angers, France

PEER-REVIEWED PUBLICATIONS

- **C LeKieffre**, JE Spangenberg, G Mabilieu, S Escrig, A Meibom, E Geslin. 2017. Surviving anoxia in marine sediments: The metabolic response of ubiquitous benthic foraminifera (*Ammonia tepida*). PLoS ONE. 12(5), e0177604.
- F Cesbron, E Geslin, **C LeKieffre**, T Jauffrais, MP Nardelli, D Langlet, G Mabilieu, F Jorissen, D Jézéquel, E Metzger, 2017. Sequestered chloroplasts in the benthic foraminifer *Haynesina germanica*: cellular organization, oxygen fluxes and potential ecological implications. J. Foraminifer. Res. 47 (3), 268-278.

PUBLICATIONS IN PREP

- **C LeKieffre**, JM Bernhard, G Mabilieu, HL Filipsson, A Meibom, E Geslin. An overview of cellular ultrastructure in benthic foraminifera: New observations of rotalid species in the context of existing literature. Marine Micropaleontology, Special issue "Foraminiferal ultrastructure". Submitted.
- KA Koho, **C LeKieffre**, H Nomaki, I Salonen, E Geslin, G Mabilieu, LH Søggaard Jensen, G-J Reichart. Changes in ultrastructural features of the foraminifera *Ammonia* spp. In response to anoxic conditions: field and laboratory observations. Marine Micropaleontology, Special issue "Foraminiferal ultrastructure". Submitted.

- H Nomaki, **C LeKieffre**, S Escrig, A Meibom, S Yagyu, EA Richardson, T Matsuzaki, M Murayama, E Geslin, JM Bernhard. Innovative TEM-coupled approaches to study foraminiferal cells. *Marine Micropaleontology*, Special issue "Foraminiferal ultrastructure". Submitted.
- T Jauffrais, **C LeKieffre**, KA Koho, M Tsuchiya, M Schweizer, JM Bernhard, A Meibom, E Geslin. Ultrastructure and distribution of kleptoplasts in benthic foraminifera from shallow-water (photic) habitats. *Marine Micropaleontology*, Special issue "Foraminiferal ultrastructure". Submitted.
- **C LeKieffre**, H Spero, AD Russell, J Fehrenbacher, E Geslin, A Meibom. Carbon integration and transfer between photosynthetic symbiotic dinoflagellates and a planktonic foraminifera. In prep.
- **C LeKieffre**, T Jauffrais, M. Giovanni, B Jesus, JM Bernhard, A Meibom, E Geslin. Inorganic carbon and nitrogen uptake and dynamics by a shallow water kleptoplast foraminifera. In prep.
- T Jauffrais, **C LeKieffre**, E Geslin, JM Bernhard, M Schweizer, B Jesus, HL Filipsson, O Maire, A Meibom. Ammonia and sulfur uptake by a kleptoplastic benthic foraminifer from an aphotic environment. In prep
- C Bird, **C LeKieffre**, A Meibom, AD Russell, J Fehrenbacher, CV Davis, BT Ngwenye and KF Darling. A heterotrophic marine protist capable of ammonium uptake from the water column. In prep
- B. Jesus, T. Jauffrais, E. Trampe, J. Gössling, **C. LeKieffre**, A Meibom, E Geslin. Kleptoplast distribution, photosynthetic efficiency and sequestration mechanisms in intertidal benthic foraminifera. In prep.

CONFERENCES

*oral presentation
** poster presentation

-
- ****C LeKieffre**, JE Spangenberg, G Mabilieu, A Meibom and E Geslin. A benthic foraminifera species respond to anoxia with a strong metabolic shift suggesting a state of dormancy. 28th International Meeting on Organic Geochemistry (IMOG), Florence, Italy, 17-22 September 2017.
- ****C LeKieffre**, JE Spangenberg, G Mabilieu, A Meibom, E Geslin. A benthic foraminiferal species respond to anoxia with a strong metabolic shift suggesting a state of dormancy. 14th Swiss Geoscience Meeting, Geneva, 18 & 19 November 2016.
- ***C LeKieffre**, H Spero, AD Russell, J Fehrenbacher, E Geslin, A Meibom. Photosynthetic process, carbon and nitrogen exchanges between a symbiotic dinoflagellate and the foraminiferal host cell. The Batsheva de Rothschild Workshop, Live foraminifera as a new model system for monitoring and reconstructing marine environments, Eilat, Israel, 10-16 September 2016.
- *E Geslin, **C LeKieffre**, PM Nardelli, O Maire, C Barras, M Schweizer, A. Thibault de Chanvalon, D. Langlet, A. Meibom, E. Metzger. Physiological functions of *Ammonia tepida* in different oxygenated conditions: evidence for dormancy under anoxia. The Batsheva de Rothschild Workshop, Live foraminifera as a new model system for monitoring and reconstructing marine environments, Eilat, Israel, 10-16 September 2016.
- ****C LeKieffre**, E Geslin, S Escrig, T Jauffrais, H Spero, AD Russell, J Fehrenbacher, A Meibom. NanoSIMS applied to the study of foraminifera. The Micropalaeontological Society Foraminifera and Calcareous Nannofossil Groups Spring Meeting, June 2016, Angers University, Angers, France, June 2016.
- **T Jauffrais, **C Le Kieffre**, B Jesus, E Metzger, A Meibom, E Geslin. Kleptoplasty in shallow water benthic foraminifera. The Micropalaeontological Society Foraminifera and Calcareous Nannofossil Groups Spring Meeting, June 2017, Angers University, Angers, France, June 2016.
- ***C Lekieffre**, E Geslin, J Spangenberg, G Mabilieu, and A Meibom. Dormant or not dormant? Benthic foraminiferal metabolism under anoxia. 2016 Ocean Sciences Meeting, New Orleans, February 21-26, 2016.
- ****C Lekieffre**, S Howard, J Fehrenbacher, A Russell, E Geslin, A Meibom. Carbon integration and transfer by the photosynthetic symbiotic dinoflagellates of the

planktonic foraminifer *Orbulina universa* observed by TEM-nanoSIMS techniques. SCOR/IGBP Working Group 138: Final Workshop & Short Course on Culturing of Planktonic Foraminifera, Wrigley Marine Science Center Santa Catalina Island, California, USA, August 30th - September 4th, 2015.

***C Lekieffre**, E Geslin, J Spangenberg, A Meibom. Feeding behaviour of a benthic species (*Ammonia tepida*) under oxic and anoxic conditions: TEM-NanoSIMS correlation. The Micropalaeontological Society Foraminifera and Calcareous Nannofossil Groups Spring Meeting, June 2015, Plymouth University, Plymouth, United Kingdom, June 16, 2015.

****M Gilis**, SK Cohen, C Kopp, **C Lekieffre** and S Escrig et al. NanoSIMS and Electron Microscopy: A powerful combination in Life Science Research. 18th International Microscopy Congress, Prague, Czech Republic, September 7-12, 2014.

****MP Nardelli**, D Langlet, F Cesbron, **C Lekieffre** and A Meibom et al. Photosynthesis in the kleptoplastidic foraminiferal species "*Haynesina germanica*". Joint Spring Meeting, Foraminifera and Nannofossil Groups, Texel, the Netherlands, June 22-25, 2014.

TEACHING EXPERIENCE

07-2017	Teaching assistant Summer school FRESCO: Living benthic foraminifera in coastal environments. University of Angers, France. Practical course: living foraminifera.
02-05/2014-2017 11/2014-2015	Environmental Engineering department, ENAC, EPFL, Lausanne, Switzerland - Environmental monitoring (practical sessions), Bachelor course - Biomineralization of foraminifera (lecture), Master course
10-11/2016 10-11/2016	Geoscience department, University of Angers, France - Evolutionary paleontology (practical and exercise sessions), Bachelor course - Bio-indicators in aquatic environments (practical and exercise sessions), Master course
09/2015 - 06/2016	Supervision of student research projects - Semester project (bibliographic report) and Master thesis: Sequestered chloroplasts in the foraminifera <i>Haynesina germanica</i> , TEM and NanoSIMS of the carbon and nitrogen metabolisms
08/2017	- Semester project (4 weeks), third year bachelor student: immersion in the lab (Electron microscopy and NanoSIMS techniques)

PROFESSIONAL CERTIFICATIONS

2016 2015	Safety certifications: FOBS 2: Specific training for safety in the laboratory (EPFL, Lausanne). COSEC training: Work safety and health protection, course for safety coordinators (EPFL, Lausanne).
2013	FOBS 1: general training on safety, prevention and health domain (EPFL, Lausanne).
2008	Informatics certification: C2i: optimal use of the computer, implementation of collaborative work remotely (blog, platform, etc.), office software (excel, word, powerpoint, etc.)

PERSONAL SKILLS

Computer skills	Microsoft office Illustrator Photoshop (basic) Image acquisition (Leica LAS software, ISC pictures) Image analysis (FIJI, ImageJ) Statistical programs (R, Rstudio, Past) Zotero.
Laboratory skills	Algae culture Confocal microscopy (basic training) Electron microscopy (sample preparation and imaging) Flow cytometry (basic training) Immunolabeling (basic training) Foraminifera culture Light microscopy Mass spectrometry Microsensors: optodes and microelectrodes (Pyroscience and Unisense) Molecular genotyping: DNA extraction, amplification, PCR (basic training) NanoSIMS Spectrophotometry.
Fieldwork skills	Basics in benthic foraminiferal taxonomy block/transect/quadrat surveys CTD cast Niskin bottles Plankton tow

MISCELLANEOUS

09/2013-08/2017

Safety and security coordinator for the Biological Geochemistry Laboratory

07/2015-12/2016

Doctoral School representative: Civil and Environmental Engineering Doctoral School, EPFL, Lausanne, Switzerland. Representative of the PhD students at the meeting with vice-provost for Research. Organization of social events (~30 to 200 people).

Scientific popularization

11/2016

Journée des gymnasiens: 3-day visit of high school students on EPFL campus.
Animations about the theme of microplastic pollution in water.

05/2014

Mystères de l'UNIL: Animations for 6 to 9 years old children on the theme of coral biology and protection, Lausanne University, Switzerland.

